Minor differences cause major effects: How differential oligomerization regulates the activities of USP25 and USP28

Kleine Unterschiede mit großer Auswirkung: Wie differenzielle Oligomerisierung die Aktivitäten von USP25 und USP28 reguliert

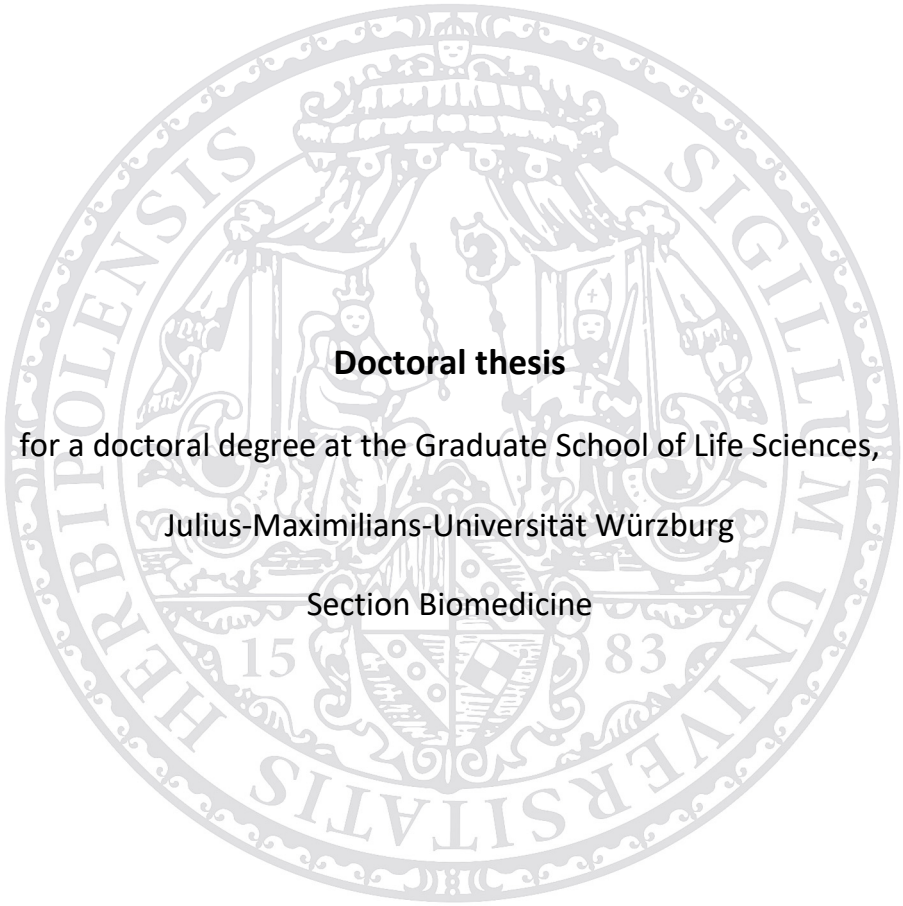

Doctoral thesis

for a doctoral degree at the Graduate School of Life Sciences,

Julius-Maximilians-Universität Würzburg

Section Biomedicine

Submitted by

Theresa Antonia Klemm

born in Ansbach

Würzburg 2019

Submitted on: ……..

Office stamp

Members of the *Promotionskomitee*:

Chairperson: Prof. Dr. Manfred Gessler

Primary Supervisor: Prof. Dr. Caroline Kisker

Supervisor (Second): Prof. Dr. Alexander Buchberger

Supervisor (Third): Prof. Dr. Nikita Popov

Date of Public Defence: ……

Date of Receipt of Certificates: ……

Wenn du mit dir am Ende bist
und du einfach nicht weiter willst
weil du dich nur noch fragst
warum und wozu und was dein Leben noch bringen soll

Halt durch, auch wenn du allein bist!
Halt durch, schmeiß jetzt nicht alles hin!
Halt durch, und irgendwann wirst du verstehen,
dass es jedem einmal so geht.

Und wenn ein Sturm dich in die Knie zwingt
halt dein Gesicht einfach gegen den Wind.
Egal, wie dunkel die Wolken über dir sind
sie werden irgendwann vorüberziehn.

Steh auf, wenn du am Boden bist!
Steh auf, auch wenn du unten liegst!
Steh auf, es wird schon irgendwie weitergehn.

(lyrics by Andreas Frege (Campino), die Toten Hosen- "*Steh auf wenn du am Boden bist*")

Abstract

Deubiquitinases are regulators of the ubiquitin proteasome system that counteract the ubiquitination cascade by removing ubiquitin from substrates and cleaving ubiquitin chains. Due to their involvment in various important pathways, they are associated with several diseases and may thus present promising drug targets. The two related ubiquitin specific proteases USP25 and USP28 share a highly conserved amino acid sequence but perform distinct biological functions. USP28 plays roles in cell cycle regulation and was also linked to several types of cancer. It adopts oncogenic functions by rescuing the oncoproteins MYC and JUN from proteasomal degradation, which is induced by the E3-ligase SCF (FBW7). Opposingly, USP28 also regulates the stability of the tumor suppressor FBW7 itself. USP25 contributes to a balanced innate immune system by stabilizing TRAF3 and TRAF6 and lately was found to promote Wnt-signaling by deubiquitinating TNKS.

Due to the high level of identity of both proteases, a recent attempt to inhibit USP28 led to cross reactivity against USP25. In our study, we characterized both USP25 and USP28 structurally and functionally using x-ray crystallography, biochemical as well as biophysical approaches to determine similarities and differences that can be exploited for the development of specific inhibitors.

The crystal structure of the USP28 catalytic domain revealed a cherry-couple like dimer that mediates self-association by an inserted helical subdomain, the USP25/28 catalytic domain inserted domain (UCID). In USP25, the UCID leads to formation of a tetramer composed of two interlinked USP28-like dimers. Structural and functional analysis revealed that the dimeric USP28 is active, whereas the tetrameric USP25 is auto inhibited. Disruption of the tetramer by a cancer-associated mutation or a deletion-variant activates USP25 through dimer formation in *in vitro* assays and leads to an increased stability of TNKS in cell studies. Furthermore, *in vitro* data showed that neither ubiquitin nor substrate binding led to the activation of the USP25 tetramer construct. With the structure of the C-terminal domain of USP25, we determined the last unknown region in the enzyme as a separately folded domain that mediates substrate interactions.

Combined the structures of the USP25 and USP28 catalytic domains and the functional characterization of both enzymes provide novel insights into the regulation of USPs by oligomerization. Furthermore, we identified individual features of each protease that might be explored for the development of specific small molecule inhibitors.

Zusammenfassung

Deubiquitinasen sind Regulatoren des Ubiquitin-Proteasom-Systems, welche der Ubiquitin-Kaskade entgegenwirken, in dem sie Ubiquitin von Substraten entfernen oder Ubiquitinketten schneiden. Durch ihr umfangreiches Vorkommen in wichtigen Signalwegen, werden sie häufig mit Krankheiten assoziiert und gelten daher als vielversprechender Ansatzpunkt für die Entwicklung von Arzneimitteln. Die zwei verwandten Ubiquitin-spezifischen Proteasen USP25 und USP28 zeichnen sich durch eine sehr hohe Konservierung der Aminosäuresequenz aus, unterscheiden sich jedoch in ihren biologischen Funktionen. USP28 ist in die Regulierung des Zellzyklus involviert und wurde auch mit mehreren Krebsarten in Verbindung gebracht. Es zeigt onkogene Merkmale, indem es die Onkoproteine MYC und JUN vor dem proteasomalen Abbau schützt, welcher durch die E3-Ligase SCF (FBW7) induziert wird. Im Widerspruch dazu reguliert USP28 jedoch auch die Stabilität des Tumorsuppressors FBW7 selbst. USP25 hingegen stabilisiert TRAF3 und TRAF6 und trägt damit zum Gleichgewicht des angeborenen Immunsystems bei. Außerdem wurde USP25 erst kürzlich eine Funktion nachgewiesen, die den Wnt-Signalweg fördert, indem es TNKS deubiquitiniert.

Die hohe Sequenzidentität beider Proteasen führte bisher dazu, dass alle Inhibitoren, die entwickelt wurden, um USP28 spezifisch zu hemmen, auch eine Kreuzreaktion mit USP25 aufweisen. In unseren Studien, haben wir Röntgenkristallographie, sowie biochemische und biophysikalische Methoden angewandt, um strukturelle und funktionelle Ähnlichkeiten und Unterschiede zwischen USP25 und USP28 zu identifizieren, die bei der Entwicklung von spezifischen Inhibitoren genutzt werden können.

Die Kristallstruktur der katalytischen Domäne von USP28 zeigt ein Kirsch-ähnliches Dimer, welches, vermittelt durch die Insertion einer helikalen Unterdomäne, der *USP25/USP28 catalytic domain inserted domain* (UCID), mit sich selbst assoziiert. In USP25, führt die UCID zu der Bildung eines Tetramers, welches aus zwei USP28-ähnlichen Dimeren besteht. Strukturelle und funktionelle Untersuchungen zeigten, dass ein USP28 Dimer aktiv ist, wohingegen ein tetrameres USP25 auto-inhibiert vorliegt. In *in vitro* Experimenten führte die Zerschlagung des USP25 Tetramers,

durch eine Krebs-assoziierte Mutation oder eine Deletionsvariante, zu einem Dimer und damit zu einer Aktivierung von USP25. In Zell-studien, induzierten die USP25 Dimere eine erhöhte Stabilität des Substrates TNKS. Außerdem zeigten die *in vitro* Daten, dass weder Ubiquitin noch die Substratbindung unsere USP25 Konstrukte aktivieren können. Durch die strukturelle Charakterisierung der C-terminalen Domäne von USP25, konnten wir den letzten bisher unbekannten Bereich des Enzyms als eine separat gefaltete Domäne beschreiben, welche Substratinteraktionen vermittelt.

Sowohl durch die Strukturen, der katalytischen Domänen von USP25 und USP28, als auch durch die funktionelle Charakterisierung beider Enzyme konnten neue Erkenntnisse zu der Regulation von USPs durch Oligomerisierung gewonnen werden. Außerdem konnten wir individuelle Merkmale in beiden Proteasen identifizieren, die genutzt werden können, um die Entwicklung von spezifischen kleinmolekularen Inhibitoren voran zu bringen.

Table of contents

I. Introduction

I.1 Deubiquitinases in the ubiquitin system

Ubiquitination is one of the most important post translational modifications in cells, due to its participation in the regulation of almost all cellular processes (1-3). Key-players of the ubiquitin system regulate the balance between cell proliferation and differentiation and contribute to the tight control of cell homeostasis and death, thus have a determining influence on the fate of a cell (4, 5). The ubiquitination reaction is implemented by a cascade of three enzymes: E1 ubiquitin activating enzyme, E2 ubiquitin conjugating enzyme and E3 ubiquitin ligase, that attach ubiquitin (Ub) with an isopeptide bond by its C-terminal carboxyl group to the amino group of a lysine residue or the free N-terminus of a substrate (6-8). Besides mono-ubiquitination and multi mono-ubiquitination on several lysine residues of the substrate, ubiquitin can itself be ubiquitinated via its seven lysine residues or its N-terminus, which leads to poly-ubiquitin chains of the same linkage type, mixed chains or further complex structures like branched ubiquitin chains (2, 3). Additional posttranslational modifications of ubiquitin itself by phosphorylation or acetylation expand the complexity of ubiquitination significantly (1, 2). All of these modifications determine different outcomes for the substrate, like a code that encrypts instructions (2, 3). The best understood translations for the labeling of a substrate with Ub-chains, are the attachment of homotypic K48-linked chains, which mainly targets proteins for proteasomal degradation and K63-linked chains, that drive mainly non-proteolytic functions, like protein interactions, DNA repair, protein sorting or regulation of signaling events (2, 3).

Ubiquitination is reversible and the proteases that perform the cleavage of ubiquitin chains or the removal of ubiquitin from substrates are called deubiquitinases (DUBs) (9). To date there are seven known DUB families (Figure 1), of which six are cysteine proteases: the ubiquitin-specific proteases (USPs), the ubiquitin C-terminal hydrolases (UCHs), the ovarian tumor proteases (OTUs), the Josephin family (9, 10) and the two recently identified families: the motif interacting with ubiquitin (MIU)-containing novel DUB family (MINDYs) (11) and the zinc finger with UFM1-specific

peptidase domain proteins (ZUFSPs) (12-15). The seventh DUB family member, the JAB1/ MPN/ MOV34 (JAMM or MPN) belong to the metalloproteases (9, 10).

In general DUBs are necessary to control ubiquitin homeostasis (16). They are responsible for the generation of free ubiquitin, by cleaving the transcribed linear precursor ubiquitin-chains or the ubiquitin-ribosomal precursor proteins (16, 17). Moreover, DUBs counteract E3-ubiquitin ligases, by removing single Ub moieties or ubiquitin-chains from substrates, which leads to the recycling of Ub on the one hand and on the other hand rescues proteins from degradation or alters signaling cascades, depending on the Ub-linkage type that is removed (9, 18).

Cystein proteases

USPs (56)

USP7 (PDB: 1NB8)

OTUs (17)

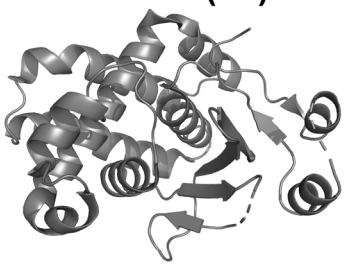

OTUB1 (PDB: 3VON)

UCH (4)

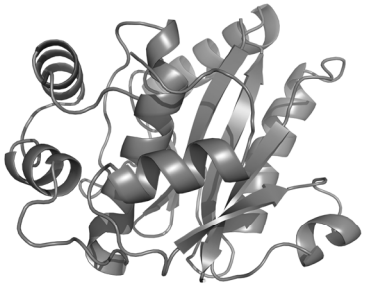

UCH-L3 (PDB: 1UCH)

Josephin (4)

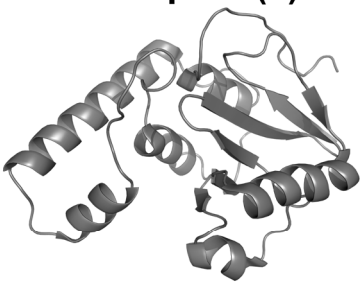

ATXN3 (PDB: 2DOS)

MINDY (5)

MINDY-1 (PDB: 5JKN)

ZUFSP (1)

ZUP1 (PDB: 6EI1)

Metalloproteases

JAMM/ MPN (12)

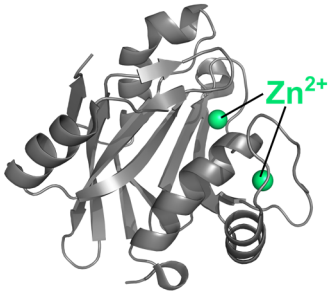

AMSH (PDB: 3RZU)

Figure 1: Examples for the DUB families. DUBs are divided due to their cleavage mechanism, into cysteine proteases and metalloproteases. For each family one example is given. The name of the enzymes and the PDB codes are given below the structures. The numeric next to the family name indicate the number of family members belonging to the specific group.

I.2 Ubiquitin specific proteases

I.2.1 Cysteine-dependent cleavage mechanism of USPs

From the 99 human DUB enzymes that were identified up to now, 56 belong to the largest family of DUBs, the USPs (19). USPs are cysteine proteases that contain a conserved catalytic triad, with a Cysteine, a Histidine and an Aspartic acid or Asparagine, that are located in close proximity to each other and form the catalytic site (20). The deubiquitinating mechanism performed by USPs, is similar to the peptide cleavage of other cysteine proteases, like the plant protease papain (21). As an example, the mechanism is shown in Figure 2 with di-Ub as the substrate and a schematic USP domain as the enzyme. Ubiquitin binding to USPs is driven by the ubiquitin binding site S1 that interacts with an Ub moiety, that is C-terminally linked to a Lysine residue of the next Ub moiety in the chain, which interacts with the S1' site on the DUB at the other side of the catalytic center. In the case of di-Ub, the distal Ub is binding to the S1 and the proximal Ub to the S1' site (10) The distal Ub is defined as the terminal Ub moiety in the Ub-chain that is connected with its C-terminus to the Lysine or N-terminal Methionine of another Ub molecule but does not have a linkage itself. In contrast, the proximal Ub is the terminal molecule in the Ub-chain that contains a free C-terminus or is linked to the substrate (10). In the catalytic triad of the DUB, Histidine acts as a base and deprotonates the thiol group of the catalytic cysteine residue, thereby facilitating the nucleophilic attack towards the carbonyl carbon of the Ub-Ub isopeptide bond. Aspartic acid meanwhile stabilizes and polarizes the Histidine in its position towards the Cysteine residue. The nucleophilic attack leads to the formation of a tetrahedral intermediate, and the negative charge is stabilized by an oxyanion hole in the enzyme. The reaction continues with the release of the proximal Ub, facilitated by the catalytic Histidine functioning as the general acid, and the formation of an acyl intermediate of the enzyme with the distal Ub. A following water attack, with the Histidine functioning again as the general base, leads to the deacylation reaction. A second negatively charged tetrahedral

intermediate is formed and stabilized by the oxyanion hole, which consequently drives the release of the distal Ub and the recovering of the catalytic triad (Figure 2) (10, 22).

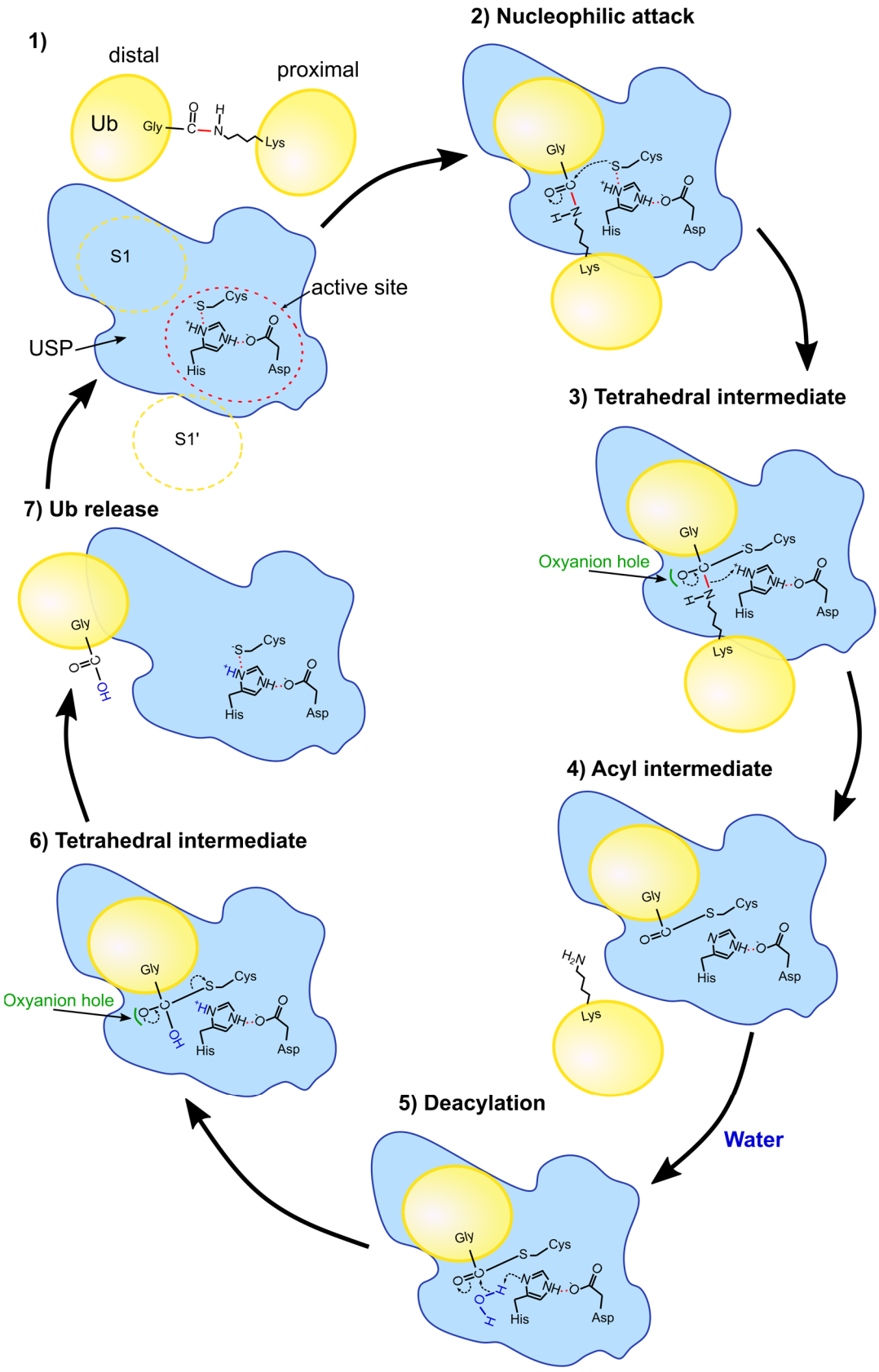

Figure 2: Isopeptide-cleavage mechanism of cysteine proteases using the example of di-Ub cleavage in USPs. **1)** Di-Ub (yellow) with a distal and proximal Ub connected by a scissile isopeptide bond in red. The USP domain is shown in blue with indicated S1 and S1' binding sites (yellow dotted circle) and the active site (red dotted circle) containing the catalytic triad with a Cysteine, Histidine and Aspartic acid residue. Histidine deprotonates the thiol group

of the Cysteine. Aspartic acid polarizes/stabilizes Histidine in its position towards Cysteine (red dotted lines). **2)** Nucleophilic attack of the deprotonated Cysteine towards the carbonyl carbon. **3)** Resulting tetrahedral intermediate with a negatively charged oxygen stabilized in an oxyanion hole (green) on the enzyme with stabilizing hydrogen bonds (not shown). **4)** Release of the proximal Ub and formation of a substrate-enzyme Acyl intermediate. **5)** Deacylation by a water molecule (blue) leads to a **6)** second tetrahedral intermediate with an oxyanion hole stabilizing the negative charge of the oxygen. **7)** Release of the distal Ub and recovery of the catalytic triad. Figure recreated and modified from Mevissen T.E.T and Komander D. (10)

I.2.2 Common domain architecture of USPs

Although ubiquitin specific proteases vary widely in their size, with the shortest comprising about 360 amino acids (aa) and the longest about 3600 aa (22), they share 6 conserved regions, which are also called boxes, in their catalytic domains that lead to a conserved USP domain fold (Figure 3A) (20). The catalytic domain folds into three subdomains, the thumb, the fingers and the palm with the catalytic triad located between the thumb (Cysteine, Box1) and the palm (Histidine, Box5 and Aspartic acid/ Asparagine Box6) (20, 23). Additional sequence insertions in the catalytic domain are common, which occur in loop regions of the USP structure, at specific insertions sites between the annotated boxes (Figure 3) (20). Some of these insertions fold into individual domains that can contribute to Ub binding, like the ubiquitin associated domains (UBA) of USP5 or USP13, that are included between box 4 and 5 and provide additional Ub binding sites (S2, S3) for poly Ub-chains (24, 25). Other insertions, in contrast, seem to consist of disordered regions with still unknown functions, like in USP9X, box 1/2 and 4/5 insertions (26). Next to their catalytic domains, most of the USPs are C- and/or N-terminally elongated, frequently containing additional ubiquitin binding regions (UBRs) consisting of UBAs, ubiquitin interacting motifs (UIMs), and zinc finger ubiquitin specific protease (ZnF UBPs) domains (9). Additionally, often ubiquitin-like (UBL) domains and less frequently domain present in USPs (DUSP) regions are integrated into the USP domain architecture (9, 27). The function of UBL domains in USPs seems to be highly diverse, contributing to catalytic efficiency of the DUBs, like the 5 UBLs in USP7 and the DUSP-UBL tandem domain in USP4 (28, 29) or leading to the association and stimulation of the proteasome as it can be seen for the UBL in USP14 (30). The DUSP domain contributes to the release of Ub in USP4, thus

promotes the catalytic efficiency of the enzyme and was suggested to be involved in protein-protein interactions (28, 31).

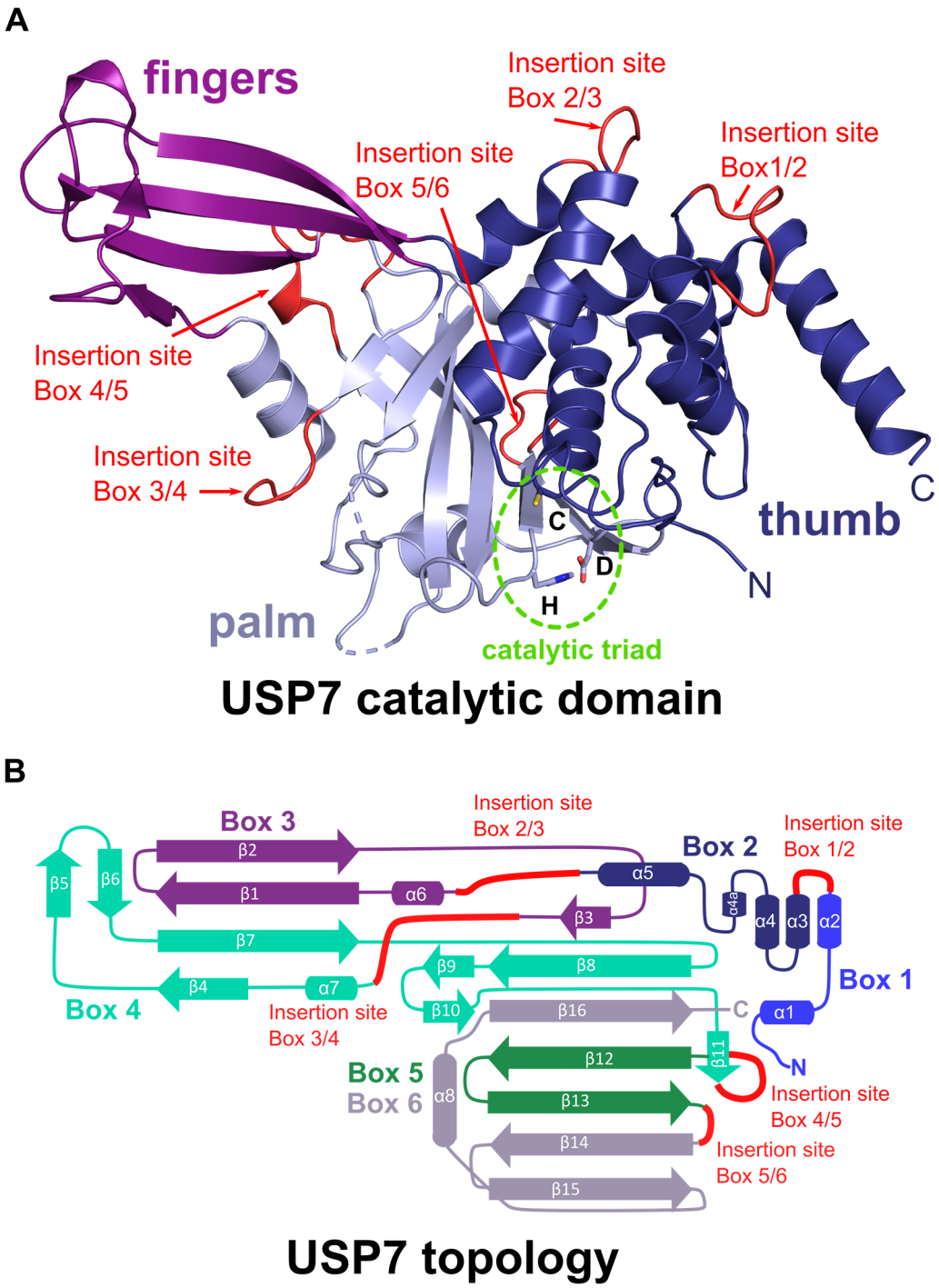

Figure 3: Structure and topology of the common USP catalytic domain using the example of USP7 (PDB: 1NB8). **A)** The structure of USP7 adopts the typical USP fold with thumb (dark blue), fingers (purple) and palm (light blue) subdomains. The site of the catalytic triad is indicated by a green dotted circle, with the residues shown as sticks. Common insertion sites in loop regions of the structure are shown and labeled in red. **B)** USP7 topology with the conserved boxes 1-6 indicated in different colors. Common insertion sites are indicated and labeled in red. Helices are shown as ovals, β-strands as arrows. Topology recreated and modified from Ye *et al*.(20).

I.3 Individual characteristics of the other DUB families

Within the 99 human DUB enzymes, 11 lack important catalytic site residues and are categorized as pseudo-DUBs, nonetheless regulating important biological functions, as activators or scaffolding proteins (32). The largest group of these pesudoenzymes belong to the JAMM/MPN family, which contains 5 pseudo-DUBs out of 12 family members (19). Several of these inactive pseudo-JAMM/MPN$^-$ members form heterodimeric complexes with active JAMM/MPN$^+$ enzymes, to allosterically activate or stabilize the active proteases, e.g. RPN8 (MPN$^-$) and RPN11 (MPN$^+$), or BRCC36 (BRCA1/BRCA2-containing complex subunit 36; MPN$^+$) and Abraxas 1 or 2 (MPN$^-$) (32). Moreover, JAMM/MPN DUBs are generally integrated into large protein complexes, like AMSH (associated molecule with the SH3 domain of STAM, Figure 1) being part of the ESCRT (endosomal sorting complex required for transport) machinery or RPN8 (MPN$^-$) and RPN11 (MPN$^+$) being part of the yeast proteasome (9, 33-35).

For the OTU DUB family, which is the second largest group of the cysteine-DUBs, a major characteristic is its specificity for Ub-chain linkages (Figure 1) (36). Linkage specificity in OTU DUBs is achieved, among other mechanisms, by the correct positioning of the proximal Ub in the S1' site located on the OTU catalytic domain or on additional UBRs (e.g. the UIM of OTUD1 or the ZnF of OTUD2). Furthermore, a second S2 Ub binding site on the OTU domain of OTUD2 revealed its importance for K11-poly Ub-chain cleavage (36).

The four members of the UCH family in humans can be subdivided into two groups. The smaller UCH (UCH-L1 and UCH-L3), are restricted by their crossover loop in the catalytic domain to only cleave small peptide conjugates, since Ub-chains cannot pass through the crossover loop (Figure 4) (9, 37, 38). The other two UCH (UCH37/UCH-L5 and BAP1 (BRCA1 (breast cancer early-onset 1)-associated protein 1)) have longer crossover loops and therefore are able to cleave Ub-chains (37, 39)

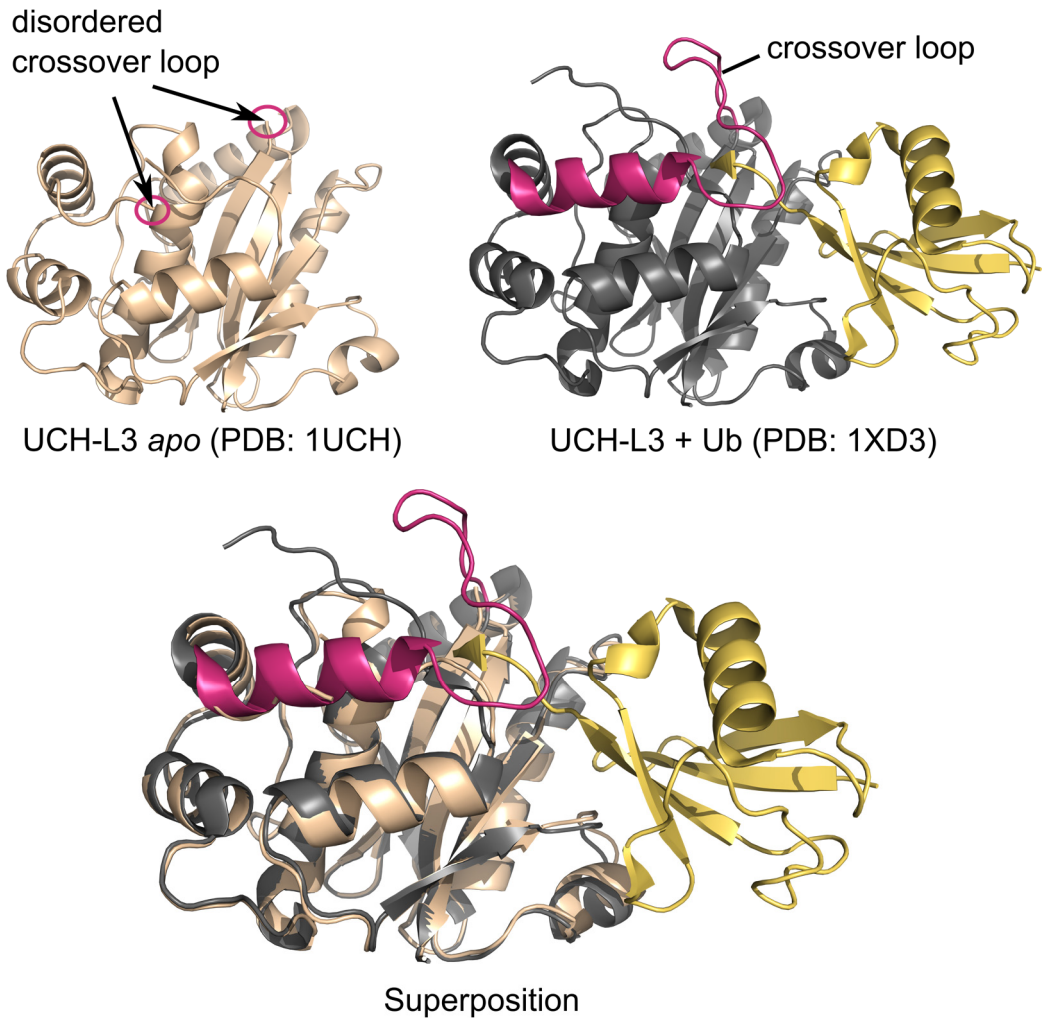

Figure 4: UCH-L3 crossover loop. Structure of UCH-L3 in the apo (left, in beige) and Ub-bound state (right, UCH-L3 in grey, Ub in yellow). The crossover loop (disordered in the apo state, indicated by pink circles and black arrows) orders upon Ub-binding (pink). The superposition of apo and Ub-bound state is displayed below. The PDB codes for the two structures are indicated.

Josephin DUBs are especially known due to their member Ataxin 3 (ATXN3), which gene mutation causes the Machado Joseph Disease (MJD), the most common spinocerebellar ataxia (Figure 1) (9). ATXN3 contains a polyQ sequence C-terminal to the Josephin domain and two UIM motifs, which aberrant extension causes the aggregation of the protein and leads to the neurodegenerative disease (40).

The two last DUB families, the MINDY and the ZUFSP, were only identified recently and show specificity for K48-linked and K63-linked ubiquitin chains, respectively (Figure 1) (11-15, 19).

I.4 USP25 and USP28- two members of the USP-family

I.4.1 Regulation by posttranslational modification

USP25 and USP28 are two closely related DUBs, that originate from a common ancestor (41). For both enzymes, at least two different isoforms have been identified, which are generated via alternative splicing. Interestingly, the longest isoform in either protease shows a muscle-tissue specificity, present in skeletal- muscle and heart tissue, while the shorter isoforms are expressed ubiquitously (41, 42). Both enzymes share the same domain architecture with a conserved USP domain that is extended by a 170 amino acid (aa) long insertion of unknown fold, located at the insertion site between box 4 and box 5 (Figure 3 and Figure 5) (20, 41). The N-terminal part of both USP25 and USP28 adopts a highly flexible structure including a UBR consisting of one UBA and two UIMs (Figure 5) (43-46). Additionally, a small-ubiquitin-like modifier (SUMO) interacting motif (SIM) is integrated in the UBR and contributes to the regulation of both enzymes (43, 45, 47). In USP25, SUMO2/3 conjugation preferably to the N-terminal K99 within the SIM hinders cleavage of tetra-Ub chains, but not the minimal substrate Ub-AMC (Ubiquitin with 7-amino-4methylcoumarin), probably due to an inhibited Ub-chain binding by the N-terminal UBR of USP25 (47). The same residue K99 was also found to be mono-ubiquitinated in the muscle specific isoform of USP25 (USP25m), promoting the activity of the enzyme (43). Interestingly, the authors of this study also proposed an auto-deubiquitinating mechanism for USP25m, facilitated by homo-dimerization/ oligomerization of the enzyme, indicating an auto-regulation of USP25 (43). A similar inhibition mechanism by SUMO conjugation to K99 was also proposed for USP28, suggesting a common regulatory function of the N-terminal domain in both enzymes by posttranslational modifications (45). Despite the related regulatory mechanism, the activity of USP28 on Ub-chains does not seem to depend on the N-terminal domain, which stands in contrast to the findings for USP25 (45, 47). Moreover, USP28 displays a preference for K11-, K48- and K63-linked Ub chains, whereas USP25 cleaves all di-Ub chain types without a specificity, except linear M1-linked chains but adopts a preference for longer K48-linked chain binding, due to its tandem-UIMs in the N-terminal domain (45, 48, 49). These small functional differences between USP25 and USP28 stand in contrast to the identical structural arrangement of the N-terminus

and the overall similar regulatory mechanisms by SUMO-inhibition and indicate additional regulatory elements within the full-length (fl) proteins that await further characterization.

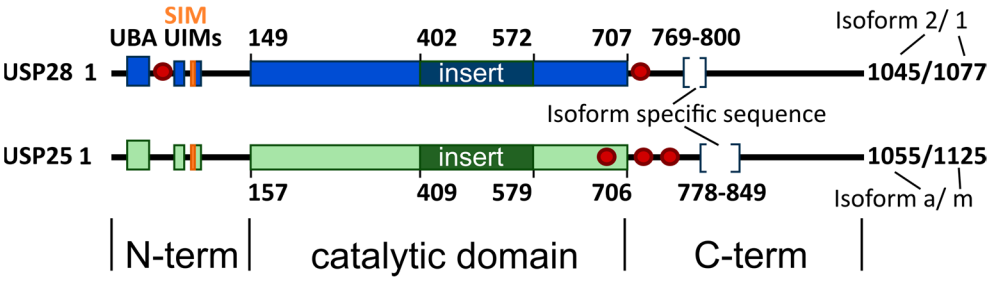

Figure 5: Domain architecture of USP25 and USP28. USP28 (Blue) and USP25 (green) display an identical domain architecture. The insertion sites of the catalytic domains are indicated for USP28 in dark blue and for USP25 in dark green. The UBA, UIM and SIM (orange) are indicated in the N-terminal domains. Phosphorylation sites are shown as red circles and the isoform specific sequences are marked in brackets.

Additional regulation of USP25 was suggested by phosphorylation of T680, T727 and S745 (with the first residue being located within the catalytic domain and the latter two C-terminally to the catalytic domain, Figure 5) through the vaccinia-related kinase 2 (VRK2), leading to an inhibition of activity towards the ubiquitinated subunit CCT4 (chaperonin containing TCP1 subunit 4) of the chaperone TCP-1 ring complex (TRiC) (50). Furthermore, phosphorylation of USP25 by the spleen tyrosine kinase (SYK) led to the downregulation of cellular USP25 protein levels independent of proteasomal degradation, but did not have an effect on the activity of the enzyme (51). Phosphorylation events after ionizing irradiation (IR) treatment, were also found for USP28 (S67, located in the N-terminal domain and S714, located C-terminally to the catalytic domain, Figure 5) and linked to the ATM (Ataxia-telangiectasia mutated) pathway of DNA damage response (DDR) (52). Nevertheless, the function of phosphorylation in USP28 is still unclear but was suggested to have an influence on substrate interaction (53, 54)

I.4.2 Biological functions for USP25 and USP28

The most striking difference between the two related DUBs is their subcellular localization, which also correlates with their distinct biological functions. While USP25 is located in the cytoplasm and associates with the endoplasmatic reticulum (ER), USP28 is mainly present in the nucleus (41, 42, 50, 55-57). The functional roles of both enzymes are introduced in the following paragraphs.

I.4.2.1 The opposing cellular functions of USP28

Due to its mainly nuclear localization, USP28 is highly involved in several pathways of the cell cycle, adopting independent functions in the DDR or mitotic surveillance (Figure 6) (58). In the DDR, for example it was shown to regulate the stability of Chk2 (checkpoint kinase 2) and 53BP1 (tumor suppressor p53 binding protein 1), which are part of the Chk2-p53-PUMA (p53 upregulated modulator of apoptosis) pathway that induces apoptosis after a DNA double strand break (52). On the contrary, USP28 is also counteracting the activity of the SCF (SKP1 (S-phase kinase-associated protein 1)/ CUL1 (Cullin 1)/ F-box protein) E3 ligase APC/C^{Cdh1} (anaphase-promoting complex/ cyclosome (cadherin-1)) on the checkpoint mediator Claspin, thereby supporting the initiation of the checkpoint in the Gap 2 (G2) phase, which leads to an activation of Chk1 and subsequent cell cycle arrest (52, 59, 60). However, an essential role for USP28 in DNA damage response has been refuted by Knobel *et al.*, who could indeed show an association of USP28 with 53BP1 by the tandem BRCT (breast cancer susceptibility gene1 COOH-terminus) domain of 53BP1, but could excluded the necessity of the protease in IR-induced DDR in cells and in mice (54). Nevertheless, USP28 in a complex with 53BP1 was again found to participate in a p53-dependent checkpoint response and was also linked to the regulation of an effective p53-DNA binding (61).

Interestingly, several groups suggested a new signaling pathway, the mitotic surveillance pathway that is activated after centrosome loss or prolonged mitosis and leads to a cell cycle arrest to prevent the growth of defective daughter cells. (58, 62-64). In this new pathway, which was suggested to function independent of DDR signaling, USP28 operates together with 53BP1 to stabilize p53, which subsequently

induces cell cycle arrest by its downstream effector p21 (58, 62-64). Combined, these publications indicate roles for USP28 in cell-cycle regulation that have rather beneficial effects for the cells, implying a tumor suppressor function for the enzyme.

Contrary to this role stands the frequent involvement of USP28 in several types of cancer (Figure 6): It was shown that overexpression of USP28 correlates with the progression of non-small cell lung cancer (NSCLC) and glioblastomas (65-68). The deubiquitination of LSD1 (lysine-specific demethylase 1) by USP28 is connected to breast cancer (56, 69) and the stabilization of the surface adhesion factor CD44 (Cluster of Differentiation 44) by USP28 promotes invasion and metastasis in bladder cancer (70). One of the better-understood functions of USP28 is the stabilization of the oncogenic transcription factor c-MYC (Avian myeloblastosis virus oncogene cellular homolog), which counteracts the SCF E3 ligase FBW7α (F-box/WD repeat-containing protein 7 α) (55). Depletion of USP28 led to reduced cell growth of human breast-, colon- and glioblastoma tumor cell lines due to decreased MYC levels (55). Overexpression of USP28 was also found in human colorectal cancer tissue, correlating with increased c-MYC levels (71). Intriguingly, USP28 is a target gene for c-MYC in intestinal cancers, indicating a positive-feedback loop for cellular MYC levels, to drive tumorigenesis of colorectal cancers (71). Initially it was thought that USP28 is interacting with MYC through FBW7α, which "piggybacks" the DUB (55). However, Diefenbacher *et al.* showed that USP28 can also stabilize c-MYC independently of FBW7 and further substrates of the E3-ligase such as c-JUN and NICD1 (Notch intracellular domain 1) by interacting with the same but unphosphorylated motif, FBW7 usually binds to (72). Interestingly, the stabilizing activity of USP28 on MYC seems to be tissue specific for the intestine and the cerebellum whereas the complete deletion of *Usp28*$^{-/-}$ in pancreas, lung and liver tissue seems to have the opposite effect in mice (73). This could be due to the effect of USP28 on FBW7. The authors observed that USP28 is counteracting the auto-ubiquitination of FBW7 and thus the complete loss of USP28 (*Usp28*$^{-/-}$) supports the degradation of FBW7 in certain tissues such as lung, liver and pancreas but not in the intestine and cerebellum (73). Overall, the dual function of USP28 on FBW7 and MYC, indicates a tight regulation of the enzyme in homeostasis, that is tissue dependently adjusted (74).

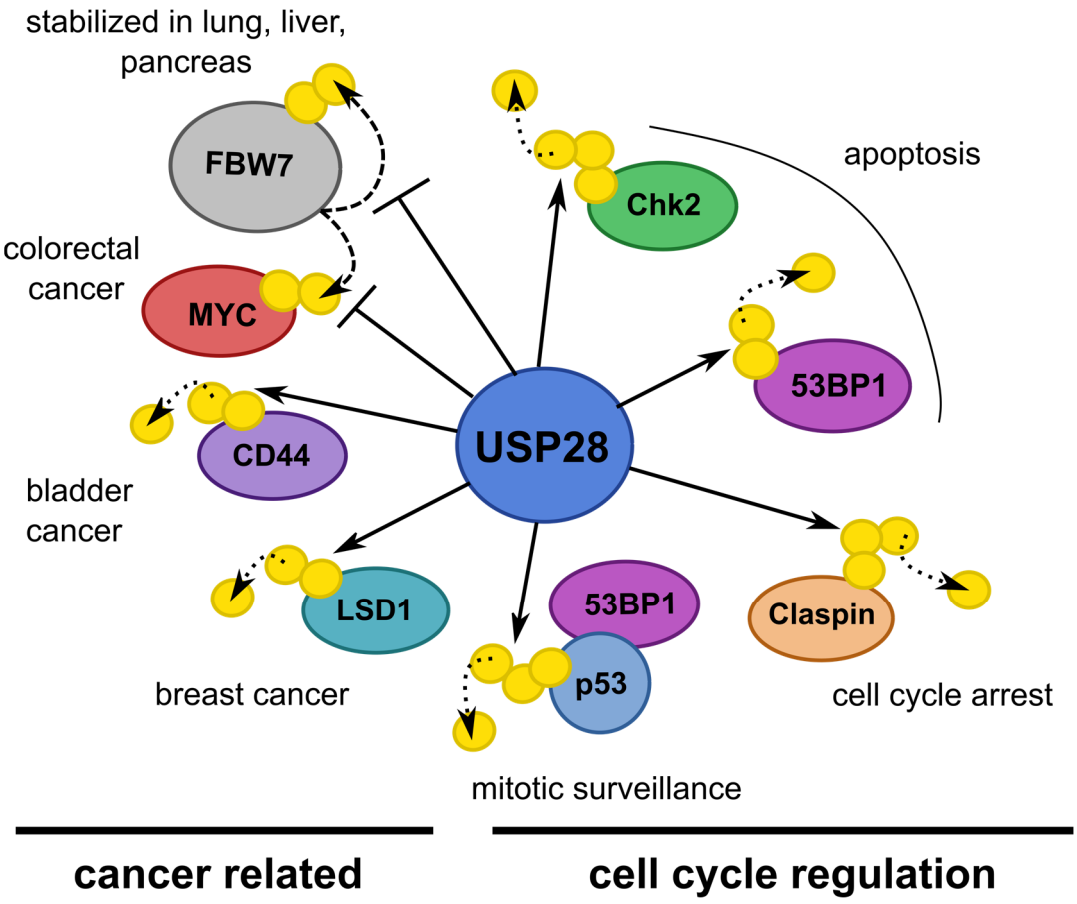

Figure 6: Schematic overview of the cellular functions and substrates of USP28. Ubiquitinated substrates of USP28 are indicated in different colors, with Ub depicted as yellow circle. The stabilization of the substrates by USP28 deubiquitination (dotted arrow, with leaving Ub), promotes/causes different outcomes. On the left side are cancer related substrates of USP28 indicated, on the right side substrates involved in cell cycle regulation. USP28 counteracts the ubiquitinating activity of the E3-ligase FBW7 on MYC and FBW7 itself (dashed arrows) by deubiquitination.

I.4.2.2 USP25 and its occurrence *in vivo*

Like USP28, also USP25 adopts several independent functions (Figure 7). The muscle-specific isoform of USP25m is specifically expressed in differentiated muscle tissue, where it interacts with the MyBPC1 (myosin binding protein C1), ACTA1 (actin alpha 1) and FLNC (filamin C), that are important regulators of muscle differentiation and maintenance (42). The interaction and stabilization by deubiquitination of MyBPC1 is specific to USP25m, whereas ACTA1 stabilization was independent from deubiquitinating activity of USP25m and also pulled down by the ubiquitous isoform of USP25 (42). Moreover, Blount *et al*. identified an association of USP25 with the ER and could show its involvement in the ER-associated degradation (ERAD) pathway, by

stabilizing the ERAD substrates CD3δ (cluster of differentiation 3δ) and the APP (β-amyloid precursor protein) (57). USP25 is thereby counteracting the activity of the E3 ligase HRD1 on CD3δ and rescues it from proteasomal degradation (57). Additionally, USP25 co-immunoprecipitated with both, its opponent HRD1 (HMG-CoA reductase degradation protein 1) and the AAA ATPase (ATPases Associated with various cellular Activities) VCP/p97 (valosin-containing protein), albeit it is still unclear whether the interaction is direct or indirect and what purpose the possible complex assumes (57).

Importantly USP25 is an essential regulatory component in the virus or lipopolysaccharide (LPS)-triggered innate immune response (75-78). Upon recognition of pathogen-associated patterns (PAMPs) several signaling pathways are induced by the innate immune system to promote the production of pro-inflammatory cytokines and type I interferons (IFN), mediating the response to infection (79). USP25 was found to stabilize tumor necrosis factor receptor-associated factor 3 (TRAF3) after LPS toll-like receptor 4 (TLR4) activation, by specifically removing K48-linked poly-Ub chains, thereby contributing to the production of type I IFNs (77). Additionally, USP25 associated with TRAF6 during Interleukin 17 (IL-17) signaling and removed K63-linked chains, thereby negatively regulating the activation of NF-κB (Nuclear Factor κB) triggered induction of pro-inflammatory cytokines (78). During viral infection, it was shown that *Usp25* gene expression is upregulated and that the USP25 protein associates with both TRAF3 and TRAF6. It stabilizes both proteins by the removal of K48- and K63-linked chains, respectively, promoting both pro-inflammatory cytokine and type I IFN production (76). Moreover, *Usp25* transcription is activated by interferon regulatory factor 7 (IRF7) after viral infection induced activation of type I IFN signaling (75). Overall, USP25 seems to be an important controller of the innate immune response, by balancing both, the production of pro-inflammatory cytokines and the activation of type I IFNs.

A more recent publication by Xu *et al.*, suggested an involvement of USP25 in Wnt-signaling by direct interaction and stabilization of tankyrases (TNKS) (80). In an active canonical Wnt-β-catenin signaling pathway, the ligand Wnt binds to the receptor frizzled, which leads to a phosphorylation cascade recruiting disheveled proteins that induce the inactivation of the β-catenin destruction complex. Therefore, β-catenin

accumulates and triggers Wnt-gene transcription, leading to, among other functions, cell proliferation and differentiation (81, 82). In the Wnt off state, the destruction complex phosphorylates β-catenin, which induces its proteasomal degradation. Importantly, the destruction complex, consists of several proteins, including Axin, which is poly-ADP-ribosylated (PARsylated) by the poly-ADP ribosyltransferase TNKS, that leads to its ubiquitination by RNF146 (ring finger protein 146) and subsequent proteasomal degradation (83-85). It has already been shown that the stabilization of Axin by inhibiting TNKS promotes β-catenin destruction and therefore causes a negative Wnt regulation (84). Xu *et al*. showed that USP25 deficiency led to decreased TNKS levels and subsequent stabilization of Axin, suggesting USP25 as a new potential target for the inhibition of aberrant Wnt-signaling in cancer (80).

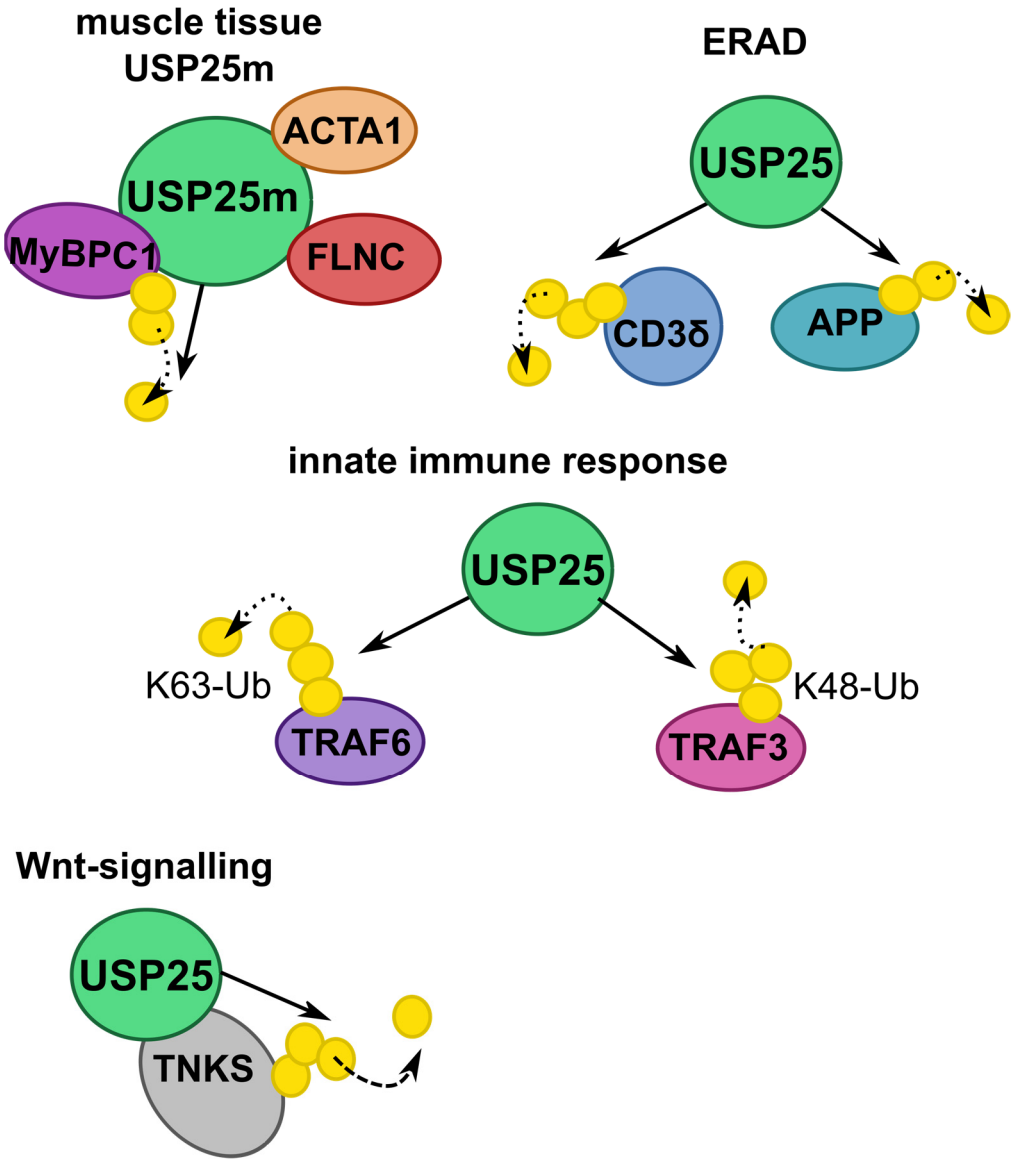

Figure 7: Schematic overview of the biological functions of USP25. USP25 (green) is involved in several pathways. Ubiquitinated substrates of USP25 are indicated in different colors, with Ub depicted as yellow circle. Deubiquitination of the substrates is shown by arrows.

I.5 Targeting structural features of USPs

Together with the other components of the ubiquitin system, deubiquitinases came recently into the focus as promising drug targets, as they are widely distributed throughout the cell and highly involved in the development and progression of human diseases (86, 87). Especially USPs are thought to be potential targets for cancer therapy, as they regulate various cellular processes that often involve the stabilization of oncoproteins, like for example MYC, which is stabilized by USP28 or

the E3-ligase MDM2 (mouse double minute 2 homolog) that negatively regulates the levels of the tumor suppressor p53 and is counteracted and stabilized by USP7 (55, 88-90). Initially small molecule inhibitors have been developed for several USPs often with a major drawback in specificity (91). Due to the upcoming structural knowledge, the inhibitors improved, by targeting individual structural features of the enzymes (92). Crystal structures of USP7 in its *apo* state revealed a distorted catalytic site with a blocked catalytic cleft that rearranges into an active state upon Ub-binding and an activation mechanism by its C-terminal Ub-like domain, due to conformational changes (23, 29, 93). Several recently published specific inhibitors exploited the auto-inhibited state of the USP7 *apo* conformation and targeted either the catalytic cleft or an allosteric site by inhibiting Ub-binding (94-99). This example shows that the structural characterization of the target enzymes is essential to selectively address the features of each DUB individually. As described above, USP25 and USP28 are involved in several important pathways and have been associated to cancer (88). Especially USP28 seems to be a promising anti-cancer target as it drives colorectal and non-small-cell lung cancer (67, 71, 100). An attempt to inhibit USP28, to find small molecule inhibitors for USP28 by a large scale high throughput screening campaign in the absence of structural knowledge, led to bispecific inhibitors against USP25 and USP28 (101, 102). Although USP25 is also arising as a potential drug target, as it was found to positively regulate the Wnt-signaling pathway, the cross reactivity of an USP28 inhibitor could also interfere with USP25s regulation of the innate immune system, thus leading to undesirable side effects (76, 80). Vice versa, this is also true for targeting USP25, which could have negative effects on cell cycle regulation, in which USP28 is involved (58). Therefore a different approach could be, to target substrate interactions of the two USPs, instead of inhibiting the active site, to specifically interfere with tumor-promoting pathways.

I.6 Aim of this thesis

Initially, the goal of this project was the structural and functional characterization of USP28, to determine specific features that could be exploited for a following structure-based drug design approach. The high sequence similarity of USP28 and USP25 necessitated also the characterization of the latter, which led to the joint work on both enzymes together with Dr. Florian Sauer and aimed to determine the individual characteristics of USP25 and USP28. A subsequent biochemical and biophysical analysis of both enzymes was pursued to identify the similarities and differences and the biological relevance of the distinct findings, which could be used in future studies to specifically target either enzyme for tumor therapy.

II. Materials and Methods

II.1 Material

II.1.1 Chemicals, reagents and media

The following list contains the chemicals used in this thesis, excluding the chemicals that were used for the preparation of the crystallization screens (Table II-11). All buffers and solutions were prepared with ultrapure water generated by the TKA GenPure system.

Table II-1: Chemicals, reagents and media

Substance	Supplier
2-Propanol	Carl Roth
4-(2-hydroxyethyl)-1-piperazineethanesulfonic acid (HEPES)	Carl Roth
Acetic acid	Carl Roth
Acrylamide/Bis-acrylamide (37.5:1)	Carl Roth
Adenosine-5'-triphosphate disodium salt (ATP)	Sigma-Aldrich
Agar	Carl Roth
Agarose NEEO ultra quality	Carl Roth
Ammonium acetate	Sigma-Aldrich
Ammonium chloride (NH_4Cl)	Sigma-Aldrich
Ammonium persulfate (APS)	Carl Roth
Ammonium sulfate	Sigma-Aldrich
Ampicillin (Amp) sodium salt	Carl Roth
Bis-Tris	Sigma-Aldrich
Bovine serum albumin (BSA)	Sigma-Aldrich
Bromphenol blue sodium salt	Carl Roth
Calcium chloride dihydrate ($CaCl_2$)	Carl Roth
Chloramphenicol (Cam)	Carl Roth
Citric acid	Sigma-Aldrich
cOmplete™, EDTA-free Protease Inhibitor Cocktail	Sigma-Aldrich (Roche)
Coomassie Brilliant Blue G-250	Carl Roth
D-(+)- Biotin	Carl Roth
D-Glucose	Carl Roth
Dimethyl sulfoxide (DMSO)	Carl Roth
Dipotassium hydrogen phosphate (K_2HPO_4)	Sigma-Aldrich

Disodium hydrogen phosphate (Na_2HPO_4)	Carl Roth
Dithiothreitol (DTT)	Carl Roth
Ethanol	Carl Roth
Ethylenediaminetetraacetic acid (EDTA)	Carl Roth
Fluorescein (FAM)-maleimide, 6-Isomer (6-FAM)	Lumiprobe
Glycerol	Carl Roth
Glycine	Carl Roth
Hydrochloric acid (HCl)	Carl Roth
Imidazole	Carl Roth
Iron(II) sulfate heptahydrate ($Fe(II)SO_4$)	Carl Roth
Isopropyl-β-D-thiogalactopyranoside (IPTG)	Carl Roth
Kanamycin sulfate (Kan)	Carl Roth
L- Isoleucine (Ile/I)	Fluka/ Sigma-Aldrich
L-Leucine (Leu/L)	Carl Roth
L-Lysine (Lys/K)	Fluka/ Sigma-Aldrich
L-Phenylalanine (Phe/F)	Fluka/ Sigma-Aldrich
L-Threonine (Thr/T)	Fluka/ Sigma-Aldrich
L-Valine (Val/V)	Fluka/ Sigma-Aldrich
Lysogeny broth (LB) medium	Carl Roth
Magnesium chloride ($MgCl_2$) hexahydrate	Carl Roth
Magnesium sulfate ($MgSO_4$)	Sigma-Aldrich
Orange G	Sigma-Aldrich
Perchloric acid	Sigma-Aldrich
Polyethylen glycol 3350 (PEG3350)	Sigma-Aldrich
Polyethylen glycol 400 (PEG400)	Sigma-Aldrich
Polyethylen glycol 4000 (PEG4000)	Sigma-Aldrich
Potassium dihydrogen phosphate (KH_2PO_4)	Carl Roth
Propargylamine (PA)	Sigma-Aldrich
Seleno methionine (SeMet)	Acros Organics
Sodium 2-mercaptoethanesulfonate (MESNa)	Sigma-Aldrich
Sodium acetate	Carl Roth
Sodium chloride (NaCl)	Carl Roth
Sodium dihydrogen phosphate (NaH_2PO_4)	Carl Roth
Sodium dodecyl sulfate (SDS)	Carl Roth
Sodium hydroxide (NaOH)	Carl Roth

Streptomycin sulfate (Strep)	Carl Roth
Strontiumchloride Hexahydrate ($SrCl_2$)	Sigma-Aldrich
Terrific Broth (TB) medium	Carl Roth
Tetramethylethylenediamin (TEMED)	Carl Roth
Tris-(2-carboxyethyl)-phosphine (TCEP)	Carl Roth
Tris-(hydroxymethyl)-aminomethan (Tris)	Carl Roth
Ubiquitin-Rhodamine110Gly (UbRh110)	UbiQ Bio
β-Mercaptoethanol	AppliChem

II.1.2 Consumables and instruments

The list of consumables excludes general glass and plastic bottles and containers.

Table II-2: Consumables

Type	Model	Supplier
24-well crystallization plates	Crystalgen SuperClear™ Plate	Jena Bioscience
384-well Microplate	Black bottom, non-binding	Greiner Bio-One
96-well crystallization plates	Crystalquick™ 1 square well, flat bottom, low profile	Greiner Bio-One
Centrifugal concentrator	Amicon® Ultra-0.5, 4 and 15 mL	Merck Millipore
Centrifuge tube	Cellstar® centrifuge tube – 15 and 50ml	Greiner Bio-One
Cover slides	Circular, Siliconised, 22mm	Jena Bioscience
Cuvettes	Rotilabo® -single-use	Carl Roth
Dialysis membranes	Spectra/Por®	Spectrum Laboratories
Filter paper		Sartorius
Gloves	Nitril gloves	Star Lab
Optical quality sealing foil	VIEWseal™	Greiner Bio-One
Polymerase chain reaction (PCR) tubes	Multiply®-Pro cup 0.2ml, Multiply®-µStrip 0.2ml chain, 8-Lid chain, flat	Sarstedt
Pierce™ Silver Stain Kit		Thermo Scientific™
Pipette tips	Pipette tips – 10, 200, 1000 ml	Mettler-Toledo
Precast SDS-Gels	Mini-PROTEAN TGX 4-20% Gels	Bio-Rad Laboratories

Reaction tubes	SafeSeal tube – 0.5, 1.5 clear and brown, 2 ml	Sarstedt
Sterile filter	Acrodisc® sterile filter for syringe – 0.22 and 0.45 µm	Pall
Syringes	Omnifix® syringes – 1,5,10 and 20 ml	B. Braun

Table II-3: Instruments

Type	**Model**	**Supplier**
Agarose gel electrophoresis system	Mini-Sub® Cell GT System	Bio-Rad Laboratories
Analytical Ultracentrifuge (AUC)	Optima XL-1	Beckman Coulter
AUC sample cell	double-sector Epon Charcoal-Filled Centerpiece, Sapphire windows	Beckmann Coulter
AUC-Rotor	An-50 Ti	Beckman Coulter
Autoclave	Systec V-150	Systec
Balance	XS 6002S Dual Range	Mettler Toledo
Balance, analytical	XS 105 Dual Range	Mettler Toledo
Block thermstat	Rotilabo® block thermostat H 250	Carl Roth
CD cuvette	Cylindrical absorption cuvette, path length 1 mm	Hellma Analytics
Cell disruption system	M-110P	Microfluidics
Centrifuges	5417 R 5424 5804 R 5430 R	Eppendorf
Centrifuges	Avanti J-26 XP Avanti J-HC	Beckmann Coulter
Circular dichroism (CD) spectropolarimeter	J-810	JASCO
Crystallographic handling tool	CrystalWand™ Magnetic	Hampton Research
Crystallographic loops	CryoLoop™	Hampton Research
Crystallographic loops	LithoLoops	MiTeGen/ Molecular Dimensions
Crystallographic sample holder	CrystalCap™ Magnetic	Hampton Research

Crystallographic sample vial	CryoVial	Hampton Research
Crystallographic storage pucks	SPINE Puck	Jena Bioscience
Electrophoresis	Mini-PROTEAN Tetra Cell	Bio-Rad Laboratories
Electrophoresis power supply	PowerPac™ Basic	Bio-Rad Laboratories
FPLC systems (Protein purification)	ÄKTA™ pure 25 ÄKTA™ avant 25 ÄKTA™ purifier 10	GE Healthcare
Gel-drying device	GelAir Gel Dryer	Bio-Rad Laboratories
Imaging System	Odyssey	LI-COR Biosciences
Imaging System	ChemiDoc™ MP Imaging System	Bio-Rad Laboratories
Incubator	B15 Compact Incubator	Heraeus
Liquid handling robot	Honeybee 963	Digilab
Liquid handling robot	LISSY 2002	Zinsser Analytic
Magnetic stirrer	MR 3002	Heidolph Instruments
MALS detector	DAWN® 8 + HELEOS® II	Wyatt Technology
Microplate reader	CLARIOstar®	BMG LABTECH
Microscope camera	AxioCam MRc	ZEISS
Microscope light source	KL 2500 LCD	ZEISS
Microscope light source	CL 1500 Eco	ZEISS
Microscopes	SteREO Discovery.V12, STEMI 2000-c	ZEISS
PCR-cycler	Mastercycler® EPgradient S Mastercycler® pro S	Eppendorf
pH meter	BlueLine 14pH	SCHOTT
Pipette (Multichannel)	Pipet-Lite Multi Pipette L8-20XLS+	Mettler-Toledo
Pipettes	XLS+ LTS PIPET 0.1-2UL XLS+ LTS PIPET 0.5-10UL XLS+ LTS PIPET 2-20UL XLS+ LTS PIPET 20-200UL XLS+ LTS PIPET 100-1000UL	Mettler-Toledo
Refractometer	Optilab T-rEX	Wyatt Technology
Rotors	JLA 16.250 JA-25.50 JS-5.0 JLA-8.100	Beckman Coulter

Sealing robot	RoboSeal	HJ-BIOANALYTIC
Shaking incubators	ISF-1-W ISF-1-X LT-X	Kühner
Spectrophotometer	BioPhotometer	Eppendorf
Spectrophotometer	NanoDrop ND 1000	Peqlab
Thermomixer	Thermomix comfort	Eppendorf
Ultra pure water system	TKA GenPure	Thermo Fisher Scientific
UV imaging system	Gel Doc™ XR System	Bio-Rad Laboratories
Vortex mixer	Vortex-Genie 2	Scientific Industries

II.1.3 Chromatography columns and resin

Table II-4: Chromatography columns and resins

Type	**Model**	**Supplier**
Affinity matrix for intein-chitin isolation	Chitin Resin	New England Biolabs
Analytical SEC FPLC column	Superdex™ 200 10/300 GL (SD 200 10/300)	GE Healthcare
Analytical SEC FPLC column	Superdex™ 75 10/300 GL (SD75 10/300)	GE Healthcare
Column body	Econo-Column®	Bio-Rad Laboratories
Immobilized metal-ion affinity chromatography resin	Protino® Ni-IDA	MACHEREY-NAGEL
Ion exchange columns	MonoQ® 5/50 GL Resource Q, 1ml Resource S, 1ml HiTrap® SP HP 5ml (SPHP)	GE Healthcare
Preparative SEC FPLC column	HiLoad™ 16/600 Superdex™ 200 pg (SD 200 16/600)	GE Healthcare
Preparative SEC FPLC column	HiLoad™ 16/600 Superdex™ 75 pg (SD75 16/600)	GE Healthcare

II.1.4 Cloning material, enzymes and recombinant proteins

Table II-5: Material for cloning

Designation	Supplier
2'-Deoxyadenosine 5'-triphosphate (dATP), sodium salt solution	Thermo Fisher Scientific
2'-Deoxycytidine 5'-triphosphate (dCTP), sodium salt solution	Jena Biosciences
2'-Deoxyguanosine 5'-triphosphate (dGTP), sodium salt solution	Thermo Fisher Scientific
2'-Deoxythymidine 5'-triphosphate (dTTP), sodium salt solution	Thermo Fisher Scientific
BSA	New England Biolabs
Dpn I	New England Biolabs
GeneRuler™ 1 kb DNA Ladder	Thermo Fisher Scientific
HF buffer (PCR)	New England Biolabs
Midori green Advance DNA stain	Biozym Scientific
NEBuffer™ 2 (Cloning)	New England Biolabs
Nucleospin Gel and PRC cleanup kit	Macherey-Nagel
Nucleospin Plasmid kit	Macherey-Nagel
Phusion® high fidelity DNA Polymerase	Thermo Fisher Scientific
Standard Taq Reaction Buffer	New England Biolabs
T4 DNA Polymerase	New England Biolabs
Taq DNA Polymerase	New England Biolabs

Table II-6: Enzymes for protein purification, recombinant proteins and protein ladder

Name	Supplier
DNaseI	AppliChem
HRV-14, 3C protease	In-house production
Human, Ubiquitin-like modifier-activating enzyme 1 (UBA1)	Kindly provided by Mark Löbel (Schindelin group), Rudolf Virchow Zentrum (RVZ), Würzburg
Lysozyme	Carl Roth
PageRuler™ Prestained Protein Ladder	Thermo Fisher Scientific

Yeast, Ubiquitin-conjugating enzyme E2 13 (Ubc13)	Kindly provided by Monika Kuhn (Schindelin group), RVZ, Würzburg
Yeast, Ubiquitin-conjugating enzyme E2-34 kDa (Cdc34, UBC3)	Kindly provided by Monika Kuhn (Schindelin group), RVZ, Würzburg
Yeast, Ubiquitin-conjugating enzyme variant MMS2 (Mms2)	Kindly provided by Monika Kuhn (Schindelin group), RVZ, Würzburg

II.1.5 Bacterial strains and plasmids

Table II-7: Bacterial strains

Organism	Strain	Usage	Supplier
Escherichia coli (E. coli)	DH5α	Cloning, plasmid amplification	Invitrogen
E. coli	BL21star (DE3) pRARE2	Protein expression	Invitrogen (BL21star) Novagen (pRARE2 plasmid from Rosetta2)
E. coli	Rosetta2 (DE3)	Protein expression	Novagen

Table II-8: Plasmids

Vector	Host	Setup	Resistance	Supplier
pCDF-14	Bacterial	6x His-[3C]-POI	Strep	Florian Sauer, RVZ Würzburg
pCDF-22	Bacterial	Thioredoxin (trx)-6x His-[3C]-POI	Strep	Florian Sauer, RVZ Würzburg
pColA-22	Bacterial	Trx-6x His-[3C]-POI	Kan	Florian Sauer, RVZ Würzburg
pET-30a	Bacterial	NdeI-POI-HindIII	Kan	Mohit Misra, RVZ Würzburg
pETM-14	Bacterial	6xHis-POI	Kan	EMBL, Hamburg
pTXB1	Bacterial	POI-Intein-CBD	Amp	D. Komander, WEHI, Melbourne

Abbreviations: POI: protein of interest, Trx: Thioredoxin , CBD: chitin binding domain, EMBL: European Molecular Biology Laboratory, WEHI: Walter and Eliza Hall Institute of Medical Research

II.1.6 Oligonucleotides

All listed primers were ordered form Sigma-Aldrich®. Primer for the generation of eukaryotic expression constructs were generated by our collaboration partners Ravi B. Kollampally and Prof. Dr. Nikita Popov and are not included in the following table. Abbreviations are given in the last row of the table.

Table II-9: List of primers used for generation of bacterial expression constructs.

Name	Sequence (5'- 3')
USP28-3C-1 fw	CTGGAAGTTCTGTTCCAGGGGCCCATGACTGCGGAGCTGCAGCAGGACG
USP28 3C-114 fw	CTGGAAGTTCTGTTCCAGGGGCCCAAAATTCAAGCTGATGGAAGAGATC
USP28 730 rv	CGACGGAGCTCGAATTCGGATCCGGTTACCCATGAGAAGAGGCTACTGAAGG
USP28 1045-Stop BamHI rv	GGGAGTTTCAACTGTGACAGTGAAATAACCGGATCCGAATTCGAGCTCCGTCG
USP28 665-Stop BamHI rv	CGACGGAGCTCGAATTCGGATCCGGTTAATCTGATTCAGTTGGGGCTGCCTC
USP25 3C-415 fw	CTGGAAGTTCTGTTCCAGGGGCCCAAGAGGGAAGAGATCAAGAGACTG
USP25 583-Stop BamHI rv	CGACGGAGCTCGAATTCGGATCCGGTTAGTCAGAGTACATTAATTCAATTGTTCG
USP28 3C-724 fw	CTGGAAGTTCTGTTCCAGGGGCCCTCAGTAGCCTCTTCTCATGG
USP28 724 fw	TCAGTAGCCTCTTCTCATGG
USP28 425-GS rv	GCTGCCTTTTTGCTGCAGAATTTT
USP28 SG-560 fw	AGCGGCAAGACTTGTATTGCAAGT
USP28 425-GSSG-560 fw	CAAAAAGGCAGCAGCGGCAAGACT
SKP1 3C-1 fw	CTGGAAGTTCTGTTCCAGGGGCCCATGCCTTCAATTAAGTTGCAG
SKP1 163-Stop BamH1 rv	CGACGGAGCTCGAATTCGGATCCGGTTACTTCTCTTCACACCA
FBW7 3C-263 fw	CTGGAAGTTCTGTTCCAGGGGCCCACACAAGTAAAACATATGATGCAAG
FBW7 707 Stop BamHI rv	CGACGGAGCTCGAATTCGGATCCGGTTATTTCATGTCCACATCAAAGTCCAGCACC
FBW7 3C 247 fw	CTGGAAGTTCTGTTCCAGGGGCCCCCAGAGAAATTGCTTGCTTTAGAT
USP28 3C 754 rv	CTCTTCTCATAGGCACGGGCGGGCCCCTGGAACAGAACTTCCAG
USP28 754 fw	GCCCGTGCCTATGAGAAGAGCGGTGTAGAA

Chimera primer USP28 528 fw	CCAGCTCCACGAACAGTCACAG
Chimera primer USP28-457-USP25-465 fw	GAATTTGCTAGTACAAAACCTGCCTGCACTTCTCCTGTTGACGATATTG
Chimera primer USP25-534-USP28-528 rv	CTGTGACTGTTCGTGGAGCTGGATGCATGGGCAAATCTGGAGGTATC
Chimera primer USP25 434 rv	TTCTAGCCTTTGTTGTAATACCGTG
Chimera primer USP25 563 fw	ACCAGAGATTTGCAGGAAAGCATATC
Chimera primer USP28 427 rv	TTCCAATTTTTGCTGCAGAATTTTTAT
Chimera primer USP28 556 fw	ATACAAGATTTAAAGACTTGTATTGC
Chimer primer USP25 434-USP28 428 fw	CGGTATTACAACAAAGGCTAGAAAGGTATGTGAAATATGGCTCAG
Chimera primer USP28 555-USP25 563 rv	GATATGCTTTCCTGCAAATCTCTGGTATCTTGTTCAATCTCACTCCTCC
Chimera primer USP28 427-USP25-435 fw	ATAAAAATTCTGCAGCAAAAATTGGAAAGATATTTAAGCTATGGTTCCGGTCC
Chimera primer USP25 563-USP28-556 rv	GCAATACAAGTCTTTAAATCTTGTATGTCATTTTCTATTTCTGTCCTCCAGCG
3C fw	CTGGAAGTTCTGTTCCAGGGGCCC
3C rv	GGGCCCCTGGAACAGAACTTCCAG
BamHI rv	CGACGGAGCTCGAATTCGGATCCGG
TNKS-ANK 3C-171 fw	CTGGAAGTTCTGTTCCAGGGGCCCGGGACTGGGGTCCCAGCAGTGAG
TNKS-ANK 957-Stop-BamHI rv	CGACGGAGCTCGAATTCGGATCCGGTTAGGGCATGGCATCTATCAGCAAAGC
Ub G76W-Stop fw	ATCTGGTCTTAAGACTGCGTGGCTGGTAAATCACGGGAGATGCACTAGTTGC
Ub G76W-Stop rv	GCAACTAGTGCATCTCCCGTGATTTACCAGCCACGCAGTCTTAAGACCAGAT
Ub K48R fw	CAGAGGTTGATCTTTGCCGGAAGACAGCTGGAAGATG
Ub K48R rv	CATCTTCCAGCTGTCTTCCGGCAAAGATCAACCTCTG
Ub S20C fw	CCCTCGAGGTGGAGCCCTGTGACACCATCGAG
Ub S20C rv	CTCGATGGTGTCACAGGGCTCCACCTCGAGG

USP25 Δtip fw	GAATTTGCCTCAAGTAAACCTGTTGGCTCTGGTGGTAGGCACATAACGGAGGAAGAAC
USP25 Δtip rv	GTTCTTCCTCCGTTATGTGCCTACCACCAGAGCCAACAGGTTTACTTGAGGCAAATTC
USP25 1055-Stop-BamHI rv	CGACGGAGCTCGAATTCGGATCCGGTTATCTTCCATCAGCAGGAGTTCG
USP25 3C-157 fw	CTGGAAGTTCTGTTCCAGGGGCCCAACCCTTATGATAGAAAAAGACAGG
USP25 3C-765 fw	CTGGAAGTTCTGTTCCAGGGGCCCTCACATGAGCATGAAGATAAAAGTCCTGAAAC
USP25 538-SGG fw	GGTAGGCACATAACGGAGGAAGAAC
USP25 706-Stop-BamHI rv	CGACGGAGCTCGAATTCGGATCCGGTTATTGTGCATCCCATTCTTCTAGTTC
USP25 C178S fw	AATGTTGGCAATACTTCTTGGTTTAGTGCT
USP25 C178S rv	AGCACTAAACCAAGAAGTATTGCCAACATT
USP25 E600A fw	GCCGTTTTAGTTCACGCAGGCCAAGCTAATGCTG
USP25 E600A rv	CAGCATTAGCTTGGCCTGCGTGAACTAAAACGGC
USP25 E600D fw	GCCGTTTTAGTTCACGACGGCCAAGCTAATGCTG
USP25 E600D rv	CAGCATTAGCTTGGCCGTCGTGAACTAAAACGGC
USP25 E600N fw	TACATGCCGTTTTAGTTCACAATGGCCAAGCTAATGCTGGGCAC
USP25 E600N rv	GTGCCCAGCATTAGCTTGGCCATTGTGAACTAAAACGGCATGTA
USP25 F458E fw	GTATGCATTGGAAGAAGCCTCAAGTAAAC
USP25 F458E rv	GTTTACTTGAGGCTTCTTCCAATGCATAC
USP25 L552E fw	CTGGAAAGTTGTGAACATCGCTGGAG
USP25 L552E rv	CTCCAGCGATGTTCACAACTTTCCAG
USP25 P535L fw	CCTCCAGATTTGCCCATGCATCTGGCACCAAGGCACATAACGGAG
USP25 P535L rv	CTCCGTTATGTGCCTTGGTGCCAGATGCATGGGCAAATCTGGAGG
USP25 P535S fw	CCTCCAGATTTGCCCATGCATTCTGCACCAAGGCACATAACGGAG
USP25 P535S rv	CTCCGTTATGTGCCTTGGTGCAGAATGCATGGGCAAATCTGGAGG
USP25 R385Q fw	CAGGCATTGGGACAACCAGAAAAAATTCACAAC
USP25 R385Q fw	GTTGTGAATTTTTTCTGGTTGTCCCAATGCCTG
USP25-464-G rv	GCCAACAGGTTTACTTGAGGCAAATTC
USP28 Δtip fw	AAAACCTGCCTCAAGCGGAAGCGGAGCTCCACGAACA
USP28 Δtip rv	TGTTCGTGGAGCTCCGCTTCCGCTTGAGGCAGGTTTT

USP28 3C-149 fw	CTGGAAGTTCTGTTCCAGGGGCCCAATCCCAATGACTGGAGGA GAGTTG
USP28 458 rv	TGAGGCAGGTTTTGTACTAGCA
USP28 529 fw	GCTCCACGAACAGTCACAGAT
USP28 707-Stop-BamHI rv	CGACGGAGCTCGAATTCGGATCCGGTTACTCCATTTGAGGGATT TTGCAAGACTGCTC
USP28 E593D fw	CAGTTCTTGTTCATGATGGACAAGCAAATG
USP28 E593D rv	CATTTGCTTGTCCATCATGAACAAGAACTG
USP28 L545E fw	GTTAAGACCTGTGAACAGAGATGGAGGAG
USP28 L545E rv	CTCCTCCATCTCTGTTCACAGGTCTTAAC
USP28 Q378R fw	GTTTAATCAGTCCCTTGGGCGGCCAGAGAAAATTCACAATA
USP28 Q378R rv	TATTGTGAATTTTCTCTGGCCGCCCAAGGGACTGATTAAAC
Abbreviations: forward primer (fw), reverse primer (rv)	

Table II-10: Oligonucleotides for real-time quantitative PCR. Generated by our collaboration partners Ravi B. Kollampally and Prof. Dr. Nikita Popov.

qRT-PCR TNKS1 fw	CCACAACCATCACAATGAGC
qRT-PCR TNKS1 rv	CTGTTCCTCCTCCAATTCCA
qRT-PCR TNKS2 fw	ATGGGCTTTCACACCGTTAC
qRT-PCR TNKS2 rv	TAGCACGTAGGCAGAGCAGA
qRT-PCR β2- macroglobulin fw	AGCCGAACATACTGAACTGCTACG
qRT-PCR β2- macroglobulin rv	CGGCCATACTGTCATGCTTAACTC
Abbreviations: quantitative real-time-PCR (qRT-PCR)	

II.1.7 Crystallization screens

Table II-11: Crystallization screens. All the screens were prepared by Nicole Bader (group of Prof. Dr. Schindelin, RVZ Würzburg) using the liquid handling robot LISSY 2002, in-house.

Name	**Supplier of original formulation**
$AmSO_4$ Suite	Qiagen
Crystal Screen™ 1+2	Hampton Research
Index	Hampton Research
JCSG+	Molecular Dimensions
MbClass II Suite	Qiagen
Nextal pH Clear	Qiagen

Nextal pH Clear II	Qiagen
Nextal-PEG Suite	Qiagen
Nextal-PEG Suite II	Qiagen
Nucleix Suite	Qiagen
Opti-Salts Suite	Qiagen
Protein Complex Suite	Qiagen
TOPAZ™ OptiMix™ 3	Fluidigm
TOPAZ™ OptiMix™ PEG	Fluidigm
Wizard 1+2	Emerald BioSystems
Wizard 3+4	Emerald BioSystems

II.1.8 Software, server, databases and deposited data

Table II-12: Software, server and databases

Name	Usage	Source
AIMLESS	Scaling of diffraction data	Evans and Murshudov,2013 (103)
APBS	Electrostatic surface potential calculation	Baker *et al*., 2001 (104)
ASTRA® VI	SEC-MALS analysis	Wyatt Technology
autoBuster	Parameter refinement	Blanc *et al*., 2004 (105)
AxioVision	Microscopy imaging software	ZEISS
Buccaneer	Chain tracing	Cowtan, 2006 (106)
CCP4	Software for X-ray structure determination	Winn *et al*., 2011 (107)
Cleario 1.2.0	Row to column transformation of the CLARIOstar data	Wolfgang Kölmel, RVZ Würzburg
COOT	Manual refinement	Emsley *et al.*, 2010 (108)
CRANK2	experimental phasing	Skubàk and Pannu, 2013 (109)
DALI	Protein structure comparison	Holm and Laakso 2016 (110)
ESPript 3.0	Depiction of sequence similarity after sequence alignment by T.Coffee	Robert and Gouet, 2014 http://espript.ibcp.fr
ExPASy ProtParam	protein parameters	Gasteiger, *et al*., 2005 (111)
GENtle 1.9.4 free software	DNA, Protein sequence handling generation of primers	Magnus Manske, University Cologne

GraphPad Prism 8.0.0	Activity assay data analysis	GraphPad
Image Lab™ 6.0.1	SDS-PAGE image analysis	Bio-Rad Laboratories
Inkscape 0.92	Preparation of all figures	www.inkscape.org, free open source software
MARS data analysis software	Activity assay data analysis	BMG Labtech
Microsoft Office 365 ProPlus Excel, Word	Activity assay data analysis Word processing	Microsoft Office
ODYSSEY	Imaging software	LI-COR
Origin	Data analysis software	OriginLab
PARROT	Density modification	Cowtan, 2010 (112)
PDB2PQR	PQR generation (for APBS)	Dolinsky *et al*., 2004 (113)
PDBeFold	Protein structure comparison	Krissinel and Henrick, 2004 (114)
PDBePisa	Calculation of protein-protein interfaces	Krissinel and Henrick, 2007 (115)
PHASER	Molecular replacement	McCoy *et al*., 2007 (116)
PHENIX refine	Parameter refinement	Adams *et al*., 2010 (117)
Protein Data Bank (PDB)	Protein structures	rcsb.org, (118)
PubMed (NCBI)	Literature research	ncbi.nlm.nih.gov/pubmed/
PyMOL	3D visualization and graphical depiction of structures	Schrödinger (119)
RaptorX	Protein structure prediction	Källberg *et al*., 2012 (120)
REFMAC	phasing	Murshudov *et al*., 2011 (121)
STARANISO server	Anisotropy correction	Tickle *et al*., 2019 (122)
T-Coffee server	Multiple sequence alignment	Notredame *et al*., 2000 (123)
UNICORN	Aekta control and data analysis	GE Healthcare
UniProt	Information about proteins	uniprot.org, (124)
XDS	X-ray data integration	Kabsch, 2010 (125)

Table II-13: PDB codes of deposited Structures

Name	**Supplier**
Crystal structure of USP25 C-terminal domain	PDB: 6H4K
Crystal structure of USP25cat	PDB: 6H4J
Crystal structure of USP28cat E593D bound to UbPA	PDB: 6H4H
Crystal structure USP28cat *apo* SeMet	PDB: 6H4L

II.2 Methods

The majority of the methods described in this thesis can also be found in the StarMethods section of Sauer and Klemm *et al*. (126). This methods part is complemented with further details and additional method information.

II.2.1 Molecular biology

II.2.1.1 Agarose gel electrophoresis

Agarose gel electrophoresis was used to analyze PCR reactions. 1 % agarose was cooked in TAE buffer and poured (~50 ml) into a gel-caster including 5 µl MidoriGreen DNA stain. The solid gel was transferred to the electrophoresis chamber, flooded with TAE buffer and loaded with 5 µl of the PCR reaction premixed with 5 µl loading dye. A DNA 1 kb standard marker (5 µl) was additionally used to determine the sizes of the PCR products. Electrophoresis was performed at 120 V for 30-40 min at room temperature. The gel was subsequently analyzed on an UV imaging system.

Table II-14: Buffers for Agarose gel electrophoresis

Name	composition
TAE buffer	40 mM Tris/HCl pH 8.0, 20 mM acetic acid, 1 mM EDTA
DNA loading dye	10 mM Tris/HCl pH 7.6, 0.15 % Orange G, 60 % Glycerol, 60 mM EDTA

II.2.1.2 Cloning strategies and plasmid isolation

All the expression constructs for USP28, USP25, TNKS-ANK, FBW7 and SKP1 were cloned into pETM-14, pCDF-14/22 or pColA-22 using the sequence and ligation independent cloning (SLIC) method (127) (list of expression constructs, see appendix Table VI-2). The vectors pCDF-14/22 and pColA-22 comprise the plasmid backbone with the resistance cassette of either pCDF or pColA vectors but have been modified to include the multiple cloning site of either pETM-14 with an N-terminal 6xHis-3C (pETM14, pCDF-14) or pETM-22 with an N-terminal trx-6xHis-3C (pCDF-22, pColA-22) tag, respectively. The initial cloning inserts of the proteins of interest were amplified from cDNA (USP25, USP28, TNKS) or available pcDNA3 vectors (FBW7, SKP1)

(provided by Nikita Popov, Tübingen) using overhang primers that overlap with the 3C-cleavage site and the BamHI- cloning site of the vectors. Expression plasmids were linearized separately using overlapping sequences (see Table II-15 and Figure 8). After *DpnI* digestion of the template DNA at 37°C for 1 h and PCR clean up with the NucleoSpin Gel and PCR Clean-up kit, single stranded overhangs were generated using the 3'-5' exonuclease activity of the T4 DNA polymerase (Table II-15). Vector and insert (ratio of 1:4, respectively) were then annealed on a thermocycler (for 5 min at 75°C, ~15 min cooling down to 20°C) and subsequently transformed (10 µl) into *E. coli* DH5α cells using a standard heat shock protocol. The transformation was then spread on an LB agar plate containing the corresponding antibiotic and the plate was incubated overnight at 37 °C. Clones were tested for the correct size of the insert, by colony PCR (Table II-15 and Figure 8) and subsequent agarose gel electrophoresis (see II.2.1). One to three clones containing the correct length of the insert, were picked and grown in 10 ml LB medium supplemented with the according antibiotics for plasmid amplification and isolation using the NucleoSpin® Plasmid kit. After cloning and plasmid isolation, all constructs were sent for sequencing (Microsynth Seqlab or Eurofins Genomics), to verify the correctness of the insert sequence.

Mutations were introduced either by site directed mutagenesis or the previously described SLIC method (Table II-15 and Figure 8). For site directed mutagenesis, the same PCR setup as for SLIC cloning was used, with primers at a concentration of 200 nM. The PCR reaction was directly transformed after PCR cleanup into DH5α cells and the inserted mutation was verified by sequencing.

The ubiquitin double mutation K48R/S20C was cloned into the wild type (wt) Ub pET-30a vector (generously provided by Mohit Misra) and the G76W mutation was inserted by cloning a C-terminal Trp-stop codon behind the Ub residue G75 of the pTXB1 construct (provided by David Komander, WEHI Melbourne).

Table II-15: Setups for SLIC and Site directed Mutagenesis

SLIC-PCR setup		SLIC- T4 digestion setup		Colony PCR	
fw primer	1 µM	vector/ insert D*NA*	1 µg	T7/3C fw primer	1 µM
rv primer	1 µM	T4 DNA polymerase	4.5 U	T7-term rv primer	1 µM
dNTPs	200 µM	NEBuffer 2	1x	dNTPs	200 µM
Phusion® polymerase	1 U	BSA	1x	Taq DNA polymerase	2.5 U
HF buffer	1x	ultrapure H_2O	add to 50 µl	Standard Taq buffer	1x
template DNA	~100 ng			template DNA	colony
ultrapure H_2O	add to 50 µl			ultrapure H_2O	Add to 50 µl

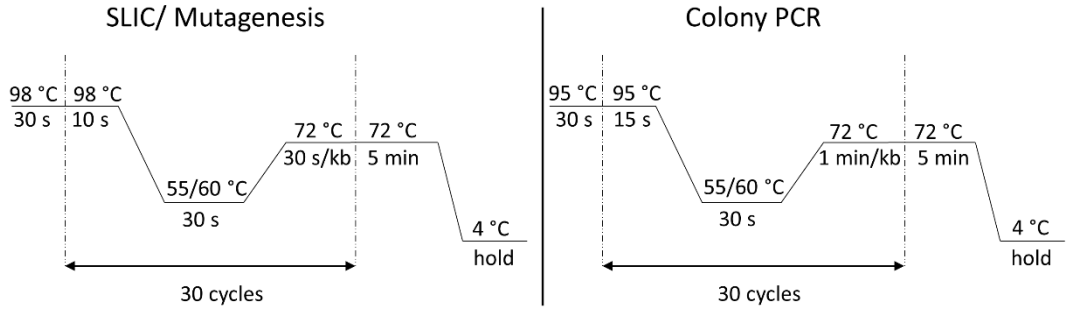

Figure 8: PCR-cycler programs: Temperature and duration steps for SLIC, Mutagenesis and colony PCRs.

II.2.1.3 Recombinant protein expression

For recombinant protein expression the chemically competent *E. coli* strains, Rosetta2 (DE3) or BL21star (DE3) pRARE2 were transformed by heat shock with the respective constructs (see list of expression constructs in appendix, Table VI-2). For the pre-culture, the entire transformation was added to 100 ml TB medium supplemented with the corresponding antibiotics for the expression vectors (50 µg/ml Strep or 100 µg/ml Kan) and the cells (34 µg/ml Cam). The pre-culture was grown at 37°C in a shaking incubator, overnight (~15 h). The next day, the main culture (2 l TB medium) supplemented with the appropriate antibiotics, was

inoculated with 1 % pre-culture and 1% glucose and cells were grown at 37°C while shaking. Protein expression was induced by the addition of 0.3 mM IPTG (final concentration) at an optical density measured at 600 nm (OD_{600}) of 3.0 and cells were incubated overnight (~15-20 h) at 20°C. Cells were then harvested by centrifugation for 13 min, at 4500 x g and 4°C. The cell pellets were either directly used for protein purification or stored at -80°C.

II.2.1.4 Seleno methionine protein expression

Table II-16: Medium and ingredients for SeMet expression

Name	Composition
M9-medium	0.1 mM $CaCl_2$, 2 mM $MgSO_4$, 4.2 mg/l $FeIISO_4$, 0.4% glucose, 0.2 mg/l biotin, 1x M9 mix
5x M9 mix	33.9 g/l Na_2HPO_4, 15 g/l KH_2PO_4, 5 g/l NH_4Cl, 2.5 g/l NaCl, pH 7.0 (autoclaved)
Amino acid mix	100 mg/l Lys/ Phe/ Thr, 50 mg/l Val/ Leu/ Iso, 30 mg/l SeMet

For the expression of SeMet substituted USP28cat or USP25ct, the plasmids were transformed into *E. coli* Rosetta2 (DE3) and *E. coli* BL21star (DE3) pRARE2 cells, respectively. Pre-cultures were grown as described above (see II.2.1.3) but cells were pelleted on the next day for 15 min at 20°C and 3220 x g and resuspended in 24 ml M9 Medium (Table II-16). 4 x 2 l M9 medium growth media including the corresponding antibiotics were inoculated with the resuspended pre-culture (5 ml for each flask). Cells were grown at 37°C while shaking at 200 rpm until an OD_{600} of 0.6 was reached. 15 min prior to the induction of protein expression (0.3 mM IPTG at 20°C, overnight ~13 h), the cultures were supplemented with the amino acid mix including SeMet (Table II-16). Cells were harvested and directly used for protein purification.

II.2.2 Protein purification

II.2.2.1 Cell lysis and affinity chromatography

Table II-17: Buffers for affinity chromatography

Name	Composition
Lysis buffer	50 mM HEPES pH 8.0, 300 mM NaCl, 1 mM TCEP
Wash buffer	50 mM HEPES pH 8.0, 1 M NaCl
Elution buffer	50 mM HEPES pH 8.0, 300 mM NaCl, 400 mM Imidazole
Dialysis buffer	50 mM HEPES pH 8.0, 300 mM NaCl, 0.05 % β-mercaptoethanol

For cell lysis, the pellet from 4 l culture was resuspended in 200 ml lysis buffer (Table II-17) supplemented with one tablet of Roche EDTA-free cOmplete protease inhibitor cocktail, 10 µl DNase and the tip of a spatula of lysozyme at 4°C. Cells were lysed in two cycles using a mechanical cell disruptor at ~1500 bar and the lysate was cleared by centrifugation (1 h, 35000 x g, at 4°C). The supernatant with the N-terminal 6xHis-tagged protein was applied twice to a gravity flow column containing (2-4 g) Protino® Ni-IDA resin followed by a 100 ml high salt washing step and two subsequent protein elution steps (15 ml and 7 ml) using imidazole in the elution buffer (for buffers, see Table II-17). Affinity chromatography was performed at room temperature, collecting the column flow through of each step on ice. After analysis of the purification steps by SDS polyacrylamide gel electrophoresis (SDS-PAGE), the elution fractions containing the protein of interest were pooled, supplemented with 3C protease for tag removal and dialyzed against 2 l dialysis buffer (Table II-17) at 4°C overnight.

II.2.2.2 Ion exchange and size exclusion chromatography

Table II-18: Buffers for size exclusion and ion exchange chromatography

Name	Composition
Storage buffer	20 mM HEPES pH 8.0, 150 mM NaCl, 1 mM TCEP
Buffer A	50 mM HEPES pH 8.0, 50 mM NaCl, 1 mM TCEP
Buffer B	50 mM HEPES pH 8.0, 1000 mM NaCl, 1 mM TCEP

For most of the protein variants (USP28 variants, USP25 catalytic domain (cat) variants, FBW7 variants, SKP1) in this project, usually one or two size exclusion chromatography (SEC) following the affinity chromatography were sufficient for protein purification. The columns (SD 200 16/600 or SD75 16/600) were equilibrated with storage buffer before the concentrated proteins were applied. Samples of the chromatogram were analyzed by SDS-PAGE and fractions containing the pure protein were concentrated, aliquoted and flash frozen in liquid nitrogen for further storage at -80°C.

The C-terminally elongated construct of USP25 (USP25cat-ct wt, aa 157-1055) and the tankyrase-ankyrin repeat region (TNKS-ANK, aa 171-957) were purified using an additional anion exchange chromatography step. After dialysis, the proteins were diluted with buffer A to a salt concentration of: ~70 mM. The proteins were then applied to a MonoQ 5/50 GL column pre-equilibrated with buffer A and eluted with a linear gradient of buffer A to buffer B. Fractions containing the proteins with the least degradation were then pooled, concentrated and further purified by SEC, often using the smaller column (SD 200 10/300 GL) which is suitable for lower protein concentrations up to 10 mg. Pure protein fractions were then handled and stored as described above.

II.2.2.3 Ubiquitin purification

Table II-19: Buffers for ubiquitin purification

Name	Composition
Ub lysis buffer	50 mM Tris/ HCl pH 7.6, 100 mM NaCl
Ub buffer A	50 mM ammonium acetate pH 4.5
Ub buffer B	50 mM ammonium acetate pH 4.5, 600 mM NaCl
Ub storage buffer	40 mM Tris/ HCl pH 7.5, 100 mM NaCl

The cell disruption was performed in the same way as mentioned in paragraph II.2.2.1 but using the Ub lysis buffer instead of the usual lysis buffer. After centrifugation, a protein precipitation step was performed using 0.4 ml of 60 % perchloric acid for 50 ml ubiquitin lysate, following 10 min incubation at 4°C while stirring. The

precipitated lysate was cleared by centrifugation (1 h, 35000 x g) and dialyzed against Ub buffer A overnight (~14 h) at 4°C. The next day it was applied to cation exchange chromatography (3x 5 ml SPHP columns) and ubiquitin was eluted utilizing a 60 CV linear gradient from Ub buffer A to Ub buffer B. Fractions containing ubiquitin were pooled and the buffer was exchanged to the Ub storage buffer while concentrating. The ubiquitin variant K48R/S20C was purified in the same way as described above, adding 1 mM TCEP to each Ub buffer.

II.2.3 Biochemical and biophysical analyses

II.2.3.1 UV/Vis spectrophotometry

DNA and protein concentrations were measured spectrophotometrically using the NanoDrop™ 1000 instrument. Prior to each measurement, a blank was performed utilizing the corresponding buffer of the sample. DNA absorbance was measured at 260 and 280 nm and the purity of the samples was determined by the absorbance ratio 260/280 nm. For protein concentrations (mg ml^{-1}) the absorbance at 280 nm with a path length of 1 cm was measured and divided by the calculated absorbance at A280 for each protein (1g/l), assuming all C residues reduced. Extinction coefficients, molecular weights and the absorption of each protein construct (Table VI-4) were obtained from the ExPASy ProtParam website (111).

The concentrations of fluorescein labeled di-Ub used in fluorescent polarization assays, was determined using equations [1] and [2]. Initially the absorbance of the labeled protein A_{prot} was calculated by taking into account the absorbance of the sample at two wavelengths 280 nm (A_{280}) and the maximal absorbance of the fluorophore (A_{max}) at 497 nm, allowing for the correction factor (CF) for fluorescein (FAM = 0.17, according to the manufacturer). The protein concentration (c_{prot}) was then calculated using the Lambert-Beer equation [2] with the extinction coefficient $\mathcal{E}_{prot}$= 8480 M^{-1} cm^{-1}, for the di-Ub variant K48R/S20C - G76W and the distance for the path length d = 1 cm.

$$\mathrm{A_{prot}} = \mathrm{A_{280}} - \mathrm{A_{max}} \times \mathrm{CF} \quad [1]$$

$$\mathrm{c_{prot}} = \frac{\mathrm{A_{prot}}}{\mathcal{E}_{\mathrm{prot}} \times \mathrm{d}} \quad [2]$$

II.2.3.2 SDS-polyacrylamide gel electrophoresis

Table II-20: Buffers and gel solutions for SDS-PAGE

Name	Composition
15% separation gel	15 % (v/v) acrylamide/bisacrylamide mix (37.5:1), 167 mM Tris/HCl pH 8.8, 0.1 % (w/v) SDS, 0.1 % (v/v) APS (freshly prepared & added with TEMED), 0.04 % (v/v) TEMED
5% stacking gel	5% (v/v) acrylamide/bisacrylamide mix (37.5:1), 125 mM Tris/HCl pH 6.8, 0.1 % (w/v) SDS, 0.1 % (v/v) APS (freshly prepared & added with TEMED), 0.1 % (v/v) TEMED
10x SDS running buffer	14.4 % (w/v) glycine, 1 % (w/v) SDS, 3% (w/v) Tris
4x SDS sample buffer	200 mM Tris-HCl pH 6.8, 8 % (w/v) SDS, 40 % glycerol (v/v), 4 % (v/v) β-mercaptoethanol, 50 mM EDTA, 0.08 % (w/v) bromphenol blue
Coomassie G250 staining	80 mg Coomassie G-250, 3 ml HCl, to 1 l ultrapure H_2O

SDS-PAGE was used to analyze proteins after purification or gel-based assays. Samples from protein purification were mixed with 1x SDS sample buffer, denatured for 5 min at 95°C and then 5 µl of the samples were run on a self-made 15% SDS gel for ~50 min at 250 V at room temperature until the loading dye reached the bottom of the gel and then left it. Gels were stained with Coomassie G250 staining as described in Lawrence and Besir 2009 (128).

For the gel-based ubiquitin cleavage activity assay (II.2.5.3) precasted Mini-PROTEAN® TGX™ gels were used. 3 µl of the samples (not denatured) were run at 120-150 V for up to ~90min and gels were stained using the Pierce™ Silver Stain Kit according to the manufacturer's instructions.

II.2.3.3 Circular dichroism spectroscopy

CD measurements were performed with a JASCO (J-810) spectropolarimeter at 20°C. UV-spectra from 190 to 260 nm were measured with (n=25) repeats using a cuvette with the path length of 0.1 cm (Hellma Analytics). Both protein samples USP25 (756-1055) and USP28 (754-1045) were diluted in 50 mM K_2HPO_4 pH 7.9 to 2.5 µM (OD_{280} 0.10) and 2.9 µM (OD_{280} 0.07), respectively. For data analysis, curves were buffer subtracted and USP25 was scaled on USP28.

II.2.3.4 Size exclusion chromatography coupled to multi-angle light scattering

Size exclusion chromatography coupled to multi-angle light scattering (SEC-MALS) was used to determine the oligomeric states of USP25 and USP28. The method combines a SEC to separate proteins and the molecular weights are determined by a Dawn Heleos 8+ light scattering detector and an Optilab T-rEX refractive index detector. Prior to the analysis, the proteins were centrifuged for at least 30 min at 25,000 x g and 4°C. The samples (100 µl with at least 3 mg/ml) were then injected on a SD200 10/300 column and eluted in storage buffer (Table II-18) with a flow rate of 0.5 ml/min at room temperature. SEC-MALS data were analyzed with the associated ASTRA software.

To test whether Ub chains have an impact on oligomerization of USP25, 30 µM of the inactive USP25cat C178S variant were incubated with either 120 µM K48 or 90 µM K63-linked tri-Ub chains overnight at 4°C. On the next day, SEC-MALS was performed using the incubated samples and the enzyme controls.

II.2.3.5 Sedimentation velocity analytical ultracentrifugation

Sedimentation velocity analytical ultracentrifugation (SV-AUC) experiments and data analysis were performed by Dr. Ingrid Tessmer. Details on data collection and analysis can be found in the StarMethods of Sauer and Klemm *et al*. (126).

For SV-AUC sample preparation, proteins were diluted in storage buffer to an absorption A_{280} of 0.5 for the individual proteins and to an A_{280} of 1 for the incubated complex samples. For interaction studies, USP25cat-ct (5 µM) and TNKS-ANK (10 µM) were incubated at a 1:2 molar ratio, respectively, for 30 min at 4°C in storage buffer (Table II-18) while being centrifuged at 25,000 x g. Samples and buffer references (400 µL each) were then loaded into standard double-sector centerpieces with sapphire windows and analyzed in an Optima XL-I analytical ultracentrifuge with an eight-hole An-50 Ti rotor at 40,000 rpm and 4°C overnight.

II.2.4 Preparation of ubiquitin substrates

II.2.4.1 Ubiquitin chain synthesis

Table II-21: Reaction mixtures and buffer for Ub chain synthesis

Name	Composition
Ub chain buffer	40 mM Tris/ HCl pH 7.5, 10 mM ATP, 10 mM $MgCl_2$, 0.6 mM DTT
Reaction mixture K48-linked chains	2.8 mM Ub, 1 µM UBA1, 25µM Cdc34 in Ub chain buffer
Reaction mixture K63-linked chains	1.4 mM Ub, 1 µM UBA1, 8 µM Ubc13, 8 µM Mms2 in Ub chain buffer
Reaction mixture K48-di-Ub	700 µM K48R/ S20C Ub, 450 µM G76W Ub, 0.6 µM UBA1, 16 µM Cdc34 in Ub chain buffer
Labeling buffer	20 mM HEPES pH 7.5, 100 mM NaCl

Ubiquitin chains were generated following the protocol of Komander *et al.* 2008 (129). The reaction mixture (2 or 5 ml, Table II-21) for K48- and K63-linked chains were incubated at 37°C and stopped after 3-4 h upon 20-fold dilution with Ub buffer A (Table II-19). The chains were isolated by cation exchange chromatography using a 1 ml Resource S column and a gradient of 60 CV from Ub buffer A to Ub buffer B (Table II-19). Fractions containing the Ub chains (mono-Ub, di-Ub, tri-Ub, and tetra-Ub) were pooled separately, concentrated and the buffer was simultaneously exchanged to keep the samples in storage buffer (Table II-18). The Ub-chains were frozen in liquid nitrogen and stored at -80°C.

K48-linked di-Ub used for fluorescence polarization assays (II.2.5.2) was generated with different Ub variants as noted in reaction mixture K48-di-Ub (Table II-21). Additionally, 1mM TCEP was added to the buffers prior to cation exchange chromatography and the di-Ub was stored in labeling buffer.

II.2.4.2 Ubiquitin labeling

The fluorescence labeling of ubiquitin with 6-FAM was performed by Dr. Florian Sauer as described in Sauer and Klemm *et al.* (126).

II.2.4.3 Preparation of ubiquitin propargylamide

Preparation of ubiquitin propargylamide (UbPA) was performed by Dr. Florian Sauer as described in Sauer and Klemm *et al*. (126).

II.2.5 DUB activity assays

II.2.5.1 *In vitro* UbRh110 fluorescence activity assay

Table II-22: Buffer for activity assays

Name	Composition
assay buffer	20 mM HEPES pH 7.5, 150 mM NaCl, 1 mM TCEP and 50 µg/ml BSA

Initial fluorescence activity assays were performed with a rhodamine110 labeled mono-Ub (UbRh110) purchased from UbiQ Bio. The stock preparation of the substrate was carried out according to the manufacturer instructions. Both substrate and enzyme were diluted in assay buffer to 750 nM and 30 nM, respectively. For the measurements, a non-binding 384-well plate was prepared with 10 µl assay buffer and 10 µl of diluted substrate. The addition of 10 µl enzyme started the reaction, which was measured at room temperature for 360 cycles à 20 s in the CLARIOStar microplate reader (excitation: 487 nm, emission: 535 nm, dichroic mirror: 507 nm, gain: 1833). The mixing of substrate, enzyme and assay buffer, led to the end concentrations of 250 nM for the substrate and 10 nM for the enzyme respectively.

For the USP25cat-ct/TNKS-ANK complex activity studies, 30 nM TNKS and 30 nM USP25cat-ct variants were mixed (in a 1:1 molar ratio) and incubated for at least 30 min on ice. The 384-well plate was prepared with 20 µl of the incubated complex mix and the reaction was started by the addition of 10 µl UbRh110.

For data analyses, the softwares MARS, Microsoft Office Excel and GraphPad Prism 8.0.0 were used. To obtain the initial activity, the fluorescence was plotted against time and the initial slope was determined. The boxplots show the initial slopes of USP25 and USP28 variants normalized to the wt proteins. Experiments were performed with at least two separately purified protein batches, which correspond

to biological replicates and measurements were done in duplicate. For statistical analysis, an unpaired t-test was performed in GraphPad Prism 8.0.0.

II.2.5.2 Fluorescence polarization measurements

To determine the catalytic efficiencies of USP25, USP28 and variants on di-Ub, fluorescence polarization measurements were performed. As a substrate, K48-linked di-Ub, fluorescently labeled at the distal Ub moiety, was used, which was prepared as described in the methods sections II.2.4.1 and II.2.4.2. The initial substrate concentration was determined as described in II.2.3.1, which was further diluted to the stock concentration of 2 µM in assay buffer (Table II-22). From 2 µM to 0.063 µM a 1:1 (v/v) dilution series was carried out in assay buffer. For the enzymes (USP25, USP28 and variants), a stock concentration of 0.5 µM was prepared in assay buffer. The reaction was performed on a black bottom, non-binding 384-well plate and started upon mixing 15 µl of the enzyme sample with 15 µl of the substrate pre-pipetted on the plate. The turnover of the substrate was measured by changes of the polarization in 113 cycles for 1 h with one flash per well, using the CLARIOStar microplate reader (excitation: 482-16 nm, emission: 530-40 nm and dichroic mirror: LP 504 nm).

Data were analyzed as described in Gersch *et al.* 2017 (130) using the software MARS, GraphPad Prism 8.0.0 and Microsoft Excel. Initial polarization values from triplicate measurements were converted to anisotropy (mA) and averaged. On the anisotropy versus time plot, a nonlinear regression analysis with one phase decay was performed with GraphPad Prism. The obtained rate constant was then plotted over the enzyme concentrations. The catalytic efficiencies k_{cat}/K_m ratio (rate constant divided by its concentration) was determined from the highest enzyme concentrations 1 µM, 0.5 µM and 0.25 µM from duplicate measurements (n=6, values) and depicted as boxplots. For statistical analysis, an unpaired t-test was calculated with GraphPad Prism.

II.2.5.3 Gel based ubiquitin chain cleavage assay

For the K48- and K63-linked tetra-Ub chain cleavage assays, the substrates were prepared as described in section II.2.4.1. Substrates and enzymes were diluted in assay buffer (Table II-22) to 2 µM and 0.5 µM respectively and pre-incubated, separately at 37°C for ~5 min. The reaction was started by mixing substrate and enzyme 1:1 (v/v). The reaction was incubated at 37°C and stopped after 1', 3', 5' and 10' min for USP28 and variants and 2', 5', 10', 15', 30'and 60' for USP25 and its variants by mixing 20 µl of the reaction with 10 µl of SDS sample buffer (Table II-20). For the time point at 0' min 10 µl enzyme and 10 µl substrate were directly pipetted to SDS sample buffer. The reaction was analyzed by SDS-PAGE (II.2.3.2) on a 4-20% precast gradient gel, stained by silver staining.

II.2.6 X-ray crystallography

II.2.6.1 Crystallization

Initially several USP28 constructs at different concentrations were screened for various crystallization conditions, using the vapor diffusion method and sitting drop 96-well plates (0.3 µl protein solution and 0.3 µl precipitant solution were mixed and equilibrated over 40 µl precipitant solution). The first USP28cat crystals (aa 149-707) grew overnight at 20°C, in the Nextal pH clear screen, in a precipitant solution containing 0.1 M citric acid pH 5.0 and 0.8 M ammonium sulfate, with a protein concentration of 2.5 mg/ml. Crystals were reproduced with protein concentrations of 2.5 mg/ml and 3.5 mg/ml using a 24-well plate and the hanging drop vapor diffusion method (1 µl protein solution and 1 µl precipitant solution were mixed and equilibrated over 500-1000 µl precipitant solution). These crystals were used for data collection but also as seed stock to obtain SeMet substituted USP28cat crystals, which grew in 0.1 M citric acid pH 5.0 and 0.4 M ammonium sulfate as precipitant in the hanging drop setup (1 µl protein solution and 1 µl precipitant solution were mixed and equilibrated over 500-1000 µl precipitant solution) at 20°C. For data collection, crystals were dipped (2-5 s) in cryoprotectant containing freshly prepared mother liquor including 22.5 % glycerol and directly flash frozen in liquid nitrogen.

Before crystallization screens for the ubiquitin bound USP28 structure were set up, the USP28cat E593D variant was mixed with a twofold excess of UbPA and incubated over night at 4°C. Unbound UbPA was removed from the sample by analytical SEC, using a SD200 10/300 column and storage buffer for elution. Crystallization trials were set up at a protein concentration of 4 mg/ml and crystals grew in several conditions. Crystals from which the structure was solved were obtained by sitting drop vapor diffusion (0.5 µl protein solution and 0.5 µl precipitant solution were mixed and equilibrated over 500 µl precipitant solution) in a precipitant solution containing 0.4 M ammonium sulfate, 0.1 M Bis-Tris pH 5.5 and 20 % w/v PEG3350 at 20°C. For cryoprotection, the crystals were dipped (2-5 s) in cryoprotectant containing freshly prepared mother liquor containing 25 % PEG400 instead of 20% PEG3350 and directly flash frozen in liquid nitrogen.

The USP25cat (aa 157-706) and USP25ct (aa 765-1055, SeMet) crystallization was performed by Dr. Florian Sauer. Both proteins crystallized within 1-2 days, utilizing the hanging drop vapor diffusion method (2 µl protein solution and 2 µl precipitant solution were mixed and equilibrated over 1 ml precipitant solution) at 20°C. Crystals of the USP25 catalytic domain with a protein concentration of 2.5 mg/ml were grown in 0.1 M HEPES pH 7.5, 12% (w/v) PEG4000 and 0.2 M $MgCl_2$ as precipitant and for the C-terminal domain at a protein concentration of 16 mg/ml in 0.1 M Tris pH 8.5, 22% PEG4000 and 0.2 M $SrCl_2$ as precipitant . Before the crystals were flash frozen in liquid nitrogen, they were cryoprotected (2-5 s) utilizing the mother liquor in which the 20% PEG4000 was replaced by 20% PEG 400.

II.2.6.2 Data collection, structure determination and refinement

All the datasets used in this thesis were collected at the European synchrotron radiation facility (ESRF), in Grenoble (France). Datasets for USP28 were collected on beamlines ID30A (USP28cat SeMet), and ID29 (USP28cat E593D-UbPA) and for USP25 on beamlines ID23-1 (USP25ct SeMet) and ID23-2 (USP25cat). Data processing and refinement was mainly carried out by Dr. Florian Sauer. For integration and scaling, XDS (125) and Aimless (103) were used. The SeMet datasets (USP28cat and USP25ct) were collected at the selenium peak wavelength and structures were solved by the

single wavelength anomalous dispersion (SAD) method, using CRANK2 experimental phasing (109) and multiple cycles of refinement (REFMAC, (121)), density modification (PARROT, (112)) and chain tracing (Buccaneer, (106)). The other structures (USP28cat E593D-UbPA and USP25cat) were solved by molecular replacement (MR) (PHASER, (116)) with the USP28cat *apo* structure as search model. Model building was completed with COOT (108) and further refinement of coordinates, B-factors and TLS-parameters was achieved with autoBuster (105) (USP25cat and USP28cat) or PHENIX-refine (117) (USP25ct and USP28cat E593D-UbPA). The USP28cat *apo* dataset was anisotropy corrected utilizing the STARANISO server (122).

For this method description see also the publication by Sauer and Klemm *et al.* and the data collection, phasing and refinement statistics (126).

II.2.7 Cell culture and cell-based assays

Conditions for cell culturing and methods for cell-based assays can be found in the, to this thesis related publication by Sauer and Klemm *et al.* 2019. A list of the eukaryotic expression constructs can be found in the appendix (Table VI-3). All of the human or mouse cell associated methods, including the cloning of the eukaryotic expression constructs, were performed by our collaboration partners Radhika K. Nair, Ravi B. Kollampally and Nikita Popov, PhD.

III. Results

The results of this thesis were obtained in collaboration with Dr. Florian Sauer. Initially USP28 and USP25 were handled as separate projects with Dr. Florian Sauer working on USP25 and me pursuing the characterization of USP28. However, it soon became clear that the results obtained in both projects should be combined and most importantly compared to delineate the similarities and the differences between the two enzymes with the potential to target them individually in the future. Therefore, both enzymes are discussed in this thesis. This work led to a joint first author publication with Dr. Florian Sauer and myself and includes the description of the structures, activity data, cell-based studies and SV-AUC results (126).

III.1 Structural and functional characterization of USP28

III.1.1 USP28: From purification to crystallization

To obtain a construct which is suitable for crystallization, several shortened USP28 variants were designed with respect to the secondary structure prediction calculated by RaptorX (Figure 9A) (120). Besides full-length USP28 (aa 1-1045, isoform 2) and constructs for the catalytic domain (aa 149-707, 114-730) also C-and N-terminally elongated variants (aa 114-1045, 1-665) were generated and utilized in interaction studies described later. Although all constructs could be expressed and purified readily, they showed remarkable differences in purity. In contrast to the catalytic domain and N-terminal elongated constructs, C-terminally elongated constructs, including the USP28 fl protein were prone to degradation (Figure 9 and supplementary Figure 53). For the purification of the different USP28 constructs, a two to three step protocol was pursued, starting with an affinity chromatography and following one or two SEC purifications. As an example, the SDS-gel of the affinity chromatography and the two SEC chromatograms from USP28cat (aa 149-707) are shown with the corresponding SDS-gels (Figure 9). Elution fractions 1 and 2 from affinity chromatography were pooled and used for further purification (Figure 9B). After overnight dialysis, in which the trx-His-tag was cleaved by 3C protease, the protein was concentrated and applied to a SD200 16/600 column for the first SEC (Figure 9C). From the eluted protein, the indicated fractions were pooled and

concentrated for a second SEC. From this purification, the peak-fractions were concentrated, stored and used for crystallization trials (Figure 9D and Figure 10).

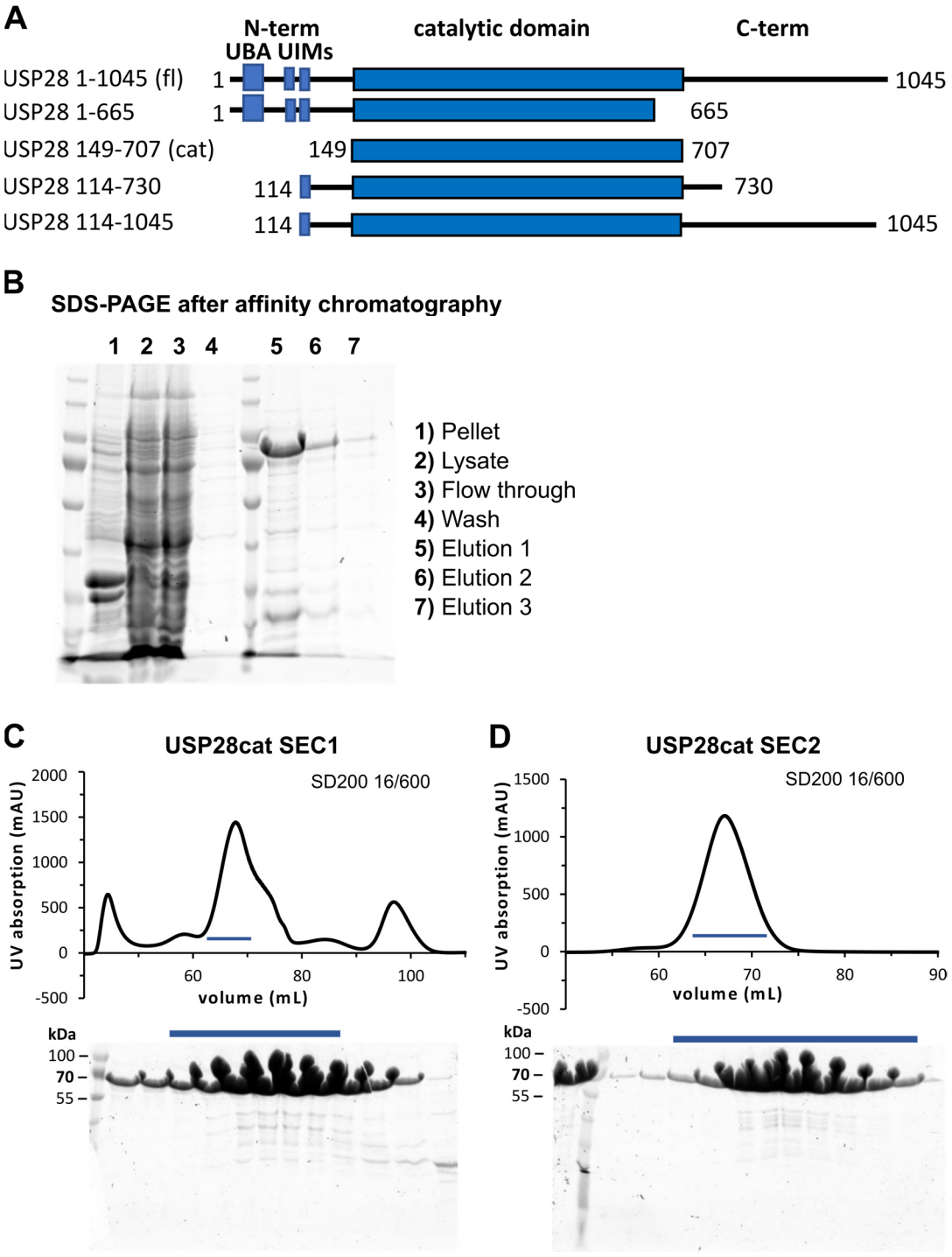

Figure 9:USP28 constructs and purification of the USP28 catalytic domain. **A)** Expression constructs for USP28. Trx/His-tag is N-terminally located, not shown in the figure. **B)** SDS-PAGE after Ni-IDA affinity chromatography. Fractions loaded on the gel are indicated. **C)** Exemplary size exclusion chromatogram of USP28cat with subsequent analysis of the elution by SDS-PAGE. Underlined are the fractions pooled for the second SEC. **C)** Second size exclusion chromatogram of USP28cat and the subsequent analysis by SDS-PAGE. Underlined are the protein fractions pooled and concentrated for crystallization.

Initial crystallization trials with the USP28cat construct were successful and crystals were obtained at a protein concentration of 2.5 mg/ml with 0.1 M citric acid pH 5.0 and 0.8 M ammonium sulfate as a precipitant (Figure 10). Data collection of native *apo* crystals was pursued at the ESRF beamline ID30A. The quality of the crystals varied substantially and therefore, the diffraction was inconsistent from not diffracting crystals to crystals diffracting up to 4 Å. To solve the phase problem SeMet substituted USP28cat was crystallized by micro seeding utilizing native *apo* crystals as seed stock. Crystals were obtained in presence of 0.1 M citric acid pH 5.0 and varying concentrations of ammonium sulfate (0.8 M, 0.6 M and 0.4 M) and in one case 0.2 M lithium sulfate was added as well. Most of the crystals did not display clear edges or formed clusters, which had to be separated prior to data collection. Diffraction quality again varied significantly, with the majority of crystals diffracting between 4 Å to 8 Å. Only one crystal with a rectangular shape displayed superior diffraction and data were collected to 3.2 Å resolution and utilized to solve the structure by single anomalous dispersion. Several trials to improve the diffraction of USP28 crystals, by dehydration, optimization of the crystal conditions or different cryoprotectants were unsuccessful.

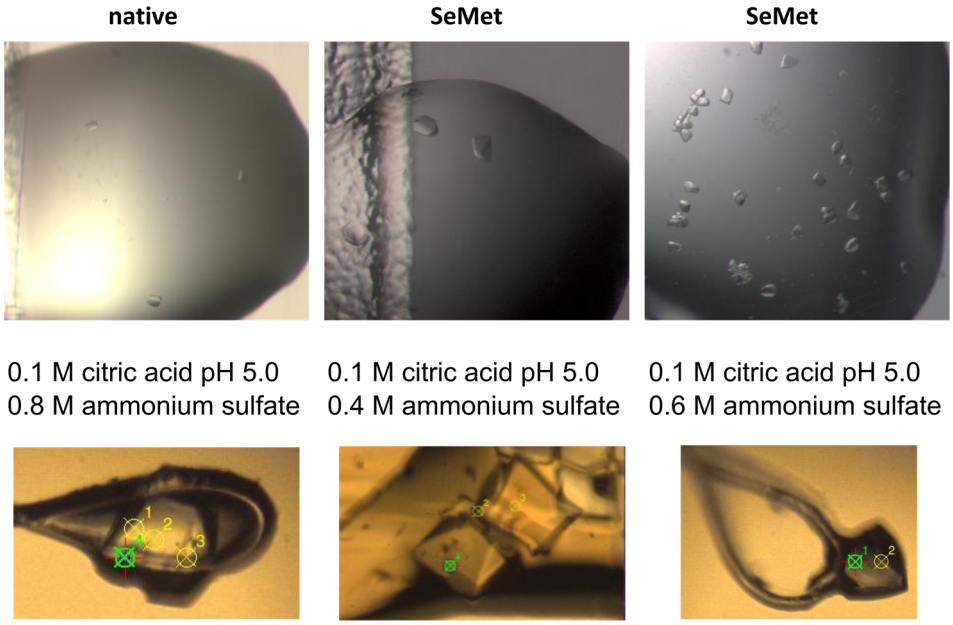

Figure 10: Crystals of USP28cat. Native or SeMet crystals grown on 96-well or 24-well plates (upper row) were harvested with litho-or nylon loops (lower row) and data were collected at the ESRF beamline ID30A (green and yellow spots on the crystals in the lower row show the position where the x-ray beam was located). Crystallization conditions of the crystals are noted in the middle. Exemplary pictures of crystals grown in these conditions are shown. Fished crystals do not correspond to the exact crystals shown in the upper row.

III.1.2 Crystal structure of the USP28 catalytic domain

The crystal structure of USP28cat was solved by SeMet-SAD phasing and was refined against STARANISO corrected data to R_{work}/R_{free} of 17.1/19.6 % extending to a resolution of 3.2 Å (Table III-1). The crystal contained two molecules in the asymmetric unit each forming a dimer with a symmetry mate. The symmetric association of two USP28 molecules leads to the formation of a cherry-couple shaped dimer with two globular domains connected by the upper part of two stem-like bipartite coiled-coils (Figure 11). The stems of the cherry-like structure correspond to the previously identified known USP25/USP28 insertion and will be named in the following **U**SP25/28 **C**atalytic domain **I**nserted **D**omain (**UCID**) (20). The UCID consist of two parts, the UCID-rod, which contains the three helices α8, α9 and α10 and the UCID-tip, which forms an 80 aa long loop (aa T454 - T534) connecting helix α9 and α10. In USP28 the UCID-tip seems to be highly flexible and is therefore only partially resolved in the structure. The two USP domains are separated by about ~35 Å, with the catalytic domains located towards the central gap, diagonally facing each other.

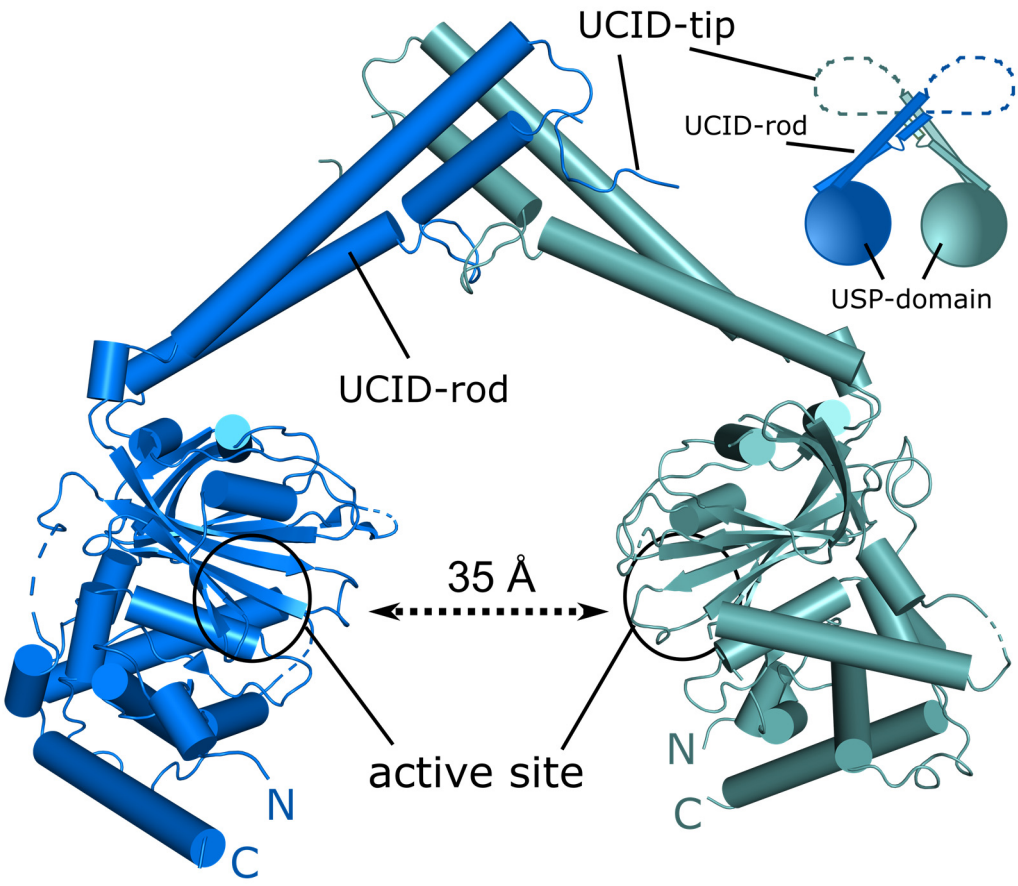

Figure 11: Structure of the dimeric USP28cat. The *apo* structure of the dimeric USP28cat (blue and teal) shown on the left side in a cartoon representation with cylindrical helices. The UCID-rod and -tip are indicated and the position of the active site is shown with a black circle. The USP domains are separated by 35 Å. Next to the structure is a schematic figure of the USP28 dimer. The partially disordered UCID-tip is shown as a dotted line.

The dimer interface of USP28 covers a large surface area of ~1860 Å² (determined by PDBePISA, Figure 12 (115)). Involved is the upper part of the UCID, starting from the α8- α9 connecting loop and the upper portion of α10 reaching to the end of the coiled-coiled part. Hydrophobic residues in the core of the interface mediate the main interactions of the two UCID's (Figure 12). Additional contacts of the α8- α9 connecting loop with itself and with residues of α9 on the other monomer stabilize the self-association. The visible part UCID-tip of each monomer is additionally interacting with upper UCID-rod of the other monomer but does not essentially contribute to the dimer interface, which is shown in next chapter.

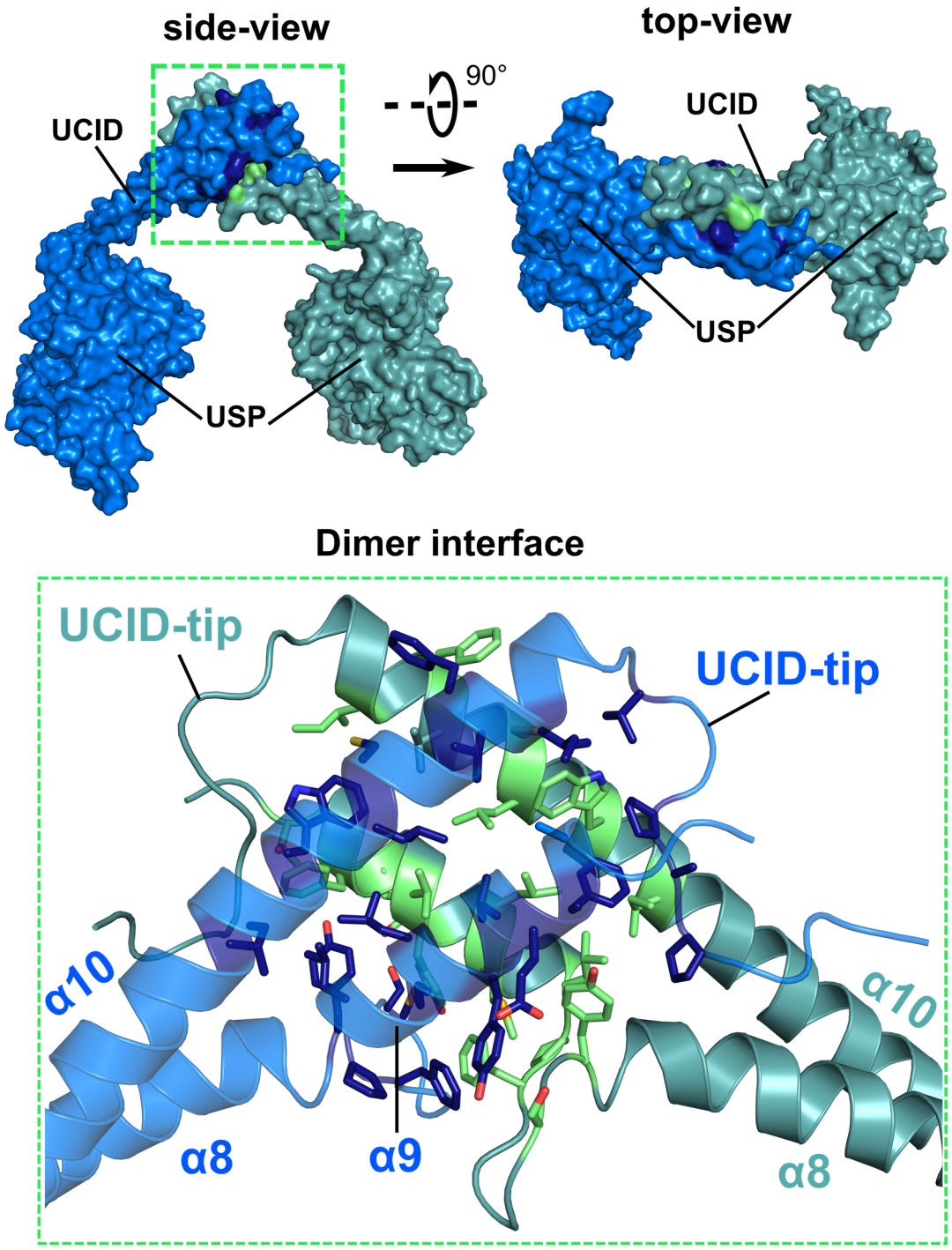

Figure 12: Dimer interface of USP28. The dimer of USP28 is depicted in surface representation from a side view (left) and a top-view (right). The green box indicates the dimer interface, with the interacting residues colored in dark blue and light green. A detailed view of the dimer interface is shown below in cartoon representation with the core interacting residues depicted as sticks and colored in dark blue and light green.

The globular part of USP28 shares high structural similarity with other USPs with the three conserved subdomains resembling, the palm, the fingers and the thumb of a right hand (Figure 13A) (23). The subdomain architecture is indicated in Figure 13A and B showing USP28 in comparison to USP7, respectively, using a similar color code

(PDB: 1NB8, (23)). The most striking difference between USP28 and USP7 is the UCID, which stretches with its long helices α8, α9 and α10 behind the fingers and palm subdomain and does not exist in USP7. The UCID is connected via two 3-10 helices (3-10-2 and 3-10-3) to the palm strands β11 and β12 of the globular domain and the position of the UCID relative to the globular domain is stabilized by several side chain interactions (Figure 14A). Another interesting difference is the close proximity of the catalytic domains' N- and C-termini in USP28, whereby R155 on the N-terminal 3-10-1 helix, forms a salt bridge with E689 of the C-terminal helix α13. In USP7 the C-terminal helix is shifted by an angle of 30° and therefore pointing away from the N-terminus (Figure 14B). The different position of the C-terminal helix in USP7 is stabilized by R543 that interacts with the backbone of the loop connecting α2 and α3. In USP28, helix α3 is much longer (dotted circle and arrow in Figure 13B, indicates shorter helix in USP7), so that the alpha 2-3 connecting loop cannot interact with the C-terminal helix (Figure 14B).

In USP28, the active site is composed of the catalytic C171 in the thumb subdomain, which is separated by the catalytic cleft from H600 and N617, located opposite to C171 on the palm subdomain (Figure 14C). Interestingly, the catalytic centers of the two molecules in the asymmetric unit adopt different conformations, with one showing an active conformation, where the catalytic triad is aligned and the other one in an inactive mode, with the histidine pointing away from the catalytic cysteine (Figure 14C).

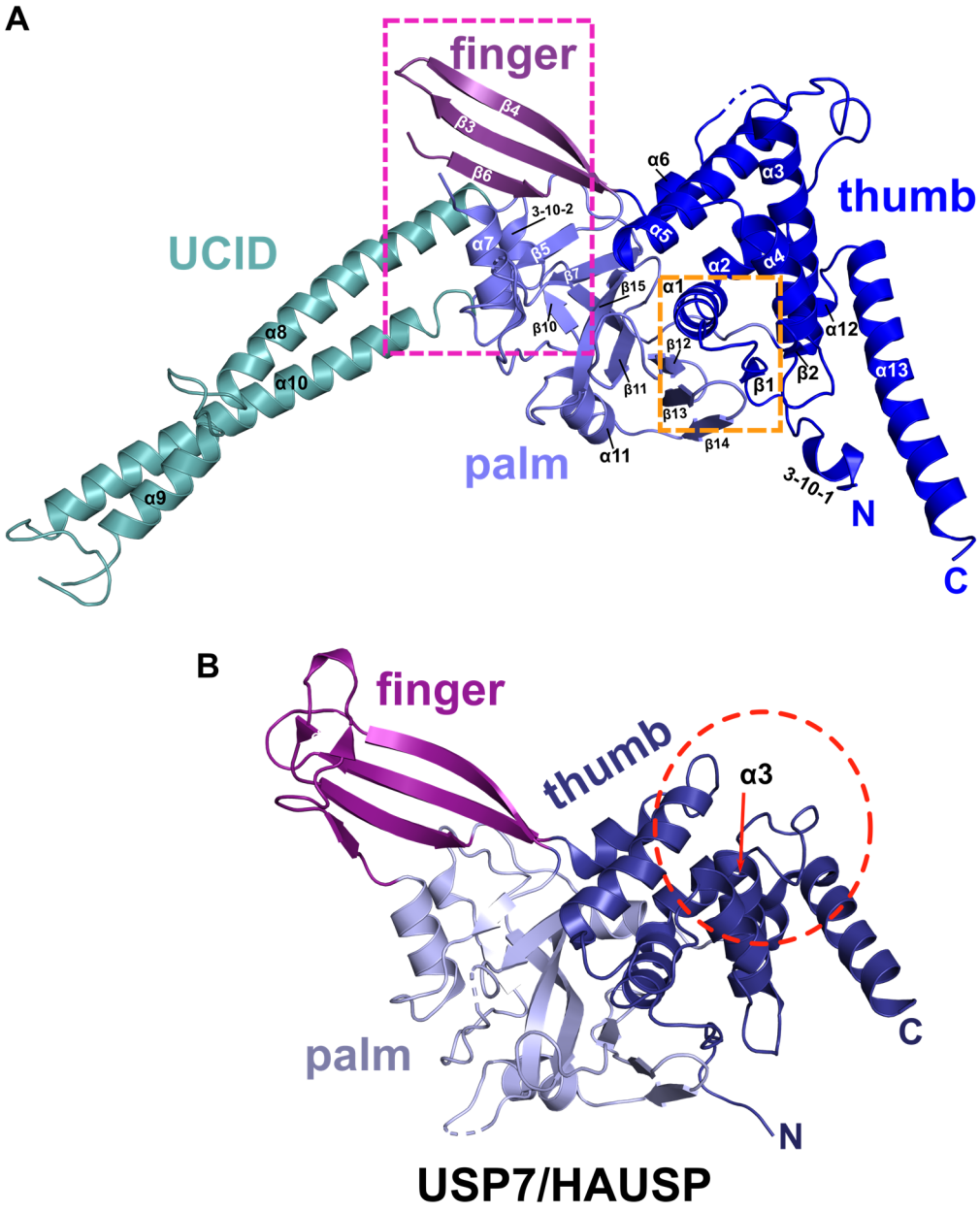

Figure 13: Comparison of USP7 and USP28. **A)** The USP28cat monomer with the USP-subdomains shown in different colors: finger (purple), palm (light blue), thumb (deep blue) and the UCID (teal). N- and C-termini are in close proximity to each other. Helices and strands are numbered. The pink and orange box indicate detailed views shown in Figure 14A and C, respectively. **B)** USP7/HAUSP in cartoon representation (PDB code: 1NB8). Same orientation as USP28 in A) with the USP-subdomains colored similarly. The red dotted circle and the red arrow indicate the shortened thumb helix α3.

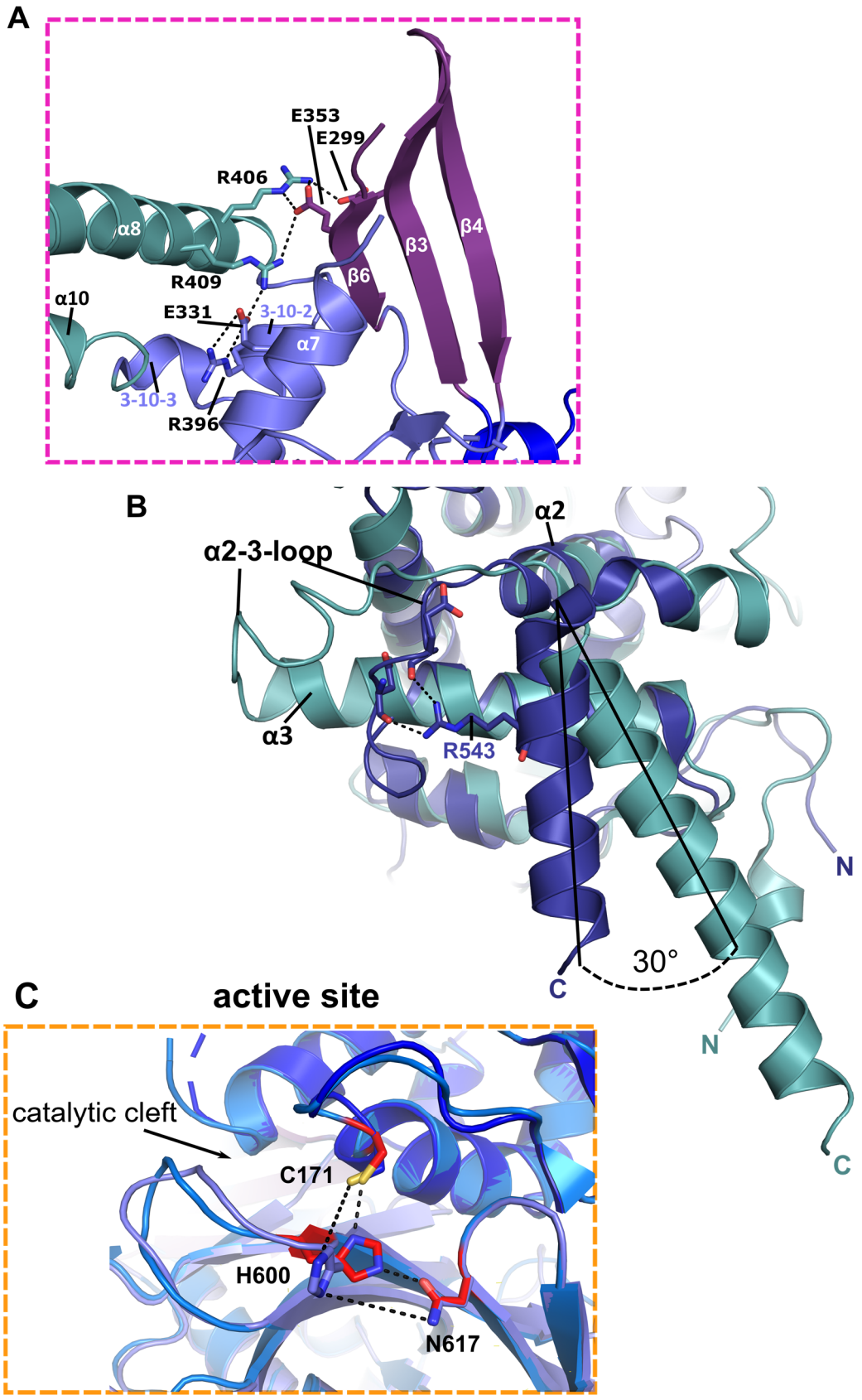

Figure 14: Detailed views of USP28 features. **A)** Detailed view of the UCID-anchoring to the USP-domain. The pink box is referring to Figure 13A indicating the position of the UCID-anchoring in the USP28 monomer. Interacting residues are shown as sticks. Dotted lines indicate hydrogen bonds or salt bridges. **B)** Superposition of USP28 (teal) and USP7 (deep blue) in the thumb view. The shifted position of the C-terminal helix is indicated. Interacting

residues of the USP7 C-terminal helix with the α2- α3 connecting loop are shown as sticks. **C)** Superposition of the two USP28 molecules in the asymmetric unit and detailed view of the active site. The orange box is referring to Figure 13A indicating the positon of the active site in the USP28 monomer. One molecule indicates a distorted catalytic site (blue residues) the other an active site (red residues

Table III-1: Data collection and refinement statistics for USP28cat *apo*. Numbers in brackets refer to the highest resolution shell. The model was refined against anisotropy corrected data (STARANISO), indicated in the additional column.

USP28cat *apo* (SeMet)

Data Collection		
PDB ID	6H4I	
Space group	I222	
Resolution range (Å)	49.58 – 3.45 (3.66 – 3.45)	49.58 – 3.22 (3.49 – 3.22)
Cell dimensions a,b,c (Å) α, β, γ (°)	 105.54, 200.52, 207.24 90, 90, 90	
Wavelength (Å)	0.9677	
Observed reflections	404279 (56772)	357341 (15141)
Unique reflections	29260 (4595)	25908 (1295)
$R_{p.i.m}$	0.046 (0.797)	0.041 (0.562)
CC1/2	0.999 (0.555)	0.999 (0.605)
Mean *I/σI*	13.4 (1.0)	15.2 (1.3)
Completeness (%)	99.7 (98.3)	94.3 (60.5)
Multiplicity	13.8 (12.4)	13.8 (11.7)
Phasing		
Method	SAD	---
Resolution	4.65	---
Anomalous completeness	99.5 (97.1)	---
Anomalous multiplicity	7.2 (6.4)	---
Figure of merit (FOM)	0.670	---
Refinement		
Resolution	---	49.59 – 3.22 (3.35 – 3.22)
Reflections work/free	---	25907 / 1096 (278 / 9)
R_{work} / R_{free}	---	17.1 / 19.6 (23.5 / 35.0)
Number of atoms		
Protein	---	7308
Ligand/ion	---	10
Water	---	-
B factors (Å²)		
Wilson B	---	109.5
Protein	---	144.9
Ligand/ion	---	167.4
Water	---	---
Rout mean square deviation (RMSD)		
Bonds (Å)	---	0.01
Angles (°)	---	1.65
Ramachandran plot favored / allowed / outliers (%)	---	93.4 / 6.0 / 0.6

III.1.3 Interface validation of the USP28 dimer

Simultaneously to the crystallization trials, we analyzed the oligomeric state of the recombinant proteins in solution by SEC-MALS. The catalytic domain of USP28 (aa 149-707) clearly eluted as a homogeneous dimer in solution, thus supporting our structural results (Figure 15A). To investigate if this result is also valid for the fl protein we purified and analyzed USP28 isoform2 (aa 1-1045). Due to severe degradation in the USP28 fl protein (see supplementary Figure 53 for the purification of the USP28 fl protein), the SEC-MALS result shows a high heterogeneity with respect to the molar mass. Nevertheless, the overall mass indicates a dimeric protein for USP28 fl in solution (Figure 15B). This indicates, that in the USP28 fl protein sample, differently degraded proteins form dimers with fl USP28, leading to an inseparable heterogeneous sample.

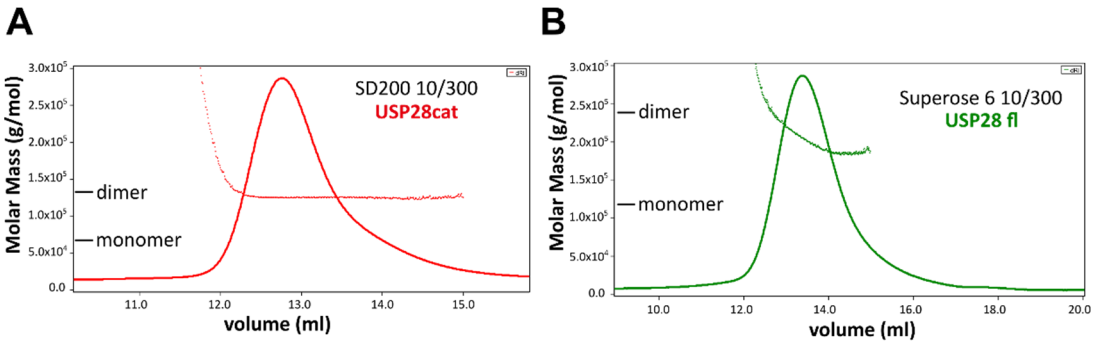

	Molecular Weight [kDa]	
	Measured	Theoretical
USP28cat	127.3 ± 0.8	129.8
USP28 fl	207.9 ± 1.3	238.2

Figure 15: Determination of the oligomeric state of USP28 by SEC-MALS analysis. SEC-MALS of **A)** USP28cat and **B)** USP28fl using the indicated SEC-columns. The chromatograms show the molar mass (dots) of the eluted proteins (continuous line: differential refractive index (dRI) signal). The theoretical masses of monomers and dimers are indicated.

The USP28cat structure indicates that dimerization is exclusively mediated by a large hydrophobic dimer interface at the upper part of the UCID rod (Figure 12). To validate the interface and further study the role of dimerization, we initially generated a catalytic domain construct, lacking the complete dimerization interface USP28cat ΔDD (aa 149 - 425 - GSSG - 560 - 707) and performed SEC-MALS (Figure 16A). The results clearly show the presence of a monomeric protein, whereas the removal of

the mainly disordered UCID-tip (USP28catΔtip, aa 149 – 458 – SGSG – 529 - 707) had no influence on oligomerization. We then decided to design a construct that would interfere less drastically with the structure of the protein and introduced a point mutation with a negative charge into the hydrophobic interface (USP28cat L545E) (Figure 16B). The USP28cat L545E variant also appeared in a monomeric state, thus further supporting the previous results.

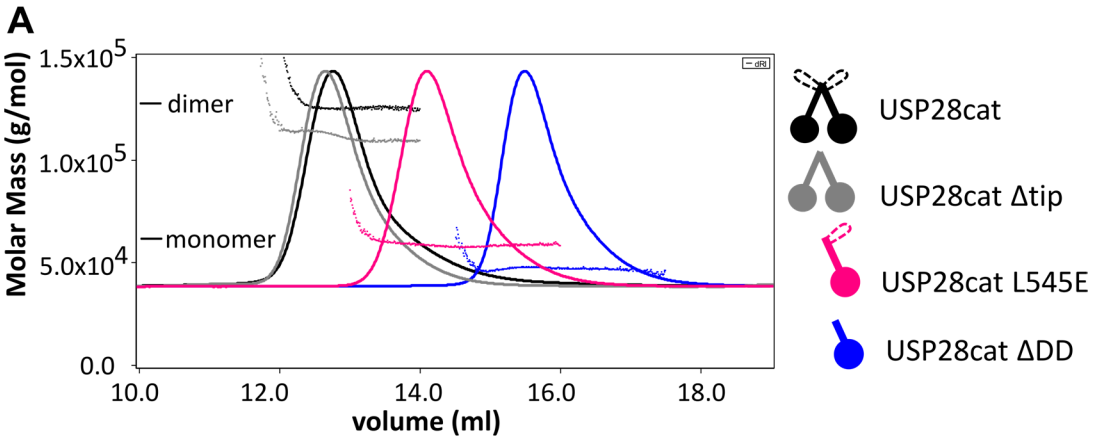

	Molecular Weight [kDa]	
	Measured	Theoretical
USP28cat**	127.3 ± 0.8	129.8
USP28cat Δtip**	112.2 ± 0.1	115.6
USP28cat L545E*	62.6 ± 0.3	64.9
USP28cat ΔDD*	47.2 ± 0.2	49.9

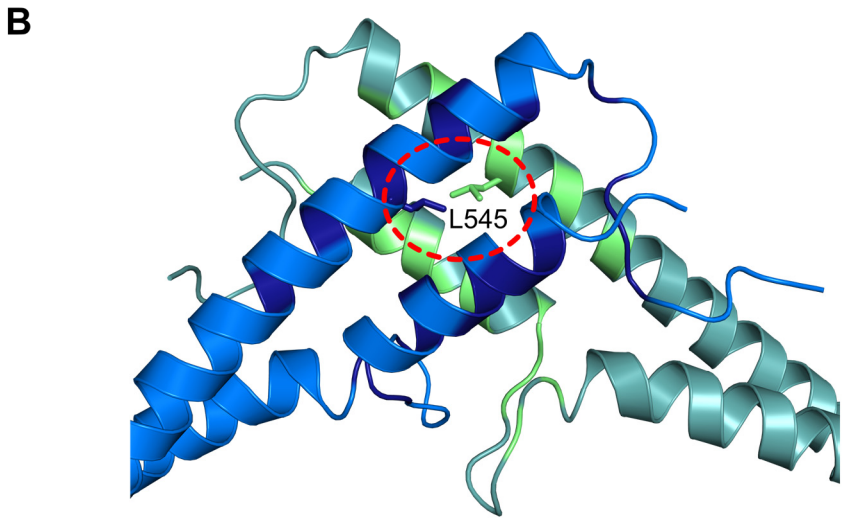

Figure 16: Dimer interface validation of USP28cat. **A)** SEC-MALS analysis of different USP28cat constructs using a SD200 10/300 column. Chromatograms show the molar mass (dots) of the eluted proteins (continuous line: differential refractive index signal (dRI)). Theoretical masses of wt-USP28cat monomer (*) and dimer (**) are indicated. The schematic figure on the right indicates the oligomeric state of the construct. **B)** Dimer interface of USP28 indicating the position of L545. The interacting residues are colored in dark blue and light green. The residue L545 is indicated by a red circle.

Since we pursued the analysis of the recombinantly purified proteins, our collaboration partner Ravi B. Kollampally in Nikita Popov's laboratory (now at the University Hospital in Tübingen, formerly at the University of Würzburg) performed co-immunoprecipitation experiments with differently tagged UPS28 constructs in HeLa cells, to verify the dimer formation *in vivo*. He could show, that HA-tagged wt USP28 is able to pull down co-expressed FLAG-tagged wt USP28, but not the FLAG-tagged L545E USP28 variant (Figure 17). These results confirm that USP28 also exists as a dimer *in vivo* and it further proves that L545 is a critical residue in the hydrophobic core interface that mediates the dimer formation.

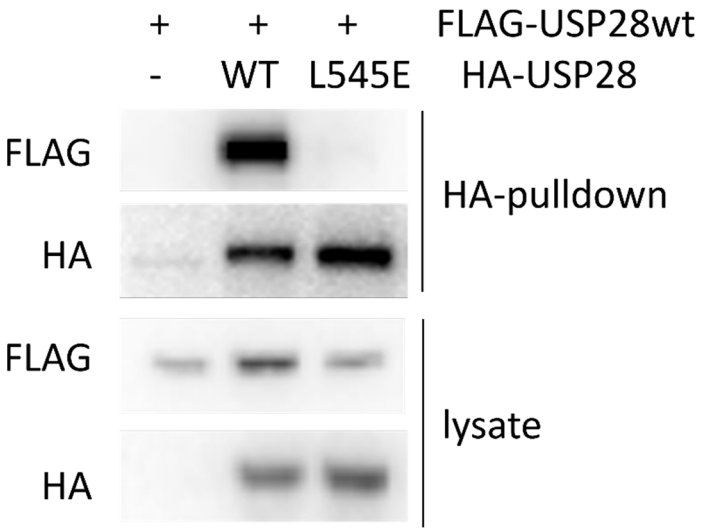

Figure 17: Validation of the USP28 interface *in vivo*. Immunoprecipitation experiment of co-expressed FLAG- and HA-tagged USP28 in HeLa cells. HA-tagged USP28 wt, but not HA-USP28 L545E pulls down FLAG-tagged USP28wt.

III.1.4 USP28 in its substrate bound state

We crystallized a variant of USP28cat E593D in its substrate bound state using the suicide probe UbPA (131) and solved the structure by molecular replacement, with the *apo* USP28 structure as a search model. The ubiquitin bound structure of USP28 was refined to R values R_{work}/R_{free} of 32.2/28% at a resolution of 3.5 Å (Table III-2). Like the *apo* structure, USP28-UbPA crystallized as a dimeric complex, with one Ub bound to each monomer (Figure 18A). Comparable to other USPs (USP7, USP2 and USP30) (23, 130, 132), ubiquitin binds with its globular surface to the synclinal S1-site of the USP domain, making direct interactions with the palm and the thumb domain (Figure 18B). From the Ub-bound structures USP2 or USP7, it is known, that a large

portion of the USP-Ub interface involves also indirect interactions via hydrogen bonds (H-bonds) with solvent molecules, which are not resolved in our structure due to the moderate resolution (23, 132).

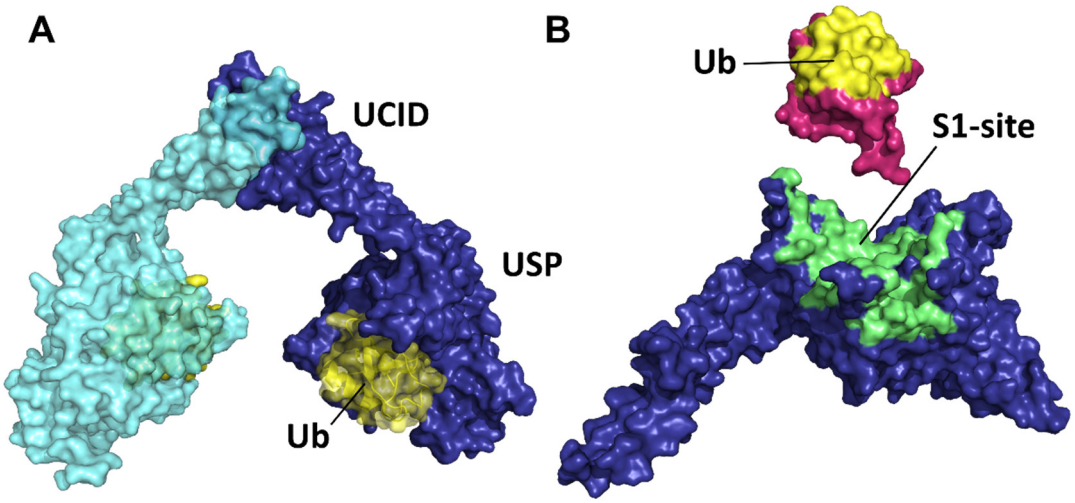

Figure 18: Structure USP28-UbPA. **A)** Dimeric USP28cat E593D (cyan, deep blue) with bound UbPA (yellow) shown as surface depiction. USP and UCID-domains are indicated. **B)** USP28-Ub Interface. The interfacing residues of USP28 (green) and Ub (pink) are shown. Ub binds to the synclinal S1-site of the USP domain. Interfacing residues are determined by PDBePISA (115).

The superposition of the *apo* structure (chain A, in light teal) to the Ub-bound structure (chain A and chain F, deep blue and yellow, respectively, Figure 19) shows a root-mean-square deviation (RMSD) of 0.9 Å, which indicates two highly identical structures (Figure 19). Main differences can be found in the position of the UCID-helices and in small conformational changes around the catalytic cleft (Figure 19). Upon ubiquitin binding, blocking loop (BL) 1 (aa R369-I382) becomes ordered and rearranges to a small β-sheet, which brings USP28 Q378 close to Ub Q40, to form a H-bond. Next to it, USP28 N597 rotates 180°, which prevents the interaction with D255 and clears the way for the Ub-tail, by moving BL2 (aa G594-G599) outwards of the catalytic cleft. On the opposite side, the switching loop (SL, aa K243-D255) becomes ordered and shields the cleft from above. The Ub-tail is anchored by L73, which binds into a hydrophobic pocket formed by the 90°C flip of Y643 and F370. At the entrance of the channel, Ub R72 is forming salt bridges with USP28 E258 on helix α5. Additional H-bonds and salt bridges stabilize the Ub-tail in the cleft. Thus, not only

the three-subdomain structure of the USP domain is conserved, but also the binding of the ubiquitin to the S1 site and especially the stabilization of its tail in the cleft seem to be highly conserved, when compared to other Ub-bound USP structures (23, 133, 134) (supplementary Figure 54).

Interestingly, the globular part of ubiquitin is also hold in place by its amino acid K48, which is interacting with D265 and E268 of USP28. A similar feature was also observed in USP7, with residues D305 and E308 coordinating K48 in Ub (23). In USP7, this interaction was suggested to bias the enzyme's Ub-binding towards Ub-moieties with a free K48 side chain (23, 97). In both molecules of our structure, ubiquitin was bound to the catalytic site of USP28. This suggests an individual activity for both monomers on ubiquitin.

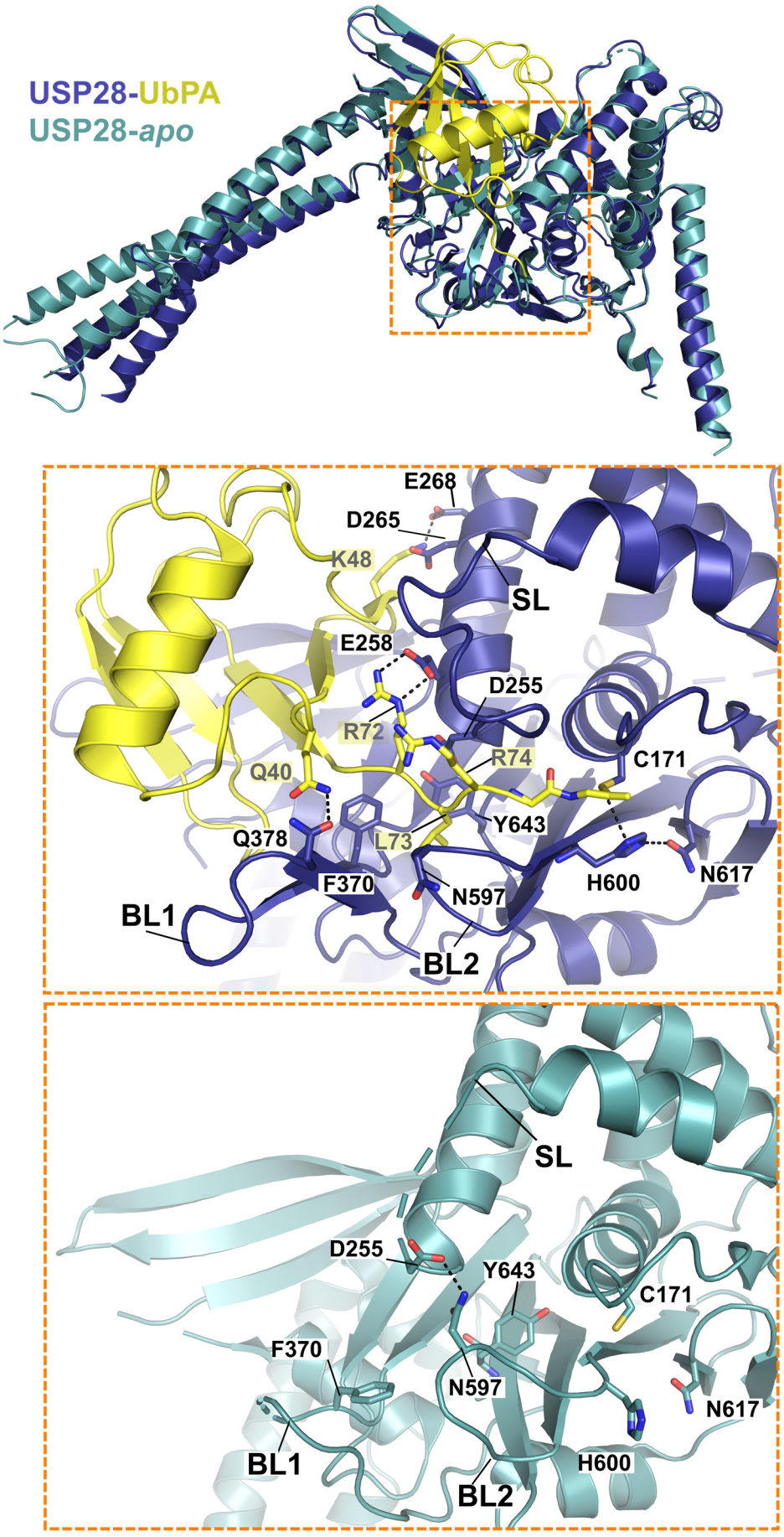
USP28-UbPA
USP28-apo
E268
D265
K48
SL
E258
D255
R72
R74
C171
Q40
Y643
L73
Q378
F370
N597
H600
N617
BL1
BL2
SL
D255
Y643
C171
F370
N597
N617
BL1
H600
BL2

Figure 19: Comparison of the two USP28 structures. Superposition of USP28cat *apo* (teal) and USP28cat-UbPA (USP28: dark-blue, UbPA: yellow) in cartoon representation. The orange box indicates the position of the detailed views shown below. The Ub-tail interactions with USP28 UbPA are shown in the middle panel, with the interacting residues indicated as sticks. The USP28cat *apo* structure is shown below in the same orientation as the Ub-bound structure. Important residues that change their conformation upon Ub-binding are shown as sticks.

Table III-2: Data collection and refinement statistics for the USP28cat E593D UbPA structure

USP28cat E593D UbPA bound (native)

Data Collection	
PDB ID	6H4H
Space group	$C222_1$
Resolution range (Å)	49.28 – 3.50 (3.78 – 3.50)
Cell dimensions a,b,c (Å) α, β, γ (°)	 171.74, 213.64, 98.56 90, 90, 90
Wavelength (Å)	1.0723
Observed reflections	197947 (41386)
Unique reflections	22722 (4692)
$R_{p.i.m}$	0.134 (1.503)
CC1/2	0.995 (0.378)
Mean *I/σI*	7.2 (0.9)
Completeness (%)	97.8 (99.5)
Multiplicity	8.7 (8.8)
Phasing	
Method	MR
Refinement	
Resolution	49.28 – 3.50 (3.66 – 3.50)
Reflections work/free	21581 / 1116 (2718 / 140)
R_{work} / R_{free}	23.2 / 28.0 (35.3 / 40.2)
Number of atoms	
Protein	8365
Ligand/ion	13
Water	---
B factors (Å²)	
Wilson B	98.5
Protein	154.8
Ligand/ion	151.5
Water	---
RMSD	
Bonds (Å)	0.004
Angles (°)	1.06
Ramachandran plot favored / allowed / outliers (%)	93.6 / 5.4 / 1.0

III.1.5 Modelling of the proximal and a second ubiquitin binding site on USP28-UbPA

Our ubiquitin bound structure, provided the ubiquitin binding mode of a distal ubiquitin to the S1 binding site of USP28. To obtain insights where the proximal ubiquitin binding site S1' and a potential S2 binding site for a longer Ub-chain is located, structural modelling was performed. Initially, a PDB search was pursued to find suitable structures of di-Ub or poly-Ub chains. Structures of Ub-chains on their own often seem to adopt a compact state, like cycled K48-linked tetra-Ub (PDB: 1F9J) or the K6-linked di-Ub (PDB: 2XK5), which makes them unsuitable for modeling trials. In complexes, however di-Ub often adopts an open conformation, like K6-linked di-Ub in complex with USP30 (PDB: 5OHP, compact versus open conformation of K6-di-Ub compared in (130)). Therefore, complex-structures of di-Ub bound to DUBs or other processors were used as preferred templates for the identification of the S1' binding site in USP28.

To determine the proximal binding site for di-Ub on USP28, a superposition of USP30 in complex with K6-linked di-Ub (Figure 20A, PDB: 5OHP, (130)) was performed, by overlaying the two USP-domains with each other, using PyMOL (119). The superposition yielded an RMSD of 1.5 Å indicating high structural similarity between the two USP domains (Figure 20B). According to this model, there is sufficient space in USP28 to accommodate the proximal Ub of the K6-linked di-Ub and no major clashes were observed. In this model, the S1' site would be located at the backside of the central palm beta-sheet with the proximal Ub pointing into the direction of the N- and C-termini of the catalytic domain (Figure 20C). Importantly, modelling of the di-Ub within the USP28 dimer illustrates the possibility that both USP28 molecules are able to simultaneously associate with di-Ub (Figure 20D). Since it is known, that USP28 has a preference for K11-, K48- and K63-linked Ub-chains (45), a second model with the structure of K63-linked di-Ub bound to the CYLD (Cylindromatosis) USP domain was generated (Figure 20E, PDB: 3WXG, (135)). Here, the alignment of both USP domains led to a high RMSD of 11.0 Å, indicating a significant discrepancy between both structures, which can be explained due to the high level of divergence of the CYLD USP domain compared to the general USP-fold (Figure 20F) (20). A closer look at the distal ubiquitin and the active site nevertheless suggest that it is an

acceptable model according to the position of the Ub-tail. The overall modeled S1' position of the K63-linked proximal Ub is almost identical to the one of the K6-linked proximal Ub, with the difference of a turned Ub, due to the differently linked lysine residue of K6- or K63-linked di-Ub (Figure 20C, D, G and H).

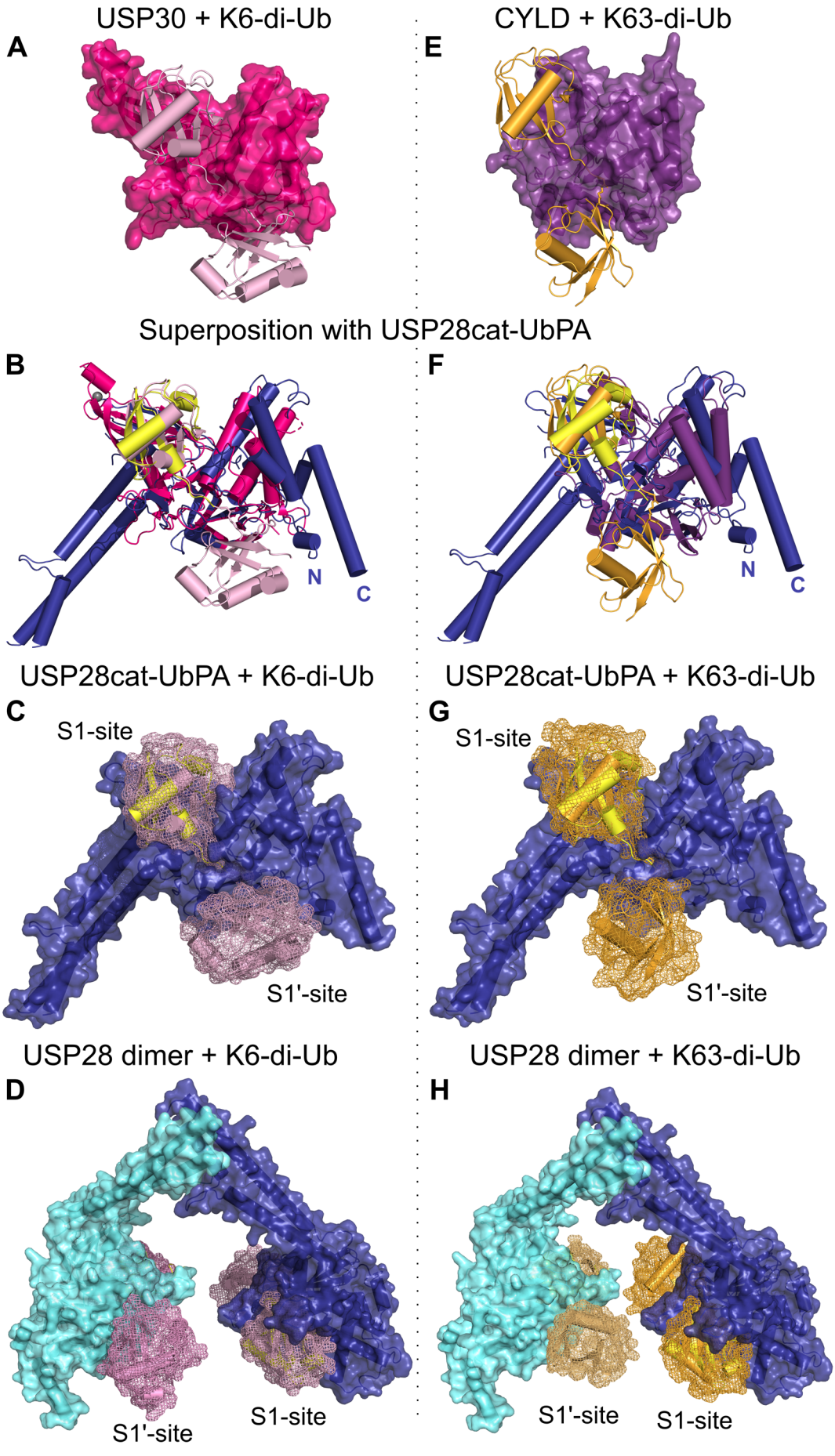
USP30 + K6-di-Ub
A
CYLD + K63-di-Ub
E
Superposition with USP28cat-UbPA
B
N
C
F
N
C
USP28cat-UbPA + K6-di-Ub
C
S1-site
S1'-site
USP28cat-UbPA + K63-di-Ub
G
S1-site
S1'-site
USP28 dimer + K6-di-Ub
D
S1'-site
S1-site
USP28 dimer + K63-di-Ub
H
S1'-site
S1-site

Figure 20: Modelling of the S1' Ub-binding site in USP28cat. **A)** Structure of K6-linked di-Ub (light pink) bound to USP30 (dark pink) (PDB: 5OHP). **B)** Superposition of USP28cat UbPA (dark blue and yellow) and USP30 K6-di-Ub (same colors as in A) depicted as cartoon with cylindrical helices. **C)** Model of USP28-UbPA with K6-di-Ub indicating the position of the S1' site of the proximal Ub. Surface depiction with K6-di-Ub in cartoon and mesh-surface. Same colors as in B). **D)** Model of USP28-UbPA dimer in surface depiction with K6-linked di-Ub (mesh-surface). Indicating the position of the proximal Ub in the dimer. **E)** Structure of K63-linked di-Ub (orange) bound to CYLD (purple) (PDB: 3WXG). **F)** Superposition of USP28cat UbPA (dark blue and yellow) and CYLD K63-di-Ub (same colors as in E) depicted as cartoon with cylindrical helices. **G)** Model of USP28-UbPA with K63-di-Ub indicating the S1' site of the proximal Ub. Surface depiction with K63-di-Ub in cartoon and mesh-surface. Same colors as in F). **H)** Model of USP28-UbPA dimer in surface depiction with K63-linked di-Ub (mesh-surface). Indicating the proximal position of the Ub in the dimer.

To estimate where a second binding site (S2) for longer Ub-chains might be located in the USP28 catalytic domain, a separate free K63- linked di-Ub was modeled into the USP28-UbPA structure. The model shows, that the distal ubiquitin molecule of a longer chain would point away from the USP28 structure with no clear binding site on the finger subdomain (Figure 21A and B).

For the positioning of K48-linked di-Ub in USP28, the structure of SARS-coronavirus papain-like protease (SARS PLpro) covalently bound to K48-linked di-ubiquitin was used (PDB: 5E6J, (136)). The alignment was performed with the Ub in the S1-site of the SARS PLpro-di-Ub structure to the UbPA in the USP28cat structure yielding an RMSD of 0.5 Å (Figure 21C and D). Unlike free K48-linked chains, the di-Ub from the SARS PLpro structure adopts an elongated conformation, which clashes with helix α3 of USP28 in our model. Furthermore, the distal Ub is positioned on top of the thumb subdomain, and is thus completely different from the concave S1-site and does not seem to be a possible S2-site.

Therefore a second model with a K48-linked di-Ub in a different conformation as found in the crystal structure of Ube2K (ubiquitin conjugating enzyme E2 K) in complex with K48-di-Ub (PDB: 6IF1) was generated. In this case, the model shows clashes of the distal Ub with helix α5 and the loop connecting thumb helix α5 and strand β3 in the finger domain (Figure 21E and F). Apart from this, the modeled S2-site would be situated behind the S1-site, where clashes would be observed with several loops connecting the thumb and the palm or the thumb and the fingers.

Overall, these superpositions indicate that conformational changes of USP28 and/or K48-linked-Ub are required to accommodate a longer chain in a possible S2-site.

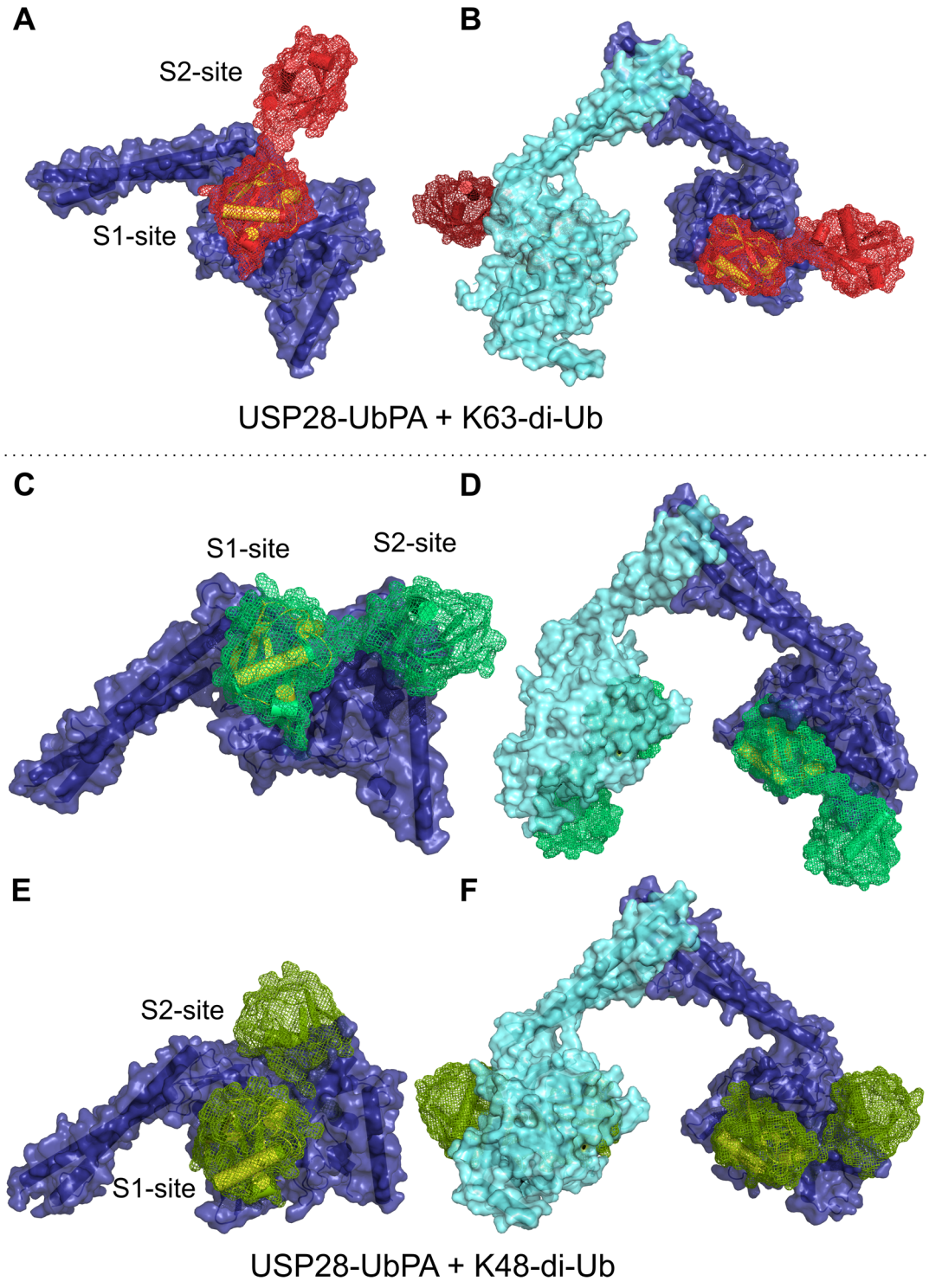

Figure 21: Modelling of a S2 Ub-binding site to USP28cat-UbPA. **A)** and **B)** Superposition of K63-di-Ub (PDB: 3H7S, red, cartoon and mesh-surface) to USP28cat-UbPA (USP28 dark blue/ cyan, cartoon and surface and Ub in yellow, cartoon). **C), D), E), F)** Superposition of K48-di-Ub (green, cartoon and mesh-surface) to USP28cat-UbPA same colors as above. C) and D) K48-di-Ub from PDB: 5E6J. E) and F) K48-di-Ub from PDB: 6IF1.

III.1.1 Dimer vs. Monomer: comparing USP28 catalytic activity

The catalytic activity of USP28 was tested utilizing several assays and different ubiquitin substrates, including fluorescently labeled mono-Ubiquitin, fluorescently labeled K48-linked di-Ub and unlabeled K48- or K63-linked tetra-ubiquitin chains (for the Ub-purification and chain synthesis see supplementary Figure 55). All activity assays were performed with the catalytic domain constructs of USP28 (USP28cat, 149-707), and different variants carrying specific point mutations or deletions.

Initially we started with a fluorescent assay, using the quenched substrate UbRh110, in which an increase of the fluorescence caused by the cleavage of the rhodamine-dye from the C-terminal glycine of ubiquitin, can be observed. The increase in fluorescence is measured over time and the initial activity of the enzymes is determined by the slope. The activity of the USP28cat wt catalytic domain was compared with the monomeric variants USP28cat ΔDD, USP28cat L545E and the dimeric variant USP28cat Δtip. Exemplary, the graph of a fluorescent-time plot depicting the mean of two biological replicates measured in duplicates (n=4) is shown (Figure 22A). All variants display an almost identical curve and the initial slope (dashed line), which stands for the initial activity, was determined from all measurement. The initial activity of all variants from two independent fluorescent-time measurements as described above (n=8) was then normalized to wt USP28cat (Figure 22B). The box plot shows no significance difference in cleavage of UbRh110 for both monomeric variants and the Δtip variant compared to the wt protein. This indicates that the UCID-tip does not influence the activity of USP28 and that monomeric and dimeric USP28 have a similar activity.

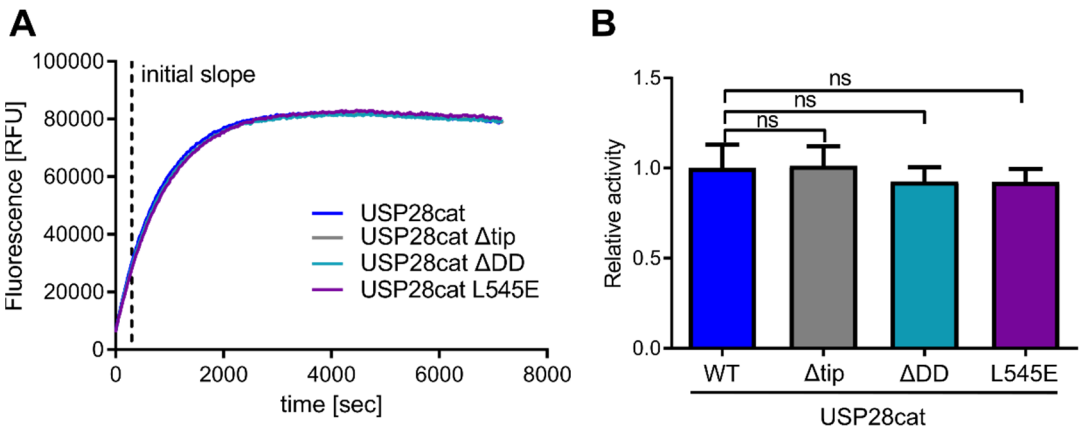

Figure 22: UbRh110 activity assay. **A)** Exemplary fluorescence-time plot of USP28cat and its variants. UbRh110 cleavage by USP28cat and indicated variants is monitored over time and the initial activity (dotted line, initial slope) is determined. **B)** Relative activity of USP28cat and its variants against UbRh110. Initial activities from A) are normalized against USP28cat and depicted as bars using the mean ± SD of n=8 measurements. Statistics show an unpaired t-test with ns, $p > 0.05$

Next, we determined the catalytic efficiency for USP28cat and the monomeric variant USP28cat L545E (Figure 23). For the fluorescence polarization measurements, we used a self-made fluorescein labeled di-Ub (K48R/S20C-G76W di-Ub-FAM). The change in polarization after cleavage of a constant amount of di-Ub in the presence of decreasing concentrations of enzyme was measured in triplicate in a plate reader, transformed to anisotropy and plotted over time. The rate constant (k_{obs}) was then determined using the GraphPad Prism, non-linear regression curve analysis and plotted over the enzyme concentration, the resulting slope indicates the catalytic efficiency k_{cat}. For the cleavage of K48-linked di-Ub in this assay, we did not observe any significant difference in the turnover rate of dimeric USP28cat (5373 $M^{-1}s^{-1}$) compared to monomeric USP28cat L545E (5111 $M^{-1}s^{-1}$).

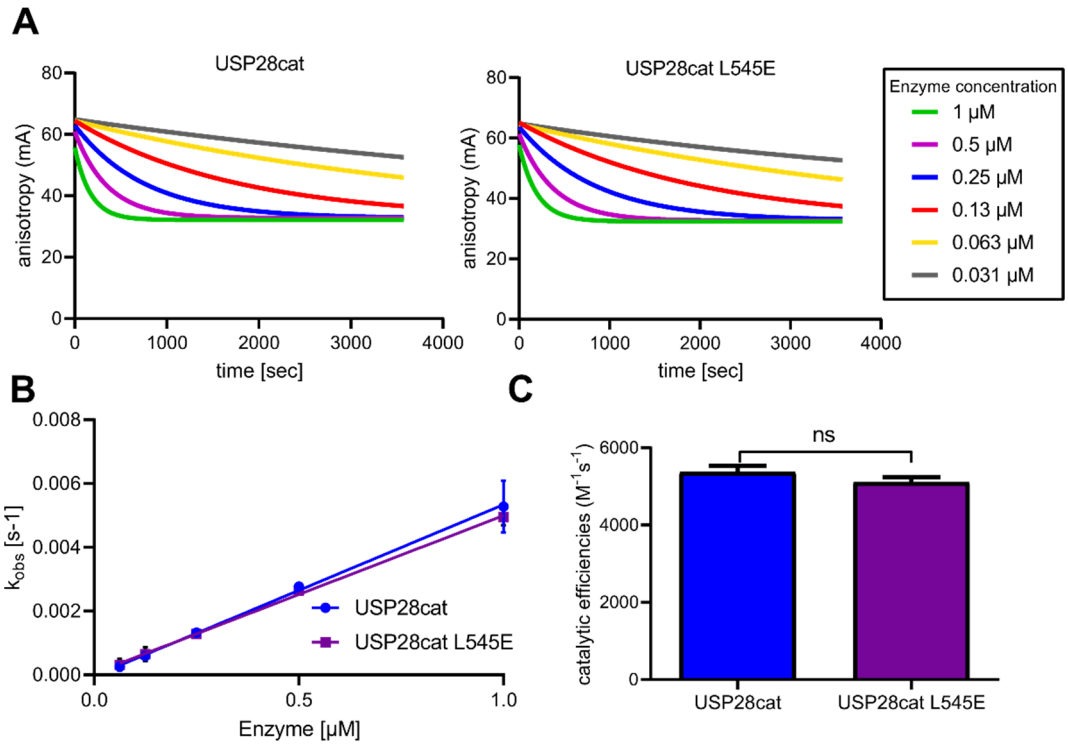

Figure 23: Fluorescence polarization measurements to determine the catalytic efficiency of monomeric and dimeric USP28. **A)** The change in anisotropy was measured over time utilizing different concentrations of USP28cat and USP28cat L545E. **B)** Linear regression curve for K48-cleavage. Rate constants k_{obs} for each concentration were determined from fitted non-linear regression curves of the anisotropy over time plot and plotted against the enzyme concentrations. Error bars depict the means ± SD of n=2 biological replicates. **C)** Catalytic efficiency of USP28cat and USP28cat L545E. Bars indicate the means ± SD of n=6. An unpaired t-test was used for statistical analysis with ns, $p > 0.05$.

To test the activity also on longer chains, we used K48- and K63-linked tetra-Ub chains and incubated them with USP28cat and the monomeric variant USP28cat L545E for different time intervals at 37°C (Figure 24). Samples were then analyzed via SDS-PAGE and the bands were visualized by silver staining. The results show, that monomeric and dimeric USP28 also display a similar activity on tetra-Ub chains, which seems to be independent of the linkage type.

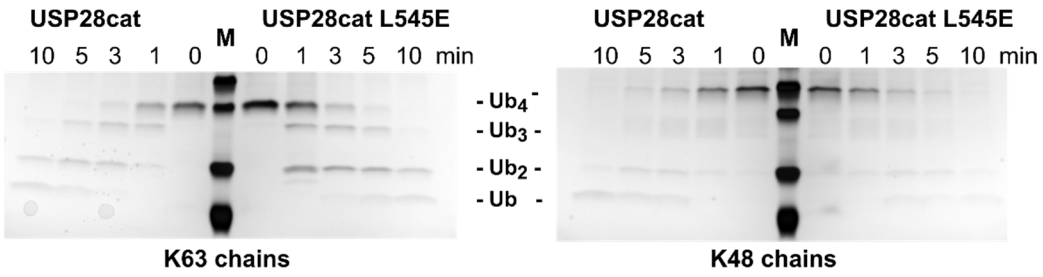

Figure 24: Gel-based tetra-Ub cleavage assay. Silver-stained SDS-gel showing K63- linked (left side) and K48-linked (right side) tetra-Ub cleavage by USP28cat and USP28cat L545E. Time points are indicated above the gel.

III.2 Structural and functional characterization of USP25

The closest relative to USP28 is USP25. Both DUBs share the same overall domain architecture, which can be divided into the N-terminal domain, the catalytic domain and the C-terminal part of the enzymes with a remarkable sequence conservation. Especially the catalytic domains share a very high identity of 57 % and both include an insertion site of the same length and position (Figure 25).

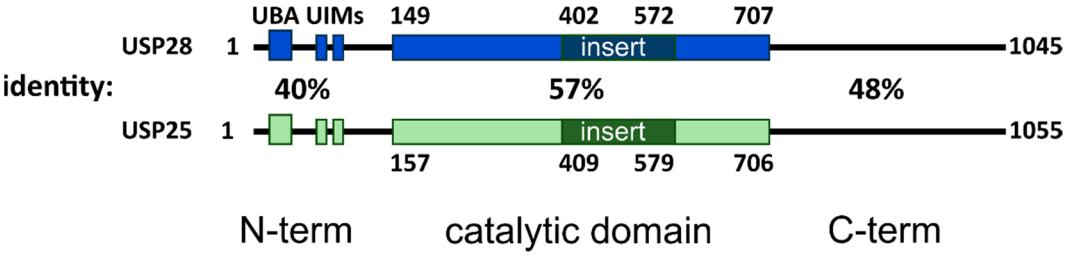

Figure 25: Domain architecture of USP28 (blue) and USP25 (green). The percentage of sequence identity between the isoform 1 of USP25 and the isoform 2 of USP28, is labeled in the center. The insertion site is marked in darker colors.

III.2.1 The oligomeric state of USP25

It has been suggested by Denuc *et al*. that USP25 assumes an oligomeric state *in vivo* (43). The authors performed a co-immunoprecipitation assay with several USP25 constructs of varying lengths and revealed that the catalytic domain of USP25 is sufficient for its oligomerization (43).

To confirm these results *in vitro*, we designed a construct of the catalytic domain of USP25 (USP25cat, aa 157-706), according to the borders of USP28 and expressed and purified the enzyme using the same protocols as used for USP28. After affinity

chromatography (data not shown), USP25cat was further purified by SEC on a SD200 16/600 column and the main peak fractions were pooled as indicated (Figure 26A). Subsequently, we examined the oligomeric state of USP25cat in solution utilizing SEC-MALS (Figure 26B). Surprisingly, we observed that USP25cat eluted earlier than USP28cat on the same column (SD200 10/300) and indicated a higher molecular mass, close to the mass of a theoretical USP25 tetramer. To determine the molecular weight with a second independent method, SV-AUC studies were performed with both USP28cat and USP25cat which confirmed that the main species of USP25cat sedimented later than the dimeric USP28cat (80% USP25cat at 6.1 S versus 93% USP28cat at 3.6 S), indicating a higher oligomeric species with respect to USP25cat (Figure 26C).

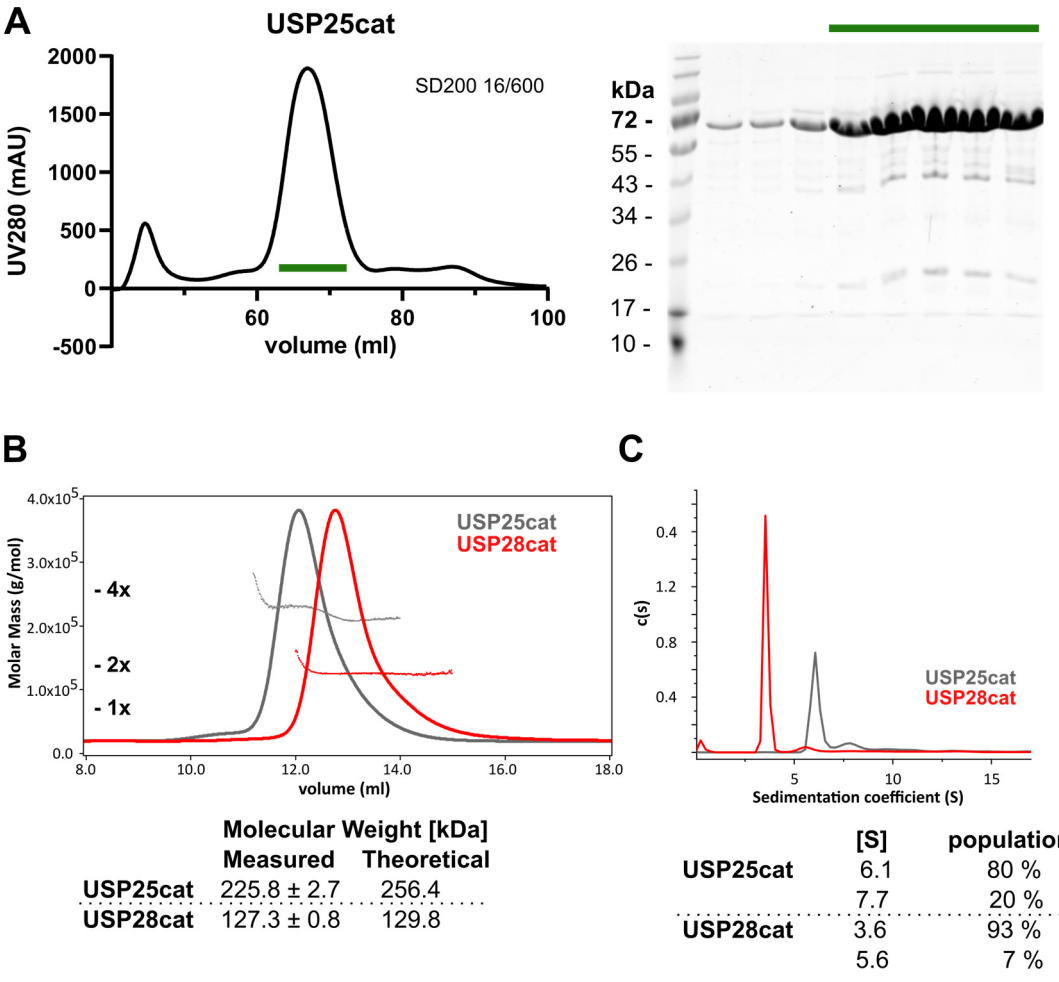

	Molecular Weight [kDa]	
	Measured	Theoretical
USP25cat	225.8 ± 2.7	256.4
USP28cat	127.3 ± 0.8	129.8

	[S]	population
USP25cat	6.1	80 %
	7.7	20 %
USP28cat	3.6	93 %
	5.6	7 %

Figure 26 Purification of USP25cat and determination of the oligomeric state. **A)** SEC of USP25cat. USP25cat was applied to the SD200 16/600 column for SEC (left side). The elution

fractions were analyzed by SDS-PAGE, with the gel shown to the right. Indicated peak fractions were pooled and used for subsequent studies. **B)** SEC-MALS analysis of USP25cat compared to USP28cat. USP25cat (grey) shows a higher molar mass (grey dotted line) compared to USP28cat (red dotted line). The theoretical masses of USP25cat are indicated. Continuous line: differential refractive index. The table with the determined and calculated masses, is shown below the chromatogram. **C)** SV-AUC of USP25cat (grey) compared to USP28cat (red). Sedimentation coefficients and occupancies are given below.

III.2.2 Structure of tetrameric USP25cat indicates an auto-inhibited state

Crystallization trials with USP25cat were performed by Dr. Florian Sauer and were successful in the presence of a precipitant solution containing HEPES pH 7.5, PEG 4000 and $MgCl_2$. The structure was solved to a resolution of 3.1 Å by molecular replacement using the USP28cat *apo* structure as a search model. Like USP28, the crystal contained two molecules in the asymmetric unit and the model was refined to an R_{work}/R_{free} of 18.1/23% (Table III-3). In contrast to USP28, however, USP25 adopts a tetrameric conformation, composed of two USP28-like dimers that are interlinked with each other (Figure 27). One molecule of USP25 assumes the same subdomain architecture as USP28 and is composed of the globular USP domain and the novel UCID domain that leads to the association with another USP25 monomer, to form a dimer. Additionally, a second interface is formed (mainly) between the UCID-tip and the globular USP-domain of a second dimer, thus connecting two USP25 dimers in an inverted fashion to form a D2 symmetrical, tetrahedral structure (Figure 27).

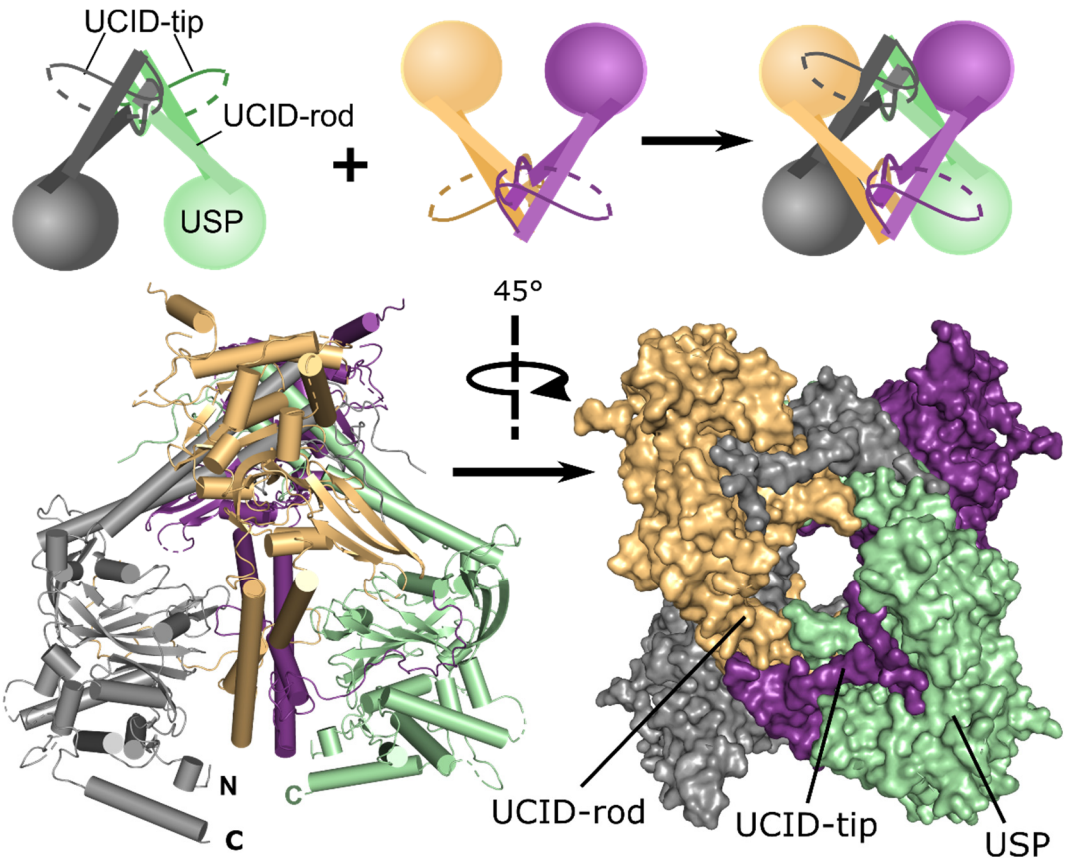

Figure 27: Structure of the USP25cat tetramer. Above the crystal structure is a schematic representation of how the tetramer is built from two USP25 dimers (grey/green and yellow/purple) that interlink with each other by the UCID-tips of one dimer with the USP domains of the other dimer. The structure of the USP25cat tetramer is shown below, in cartoon and rotated by 45° in surface depiction in the same colors.

The interaction is enabled by a kink of the C-terminal part of the UCID-tip that extends in a perpendicular direction from the rod towards the USP domain of the other molecule, where it binds into a cleft formed between thumb helix α5 and the palm β-sheet (Figure 28A). The position of the tip is stabilized by residue F522, which binds into a hydrophobic pocket of the cleft and furthermore, by additional hydrogen bonds formed with residues of the palm, thumb and finger subdomains. Interestingly, K520 of the UCID tip forms a salt bridge with E275 of the thumb helix α5 and further hydrogen bonds with D272 and Y300 (Figure 28B). The same residues can be found in USP28 (D265, E268, Y293), where they stabilize ubiquitin binding by coordinating Ub-K48 (Figure 19). Besides the UCID-tip/USP interactions, the tetramer is further stabilized by the proximity of the loop between α8 and α9 of the other dimer mate

to BL1 in the USP domain, leading hydrogen bond formation between R445 and E387, thus every molecule in the tetramer is interlinked with each other (Figure 28C).

Superposition of the ubiquitin bound structure of USP28 with the tetrameric USP25 structure indicates that the UCID-tip of USP25 occupies a major fraction of the ubiquitin binding site (Figure 28D). We therefore assumed that USP25 adopts an auto-inhibited state in its tetrameric conformation.

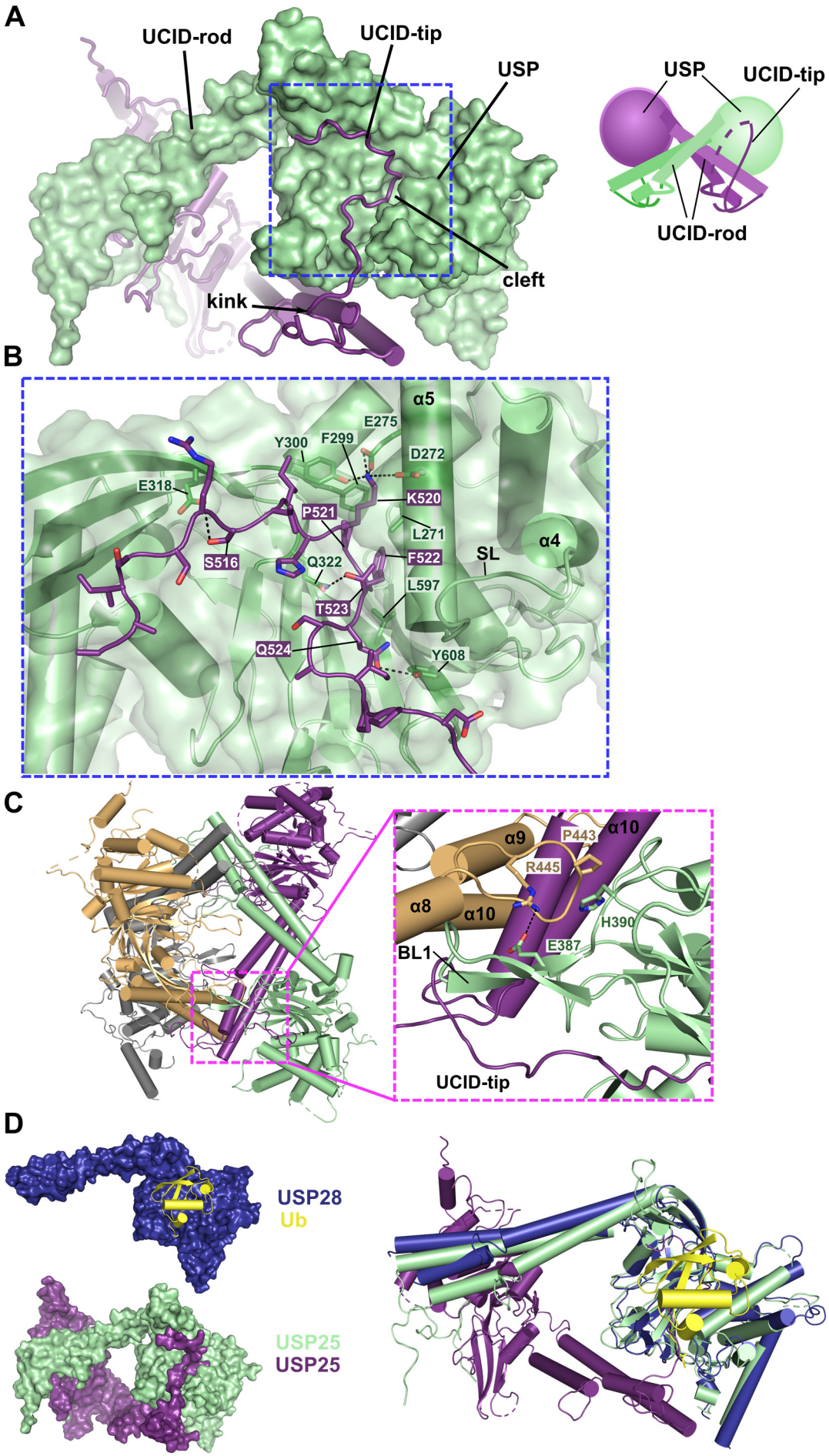
A
UCID-rod
UCID-tip
USP
cleft
kink
USP
UCID-tip
UCID-rod
B
α5
E275
Y300
F299
D272
E318
K520
P521
L271
α4
SL
S516
Q322
F522
L597
T523
Q524
Y608
C
α9
P443
α10
R445
α8
α10
H390
E387
BL1
UCID-tip
D
USP28
Ub
USP25
USP25

Figure 28: Interface of the USP25 tetramer. **A)** The UCID-tip is binding to the USP domain. Due to a kink the UCID-tip (purple molecule, cartoon representation) is directed towards the USP domain of the other molecule (green, surface depiction), where it binds into a cleft. Left-side crystal structure and right side schematic overview. **B)** Detailed view of the UCID-tip/USP interaction. The UCID-tip is anchored by F522, which binds into a hydrophobic pocket of the USP domain and is stabilized by H-bonds and salt-bridges (black, dotted lines) to the thumb, palm and finger subdomains. **C)** Interconnection of all molecules. "The other dimer mate" (yellow) interacts with BL1 of the USP domain (green) by the α8-α9 connecting loop. **D)** The UCID-tip/ USP interaction of USP25 blocks ubiquitin binding. Left side: comparison of USP28-UbPA (dark blue and yellow, upper panel) and the USP25-tetramer interface purple and green, lower panel). Right side: Superposition of USP28-UbPA and two molecules of USP25 forming the main tetramer interface.

Table III-3:USP25cat data collection and refinement statistics

USP25cat (Native)

Data Collection	
PDB ID	6H4J
Space group	$C222_1$
Resolution range (Å)	48.54-3.07 (3.28-3.07)
Cell dimensions a,b,c (Å) α, β, γ (°)	 81.87, 202.25, 169.50 90, 90, 90
Wavelength (Å)	0.8729
Observed reflections	722733 (129388)
Unique reflections	26854 (4806)
$R_{p.i.m}$	0.067 (0.754)
CC1/2	0.999 (0.509)
Mean *I/σI*	11.9 (1.2)
Completeness (%)	100 (100)
Multiplicity	26.9 (26.9)
Phasing	
Method	MR
Refinement	
Resolution	48.54 – 3.07 (3.19 – 3.07)
Reflections work/free	25462/ 1365 (2841 / 154)
R_{work} / R_{free}	18.1 / 23.0 (23.3 / 28.4)
Number of atoms	
Protein	7556
Ligand/ion	3
Water	29
B factors (Å²)	
Wilson B	86.6
Protein	104.6
Ligand/ion	114.0
Water	69.0
RMSD	
Bonds (Å)	0.01
Angles (°)	1.06
Ramachandran plot favored / allowed / outliers (%)	93.68 / 6.0 / 0.32

III.2.3 Interface validation of USP25cat

The structure of USP25cat indicates a strong involvement of the UCID tip in the USP25cat tetramer interface. Therefore, we generated a construct lacking this region USP25cat Δtip (aa 157-464-GSGG-538-706) and investigated its oligomeric state using SEC-MALS analysis (Figure 29). The data show, that the removal of the UCID-tip leads to USP25 dimers, confirming that the tip is essential for the tetramer formation. Using this mutant, USP25cat Δtip, and introducing two charged point mutations into the dimer interface (USP25cat tip F458E L552E) we were able to generate a monomeric USP25cat. This indicates that the USP25 dimer interface is equivalent to the one observed in USP28. To further dissect the USP25 tetramer-interface, we introduced the monomer-mutations into the catalytic domain construct of USP25cat and observed the same breakdown of the USP25 oligomer. This indicates that the tetramer can only form from a USP28-like dimer and that the tip cannot independently bind to the USP core domain. Additionally, this result implies that only the USP28-like dimer interface is independently stable and that a “second dimer interface” as found in the USP25 tetramer, depends on the presence of the USP28-like dimer.

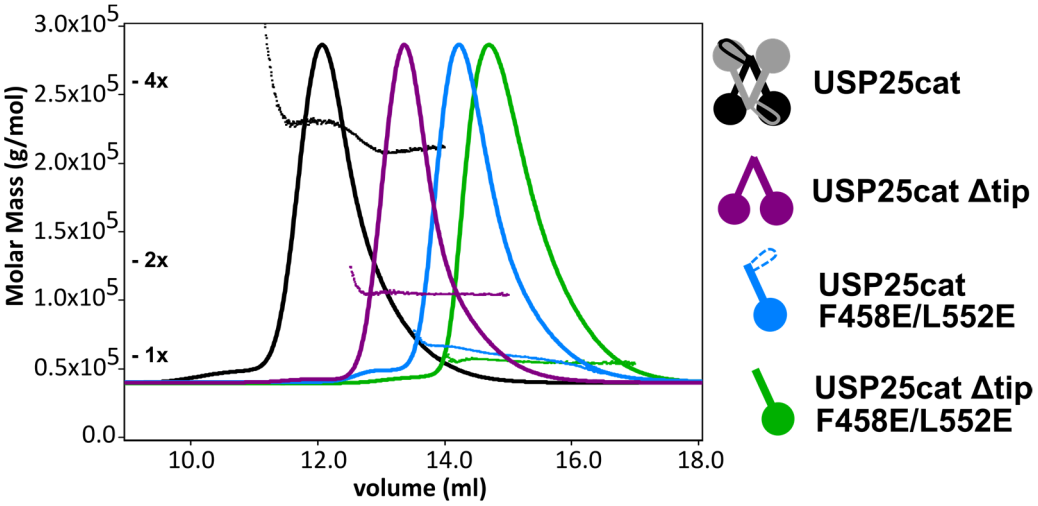

	Molecular Weight [kDa] Measured	Theoretical
USP25cat****	225.8 ± 2.7	256.4
USP25cat Δtip**	105.3 ± 1.2	113.8
USP25cat F458E/L552E*	64.5 ± 0.4	64.1
USP25cat Δtip F458E/L552E*	56.4 ± 0.6	56.9

Figure 29: SEC-MALS analysis of USP25cat and its variants to validate the dimer and tetramer interface. Theoretical masses of tetrameric (4x), dimeric (2x) and monomeric variants (1x) are indicated in the graph. Table with determined and theoretical masses of the variants tetrameric ****, dimeric ** and monomeric *, are shown below the chromatogram. Peaks indicate the dRI-signal (continuous line) combined with the molar mass (dotted lines) and are normalized.

III.2.4 Catalytic activity of USP25

Based on the structural analysis of the USP25cat tetramer, we assumed an auto-inhibited state for the protease. By probing the catalytic activity of USP25 and its different oligomeric variants we could confirm the hypothesis of an auto-inhibited tetramer in several activity assays. In the UbRh110 activity assay the dimeric USP25cat Δtip showed a ~7-fold higher activity compared to the tetrameric USP25cat (Figure 30A). The monomeric variant, USP25cat F458E/L552E, showed a minimal but significantly lower activity than the dimeric USP25 but still a higher cleavage rate then the wt protein. In a second experiment, the catalytic efficiency k_{cat} against K48-linked di-Ub was determined (Figure 30 B). In accordance with the previous results USP25cat Δtip displays a 6-fold increased turnover rate compared to the wt catalytic domain, whereas the monomeric USP25 cleaves K48-linked di-Ub with a ~5-fold increased efficiency.

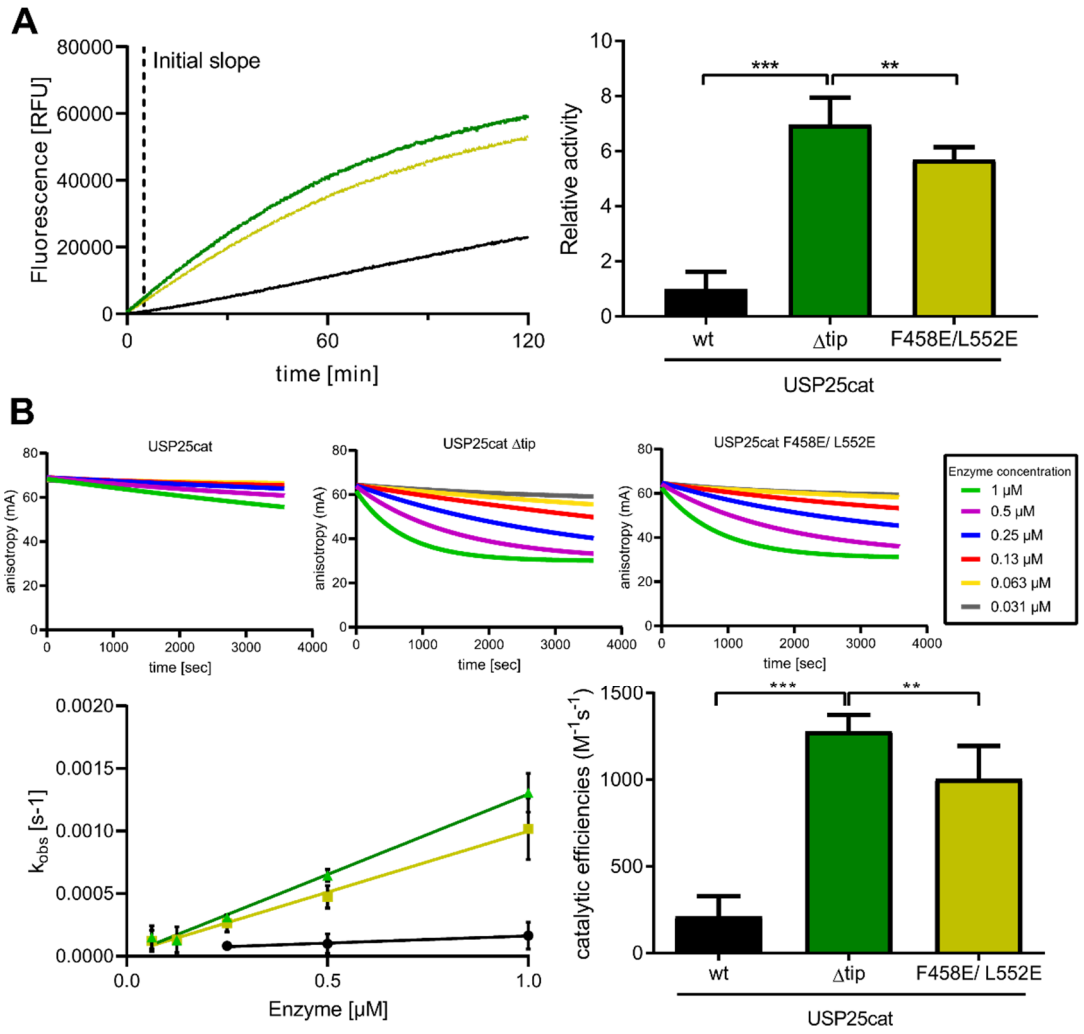

Figure 30: Catalytic activity of USP25cat and its variants. **A)** UbRh110 cleavage assay. Increasing fluorescence over time indicates the cleavage of Rh110 from Ub by USP25cat and its variants (exemplary graph on the left, same color code as in the graph on the right side). The initial velocity is determined by the initial slope (dotted line). The initial activity is normalized to USP25cat wt and depicted as mean ± SD of n= 7 measurements. **B)** Catalytic efficiency of USP25cat and its variants. Fluorescence polarization measurements of indicated enzyme concentrations (upper panels, depicted as anisotropy over time plots) were fitted with non-linear regression curves. Observed rate constants (k_{obs}) are plotted over the enzyme concentration and fitted by nonlinear regression curves (lower panel, left side, same color code as above). Error bars represent means ± SD of n=2 biological replicates. The catalytic efficiencies of USP25 are shown as box plot with means ± SD of n=6 (graph on the right side). For statistical analysis an unpaired t-test was used with **p > 0.01 and *** p > 0.001.

To further examine the activity at a more physiological level, we used tetra-Ub chains (K48- and K63-linked) and compared the cleavage of tetrameric USP25cat with dimeric USP25cat Δtip and monomeric USP25cat F458E/L552E (Figure 31). The cleavage reaction was stopped at the indicated time points and visualized by SDS-PAGE and silver staining. It can be clearly observed that the dimeric and monomeric variants of USP25cat cleaved the K48- and K63-linked tetra-Ub chains completely

after 30 min, whereas the tetrameric USP25cat seems to process the substrate at a slower rate and tetra-Ub remains present after 30 min. A clear preference for any of the two tetra-Ub-chain linkage types is not visible.

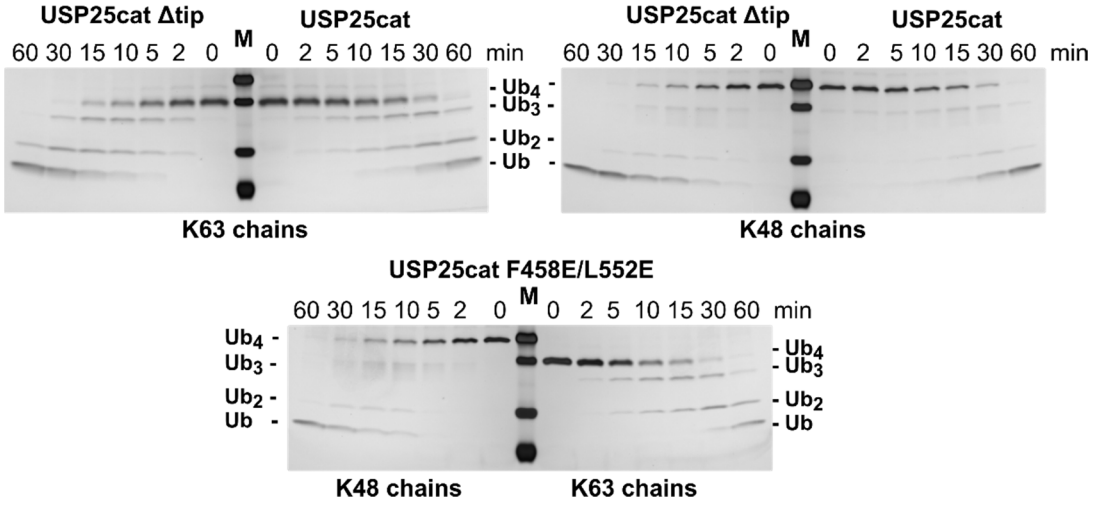

Figure 31: Gel-based tetra-Ub cleavage assay. Cleavage of K63- and K48-linked tetra-Ub by USP25cat and variants was stopped at indicated time points, analyzed by SDS-PAGE and visualized by silver staining.

III.2.5 Is the inhibitory effect of USP25 transferable to USP28?

Due to the high identity of both enzymes' catalytic domains (57 %) the question arises: What is the major difference of USP28 and USP25 that leads to the differential oligomerization? Would it be possible to transfer the inhibitory effect of USP25 to USP28?

First, we focused on the sequence comparison of USP25 and USP28 (Figure 32A). Interestingly, the most dissimilar sequence is located in the UCID tip-region (aa USP28 T454-T534, USP25 S461-T541). Apart from the same length of 81 residues, only 38 % of the amino acids are identical or conserved. In contrast, further sequence analyses indicate that both, the globular USP-domain and the UCID-rod (helices α8, α9, α10) are highly identical with 67% and 54%, respectively (identities for the USP-domains and the UCID-rods were calculated by the basic local alignment search tool (BLAST), (137)). By depicting the amino acid conservation of USP28 and USP25 on one molecule of the USP25 structure, this became even more evident. Especially, the ubiquitin-binding site in USP28 and the tip-binding site in USP25 are virtually identical, when comparing the position of the Ub in USP28 and the conservation depicted on the USP25 structure (Figure 32B).

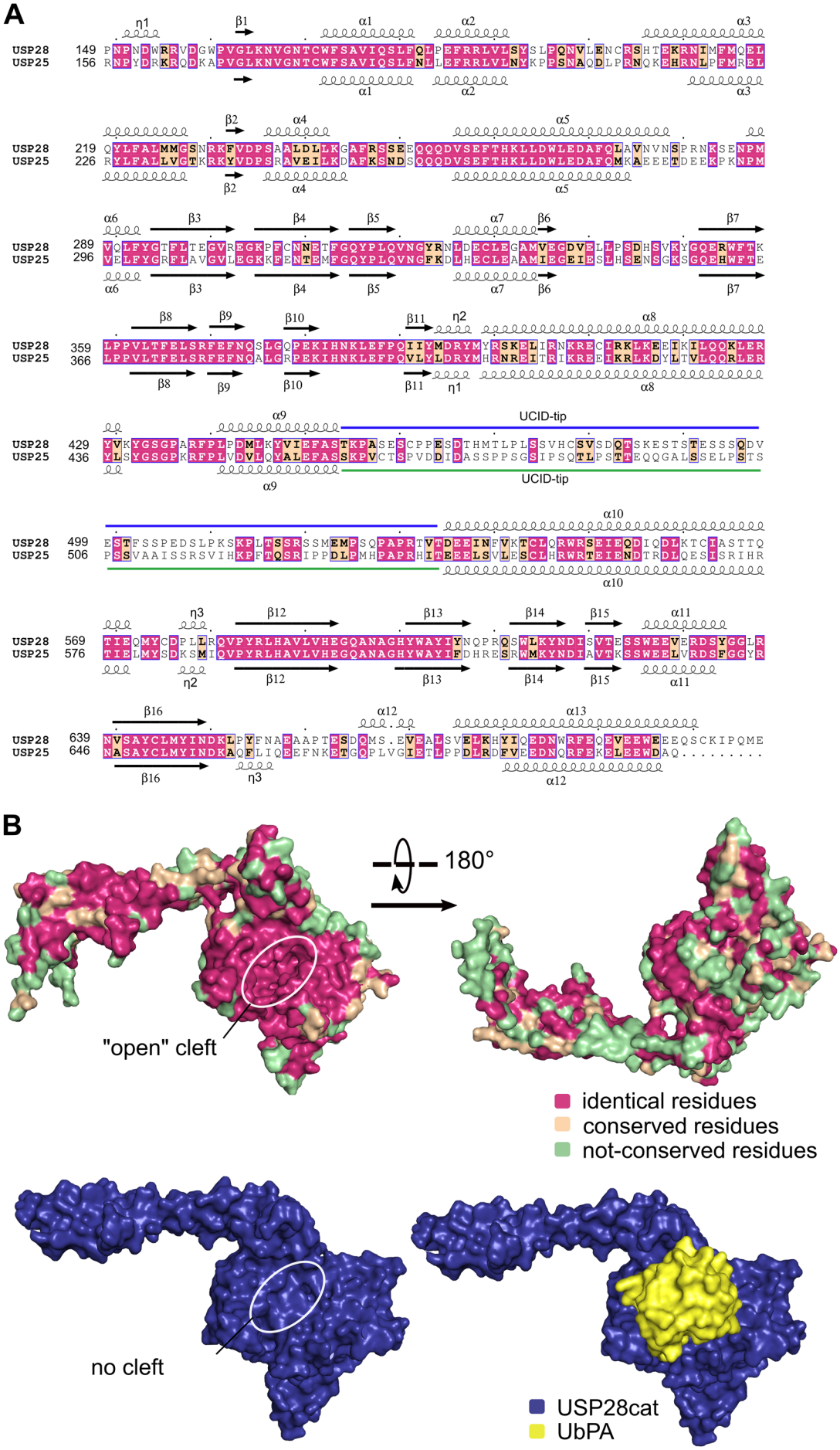
A
USP28
USP25
UCID-tip
B
180°
"open" cleft
identical residues
conserved residues
not-conserved residues
no cleft
USP28cat
UbPA

Figure 32: Sequence alignment and conservation of USP28 and USP25. **A)** The sequence alignment of the catalytic domains of USP28 (149-707) and USP25 (157-706) was performed with T-Coffee (123) and the sequence similarity was depicted with ESPript 3.0 (138). The pink background indicates identical residues, the beige background type conserved residues and no background not-conserved residues. Secondary structure elements are numbered with curls indicating α-helices, arrows for β-strands and η indicating 3-10-helices. The UCID-tip is shown by a green and blue line for USP25 and USP28, respectively. **B)** Sequence conservation of USP25 and USP28. Identical (pink) type conserved (beige) and not-conserved (green) residues are depicted on the USP25cat structure (upper panels). USP28cat without and with UbPA are shown below in the same orientation (dark blue and yellow, respectively). The UCID-tip binding cleft is open in USP25 and missing in USP28.

This prompted us to generate two USP28-chimeras, that contained either the UCID-tip amino acid sequence of USP25 (USP28-tip-chimera, aa USP28-149-457_USP25-465-534_USP28-528-707) or the "roof" of the USP25-UCID, which is defined as the upper part of the UCID, starting shortly in front of the α8-α9 connecting-loop (USP28-roof-chimera, aa USP28-149-427_USP25-433-562_USP28-555-707, Figure 33A). As the counterpart, we also generated the USP25-roof-chimera, containing the upper part of the USP28-UCID (aa, USP25-157-434_USP28-428-555_USP25-563-706). For all three variants we determined a dimeric state by SEC-MALS analysis (Figure 33A), which indicates, that neither the USP25-tip by itself nor the USP25 globular domain alone are able to adopt the higher oligomeric state, but that the combination of both is required for tetramerization. A major difference between USP28 and USP25, however, is the presence of the open tip-binding cleft in USP25, which is not present in USP28 (Figure 32B). The superposition of both enzymes with one molecule from USP25 and one from the USP28cat-UbPA structure reveals that the closed conformation in USP28 is mediated by a shifted position of helix α5 (Figure 33B). Furthermore, there is a major difference between USP25 and USP28 in the length of the two helices (α3 and α4) with α3 being longer and α4 shorter in USP28. Due to the longer helix α3 E208 is pointing into the opposite direction than the corresponding residue E215 in USP25, which stabilizes the pulled in conformation of helix α5 by interacting with K269. An additional H-bond of E215 with R217 leads to the positioning of R217 towards helix α4, where it interacts with D251. In USP28 D251 is not conserved and substituted by G244, which is due to the shorter helix α4 already part of the switching loop. Importantly, in USP25, the longer helix α4 places F253 on top of F266, close enough for π-stacking interactions, which further stabilizes the

position of helix α5 leading to an open cleft conformation that is able to accommodate the UCID-tip in a tetrameric state.

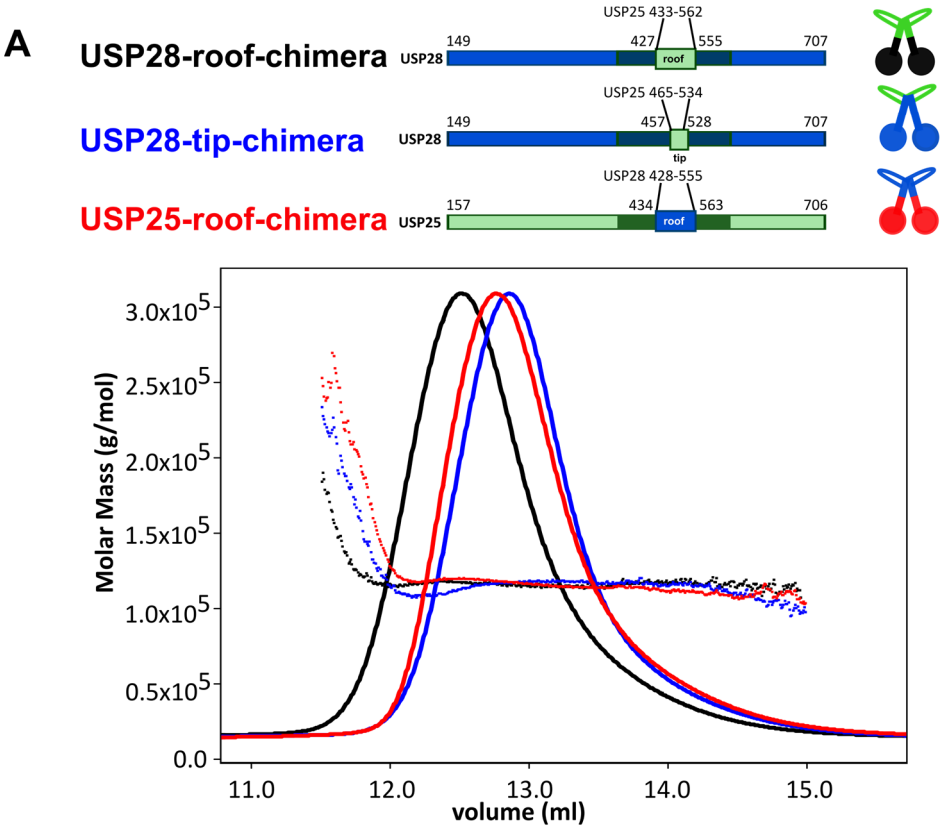

	Molecular Weight [kDa]	
	Measured	Theoretical
USP28-roof-chimera	117.0 ± 1.7	130.0
USP28-tip-chimera	116.2 ± 1.0	130.5
USP25-roof-chimera	117.3 ± 2.0	128.5

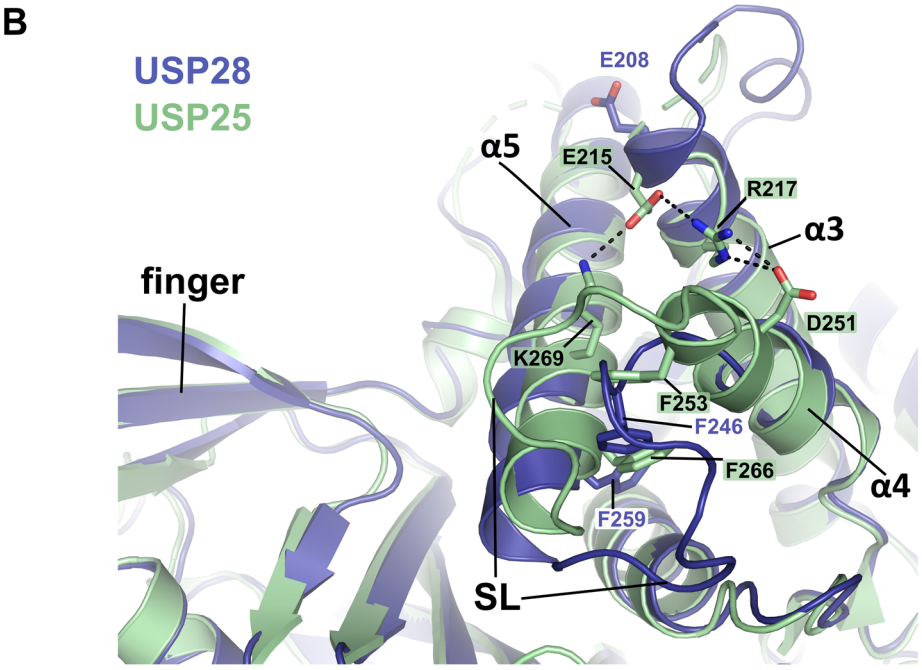

Figure 33: Non-transferable tetramerization of USP25. **A)** SEC-MALS analysis of USP28 and USP25-chimera variants. Chimeric USP28 and USP25 constructs are shown above the chromatogram with indicated sequence borders and schematic figures to the right. The color code is the same as for SEC-MALS chromatograms with the USP28-roof-chimera in black, the USP28-tip-chimera in blue and the USP25-roof-chimera in green. All variants indicate a dimeric state; theoretical and measured values of the molecular weight are given below. **B)** Superposition of USP25 (green) and USP28 (dark blue) with a detailed view of the open and closed tip-binding cleft, respectively. The open cleft in USP25 is stabilized by π-stacking interactions and further H-bonds on helix α3, α4 and α5. Interacting residues are shown as sticks.

Next, we investigated if a USP25 tetramer can be formed spontaneously from two separately expressed dimers. To prevent tetramer formation upon expression of the USP25 catalytic domain, we used the dimer-variant USP25cat Δtip, which was incubated with twice the amount of the separately purified dimeric UCID-subdomain of USP25 (aa 415-583). Surprisingly, SEC-MALS analysis showed no significant change in the elution volume and mass of the catalytic domain (Figure 34). We therefore conclude, that even in the presence of all the tetramer interacting components, a spontaneous association of the UCID-subdomain with the globular USP-domain does not occur.

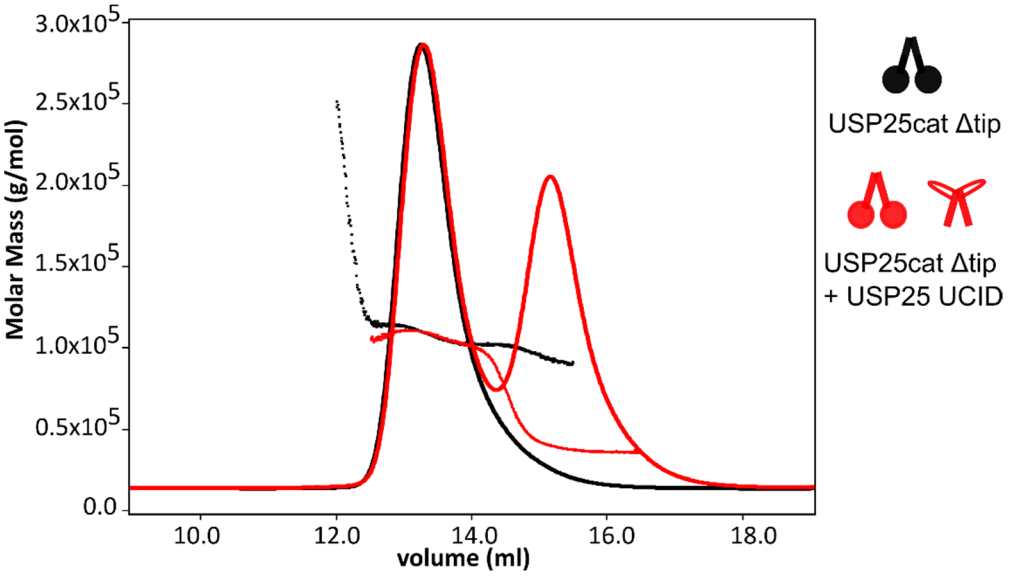

	Molecular Weight [kDa]	
	Measured	Theoretical
USP25cat Δtip	108.0 ± 0.4	113.8
USP25 UCID	42.0 ± 0.2	38.0
USP25cat Δtip after incubation with UCID	106.2 ± 0.5	113.8

Figure 34: SEC-MALS analysis of a 1:2 mixture of USP25cat Δtip and the isolated UCID (red) compared to the USP25cat Δtip variant (black). Schematic figure of the constructs are

depicted on the right side. No association of the UCID to the dimeric USP25 construct can be observed. The experimentally determined and theoretical molecular weights are indicated below the chromatogram.

III.3 Differential activity of USP25 and USP28

Despite the high sequence identity of USP25 and USP28 in the catalytic domains severe structural differences between both enzymes could be determined, leading to USP25's exceptional tetramerization, described above. Following this thread, we compared subsequently their catalytic activities. An initial UbRh110 cleavage assay confirmed our previous results of the auto-inhibited USP25 tetramer, which becomes activated upon removal of the UCID-tip by dimerization (Figure 35A and B). The previous results obtained with the USP28cat Δtip variant, clearly demonstrated that the UCID-tip does not play a major role in the catalytic activity of the dimeric enzymes (Figure 22 and Figure 35). Interestingly, the activated USP25cat Δtip dimer displayed a 6-fold lower activity compared to the USP28cat dimers (USP28cat and USP28cat Δtip) (Figure 35B). A closer look at the structures of USP25cat and USP28cat-UbPA revealed an important difference in BL1. In both structures, BL1 adopts a β-hairpin conformation (Figure 35B and C). In contrast to USP28, the BL1 in USP25 is connected with BL2 by side chain interactions of R385 with Q602 (Figure 35 B). This positioning of R385 towards BL2 is additionally stabilized by a salt bridge with E387. The coupling of BL1 and BL2 in USP25 might interfere with the independent movement of both loops upon substrate binding and could therefore be the reason for the observed decreased catalytic activity. R385 in USP25 is not conserved and replaced by Q387 in USP28 (Figure 35). Interestingly, in USP28 this residue is pointing into the opposite direction and interacts with Q40 in ubiquitin, thereby supporting the positioning of the Ub-tail. Since the Ub-tail also contains two positively charged Arg-residues, the R385 in USP25 might lead to repulsive forces that impede the binding to the catalytic cleft. To investigate our hypotheses, we generated two dimeric mutants with the substituted residues USP25cat Δtip R385Q and USP28cat Q378R and performed activity assays (Figure 35 D and E). The R385Q USP25cat Δtip variant showed an increase in catalytic activity in the presence of the UbRh110 substrate, as well as in the catalytic efficiency towards cleaving K48-linked di-Ub of about 2-fold compared

to USP25cat Δtip. Surprisingly, however, the USP28cat Q387R variant displays only 20% reduced activity on UbRh110 compared to the wt protein but we observed no change in the catalytic efficiency upon cleavage of K48-di-Ub. These results indicate that both the affinity of the substrate to the USP28cat Q378R variant (K_M) as well as the turnover rate (k_{cat}) change in the same way, so that the catalytic efficiency (k_{cat}/K_M) stays the same as for the wt protein. Although we could ‘‘activate’’ USP25 by a factor of 2 and reduce the activity for USP28 through the generation of the USP25cat Δtip R385Q and USP28cat Q378R variants, respectively, a two-fold gap in the catalytic activity of both enzymes remains, suggesting that there is another important difference between both enzymes, which we have not identified so far.

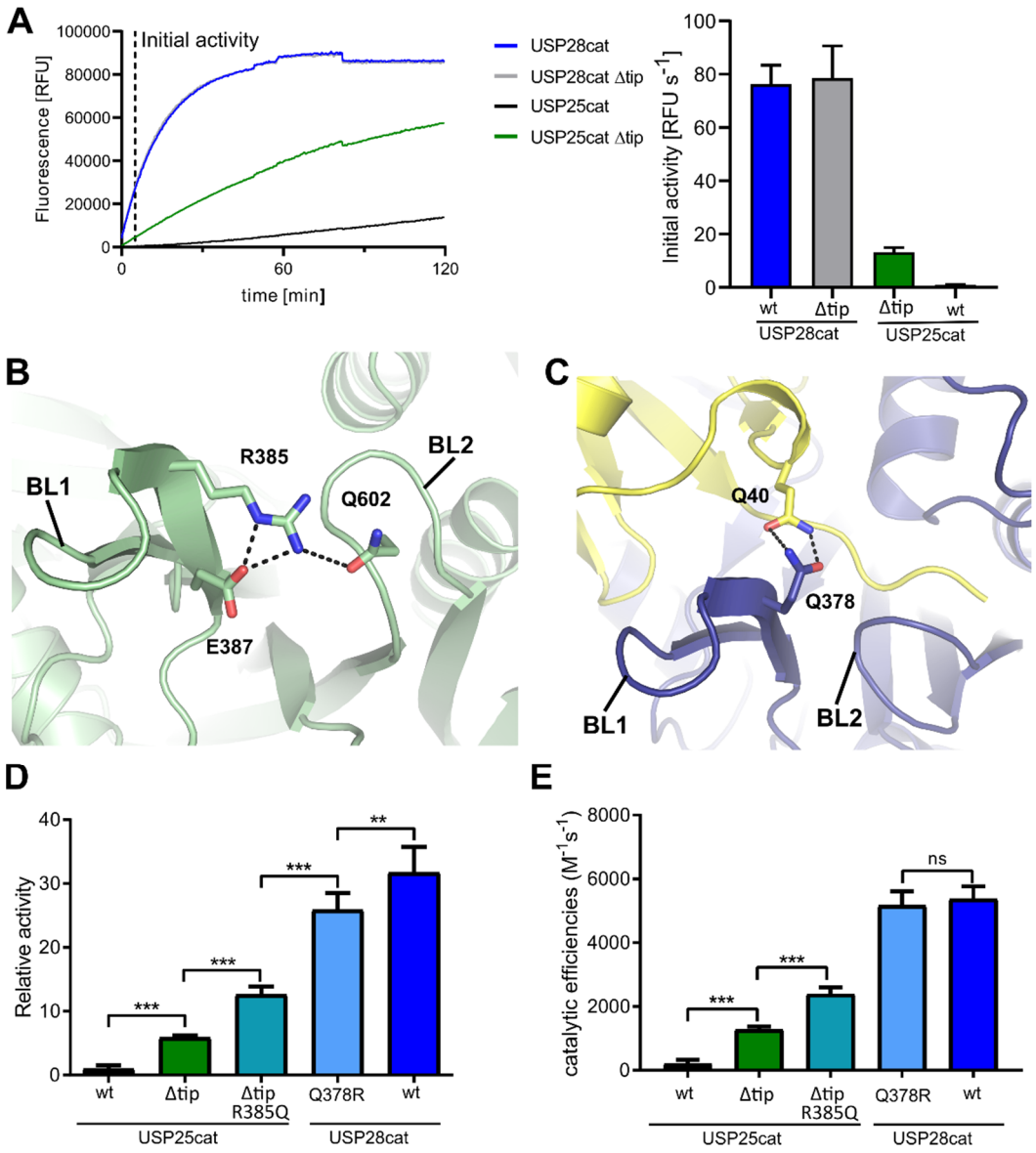

Figure 35: Differential activity of USP25 and USP28. **A)** Comparison of the catalytic activity of USP25 and USP28 in the presence of UbRh110. Fluorescence time plot (left side) of USP25, USP28 and the Δtip variants. The initial activity is indicated by dotted line. The boxplot on the right side is indicating the initial activities. Dimeric USP28 displays a 6-fold increased activity compared to dimeric USP25cat Δtip. **B)** BL1 and BL2 of USP25 are coupled. Interacting residues R385, Q602 and E387 are indicated as sticks. **C)** Q387 of USP28 interacts with ubiquitin residue Q40. Same orientation of BL1 and BL2 in the USP28cat UbPA structure. BL1 and BL2 are not linked. **D)** UbRh110 cleavage assay to determine the differences in activity between USP25, USP28 and their variants. Boxes indicate mean ± SD of the initial slopes from n=8 measurements normalized to USP25cat wt. **E)** Differences in the catalytic efficiency on K48-linked di-Ub cleavage of USP25, USP28 and their variants. Fluorescence polarization measurements were performed with different enzyme concentrations. Observed rate constants were divided by the concentrations to determine the catalytic efficiencies. The boxplot indicates the catalytic efficiency as mean ± SD of n=5-6 values. For all statistical analysis an unpaired t-test with *** $p \leq 0.001$, ** $p \leq 0.01$ and ns $p > 0.05$ was used.

III.4 USP25 auto-inhibition in the context of disease: Cancer-associated mutations activate USP25cat

To follow up the question: "What might be the biological relevance of an auto-inhibited USP25?" and to validate our previous findings, we focused on cancer-associated mutations within the catalytic domain that might have an effect on oligomerization or activity of the enzyme. Analysis of the catalogue of somatic mutations in cancer (COSMIC) database (139), revealed two mutations of USP25 residues that are located in the catalytic domain: P535 was mutated one time to Serine (mutation ID: COSM4469547) and three times to Leucine (mutation ID: COSM1413407) and E600 was mutated to Aspartic acid (mutation ID: COSM53509) in 3 independent patient samples. The mutation of P535 to L/S was found in several different tissues including the intestine, skin and biliary tract with the histology of carcinoma and the central nervous system with the histology of glioma (140, 141). In contrary, the mutation E600D was found three times in the liver with the histology of carcinoma that was associated with Hepatitis C virus infection (142, 143).

P535 is located, close to the C-terminal end of the UCID-tip (Figure 36A). The amino acid forms a *cis*-configuration leading to the above described backbone kink of the UCID tip, directing it towards the USP-domain of another dimer to form the tetramer interface. The *cis*-amide bond of P535 is further stabilized by neighboring aromatic-proline (H534 and P468, Y436 with P535) or proline-proline interactions (P537 with P463). In USP28 the majority of these stabilizing residues are identical with the exception of USP25 H534, which is substituted by USP28 Q527 (Figure 36B). This missing neighboring aromatic residue, which forms the major stabilizing interaction of the *cis*-peptide bond is possibly the reason why the conserved P528 forms a *trans*-peptide bond in USP28 instead. The *trans*-amide bond in USP28 leads to UCID-tip protrusion along the UCID- rod of the dimer mate instead of forming the kink towards a tetramer interface. The cancer mutation P535L/S should lead to the formation of a *trans*-peptide bond since neither serine nor leucine can adopt a *cis*-configuration and would thus possibly prevent the formation of the tetramer.

The second cancer-associated mutation E600D is located close to the catalytic center of USP25 (Figure 36C). In our structure, we observe that this residue is involved in the

disruption of the active site by pulling the catalytic H607 into the opposite direction of the catalytic cysteine. Furthermore, it also interacts with R556 on α10 of the UCID-rod of the molecule that interlinks the tetramer with its UCID-tip. E600 is also conserved in USP28 (USP28 E593) leading to the same ‘‘distorted catalytic site’’ in the USP28cat *apo* structure (Figure 36D). We structurally characterized the mutation in USP28cat E593D in the Ub-bound state (Figure 36D). The mutation towards Aspartic acid conserved the negative charge but led to a shortened side chain. In the USP28cat E593D-UbPA structure the interaction of the shorter D593 with H600 is no longer possible and H600 points towards the catalytic C171 leading to an ‘‘active’’ conformation of the catalytic site.

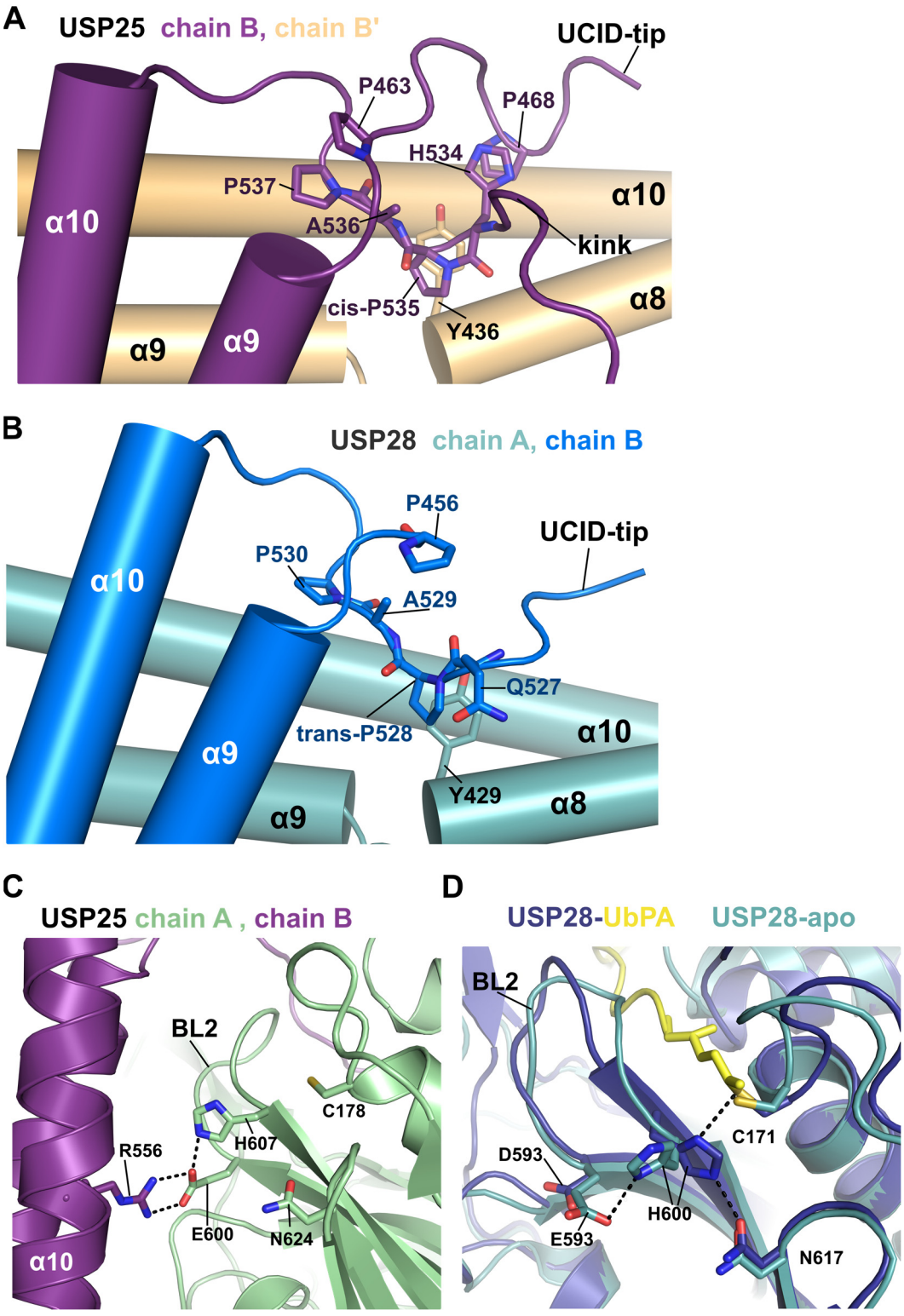

Figure 36: Position of the cancer-associated mutations. **A)** UCID-tip conformation in USP25cat. Chain B and chain B' form a USP28-like dimer in USP25. P535 adopts a *cis*-configuration that is stabilized by neighboring aromatic-proline and proline-proline interactions, indicated as sticks. *Cis*-P535 leads to a kink in the UCID-tip directing it towards the tetramer interface. **B)** UCID-tip conformation in USP28cat. USP28 dimer is formed by chain A and chain B. The conserved P528 residue forms a *trans*-peptide bond in USP28. Most of the residues are conserved between USP28 and USP25. Q527 is not able to stabilize a *cis*-configuration in USP28. **C)** Active site of USP25cat. E600 is interacting with H607 in the

opposite direction of the catalytic C178, leading to a distorted catalytic site. E600 is also interacting with R556 thereby stabilizing the tetramer. Residues are shown as sticks, H-bonds and salt bridges as dotted lines. **D)** Superposition of USP28cat *apo* and USP28cat E593D-UbPA. E593 in USP28 *apo* (teal) is interacting with H600 leading to a distorted catalytic site. In the structure of E593D-UbPA, H600 is interacting with the catalytic C171 pointing away from E593D.

To further dissect the effects of the mutations on oligomerization and catalytic activity, we purified the three variants USP25cat P535L, USP25cat P535S and USP25cat E600D and determined the oligomeric state of these cancer-associated mutations by SEC-MALS analysis (Figure 37A). As expected, we observed a delayed elution volume for the P535L/S variant compared to USP25cat and only observed dimers in solution, indicating that the introduction of a *trans*-amino-acid leads to the disruption of the tetramer formation in USP25. The other cancer-associated mutation E600D preserved the primarily tetrameric state of USP25cat wt. Next, we analyzed the catalytic activities of the variants compared to the wt protein and the dimeric USP25cat Δtip variant, utilizing the UbRh110 substrate (Figure 37B). Both Pro variants display an increased activity of about 6-fold compared to the tetrameric wt USP25cat, nearly comparable to the dimeric USP25cat Δtip variant. Surprisingly, we determined also an about 5-fold increased activity of the tetrameric USP25cat E600D variant. Further analysis of USP28cat E593D also indicate a slight but significant increase in catalytic activity towards UbRh110 compared to USP28cat wt (Figure 37C). To study the E600D variant also in an active dimeric form of USP25 we generated the USP25cat Δtip E600D variant and analyzed its catalytic efficiency towards K48-linked di-Ub in comparison to USP25cat wt, Δtip and the P535L variant (Figure 37D). In support of our previous results, we observed a comparable catalytic efficiency of the P535L and Δtip variants, which was approximately 6-fold higher than for wt-USP25. For the dimeric cancer-associated mutation Δtip E600D, a hyperactivation of the enzyme was visible with a 2-fold higher catalytic efficiency compared to the other dimeric variants. To probe if the cause of this hyperactivation is due to the ‘‘activated catalytic site’’ by prohibiting the interaction of E600 with H607, we generated mutations of E600 to Alanine and Asparagine. Both mutations should lead to the same hyperactivity, if an inactive catalytic site caused by the native E600 residue is the sole reason for the reduced catalytic activity, as observed in the USP25cat structure

(Figure 36C). Surprisingly, we observed only a slight, but significant change in activity for the USP25cat Δtip E600A and E600N variants, comparable to the slight activation of USP28 containing the E593D mutation (Figure 37C and E). Based on these results, we can only conclude that the conservation of the negative charge is essential for the unique hyperactivation of USP25 but further analyses are required to explain its origin.

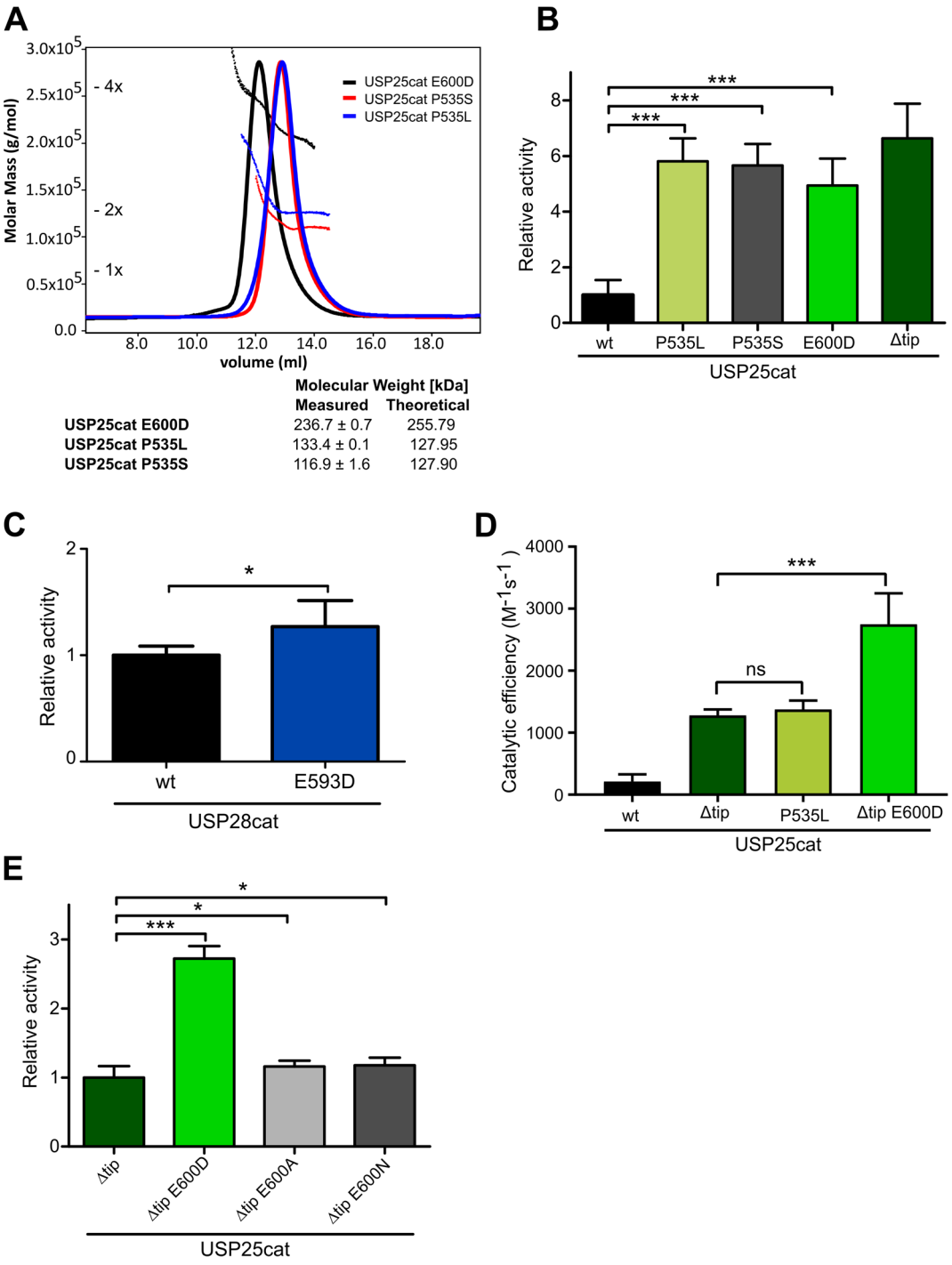

Molecular Weight [kDa]	Measured	Theoretical
USP25cat E600D	236.7 ± 0.7	255.79
USP25cat P535L	133.4 ± 0.1	127.95
USP25cat P535S	116.9 ± 1.6	127.90

Figure 37: Analysis of cancer variants. **A)** SEC-MALS analysis of USP25cat P535L/S and E600D. Both Proline mutations lead to the formation of a dimeric state, whereas E600D stays in a

tetrameric conformation. Experimentally determined and theoretical molecular masses of the particular oligomeric states are given below. Numbers on the left indicate monomeric (1x), dimeric (2x) and tetrameric (4x) theoretical masses of USP25cat wt. Data are normalized. **B)** and **C)** UbRh110 cleavage assay of USP25cat variants (B) and USP28cat compared to E593D (C). Data are normalized to the respective wt catalytic domains. The box plot indicates the mean ± SD of n ≥ 6 measurements. **D)** Catalytic efficiency of USP25 variants towards cleaving K48-linked di-Ub. The box plot indicates the mean ± SD of n ≥ 5 measurements. **E)** UbRh110 cleavage assay of USP25cat Δtip and E600 variants. Only the USP25cat Δtip E600D variant shows a hyperactivity. The box plot indicates the mean ± SD of n = 8 measurements. For all statistical analyses an unpaired t-test was used with ns, $p > 0.05$, * $p \leq 0.05$ and *** $p \leq 0.001$.

III.5 Substrate interaction studies

III.5.1.1 FBW7: substrate and interaction partner of USP28?

Several *in vivo* studies indicate that USP28 is counteracting the E3 ligase activity of the SCF (FBW7) on its substrates but also reverses its auto-ubiquitination (55, 72, 144). An interaction of USP28 with the two isoforms FBW7 α and γ was shown *in vivo* by pull down experiments (55). To study the association of USP28 and FBW7 *in vitro* and to further dissect the interacting domains, we performed analytical size exclusion chromatography using overlapping constructs of USP28.

Initial trials to obtain full-length FBW7 were not successful (data of expression tests not shown). Since crystal structures of an N-terminally shortened FBW7 variant in complex with SKP1, another component of the SCF-ligase (Figure 38A) have been solved, indicating the possibility to obtain suitable stable proteins, we generated a FBW7 construct comprising the same range (aa 262-707) and co-expressed and purified it together with SKP1 (145). The protein complex was purified by affinity chromatography following SEC (supplementary Figure 56). As the construct FBW7 262-707 does not contain the dimerization domain (DD) and we could not obtain FBW7 protein containing the full DD (data not shown), we generated a second FBW7 variant (aa 247-707) that partially includes the oligomerization sequence (Figure 38 A). After purification, we performed SEC-MALS analyses and determined a molecular mass of 119 kDa and 129 kDa for FBW7 262-707-SKP1 and FBW7 247-707-SKP1, respectively. Surprisingly, the results indicate for both samples rather a dimeric state of FBW7 (Figure 38B, D) and not as expected a monomeric form. Overall, the molar masses of the FBW7/SKP1 SEC-MALS results would roughly fit to a composition of a

dimeric FBW7 with one SKP1 bound to it (Figure 38D). For SKP1 alone we obtained a molecular weight of about 28 kDa, which is much higher than the expected monomeric form of 19 kDa and lower then a calculated dimer of about 37 kDa (Figure 38C, D). Since SKP1 is capable of forming dimers but also exists as a monomeric species our SEC-MALS result probably indicates an inseparable mixture of both (146).

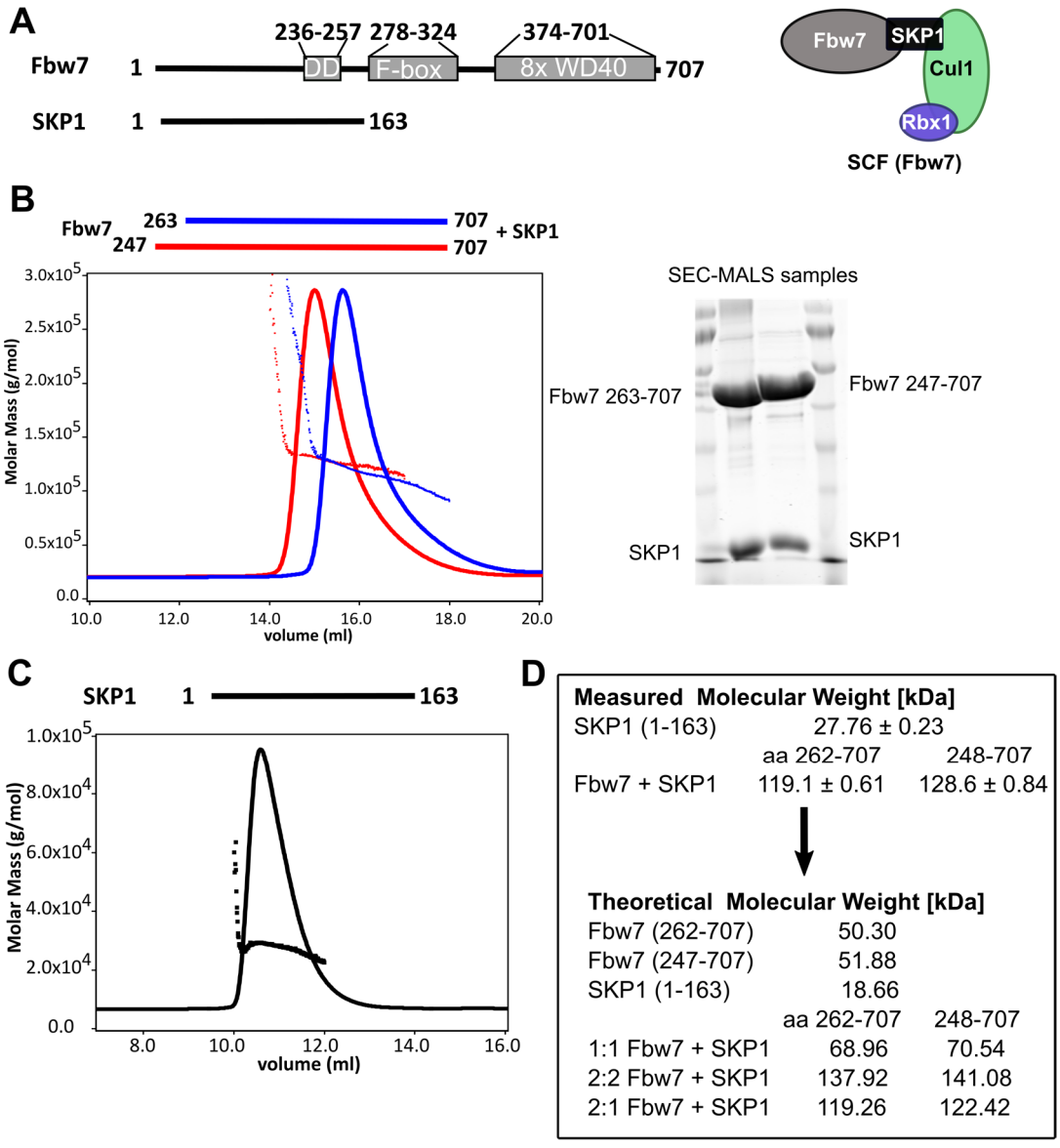

Figure 38: Constructs and SEC-MALS analysis of FBW7 and SKP1. **A)** Domain architecture of FBW7 and SKP1. FBW7 contains a dimerization domain DD, F-box and a WD40 repeat. FBW7 and SKP1 assemble together with CUL1 and RBX1 into a SCF E3 ligase. **B)** SEC-MALS analyses of FBW7 variants in complex with SKP1. Samples were analyzed on the SDS Gel, to the right. **C)** SEC-MALS analysis of SKP1. **D)** Experimentally determined and theoretical values of the FBW7/SKP1 complex determined by SEC-MALS.

We then attempted to map the interacting domain of USP28 to FBW7 262-707-SKP1 through the use of overlapping USP28 constructs (1-665, 114-730 and 114-1045, for purifications of the USP28 variants, see supplementary Figure 53) and incubated the potentially formed complexes for one hour in a 1:1 ratio of 30 µM each. Analytical SEC of the incubated samples was performed and compared to the control protein chromatograms of the single proteins, which indicated that no interaction of USP28 with FBW7 could be observed (Figure 39A). In addition, the monomeric variant of USP28cat did also not lead to an association with FBW7 262-707 (Figure 39A).

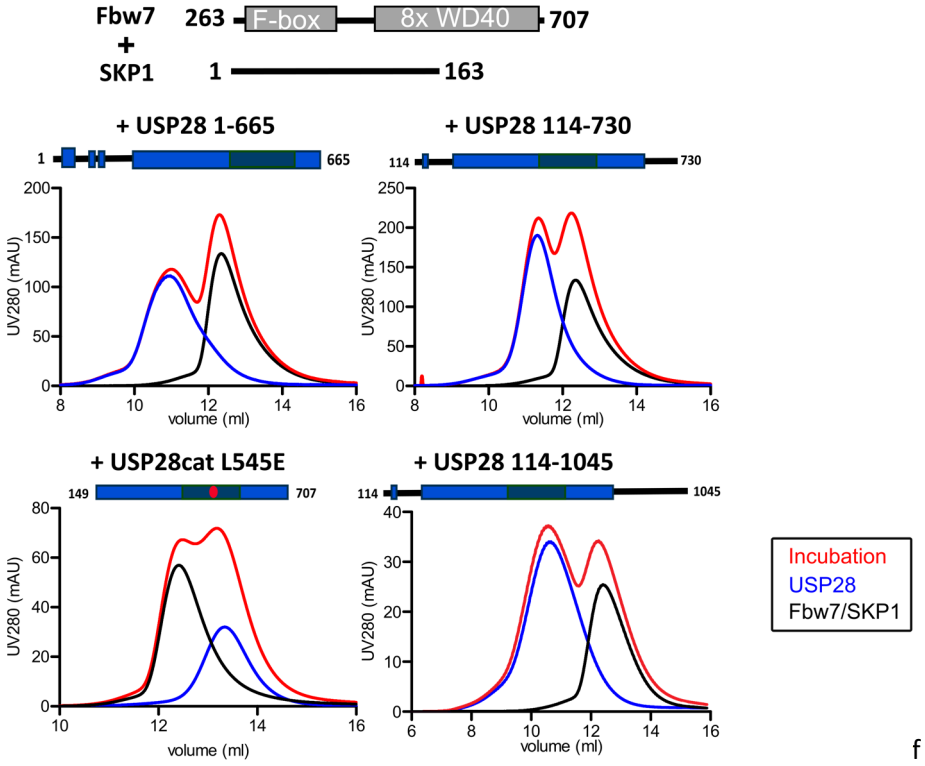

Figure 39: Interaction studies of USP28 and FBW7. Analytical SEC of the complex FBW7/SKP1 (black), USP28 variants (blue) and an incubated sample of FBW7/SKP1 and USP28 variants (red). The different USP28 variants are indicated above the chromatograms.

III.5.1.2 SV-AUC *in vitro* studies to determine the oligomeric state of TNKS-USP25 complexes

The structure and activity data revealed an auto-inhibited USP25 molecule due to a tetrameric assembly. This raises the questions: How is the USP25 tetramer regulated towards an active dimer? Does substrate binding influence the oligomeric state and thereby regulate the activity of USP25 and/ or is substrate binding compatible with the tetrameric state of USP25? Recently identified interaction partners and

substrates of USP25 are TNKS (80). Xu *et al* showed direct binding of TNKS1-ANK (aa 178-957) to a C-terminal peptide of USP25 containing residues 1049-1055, with a K_d of 6.5 μM (80). Since this interaction has already been established, TNKS1 is an ideal substrate to address the above raised questions. We purified and expressed C-terminally elongated USP25 (aa 157-1055, for the purification see supplementary Figure 57) and the TNKS-ANK repeat (aa 171-957, for the purification see supplementary Figure 58) separately and incubated both proteins in a 1:2 molar ratio respectively, prior to our analysis by SV-AUC (Figure 40A). As a control for USP25 in its activated state, we also prepared the C-terminally elongated P535L mutant (USP25 157-1055 P535L, for the purification see supplementary Figure 59). The control experiment with the isolated proteins indicated two major species for USP25cat-ct with a sedimentation coefficient of 4.5 S and 6.7 S (Figure 40B, upper panel). Using the sedimentation coefficient with the highest population of 81% of the P535L variant at 4.3 S, we could directly assign the lower population of USP25cat-ct to a dimeric state of the enzyme, which suggests the tetrameric state for the higher populated (72 %) species at 6.7 S. TNKS-ANK alone sedimented at 2.8 S with a population of 85%. Next, we analyzed the pre-incubated complexes of USP25cat-ct/TNKS-ANK and USP25cat-ct P535L/TNKS-ANK using the same method (Figure 40B, lower panel). The complex of USP25cat-ct/TNKS-ANK sediments with three major species at 2.7 S, 6.2 S and 9.0 S. For the P535L-TNKS-ANK variant, two principal species are visible, at 2.9 S and at 6.2 S. Due to the control experiments, we were able identify the species at ~3 S in the complex samples as TNKS-ANK (compare Figure 40B, upper and lower panel). The second species in the P535L/TNKS-ANK complex must therefore represent a dimeric USP25cat-ct with one or two associated TNKS-ANK molecules and the last species in the USP25cat-ct/TNKS-ANK sample at 9.0 S corresponds to a tetrameric USP25cat-ct assembly with 1-4 TNKS-ANK molecules (Figure 40).

Utilizing our UbRh110 activity assays, permitted the analysis whether substrate binding influences the activity of USP25. Consistent with our previous data we observed a reduced activity for tetrameric USP25cat-ct compared to the dimeric USP25cat-ct P535L variant. The same result was obtained for the tetrameric USP25 bound to TNKS-ANK in a higher order complex compared to the dimeric USP25cat-ct

P535L associated with TNKS-ANK. Interestingly, both complexes display a significantly decreased activity compared to their isolated USP25 variants.

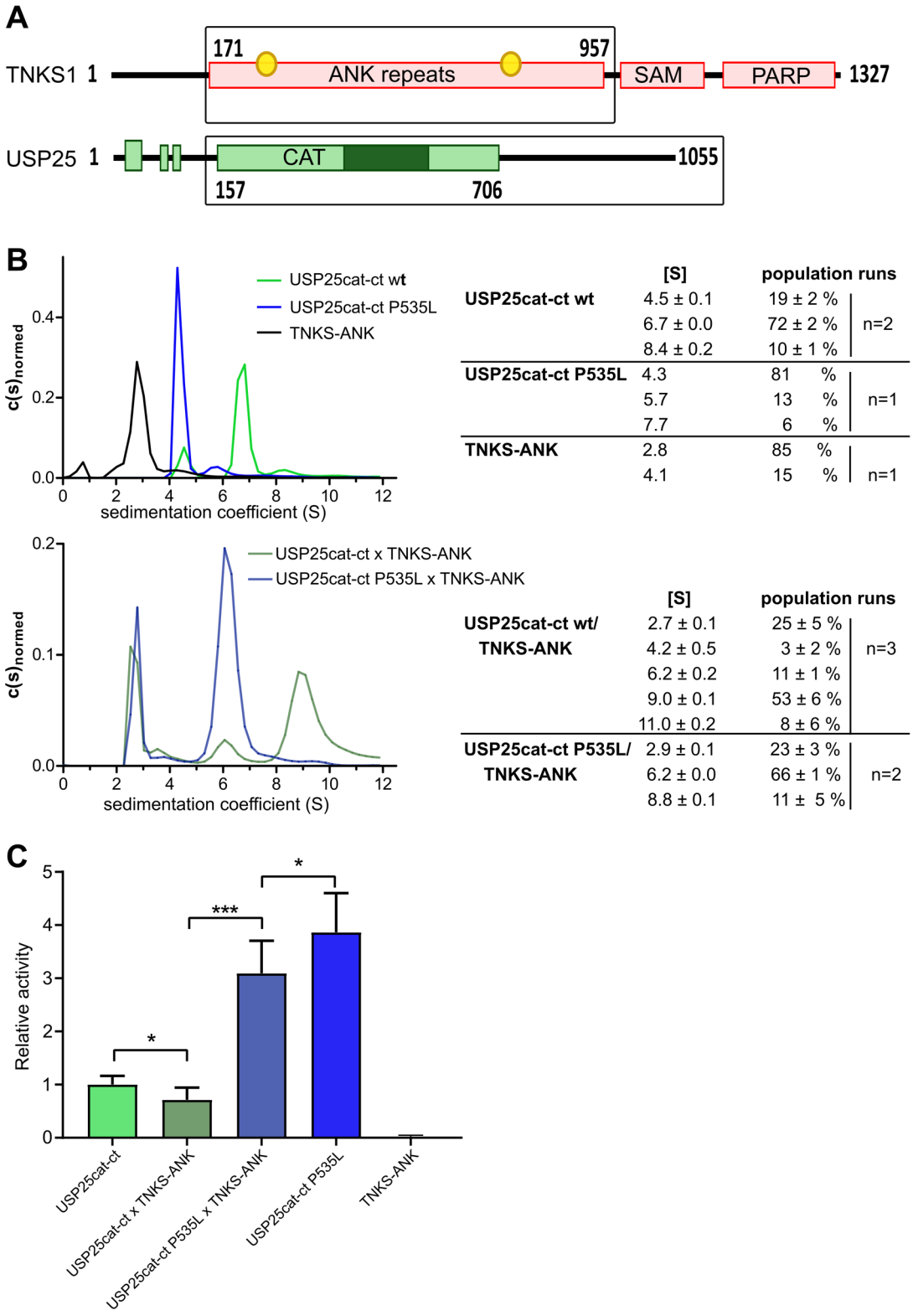

	[S]	population	runs
USP25cat-ct wt	4.5 ± 0.1	19 ± 2 %	n=2
	6.7 ± 0.0	72 ± 2 %	
	8.4 ± 0.2	10 ± 1 %	
USP25cat-ct P535L	4.3	81 %	n=1
	5.7	13 %	
	7.7	6 %	
TNKS-ANK	2.8	85 %	n=1
	4.1	15 %	

	[S]	population	runs
USP25cat-ct wt/ TNKS-ANK	2.7 ± 0.1	25 ± 5 %	n=3
	4.2 ± 0.5	3 ± 2 %	
	6.2 ± 0.2	11 ± 1 %	
	9.0 ± 0.1	53 ± 6 %	
	11.0 ± 0.2	8 ± 6 %	
USP25cat-ct P535L/ TNKS-ANK	2.9 ± 0.1	23 ± 3 %	n=2
	6.2 ± 0.0	66 ± 1 %	
	8.8 ± 0.1	11 ± 5 %	

Figure 40: Interaction studies of USP25cat-ct with TNKS-ANK. **A)** Domain architecture of TNKS1 and USP25. TNKS1 contains an ankyrin repeat region (ANK repeats), a sterile alpha

motif (SAM) and a poly-ADP-ribosyl-polymerase (PARP) domain. Two ubiquitination sites are indicated by yellow circles. Constructs used in this study are boxed. **B)** SV-AUC of the individual USP25cat-ct, P535L and TNKS-ANK samples (upper panel) and after complex formation (lower panel). On the right side, sedimentation coefficients and populations of the species are indicated. **C)** UbRh110 activity assay of USP25cat-ct, P535L and USP25-TNKS complexes. Bars represent the mean ± SD of the initial slope from n ≥ 8 measurements. For statistical analysis, an unpaired t-test was used with * $p \leq 0.05$, *** $p \leq 0.001$.

III.5.1.3 Stabilizing effect of USP25 dimers on the substrate tankyrase

Consistently, we could show that USP25 assembles into a tetramer and only displays increased activity when it adopts a dimeric state. All of our experiments, however, were performed *in vitro* and we therefore wanted to address if this is also the case *in vivo*. All of the *in vivo* experiments were performed by our collaboration partners Ravi B. Kollampally and Nikita Popov and were published along with most of the *in vitro* data in Sauer and Klemm *et al*. (126).

We probed the activity of overexpressed USP25 wt and its variants by investigating the stability of TNKS1/2 (using a bispecific antibody against TNKS1 and TNKS2) and downstream targets of the Wnt-signaling pathway in mouse KPC cells (Figure 41A). An upregulated Wnt-signaling leads to the accumulation of β-Catenin, which then increases the expression of *c-myc,* a target gene of the transcription co-activator (147). The data clearly indicates a higher stability of TNKS1/2 in cells with the overexpressed USP25 dimer variants USP25 Δtip and USP25 P535L compared to wt USP25 and also the catalytically dead mutants of each variant (CD). Consistently also β-Catenin and c-MYC proteins seem to accumulate due to the higher activity of dimeric USP25 on TNKS1/2. Additionally, we also observe increased levels of TNKS, and downstream targets, in cells overexpressing the cancer-associated mutation USP25 E600D, that led to a hyperactive USP25 *in vitro*. Importantly mRNA levels of TNKS1 and TNKS2 are not elevated in the overexpressed cells, indicating the direct effect of USP25 on the protein level (Figure 41B).

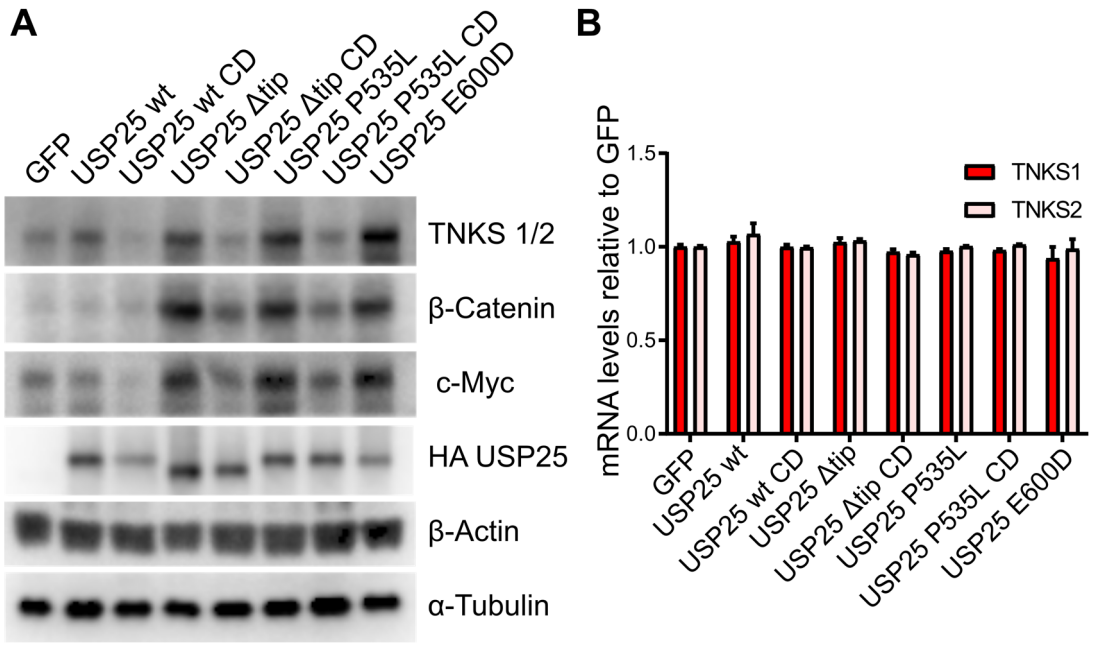

Figure 41: Stabilization of TNKS by USP25 variants *in vivo*. **A)** Retroviral over expression of USP25 variants in mouse KPC cells. Endogenous TNKS 1/2 is stabilized by dimer variants of USP25. Downstream targets of TNKS1/2 in the Wnt-signaling pathway (β-Catenin and c-MYC) accumulate upon TNKS stabilization. β-Actin and α-Tubulin function as loading controls. CD indicates the catalytically dead variants of USP25 containing the mutation C178A. **B)** mRNA levels of TNKS 1/2 upon overexpression of USP25 variants indicate no change.

III.5.2 Does ubiquitin or ubiquitin chains effect the oligomeric state of USP25?

Lastly, we also tested if the substrate Ub influences the oligomeric state of USP25. We incubated inactive USP25cat C178S with an excess of either K48- or K63-linked tri-Ub chains and performed SEC-MALS analysis and compared these results with a SEC-MALS study of USP25cat C178S in the absence of ubiquitin (Figure 42A and B). Neither chain type let to the disruption of the USP25 tetramer. Additionally, we incubated USP25cat with the suicide probe UbPA, which led to the disruption of the tetramer, to a dimeric species with bound ubiquitin Figure 42C).

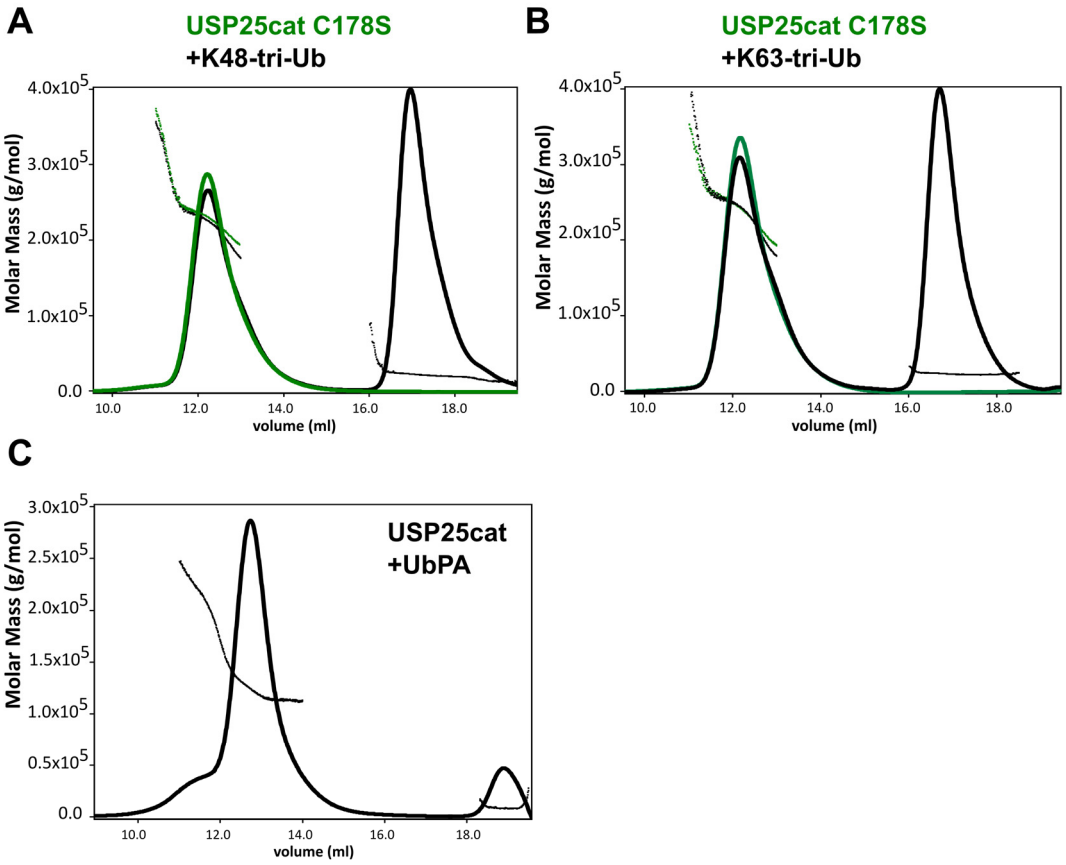

	Molecular Weight [kDa] Measured	Theoretical
USP25cat C178S	222.8 ± 5.3	256.4
USP25cat C178S + K48-tri-Ub (A, left peak)	213.1 ± 5.2	
K48-tri-Ub (A, right peak)	21.7 ± 0.8	25.5
USP25cat C178S + K63-tri-Ub (B, left peak)	223.0 ± 1.0	
K63-tri-Ub (B, right peak)	23.7 ± 0.3	25.5
USP25+ UbPA	134.3 ± 2.1	145.2 (2x USP25+ 2x UbPA)

Figure 42: SEC-MALS analyses of USP25 incubated with different Ub variants. **A)** The inactive USP25cat C178S variant incubated with K48-tri-Ub (black) compared to USP25cat C178S (green). **B)** Same as in A but using K63-linked tri-Ub chains. **C)** Active USP25cat incubated with UbPA leads to the disruption of the tetramer. Experimentally determined and theoretical molecular weights are given below.

III.6 C-terminal domains of USP25 and USP28

After having solved the structures of the catalytic domains of USP25 and USP28, which allowed us to shed light on the mechanism of oligomerization and its impact on their catalytic activities we focused on the region located C-terminally to the two catalytic domains. For both enzymes, the C-terminal part of the protein comprises more than a third of the entire protein and was so far structurally uncharacterized. Secondary structure predictions, calculated by RaptorX (120), indicate an all α-helical

domain for the C-terminal parts of USP28 and USP25, which are separated from the catalytic domains by a linker. Those structural predictions were used to define the construct boundaries for the C-terminal domains (CTs) of USP25 (aa 765-1055) and USP28 (723-1045). For the purification of the C-terminal domains, affinity chromatography with a subsequent SEC was performed (see supplementary Figure 60 for USP25CT and Figure 61 for USP28CT-2).

Crystallization trials were so far not successful for USP28CT, but led to crystals for USP25CT, of which we solved the crystal structure by SAD phasing using crystals grown from SeMet derivatized protein, to a resolution of 2.05 Å (Table III-4). The model was refined to R_{work}/R_{free} = 19/22% and reveals a unique helical fold, which could not be found upon DALI or PDB eFOLD structure comparison (Figure 43A) (110, 114). The C-terminal domain is composed of two subdomains sub1 (α1- α4) and sub2 (α5- α11, 3-10-1). A prominent linker between helix α10 and α11 is wrapping around the entire sub2 positioning helix α11 on top of helix α5, next to the border separating sub1 and sub2 (Figure 43A). Remarkably, the two subdomains are divided with respect to their electrostatic potential, with sub1 carrying a mainly positive and sub2 a mainly negative potential (Figure 43 B). The last amino acid that was visible in our structure is R1049, which is part of the known interface for the TNKS interaction (1049-**R**TPA**DG**R-1055) (80).

Since the sequence identity between the C-terminal domains of USP25 and USP28 is very high (48%), we also generated a shorter USP28 construct (USP28CT-2, aa 754-1045) corresponding to the USP25 construct (for the purification see supplementary Figure 61). To compare the fold of USP28CT-2 with USP25CT, we performed CD spectroscopy (Figure 43C). The matching spectra indicate for both constructs a predominantly α-helical domain, confirming the structural results for USP25CT. Additional SEC-MALS analysis indicate for both proteins a monomeric formation in solution (Figure 43D). Unfortunately, crystallization trials utilizing the USP28CT-2 construct were also not successful and further optimization of the USP28CT constructs may be required.

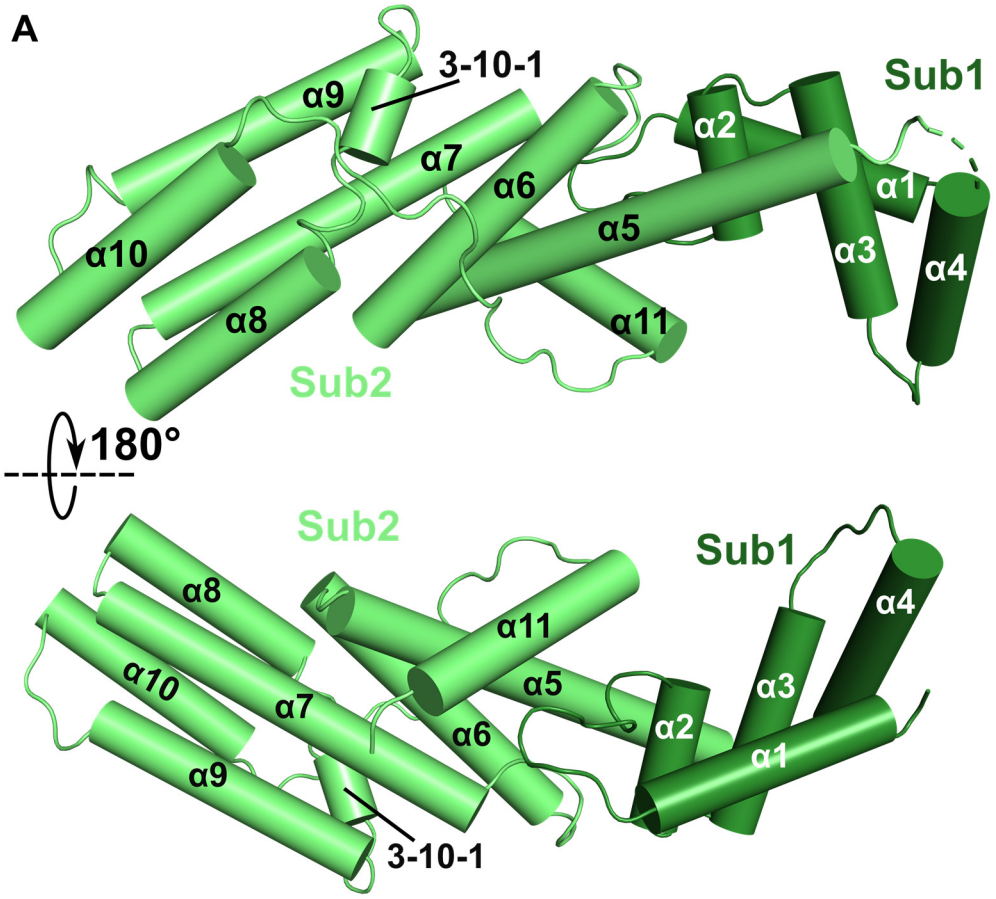

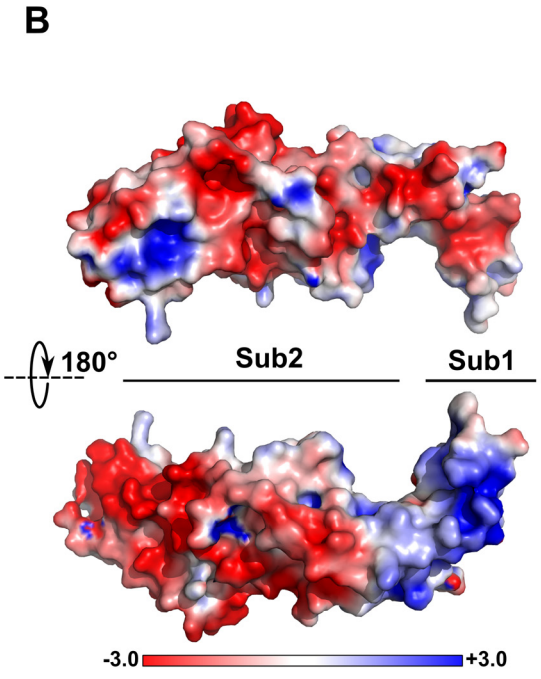

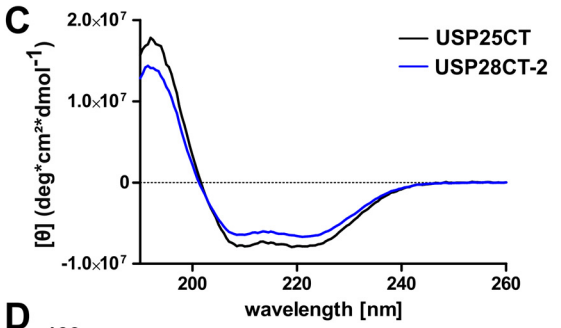

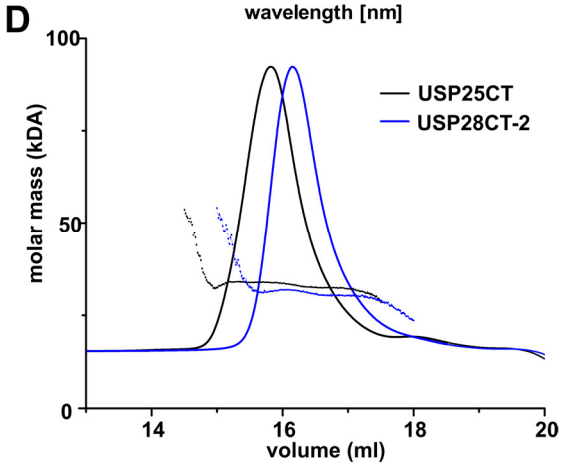

	Molecular Weight [kDa]	
	Measured	Theoretical
USP25CT	33.2 ± 0.3	34.5
USP28CT-2	31.2 ± 0.4	34.3

Figure 43: The structure of USP25 C-terminal domain. **A)** Structure of the USP25 C-terminal domain. The structure of USP25CT is composed of 11 α-helices and one 3-10 helix and split into two subdomains, Sub1 (light green) and Sub2 (dark green). **B)** Bipolar electrostatic potential of USP25CT. Sub1 is mostly positively (blue) and Sub2 mainly negatively charged (red). **C)** CD-spectroscopy of USP25CT and USP28CT-2. USP25CT (black) and USP28CT-2 (blue) indicate that the fold of both domains is highly similar and mainly α-helical. **D)** SEC-MALS analysis of USP25CT and USP28CT-2. Both proteins are monomeric. Experimentally determined and theoretical molecular weights are indicated.

Table III-4: Data collection and refinement statistics for USP25CT

USP25ct (SeMet)	
Data Collection	
PDB ID	6H4K
Space group	$P4_32_12$
Resolution range (Å)	43.50 – 2.05 (2.11 – 2.05)
Cell dimensions a,b,c (Å) α, β, γ (°)	 87.01, 87.01, 86.79 90, 90, 90
Wavelength (Å)	0.9790
Observed reflections	1064779 (65898)
Unique reflections	21553 (1608)
$R_{p.i.m}$	0.024 (0.759)
CC1/2	0.999 (0.512)
Mean *I/σI*	19.4 (1.4)
Completeness (%)	100 (99.7)
Multiplicity	49.4 (41.0)
Phasing	
Method	SAD
Resolution	2.62
Anomalous completeness	100 (99.7)
Anomalous multiplicity	23.7 (11.0)
<FOM>	0.529
Refinement	
Resolution	43.51 – 2.05 (2.09 – 2.05)
Reflections work/free	37760 / 2171 (2325 / 144)
R_{work} / R_{free}	19.2 / 22.1 (33.9 / 38.9)
Number of atoms	
Protein	2196
Ligand/ion	2
Water	57
B factors (Å²)	
Wilson B	46.1
Protein	60.5
Ligand/ion	61.6
Water	55.8
RMSD	
Bonds (Å)	0.01
Angles (°)	1.16
Ramachandran plot favored / allowed / outliers (%)	99.25 / 0.75 / 0

IV. Discussion

The following selection discusses the key findings of this project and critically assesses them in a biological context. The results are also presented and discussed in Sauer and Klemm *et al.*, published back to back with Gersch *et al.* 2019 (126, 148). Furthermore, the structure of the auto-inhibited USP25 catalytic domain was published by Liu *et al.* 2018 during revision of our manuscript (149). All three publications come to very similar conclusions and the results of this dissertation are also evaluated in consideration of these additional publications.

IV.1 Insertion site mediates oligomerization of USP25 and USP28

USP25 and USP28 are two closely related DUBs that share an overall domain architecture including an insertion site of about 170 aa within their catalytic domains (20). Despite the overall high sequence identity and conservation of USP25 and USP28 our structural and biochemical analysis revealed major differences in their oligomeric composition mediated by a novel helical domain (UCID) that corresponds to the common insertion site. In USP28 the UCID leads to the assembly of a dimer, whereas in USP25 a tetramer is formed by two interlinked USP28-like dimers.

IV.1.1 USP28 a constitutively active dimer

IV.1.1.1 The dimeric structure of USP28

The overall shape of the dimeric USP28cat can be readily compared to a cherry-couple. The globular USP domains resemble the cherries that are connected by the stems, which correspond to the upper part of the UCID-rod mediating dimer formation. Even the UCID-tip, which is mainly disordered and not visible in our structure, could be assigned to leaves on top of the stems (Figure 44).

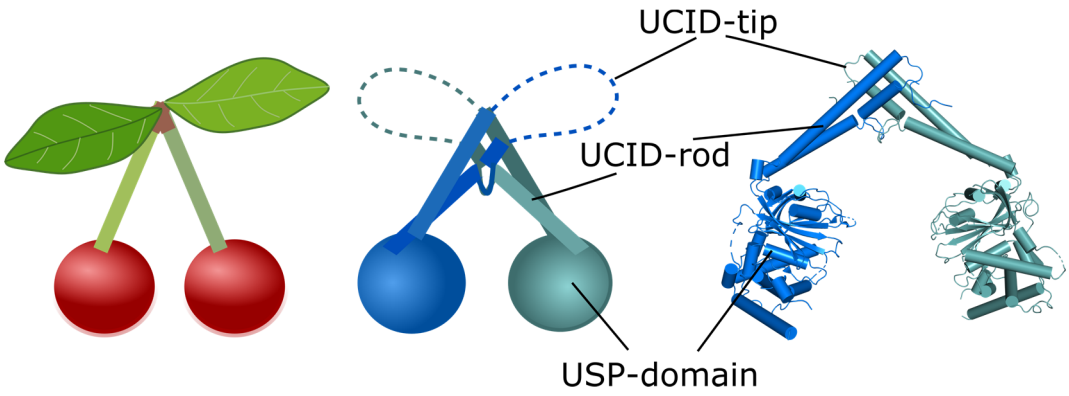

Figure 44: USP28 cherry-couple like structure. Comparison of the USP28cat *apo* structure (right) with a cherry-couple (left). Schematic figure of USP28cat is shown in the middle. The UCID-tip, -rod and UPS domain are indicated.

A closer look at the structure reveals that the USP domains adopt the common USP fold including the palm, fingers and thumb subdomains. The helical UCID stretches behind the fingers between two beta strands of the palm subdomain assigned as insertion point box 4/5 according to the USP-box annotation of Ye *et al*. (20). USP25 and USP28 share the site of insertion with 10 other USPs (20). In three of them, the insertion extends the S1 Ub-binding site of the USP by further UBAs or UIMs (USP5, USP13 and USP37) that directly contribute to the binding of Ub and partial specificity of the DUBs (24, 150, 151). In the case of CYLD, the site corresponds to a small zinc-binding B-Box that is dispensable for activity but influences the localization of the protein in the cell (129). Despite the fact that insertions were also observed in other USPs with varying positions, so far only the insertion within USP25 and USP28 is known to mediate oligomerization (126, 148, 149).

The anchoring of the UCID to the palm and fingers of the USP domain leads to a relatively fixed position of helix α8 and the lower part of α10, so that only small movements of the upper part of the UCID are possible, due to the loop between α8 and α9 (Figure 19 superposition). Furthermore, the connection of the UCID to the USP core leads to a restriction of the flexibility of the fingers that has been described in other USPs like USP8 and USP18 (152, 153). Upon removal of the complete UCID from USP28 Gersch *et al.* showed that both activity and stability of the protein was strongly reduced (148). In our studies, we observed that partial removal of the UCID (USP28cat ΔDD), leading to a monomeric variant, or the removal of the disordered

UCID-tip (USP28cat Δtip), which remains dimeric, had no influence on the activity of the protein and both variants were indistinguishable from the wt protein. We can therefore conclude that the UCID is only indirectly involved in the enzymes activity through stabilization of the core USP domain.

The symmetrical association of the upper part of the UCID rod separates the two globular USP domains by about 35 Å and directs the N- and C-termini of each molecule, which are connected with each other by polar contacts, to opposite sites.

Interestingly, the S1 ubiquitin binding sites of the USP28 dimer are also positioned towards the same direction to which the other molecules N- and C-termini are pointing. Since the catalytic domains of DUBs recognize the Ub by their primary S1 sites (10), it is tempting to speculate that the N-terminus of one molecule within the dimer, which interacts with Ub by its UBR, "feeds" the other molecule's USP domain in *trans* (Figure 45 A). But also *cis*-"feeding" by the N-terminal domain would be conceivable, with the UBR in the N-terminal domain pushing one molecule of the Ub-chain after another into the catalytic site of the DUB (Figure 45 B). Additionally, an interplay of the N- and C-terminal domains seems plausible due to the close proximity of both termini in the catalytic domain.

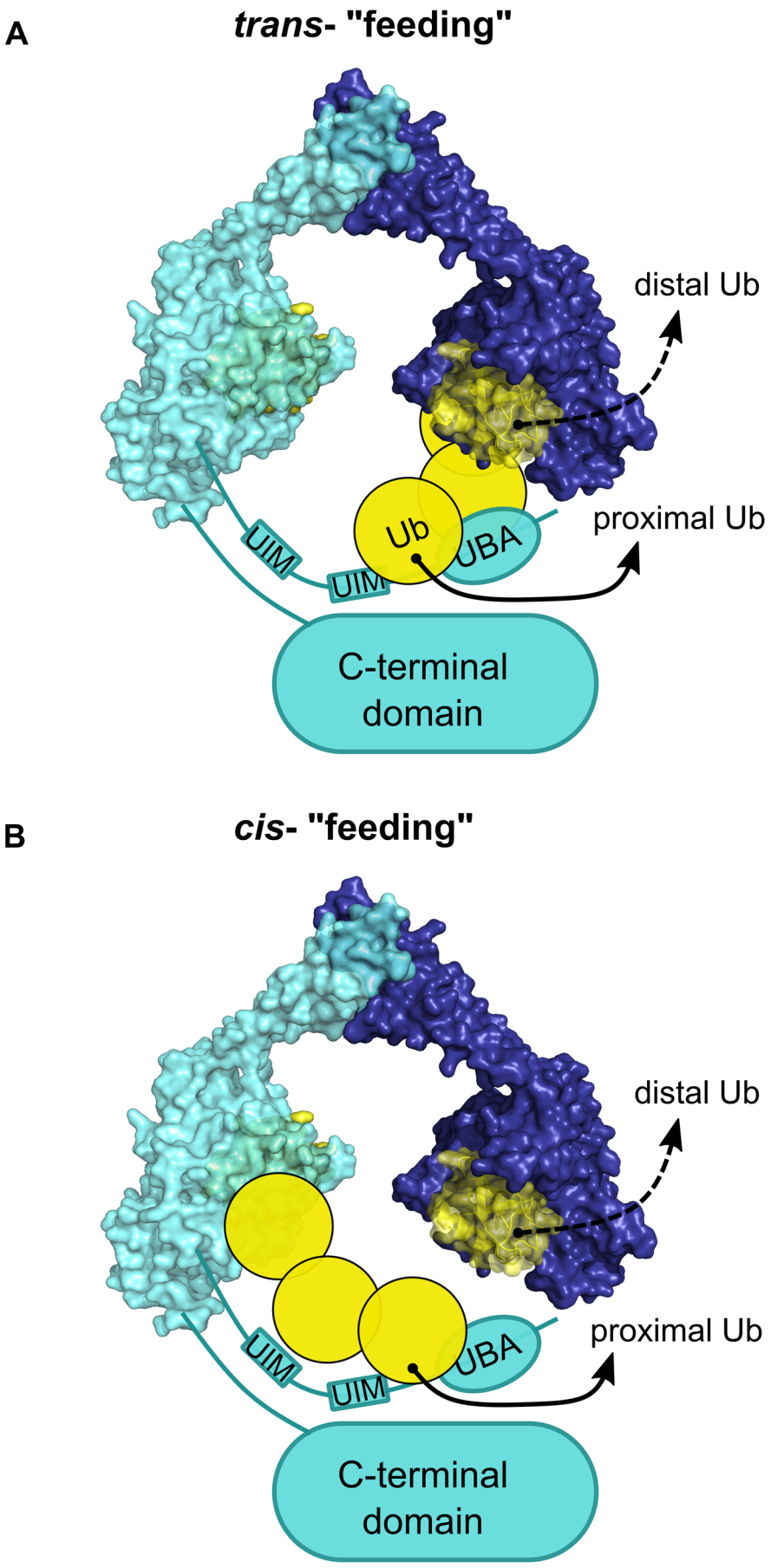
A
trans- "feeding"
distal Ub
proximal Ub
Ub
UBA
UIM
UIM
C-terminal domain
B
cis- "feeding"
distal Ub
proximal Ub
UBA
UIM
UIM
C-terminal domain

Figure 45: Models for USP28 chain-cleavage. **A)** *Trans*-feeding of one monomer to the other monomer in the dimer and **B)** *Cis*-feeding of one molecule in the dimer to itself. The structure of USP28cat- UbPA is supplemented with schematic drawings of the N-terminal and C-terminal domains. Ubiquitin chains are indicated by yellow circles. Distal and proximal Ub molecules are marked. The N-terminal domain contains two Ub interacting motifs (UIM) and one Ub associated domain (UBA).

IV.1.1.2 Ubiquitin binding sites in USP28

Distal Ub-binding to the S1 site of the USP domains has already been described in several publications (23, 25, 130, 132). Despite our low-resolution structure of USP28-UbPA at 3.5 Å we could identify a similar binding mode compared to other USPs (23, 132). A superposition of our Ub-bound structure with the USP28-UbPA structure from Gersch *et al.* (6HEK) revealed an RMSD of 0.6 Å, indicating almost identical structures and also precludes that the point mutation E593D in our structure influences Ub-binding (Figure 46) (126, 148). Smaller differences between the structures can be found in the position of the upper UCID, which can be due to the flexibility of this part (126, 148).

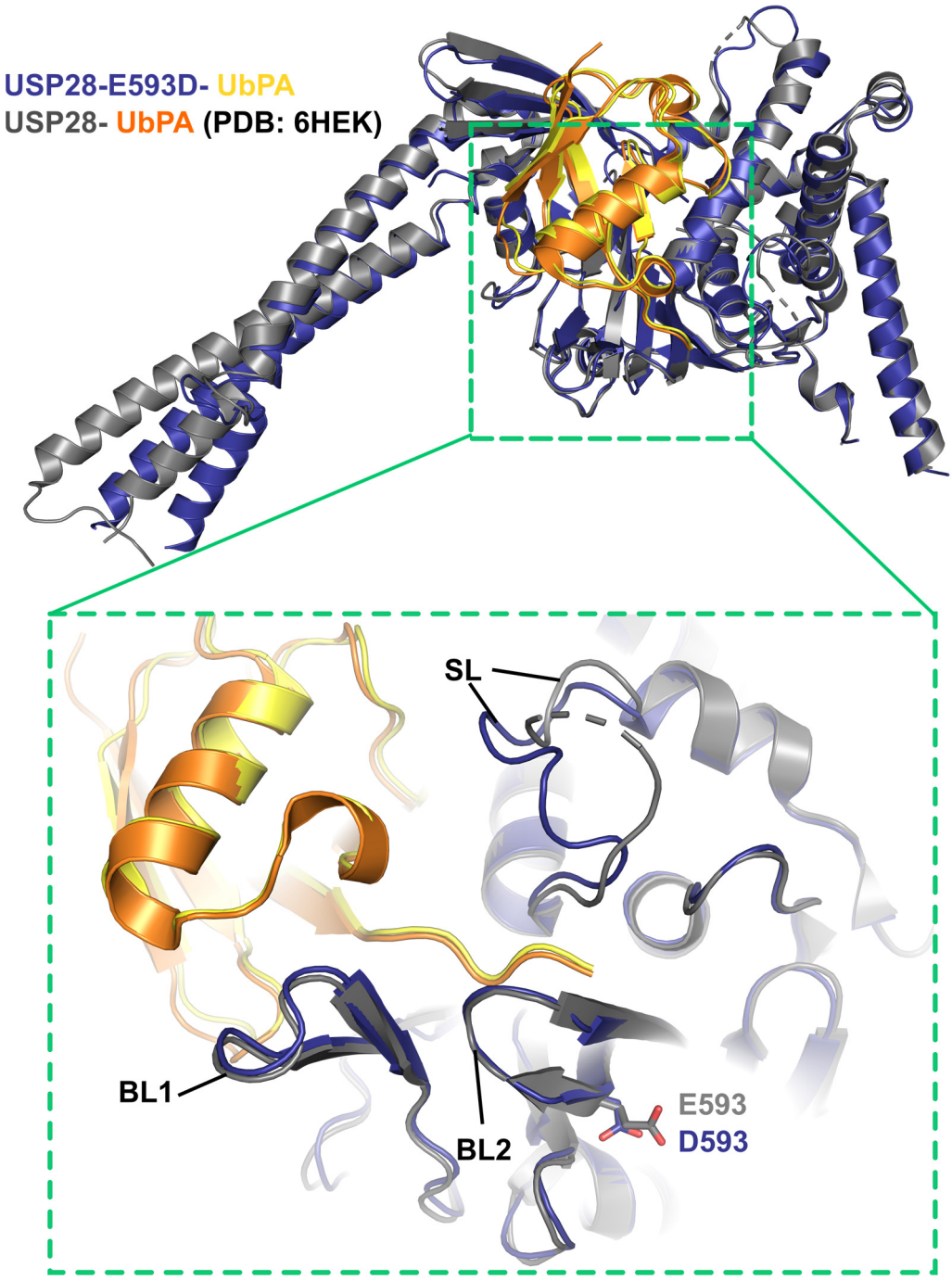

Figure 46: Superposition of USP28 E593D-UbPA and USP28-UbPA (6HEK). Overview (upper part) and detailed view of the catalytic cleft (green box, lower part) after superposition of USP28cat E593D-UbPA (dark blue and yellow) and USP28cat UbPA (grey and orange) indicating only slight differences between the two structures. The amino acids E593 and D593 are shown as sticks in the detailed view.

Furthermore, both monomers within the dimer have UbPA bound to its core USP domain confirming an independent activity of both molecules towards a minimal Ub-substrate and that Ub-binding can be achieved simultaneously. Based on the

modelling of di-Ub to our bound distal-Ub, we were able to predict the location of the proximal Ub in the S1' binding site at the opposite side of the palm domain, with the proximal Ub pointing into the same direction as the N-and C-termini of the molecule it binds to (Figure 47). Interestingly, modelling indicates sufficient space for the simultaneous binding of di-Ub supporting the statement of two independently active USP molecules in the dimer.

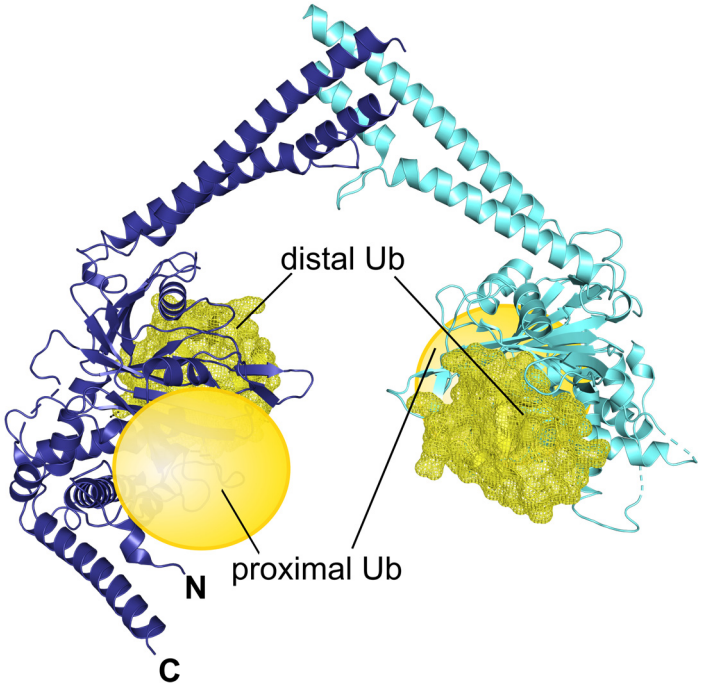

Figure 47: Position of the distal and proximal Ub in USP28. Structure of USP28cat E593D UbPA with schematic Ub (yellow circle) in the predicted proximal Ub site.

While the prediction of the S1' binding site is supported by previous findings, modelling of further Ub-binding sites (S2) onto the catalytic domain of USP28was rather unsuccessful. The model of K48-linked di-Ub to USP28 indicated serious clashes of the distal Ub with the USP domain, thus suggesting that large conformational changes of both USP28 and Ub have to take place for a longer K48-linked Ub chain to bind. For K63-linked di-Ub the modeled S2 site would only provide a minimal interaction platform with the fingers of USP28, if no rearrangements of both protein take place. In summary, structures containing a di-Ub bound to USP28 are required to clearly identify the S1' site for the proximal Ub moiety and the S2 Ub-binding site. Additionally, the second Ub-binding site (S2) may not be present on the

USP domain of USP28 but could be contributed by other domains of the enzyme. It has already been shown, that the N-terminal domain, despite its Ub-interacting sites, is dispensable for the catalytic activity and does not influence the cleavage preference of K48, K63 and K11- linked di-Ub (45). Although stated otherwise, the chain cleavage assay of Zhen *et al*. indicates a slightly increased activity on longer Ub-chains but not di-Ub for an N-terminally elongated USP28 catalytic domain (USP28 1-757) compared to the N- and C-terminal shortened construct (160-757) (45). This might indicate that the UBA and UIMs in the N-terminal domain serve as additional Ub-binding sites (S2, S3/S2',S3'), thereby supporting a more efficient cleavage of longer chains or as suggested above, "feed" the catalytic domains of the dimer in *cis* or *trans* (Figure 45 A and B). Shorter chains like di-Ub would only require the S1/S1'-Ub binding site for efficient cleavage, which would explain the similar catalytic activity of both constructs on di-Ub in Zhen *et al*. (45). In our activity assays we only used N-terminally shortened constructs of the catalytic domain of USP28 (149-707), which were able to cleave both K48- and K63- linked tetra-Ub chains. Nevertheless, without a comparison of the N- or C-terminal elongated or the full-length enzyme, we can only state that a cleavage of longer chains is possible without the N-terminus, but we currently have no information if and how the N- or C-terminal domain contribute to the catalytic activity or substrate affinity of the enzyme. Future work should address the roles of USP28's N- and C-terminal domains on the catalytic activity and efficiency towards cleaving longer Ub-chains.

IV.1.1.3 Ub-chain cleavage of USP28

In our K48- and K63-linked tetra-Ub chain cleavage assay we could not identify a clear preference of the enzyme to cleave either chain type. Strikingly though, for K63-linked chains USP28 seems to preferably cleave the higher Ub-chains (tetra-Ub or tri-Ub) first, whereas the di-Ub chains accumulate before they are processed. The cleavage of the K48-linked chains seems to be more stochastically. The same result was observed for USP25 chain cleavage. According to Pruneda and Komander the preferable cleavage of longer chains might be an indication for an S2/ S2' site on the enzyme (154). However, upon modelling K63-linked di-Ub chains to the USP28

catalytic domain structure, we were not able to determine a promising S2 site on USP28. Furthermore, in comparison to the SARS PLpro protease, which has been shown to be specific for K48-linked poly-Ub, the effect of accumulating di-Ub upon chain cleavage in USP28 is only marginal (136). Therefore, we suggest that USP28 has a slight preference for K48-linked di-Ub compared to K63-linked di-Ub, which has also been pointed out by Zhen *et al* (45).

IV.1.1.4 The function of dimeric USP28 and substrate interaction

In our *in vitro* studies, we were able to generate a USP28 monomer by introducing a charged amino acid into the hydrophobic dimer interface. Interestingly, we did not observe any differences in activity or in catalytic efficiency of a monomeric USP28 compared to the dimeric wt protein. Nevertheless, we confirmed the existence of the dimer *in vivo* by showing the self-association of USP28 in HeLa cells and conversely dimer formation was prevented using the same mutation, L545E as in our *in vitro* studies.

Intriguingly, Gersch *et al.* could show that dimer formation of USP28 *in vivo* is irrelevant for the stabilization of LSD1, since both the wt protein and a monomeric variant indicate similar activity on the substrate (148). A clear function for the dimeric USP28 is thus still unknown.

Notably, several substrates of USP28 have been found to be oligomeric, which might indicate the need for a dimeric USP28 to interact with its substrates and to efficiently process multiple components. In 53BP1 for example, the intact oligomerization domain is required for the interaction with p53 via its tandem-BRCT-domain (61). USP28 also interacts with 53BP1 on the opposite side of the BRCT-domain, suggesting a common role in the regulation of p53 (61, 155). Another substrate of USP28 is the substrate recognition component FBW7 of the SCF-E3 ligase, which includes a dimerization domain upstream of the F-box (156, 157). Dimerization of FBW7 is regulating substrate interactions and further leads to specific and robust substrate degradation (157, 158). USP28 counteracts FBW7 auto-ubiquitination and stabilizes specific substrates of the E3-ligase, like MYC and JUN (71, 144). A binary complex of USP28 with FBW7α was identified by pulldown experiments *in vivo* (55). In our

studies, we tried to elucidate the interacting domains of both proteins. Unfortunately, we were only able to express a shortened construct of FBW7 lacking the full dimerization domain. *In vitro* preparation of FBW7 was only successful by co-purification with SKP1, another component of the SCF-complex. Surprisingly, upon examination of the molecular mass of our recombinantly purified FBW7/SKP1 samples we determined for both FBW7 constructs (aa 262-707 and 247-707) a hetero-oligomeric complex that indicated higher molar masses than predicted for the anticipated heterodimeric form. The measured molecular weights corresponds to the theoretical calculated molecular weights of a self-associated FBW7 in complex with one SKP1, despite the completely (FBW7 262-707) or partially missing (FBW7 247-707) dimerization domain. The 2:1 ratio is also in agreement with the intensity of the protein bands we observed in the SDS-PAGE from the samples obtained after SEC-MALS analysis. Our data thus suggest that the dimerization domain in FBW7 may be even further extended towards the C-terminal domain, than the previous publication proposed (157). Interaction studies of the shorter FBW7 construct 263-707 in complex with SKP1 together with overlapping constructs of USP28, thereby covering the complete USP28 sequence, however, were not successful. Based on analytical size exclusion chromatography experiments, we could not obtain a stable complex or any evidence for complex formation *in vitro*. It is currently unclear whether the lack of interaction is due to the missing N-terminal part of FBW7, or if further components or proteins are required for stable complex formation. Since USP28 is counteracting FBW7 auto-ubiquitination, ubiquitin might be the missing player of the interacting complex. Moreover, in a ‘‘piggyback’’ model, it has been suggested, that USP28 interacts with MYC via binding to FBW7 (55). Therefore, also the absence of MYC might hinder an interaction of the ligase and the DUB. In this thesis the validation of the interaction was only initiated with one construct of FBW7 and overlapping USP28 variants. Future studies should extend the *in vivo* work, to determine possible posttranslational modifications or other proteins that might be involved in the interaction of USP28 and FBW7, for example with combined pull down and mass spectrometry analyses. *In vitro*, further effort should be made towards the generation of longer constructs of FBW7 and the development of a method for FBW7 auto-ubiquitination. Once a direct interaction is verified, additional methods should

be applied to probe complex formation, reaching from native gel analyses, over isothermal titration calorimetry (ITC) or thermal shift assays to co-crystallization trials. Additionally, interaction studies could be extended to other interaction partners, like MYC-peptides (46-74) that were able to pull down USP28 with and without FBW7 from *in vivo* cell lysates (72).

IV.1.2 USP25 an auto-inhibited tetramer

IV.1.2.1 The exceptional tetramerization of USP25

In contrast to USP28, we observed that the UCID of USP25 does not only mediate dimer formation but led to a higher order oligomer. The crystal structure of the catalytic domain of USP25 revealed the association of two USP28 like dimers that interlink through their UCID-tips to form a tetramer. Interestingly, the interaction of the UCID-tip with the USP domain of a neighboring molecule within the tetramer blocks the Ub-binding site and leads to an auto-inhibited state of the enzyme.

Our interface validation clearly showed that the USP25 tetramer can only be formed from USP28 like dimers (Figure 48 A) and that a "second dimer interface" of two USP25 molecules coupled by the UCID-tips to the USP domains does not stably exist (Figure 48 B).

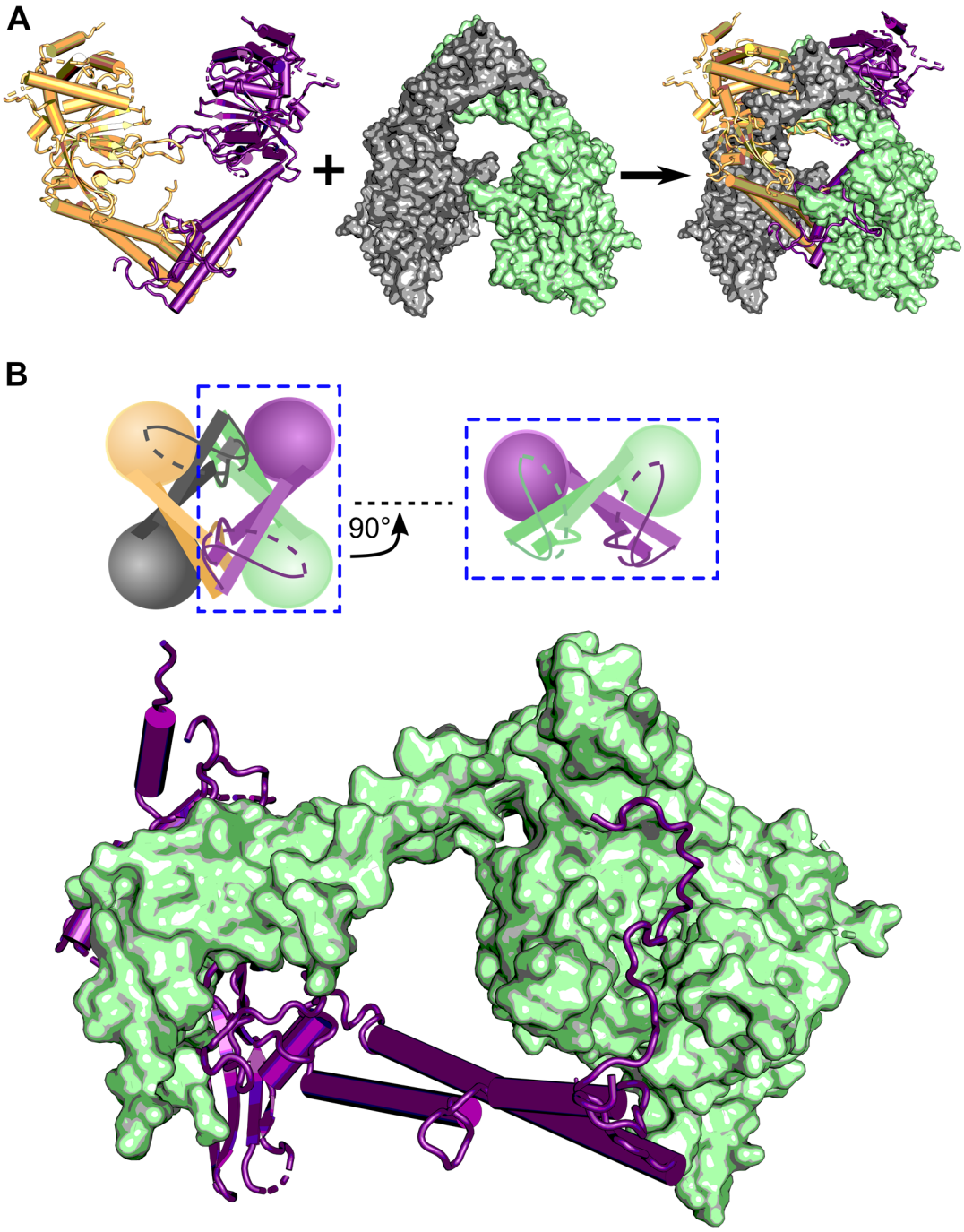

Figure 48: USP25 tetramer assembly. **A)** Model of the USP25 tetramer assembly. The USP25 tetramer is composed of two USP28-like dimers (yellow, pink and grey, green). **B)** "Second dimer interface" of USP25. Schematic view (above) and structural view of the "second dimer interface", which does not stably exist.

Nonetheless, the UCID-tip is the major driver towards tetramerization, since a removal led to the formation of dimers. Additionally, a sequence comparison of USP25 and USP28 identified that the most dissimilar region between the two proteins is located in the UCID-tip and a very high identity can be found at the UCID-binding

site on the USP domains. Chimeric variants of USP28 with the UCID-tip of USP25 or the UCID-roof of USP25, however, did not form tetramers, indicating that tetramerization is unique to USP25 and that only minor differences are sufficient to prevent tetramer formation. The inability of the USP28 chimeras to form tetramers might also be due to the missing cleft in the USP domain of USP28, to which the UCID-tip of USP25 is binding in the tetramer. In USP25 cleft opening is facilitated by helix α5, which has been shown in USP7 to be important for the regulation of its catalytic activity (93). In USP7 an activating peptide of its C-terminus is binding on the opposite side of helix α5 compared to the UCID-tip of USP25 and pushes it into an active conformation (Figure 49) (29, 93). Nevertheless, it is still unclear whether the cleft in the USP domain of USP25 is open, because of the binding of the UCID-tip that acts as a wedge and pushes helix α5 into an inactive position, as suggested by Gersch *et al.* (148), or if it is generally open so that the UCID-tip is able to bind to the open cleft. Intriguingly, USP25 tetramerization seems to be unidirectional *in vitro*, i.e. a dissociated tetramer does not reassemble from dimers, which we have shown by the incubation of the USP25cat Δtip variant with the UCID of USP25 that didn't lead to an interaction. This result suggests that the cleft closes as soon as the tetramer is disrupted. But how is tetramer formation then achieved initially? To address this question, and to determine the requirements to build an auto-inhibited tetramer, the structure of the dimeric USP25 should be solved as a basis for comparison with the tetrameric structure and to elucidate the conformational changes that probably take place.

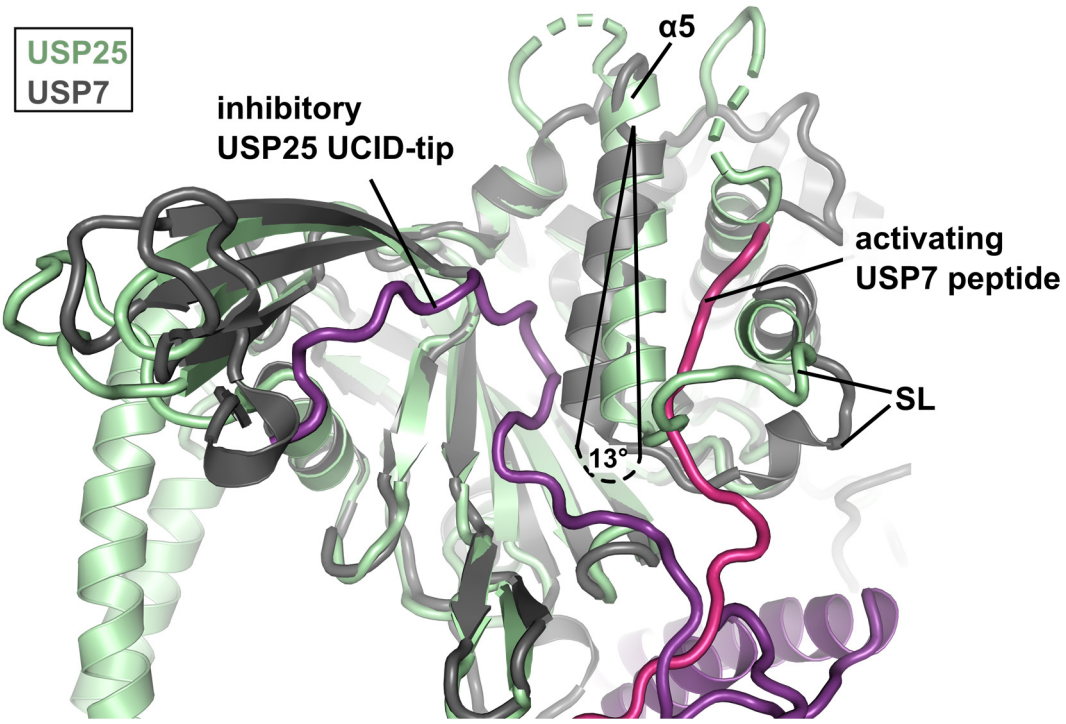

Figure 49: Superposition of USP7 (grey) and USP25 (green). The activating peptide of USP7 (pink) and inhibitory UCID-tip of USP25 (purple) are positioned on opposite sides of helix α5, which shifts by 13°. The switching loop (SL) in different positions is indicated.

IV.1.2.2 The auto-inhibition of USP25

We and two other groups could show the auto-inhibited tetrameric state of USP25, indicating its scientific importance (126, 148, 149). Upon removal of the "inhibitory" UCID-tip USP25 was activated ~6-fold and assumed a dimeric assembly, thus, indicating, that this oligomeric change from a tetramer to a dimer has to take place to fully activate the enzyme. Although the Ub-S1-binding site is blocked in the USP25 tetramer, we observed a minor activity of tetrameric USP25cat against all substrates. Especially tetra-Ub chains were cleaved after approximately 60 min compared to dimeric USP25cat Δtip, which required approximately 30 min. However, when we incubated tetrameric USP25cat with Ub-chains we could not observe a significant disruption of the tetramer, neither a dissociation of the control-wt catalytic domain after overnight incubation at 4°C, indicating that our tetrameric sample is stable and cannot be disrupted by Ub-chains. The marginal tetramer activity could be due to impurities of degraded USP25 within our samples, which was also observed on the SDS-PAGE after purification (Figure 26A). Since our SEC-MALS results indicate mainly

a tetrameric sample, the degradation might only lead to partially opened Ub-binding sites by degradation of only one UCID-tip within the tetramer (Figure 50). This would still keep the tetramer intact but lead to a partial activity of USP25. Furthermore, we cannot exclude small amounts of active dimers in our samples, since we showed that already a *cis-trans* mutation in the UCID-tip at position P535 is sufficient to disrupt the tetramer. Nevertheless, the tetrameric sample displays a strongly reduced activity compared to a dimeric sample, supporting the auto-inhibited structure.

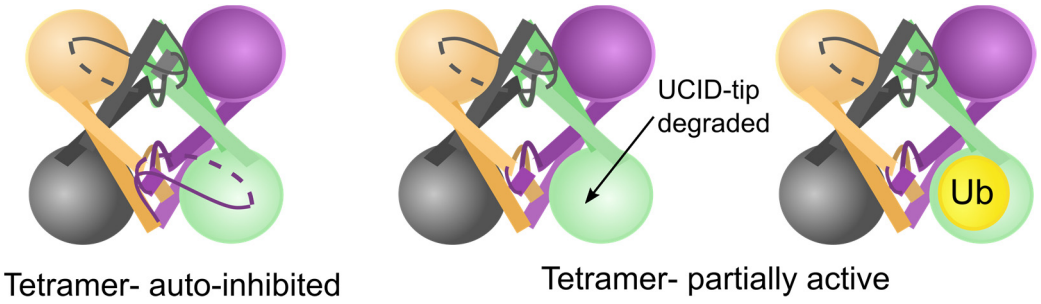

Figure 50: Model of the partially active USP25 tetramer. Schematic model of the USP25 tetramer in an auto-inhibited (left) or partially active mode (right side), due to a degraded UCID-tip (middle). Ub is indicated as yellow circle.

IV.1.2.3 Regulation of USP25 oligomerization and activity

In our studies, we observed that USP25 exists as an auto-inhibited tetramer and that it is active in a dimeric state. We could show that the cancer-associated mutation P535L prevented formation of the tetramer and led to an activation of USP25 *in vitro* and displayed an increased stabilization of the substrates TNKS1/2 *in vivo* compared to wt USP25, demonstrating that the auto-inhibited state is not an *in vitro* artefact. This result directly leads to the question, how is USP25 activated? In the studies by Gersch *et al.* and Liu *et al.* dimeric states of USP25 were identified in protein samples purified from N-terminal elongated constructs whereas constructs of USP25 containing the catalytic domain and C-terminal elongated samples were throughout tetrameric (148, 149). These combined findings suggest that a self-regulation of USP25 may be possible, with the N-terminal domain being the modulator of the higher oligomeric state and thereby also of its activity (148, 149). However, how the regulation in USP25 is achieved and if additional proteins are involved, requires further investigations. Notably, Liu *et al.* showed that dimeric and tetrameric species

could be separated and remained in their respective oligomeric states indicating no equilibrium between the two states *in vitro* (149). In contrast, Gersch *et al.* noticed the dissociation of the tetrameric species on native PAGE after incubation on ice utilizing samples from cell lysates of recombinantly expressed USP25 full-length proteins in HEK293 cells (148). Additionally, they found higher levels of endogenous dimeric USP25 than tetrameric USP25 confirming that the tetramer clearly exists in cells but that the auto-inhibited enzyme is rapidly "activated" in its natural environment (148). Combined, these findings suggest that besides the N-terminal domain of USP25 another component or condition provided by the cells regulates the oligomeric state of USP25. Consistently with the data obtained from the other two groups, we could show that a dissociated tetramer cannot reform, demonstrating a unidirectional activation mechanism in USP25.

A self-activating mechanism has also been suggested for USP7, in which the C-terminal tail of USP7 binds into a cleft on the opposite side of helix α5, compared to the USP25-tip binding cleft, leading to the stabilization of the SL in a catalytically competent position (Figure 49) (29, 93, 159). A recent publication further deciphered the activation mechanism of USP7: Initially, the ubiquitinated substrate associates with the N-terminal TRAF domain of USP7. The C-terminally located UBLs 4 and 5 facilitate the binding of Ub to the S1 site of USP7 which rearranges the catalytic triad to an active conformation that is then stabilized by the binding of the C-terminal tail into the cleft, leading to fast processing of the substrate (160). This mechanism indicates that both Ub and substrate binding collaborate towards the auto-activation of USP7 supporting the hypothesis that further components are required for the activation of USP25. Interestingly, additional regulation mechanisms for USP25 and USP28 by posttranslational modifications have already been described (43, 45, 47). Sumoylation of both enzymes at position K99 residue in the SIM motifs, located between the two UIMs in the N-terminal domain impaired Ub-chain cleavage for both USP25 and USP28 (45, 47), whereas ubiquitination of the same residue within USP25m led to activation (43). Unfortunately, the oligomeric states of the posttranslationally modified enzymes were not investigated. In future work, it would be of great interest, whether sumoylation of USP25 preserves the tetrameric state of USP25 or regulates the activated dimeric form. Furthermore, ubiquitination of the N-

terminal domain of USP25 might be the missing key for the activation mechanism leading to the formation of the dimer. In our analyses we could not observe a significant disruption of the tetramer by Ub-chains nor by the ANK-repeat region of the substrate TNKS. Notably, however, we only used catalytic domain constructs or C-terminally elongated constructs that displayed relatively stable tetramer formation *in vitro*. A possible collaboration of Ub-chains and an N-terminally elongated construct should be analyzed in future work to determine the influence of both on the oligomeric state of USP25 *in vitro*. We only observed a clear dissociation of the USP25cat tetramer *in vitro*, after incubation with the suicide probe UbPA. The dimeric state of USP25 in complex with UbPA was also determined and validated by SEC-MALS and Small-angle X-ray scattering (SAXS) data in Gersch *et al.* (148). How the covalent bond between UbPA and the catalytic cysteine can form, although the main S1-Ub recognition site is blocked is still unclear, especially, since we do not observe the dissociation of the tetramer in the presence of Ub-chains. We therefore assume that only tight interactions or covalent binding with the catalytic site rearrange the USP domain in a way that the UCID-tip loses its anchoring and USP25 dissociates into two dimers.

Overall, the results from three independent groups, which identified an auto-inhibited tetrameric USP25 that is activated upon dimerization, indicates another layer of regulation in DUB activation by oligomerization (126, 148, 149).

IV.1.2.4 Hyperactivation of USP25 by the cancer mutation E600D

In our investigations of cancer-associated mutations in USP25, we also focused on the point mutation E600D that led to a hyperactive USP25 compared to the wt and dimeric USP25cat. Interestingly, the mutation did not influence the oligomeric state of USP25 although E600 is interacting with the UCID-rod of the other dimer in the tetramer. Moreover, a corresponding mutation in USP28 E593D only led to a small increase in activity not comparable to the hyper activation of dimeric USP25, indicating a specific activation mode for USP25. Additionally, we only observed the super activation of USP25 activity, when the negative charge of E600 was conserved (Aspartic acid), but not in the Alanine or Asparagine variants. Intriguingly, in USP30

the same position is occupied by H445, which is interacting with the proximal Ub of a K6-linked di-Ub and contributes to the linkage specificity of the enzyme (Figure 51) (130). Since the superposition of the USP30 K6-di-Ub structure to USP28cat E593D UbPA indicates a similar position of the proximal Ub, the participation of USP28 E593 and USP25 E600 in proximal Ub-binding is quite likely. Moreover Gersch *et al*. could show that the mutation H445E in USP30 abrogated specificity for K6-linked di-Ub and increased especially cleavage for K11- and K48-linked chains, whereas the overall activity against Ub-KG-TAMRA was strongly reduced compared to the wt protein (130). These results suggest that also in USP25 residue E600 and in USP28 E593 might be involved in the processing of Ub by interacting with the proximal moiety. How and why the mutation USP25 E593D promotes hyperactivation and if the proximal Ub is involved, requires further analysis. Contradicting to the proximal-Ub hypothesis, however, is the fact that we also used UbRh110 as a substrate, which does not contain a second Ub moiety, but was also processed with an increased activity by USP25 E600D but not by E600A or E600N. Therefore, hyperactivation may also be caused by structural rearrangements of the USP domain of USP25 that require a negative charge but do not take place in USP28. To address this question more conclusively a structure of a dimeric USP25 *apo* and Ub-bound complex are required. Additionally, further mutations in this position to positively charged and other amino acids could be informative, to narrow down specific conditions for hyperactivation.

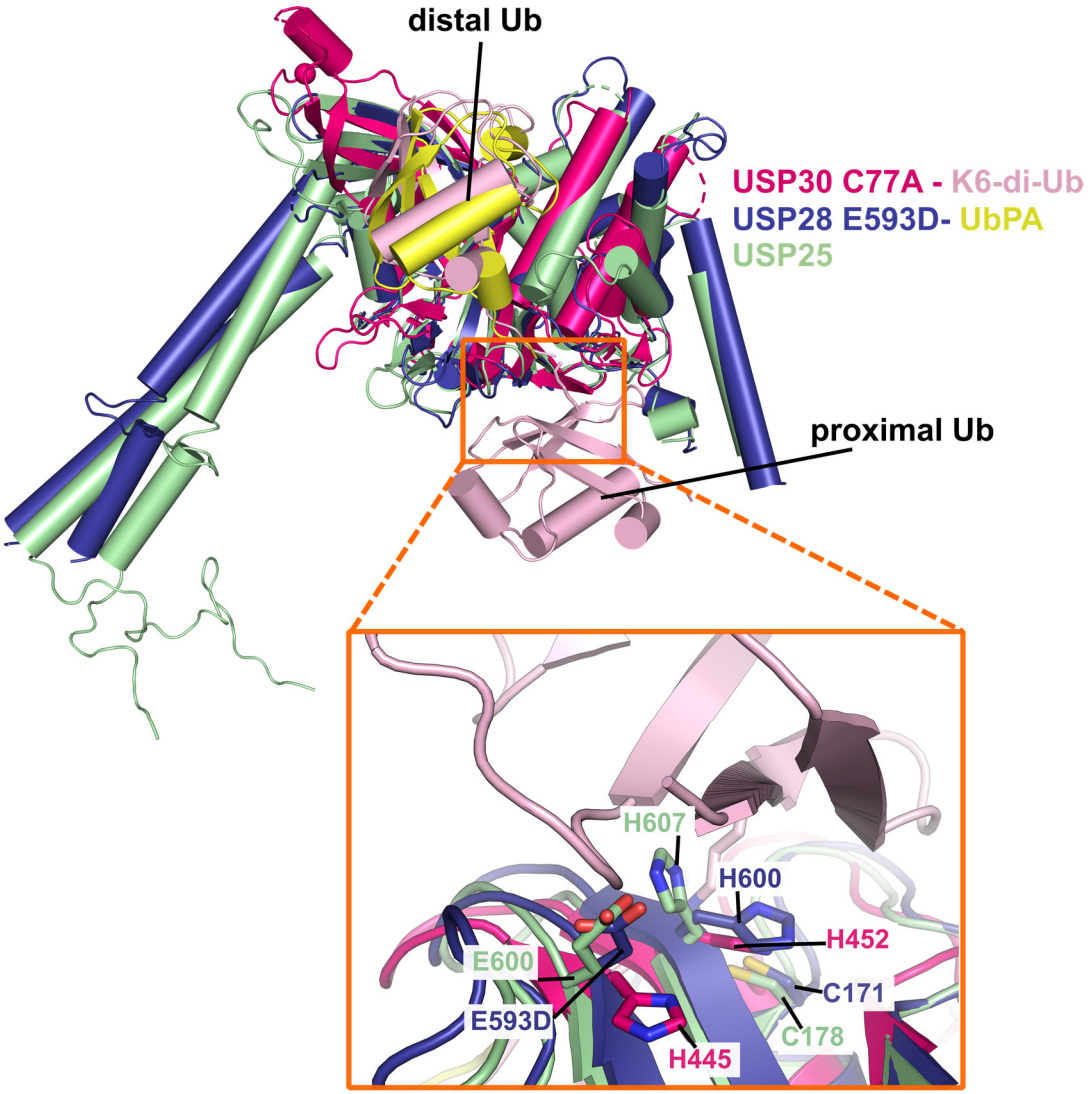

Figure 51: Superposition of USP30 in complex with K6-di-Ub, USP25 and USP28-UbPA. The overlay of the structures (USP30 C77A- K6 di-Ub (PDB: 5OHP) in dark pink and light pink, USP28 E593D-UbPA in dark blue and yellow and USP25 in green) displays a model for proximal Ub-binding in USP28 and USP25. The detailed view indicates the same position of amino acids E600 (USP25), D593 (USP28 E593D) and H445 (USP30). In USP30 C77A K6-di-Ub H445 is involved in proximal Ub-binding. Catalytic residues in USP25 with H607 and C178, USP28 H600 and C171, and USP30 H452 are shown.

IV.1.2.5 Stabilization of TNKS by USP25

Only recently TNKS1/2 were identified as substrates for USP25 and described to directly interact with the C-terminal tail of USP25 (80). We showed that USP25 can interact with TNKS both, in its dimeric and its tetrameric form and that simple substrate binding, does not induce dissociation of the USP25 tetramer. In cell-based assays we could then demonstrate, that artificially introduced mutations within

USP25 that cause dimer formation led to an increased stabilization of TNKS, which was independent from its transcription levels. Additionally, both of the cancer-associated mutations indicated a similar effect of upregulated substrate as expected from our *in vitro* assays. Highly compatible results were also obtained by Liu *et al.* showing an increased stabilization of TNKS in HEK293 cells for dimeric USP25 compared to wt USP25 (149). Taken together, this indicates a biological relevance for the auto-inhibited tetrameric USP25, whose regulation mechanism of auto-inhibition and activation still needs to be elucidated.

IV.2 Differential activity of USP25 and USP28 dimers

Our combined structural and biochemical analyses revealed the oligomeric state as the most important distinction between USP25 and USP28. As discussed above, tetramerization adds another layer of regulation to USP25, which needs to be overcome to fully activate the protein. The active form of USP25 is dimeric, which is similar to the constitutively active USP28 dimer. Nevertheless, and despite the same conformation, we observed striking differences in their activities, with the USP25 dimer being 6-fold less active and efficient than the USP28 dimer. We could enhance the activity of the USP25 dimer 2-fold by substituting R385 with Glutamine, the latter being the amino acid present in this position in USP28 (Q378). Since R385 in USP25 is interacting with an amino acid in BL2, the mutation to Glutamine could uncouple BL1 and BL2 of USP25, which might permit faster Ub processing. Moreover, Q378 in USP28 interacts with Q40 of Ub, indicating, that the point mutation in USP25 R385Q contributes to the stabilization of Ub, leading to a more efficient cleavage. The opposing mutation in USP28 Q378R also led to an expected decrease in UbRh110 cleavage, but surprisingly, did not affect the catalytic efficiency in K48-linked di-Ub processing, indicating that both the turnover rate (k_{cat}) and the substrate affinity (K_M) change proportionally. To verify this assumption, assays should be performed to determine the K_M and k_{cat} for this variant and wt USP28 separately.

Another reason for the overall higher activity of dimeric USP28 compared to dimeric USP25 could also lie in the position of helix α5. As already discussed above, this helix plays an important role in the activation of USPs and based on our structures we

speculate, that the shift of helix α5 is the main reason for the "open" cleft in USP25, to which the UCID-tip is binding. Interestingly, in the USP25 tetramer structure we also observe interactions on the other side of the tip-binding cleft, stabilizing helix α5 in the pulled up position. Coherent with this observation, the SL in USP25 is shorter, compared to USP28, which is due to a longer helix α4 and thereby supports the positioning of helix α5. In USP28 the SL seems to be a highly flexible loop that was disordered in the *apo* structure, and became ordered upon Ub-binding acting as a lid on top of the catalytic cleft (Figure 19). Combined, the shorter SL in USP25 and the pulled up position of helix α5, might impede with a dynamic exchange of ubiquitin in the catalytic cleft and could thereby cause the decreased activity and efficiency compared to USP28. The significance for a flexible BL1 and SL in USPs for Ub processing has already been shown for other DUBs like, USP7, USP4 and USP14 (29, 134, 161).

IV.3 The C-terminal domain as interaction platform?

In several publications, the C-terminal region of USP25 was suggested to be the interacting part for substrate binding. Besides TNKS1/2 that interact with the very C-terminal amino acids of USP25 also TRAF3, TRAF6 and SYK could be associated with the C-terminal region of USP25 (51, 76, 80). Our analysis of the C-terminal region showed that the last 765 amino acids assume a folded domain that is connected by a linker of about 60 amino acids to the USP domain. The C-terminal domain of USP25 is mostly α-helical with a novel fold. In addition, we showed that the tetrameric state of USP25 is preserved in a C-terminally elongated USP25 catalytic domain, indicating that the USP25ct does not regulate auto-inhibition. So far, we could not determine the crystal structure for the C-terminal domain of USP28 but our analysis utilizing CD-spectroscopy indicated also a helical fold that is most likely similar to the C-terminal domain of USP25. Comparable results for USP25 and USP28ct were also obtained by Gersch *et al.* (148).

With the C-terminal domain acting as an interaction platform and the N-terminal domain playing a role towards activation and regulation of USP25, as discussed

before, it will be exciting to elucidate how both domains collaborate in the regulation and activation mechanism of USP25.

In USP28, several binding sites for substrate interactions are not defined so far but the high sequence conservation of the C-terminal domains of USP28 and USP25 suggests a similar function. In the dimeric crystal structure of the catalytic domain of USP28, the close proximity of N- and C termini imply a tight collaboration of both domains. The proposal of a substrate platform with respect to the C-terminal domain can be used to complete our previous model for *cis*- or *trans*-feeding of dimeric USP28, which can also be extended to the active dimeric USP25:

Ub-bound substrates, associate with the C-terminal domain utilizing their interaction motifs. The substrate bound Ub-chains are stabilized through the N-terminal domain providing further Ub-binding sites. Together, the C- and N-terminal domains feed the USP domains in *cis* or *trans* (Figure 52).

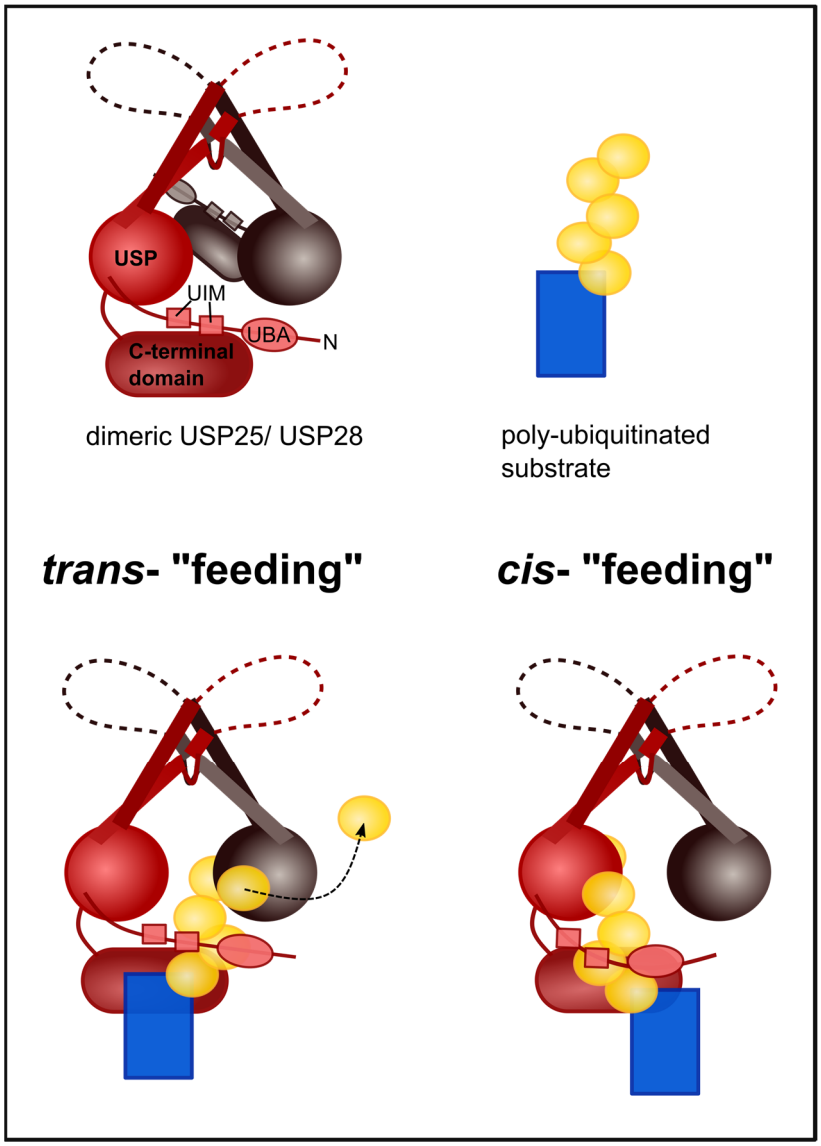

Figure 52: Extended model for substrate processing in USP25 and USP28. Schematic model for Ub-chain cleavage attached to its substrates. The upper panel indicates a model for dimeric USP25/28 including the N- and C-terminal domain (left side) and a poly-ubiquitinated substrate (yellow circles and blue rectangle respectively). The lower panel indicates different models for substrate processing by *trans*-feeding of one monomer in the dimer to the other (left side) or *cis*-feeding (right side) of the monomer to itself. The C-terminal domain interacts with the substrate. Ub chains are processed through the support of the N-terminal domains.

IV.4 Closing remarks

Since deubiquitinases come more and more into focus as pharmaceutical targets, the elucidation of their biological function, their regulation mechanisms, and their activation or inhibition conditions are essential for future medical approaches. Because of their biological functions, the two DUBs USP25 and USP28 are of specific interest for the development of anti-cancer drugs (88). Due to their high identity, previous trials to target only one of the two USPs were not successful (101). Our analysis on USP25 and USP28 highlights important structural and functional differences that can be exploited for the development of specific small molecules using structure based drug design. The auto-inhibition of USP25 by higher order oligomerization *in vitro* and *in vivo* indicates a novel regulation mechanism of USPs with biological and scientific significance (126, 148, 149). Both USP25 and USP28 are active in a cherry-couple-like dimeric state, with two independent catalytic sites. The relevance of dimerization is still unclear, although a *trans*-model for ubiquitin processing can be envisioned and we propose a significance towards substrate binding. Future work should address the function of the dimeric USP25/28 and investigate substrate-enzyme interactions, also with respect to the C-terminal domains. Together with the previously published NMR structure of the USP25 N-terminal domain (43), our structures of the USP25 catalytic and C-terminal domains provide a full view of the entire enzyme. These structural insights are the foundation for future investigations to understand the regulation mechanisms and function of ubiquitin specific proteases.

V. Literature

1. Swatek KN, Komander D. Ubiquitin modifications. Cell Res. 2016;26(4):399-422.

2. Yau R, Rape M. The increasing complexity of the ubiquitin code. Nat Cell Biol. 2016;18(6):579-86.

3. Komander D, Rape M. The ubiquitin code. Annu Rev Biochem. 2012;81:203-29.

4. Rape M. Ubiquitylation at the crossroads of development and disease. Nat Rev Mol Cell Biol. 2018;19(1):59-70.

5. Gomez-Diaz C, Ikeda F. Roles of ubiquitin in autophagy and cell death. Semin Cell Dev Biol. 2018.

6. Schulman BA, Harper JW. Ubiquitin-like protein activation by E1 enzymes: the apex for downstream signalling pathways. Nat Rev Mol Cell Biol. 2009;10(5):319-31.

7. Ye Y, Rape M. Building ubiquitin chains: E2 enzymes at work. Nat Rev Mol Cell Biol. 2009;10(11):755-64.

8. Buetow L, Huang DT. Structural insights into the catalysis and regulation of E3 ubiquitin ligases. Nat Rev Mol Cell Biol. 2016;17(10):626-42.

9. Komander D, Clague MJ, Urbe S. Breaking the chains: structure and function of the deubiquitinases. Nat Rev Mol Cell Biol. 2009;10(8):550-63.

10. Mevissen TET, Komander D. Mechanisms of Deubiquitinase Specificity and Regulation. Annu Rev Biochem. 2017;86:159-92.

11. Abdul Rehman SA, Kristariyanto YA, Choi SY, Nkosi PJ, Weidlich S, Labib K, et al. MINDY-1 Is a Member of an Evolutionarily Conserved and Structurally Distinct New Family of Deubiquitinating Enzymes. Mol Cell. 2016;63(1):146-55.

12. Kwasna D, Abdul Rehman SA, Natarajan J, Matthews S, Madden R, De Cesare V, et al. Discovery and Characterization of ZUFSP/ZUP1, a Distinct Deubiquitinase Class Important for Genome Stability. Mol Cell. 2018;70(1):150-64 e6.

13. Hewings DS, Heideker J, Ma TP, AhYoung AP, El Oualid F, Amore A, et al. Reactive-site-centric chemoproteomics identifies a distinct class of deubiquitinase enzymes. Nat Commun. 2018;9(1):1162.

14. Hermanns T, Pichlo C, Woiwode I, Klopffleisch K, Witting KF, Ovaa H, et al. A family of unconventional deubiquitinases with modular chain specificity determinants. Nat Commun. 2018;9(1):799.

15. Haahr P, Borgermann N, Guo X, Typas D, Achuthankutty D, Hoffmann S, et al. ZUFSP Deubiquitylates K63-Linked Polyubiquitin Chains to Promote Genome Stability. Mol Cell. 2018;70(1):165-74 e6.

16. Park CW, Ryu KY. Cellular ubiquitin pool dynamics and homeostasis. BMB Rep. 2014;47(9):475-82.

17. Callis J. The ubiquitination machinery of the ubiquitin system. Arabidopsis Book. 2014;12:e0174.

18. Amerik AY, Hochstrasser M. Mechanism and function of deubiquitinating enzymes. Biochimica et Biophysica Acta (BBA) - Molecular Cell Research. 2004;1695(1):189-207.

19. Clague MJ, Urbe S, Komander D. Breaking the chains: deubiquitylating enzyme specificity begets function. Nat Rev Mol Cell Biol. 2019.

20. Ye Y, Scheel H, Hofmann K, Komander D. Dissection of USP catalytic domains reveals five common insertion points. Mol Biosyst. 2009;5(12):1797-808.

21. Verma S, Dixit R, Pandey KC. Cysteine Proteases: Modes of Activation and Future Prospects as Pharmacological Targets. Front Pharmacol. 2016;7:107.

22. Clague MJ, Barsukov I, Coulson JM, Liu H, Rigden DJ, Urbe S. Deubiquitylases from genes to organism. Physiol Rev. 2013;93(3):1289-315.

23. Hu M, Li P, Li M, Li W, Yao T, Wu JW, et al. Crystal structure of a UBP-family deubiquitinating enzyme in isolation and in complex with ubiquitin aldehyde. Cell. 2002;111(7):1041-54.

24. Zhang YH, Zhou CJ, Zhou ZR, Song AX, Hu HY. Domain analysis reveals that a deubiquitinating enzyme USP13 performs non-activating catalysis for Lys63-linked polyubiquitin. PLoS One. 2011;6(12):e29362.

25. Ye Y, Akutsu M, Reyes-Turcu F, Enchev RI, Wilkinson KD, Komander D. Polyubiquitin binding and cross-reactivity in the USP domain deubiquitinase USP21. EMBO Rep. 2011;12(4):350-7.

26. Paudel P, Zhang Q, Leung C, Greenberg HC, Guo Y, Chern YH, et al. Crystal structure and activity-based labeling reveal the mechanisms for linkage-specific substrate recognition by deubiquitinase USP9X. Proc Natl Acad Sci U S A. 2019;116(15):7288-97.

27. Zhu X, Ménard R, Sulea T. High incidence of ubiquitin-like domains in human ubiquitin-specific proteases. 2007;69(1):1-7.

28. Clerici M, Luna-Vargas MP, Faesen AC, Sixma TK. The DUSP-Ubl domain of USP4 enhances its catalytic efficiency by promoting ubiquitin exchange. Nat Commun. 2014;5:5399.

29. Faesen AC, Dirac AM, Shanmugham A, Ovaa H, Perrakis A, Sixma TK. Mechanism of USP7/HAUSP activation by its C-terminal ubiquitin-like domain and allosteric regulation by GMP-synthetase. Mol Cell. 2011;44(1):147-59.

30. Kim HT, Goldberg AL. UBL domain of Usp14 and other proteins stimulates proteasome activities and protein degradation in cells. 2018;115(50):E11642-E50.

31. de Jong RN, Ab E, Diercks T, Truffault V, Daniels M, Kaptein R, et al. Solution structure of the human ubiquitin-specific protease 15 DUSP domain. J Biol Chem. 2006;281(8):5026-31.

32. Walden M, Masandi SK, Pawlowski K, Zeqiraj E. Pseudo-DUBs as allosteric activators and molecular scaffolds of protein complexes. Biochem Soc Trans. 2018;46(2):453-66.

33. McCullough J, Row PE, Lorenzo O, Doherty M, Beynon R, Clague MJ, et al. Activation of the endosome-associated ubiquitin isopeptidase AMSH by STAM, a component of the multivesicular body-sorting machinery. Curr Biol. 2006;16(2):160-5.

34. Worden EJ, Padovani C, Martin A. Structure of the Rpn11-Rpn8 dimer reveals mechanisms of substrate deubiquitination during proteasomal degradation. Nat Struct Mol Biol. 2014;21(3):220-7.

35. Matyskiela ME, Martin A. Design principles of a universal protein degradation machine. J Mol Biol. 2013;425(2):199-213.

36. Mevissen TE, Hospenthal MK, Geurink PP, Elliott PR, Akutsu M, Arnaudo N, et al. OTU deubiquitinases reveal mechanisms of linkage specificity and enable ubiquitin chain restriction analysis. Cell. 2013;154(1):169-84.

37. Eletr ZM, Wilkinson KD. Regulation of proteolysis by human deubiquitinating enzymes. Biochimica et Biophysica Acta (BBA) - Molecular Cell Research. 2014;1843(1):114-28.

38. Larsen CN, Krantz BA, Wilkinson KD. Substrate specificity of deubiquitinating enzymes: ubiquitin C-terminal hydrolases. Biochemistry. 1998;37(10):3358-68.

39. Zhou Z-R, Zhang Y-H, Liu S, Song A-X, Hu H-Y. Length of the active-site crossover loop defines the substrate specificity of ubiquitin C-terminal hydrolases for ubiquitin chains. 2012;441(1):143-9.

40. Matos CA, de Almeida LP, Nobrega C. Machado-Joseph disease/spinocerebellar ataxia type 3: lessons from disease pathogenesis and clues into therapy. J Neurochem. 2019;148(1):8-28.

41. Valero R, Bayes M, Francisca Sanchez-Font M, Gonzalez-Angulo O, Gonzalez-Duarte R, Marfany G. Characterization of alternatively spliced products and tissue-specific isoforms of USP28 and USP25. Genome Biol. 2001;2(10):RESEARCH0043.

42. Bosch-Comas A, Lindsten K, Gonzalez-Duarte R, Masucci MG, Marfany G. The ubiquitin-specific protease USP25 interacts with three sarcomeric proteins. Cell Mol Life Sci. 2006;63(6):723-34.

43. Denuc A, Bosch-Comas A, Gonzalez-Duarte R, Marfany G. The UBA-UIM domains of the USP25 regulate the enzyme ubiquitination state and modulate substrate recognition. PLoS One. 2009;4(5):e5571.

44. Yang Y, Shi L, Ding Y, Shi Y, Hu HY, Wen Y, et al. Structural and Functional Investigations of the N-Terminal Ubiquitin Binding Region of Usp25. Biophys J. 2017;112(10):2099-108.

45. Zhen Y, Knobel PA, Stracker TH, Reverter D. Regulation of USP28 deubiquitinating activity by SUMO conjugation. J Biol Chem. 2014;289(50):34838-50.

46. Wen Y, Shi L, Ding Y, Cui R, He WT, Hu HY, et al. The N-terminal ubiquitin-binding region of ubiquitin-specific protease 28 modulates its deubiquitination function: NMR structural and mechanistic insights. Biochem J. 2015;471(2):155-65.

47. Meulmeester E, Kunze M, Hsiao HH, Urlaub H, Melchior F. Mechanism and consequences for paralog-specific sumoylation of ubiquitin-specific protease 25. Mol Cell. 2008;30(5):610-9.

48. Faesen AC, Luna-Vargas MP, Geurink PP, Clerici M, Merkx R, van Dijk WJ, et al. The differential modulation of USP activity by internal regulatory domains, interactors and eight ubiquitin chain types. Chem Biol. 2011;18(12):1550-61.

49. Kawaguchi K, Uo K, Tanaka T, Komada M. Tandem UIMs confer Lys48 ubiquitin chain substrate preference to deubiquitinase USP25. Scientific reports. 2017;7:45037.

50. Kim S, Lee D, Lee J, Song H, Kim HJ, Kim KT. Vaccinia-Related Kinase 2 Controls the Stability of the Eukaryotic Chaperonin TRiC/CCT by Inhibiting the Deubiquitinating Enzyme USP25. Mol Cell Biol. 2015;35(10):1754-62.

51. Cholay M, Reverdy C, Benarous R, Colland F, Daviet L. Functional interaction between the ubiquitin-specific protease 25 and the SYK tyrosine kinase. Exp Cell Res. 2010;316(4):667-75.

52. Zhang D, Zaugg K, Mak TW, Elledge SJ. A role for the deubiquitinating enzyme USP28 in control of the DNA-damage response. Cell. 2006;126(3):529-42.

53. Kessler BM, Edelmann MJ. PTMs in conversation: activity and function of deubiquitinating enzymes regulated via post-translational modifications. Cell Biochem Biophys. 2011;60(1-2):21-38.

54. Knobel PA, Belotserkovskaya R, Galanty Y, Schmidt CK, Jackson SP, Stracker TH. USP28 is recruited to sites of DNA damage by the tandem BRCT domains of 53BP1 but plays a minor role in double-strand break metabolism. Mol Cell Biol. 2014;34(11):2062-74.

55. Popov N, Wanzel M, Madiredjo M, Zhang D, Beijersbergen R, Bernards R, et al. The ubiquitin-specific protease USP28 is required for MYC stability. Nat Cell Biol. 2007;9(7):765-74.

56. Wu Y, Wang Y, Yang XH, Kang T, Zhao Y, Wang C, et al. The deubiquitinase USP28 stabilizes LSD1 and confers stem-cell-like traits to breast cancer cells. Cell reports. 2013;5(1):224-36.

57. Blount JR, Burr AA, Denuc A, Marfany G, Todi SV. Ubiquitin-specific protease 25 functions in Endoplasmic Reticulum-associated degradation. PLoS One. 2012;7(5):e36542.

58. Lambrus BG, Holland AJ. A New Mode of Mitotic Surveillance. Trends Cell Biol. 2017;27(5):314-21.

59. Bassermann F, Frescas D, Guardavaccaro D, Busino L, Peschiaroli A, Pagano M. The Cdc14B-Cdh1-Plk1 axis controls the G2 DNA-damage-response checkpoint. Cell. 2008;134(2):256-67.

60. Bassermann F, Pagano M. Dissecting the role of ubiquitylation in the DNA damage response checkpoint in G2. Cell Death Differ. 2010;17(1):78-85.

61. Cuella-Martin R, Oliveira C, Lockstone HE, Snellenberg S, Grolmusova N, Chapman JR. 53BP1 Integrates DNA Repair and p53-Dependent Cell Fate Decisions via Distinct Mechanisms. Mol Cell. 2016;64(1):51-64.

62. Lambrus BG, Daggubati V, Uetake Y, Scott PM, Clutario KM, Sluder G, et al. A USP28-53BP1-p53-p21 signaling axis arrests growth after centrosome loss or prolonged mitosis. J Cell Biol. 2016;214(2):143-53.

63. Meitinger F, Anzola JV, Kaulich M, Richardson A, Stender JD, Benner C, et al. 53BP1 and USP28 mediate p53 activation and G1 arrest after centrosome loss or extended mitotic duration. J Cell Biol. 2016;214(2):155-66.

64. Fong CS, Mazo G, Das T, Goodman J, Kim M, O'Rourke BP, et al. 53BP1 and USP28 mediate p53-dependent cell cycle arrest in response to centrosome loss and prolonged mitosis. Elife. 2016;5.

65. Ren K, Li Y, Lu H, Li Z, Han X. miR-3940-5p Functions as a Tumor Suppressor in Non-Small Cell Lung Cancer Cells by Targeting Cyclin D1 and Ubiquitin Specific Peptidase-28. Transl Oncol. 2017;10(1):80-9.

66. Zhang L, Xu B, Qiang Y, Huang H, Wang C, Li D, et al. Overexpression of deubiquitinating enzyme USP28 promoted non-small cell lung cancer growth. J Cell Mol Med. 2015;19(4):799-805.

67. Li P, Huang Z, Wang J, Chen W, Huang J. Ubiquitin-specific peptidase 28 enhances STAT3 signaling and promotes cell growth in non-small-cell lung cancer. Onco Targets Ther. 2019;12:1603-11.

68. Wang Z, Song Q, Xue J, Zhao Y, Qin S. Ubiquitin-specific protease 28 is overexpressed in human glioblastomas and contributes to glioma tumorigenicity by regulating MYC expression. Exp Biol Med (Maywood). 2016;241(3):255-64.

69. Cao C, Vasilatos SN, Bhargava R, Fine JL, Oesterreich S, Davidson NE, et al. Functional interaction of histone deacetylase 5 (HDAC5) and lysine-specific demethylase 1 (LSD1) promotes breast cancer progression. Oncogene. 2017;36(1):133-45.

70. Zhu J, Huang G, Hua X, Li Y, Yan H, Che X, et al. CD44s is a crucial ATG7 downstream regulator for stem-like property, invasion, and lung metastasis of human bladder cancer (BC) cells. Oncogene. 2019;38(17):3301-15.

71. Diefenbacher ME, Popov N, Blake SM, Schülein-Völk C, Nye E, Spencer-Dene B, et al. The deubiquitinase USP28 controls intestinal homeostasis and promotes colorectal cancer. J Clin Invest. 2014;124(8):3407-18.

72. Diefenbacher ME, Chakraborty A, Blake SM, Mitter R, Popov N, Eilers M, et al. Usp28 counteracts Fbw7 in intestinal homeostasis and cancer. Cancer Res. 2015;75(7):1181-6.

73. Schülein-Völk C, Wolf E, Zhu J, Xu W, Taranets L, Hellmann A, et al. Dual regulation of Fbw7 function and oncogenic transformation by Usp28. Cell reports. 2014;9(3):1099-109.

74. Taranets L, Zhu J, Xu W, Popov N. Fbw7 and Usp28 - enemies and allies. Mol Cell Oncol. 2015;2(3):e995041.

75. Ren Y, Zhao Y, Lin D, Xu X, Zhu Q, Yao J, et al. The Type I Interferon-IRF7 Axis Mediates Transcriptional Expression of Usp25 Gene. J Biol Chem. 2016;291(25):13206-15.

76. Lin D, Zhang M, Zhang MX, Ren Y, Jin J, Zhao Q, et al. Induction of USP25 by viral infection promotes innate antiviral responses by mediating the stabilization of TRAF3 and TRAF6. Proc Natl Acad Sci U S A. 2015;112(36):11324-9.

77. Zhong B, Liu X, Wang X, Liu X, Li H, Darnay BG, et al. Ubiquitin-specific protease 25 regulates TLR4-dependent innate immune responses through deubiquitination of the adaptor protein TRAF3. Sci Signal. 2013;6(275):ra35.

78. Zhong B, Liu X, Wang X, Chang SH, Liu X, Wang A, et al. Negative regulation of IL-17-mediated signaling and inflammation by the ubiquitin-specific protease USP25. Nat Immunol. 2012;13(11):1110-7.

79. Hu H, Sun SC. Ubiquitin signaling in immune responses. Cell Res. 2016;26(4):457-83.

80. Xu D, Liu J, Fu T, Shan B, Qian L, Pan L, et al. USP25 regulates Wnt signaling by controlling the stability of tankyrases. Genes Dev. 2017;31(10):1024-35.

81. Zhan T, Rindtorff N, Boutros M. Wnt signaling in cancer. Oncogene. 2017;36(11):1461-73.

82. Pai SG, Carneiro BA, Mota JM, Costa R, Leite CA, Barroso-Sousa R, et al. Wnt/beta-catenin pathway: modulating anticancer immune response. 2017;10(1):101.

83. Callow MG, Tran H, Phu L, Lau T, Lee J, Sandoval WN, et al. Ubiquitin ligase RNF146 regulates tankyrase and Axin to promote Wnt signaling. PLoS One. 2011;6(7):e22595.

84. Huang SM, Mishina YM, Liu S, Cheung A, Stegmeier F, Michaud GA, et al. Tankyrase inhibition stabilizes axin and antagonizes Wnt signalling. Nature. 2009;461(7264):614-20.

85. Zhang Y, Liu S, Mickanin C, Feng Y, Charlat O, Michaud GA, et al. RNF146 is a poly(ADP-ribose)-directed E3 ligase that regulates axin degradation and Wnt signalling. Nat Cell Biol. 2011;13(5):623-9.

86. Harrigan JA, Jacq X, Martin NM, Jackson SP. Deubiquitylating enzymes and drug discovery: emerging opportunities. Nature Reviews Drug Discovery. 2017;17:57.

87. Salami J, Crews CM. Waste disposal-An attractive strategy for cancer therapy. Science. 2017;355(6330):1163-7.

88. D'Arcy P, Wang X, Linder S. Deubiquitinase inhibition as a cancer therapeutic strategy. Pharmacol Ther. 2015;147:32-54.

89. Li M, Brooks CL, Kon N, Gu W. A dynamic role of HAUSP in the p53-Mdm2 pathway. Mol Cell. 2004;13(6):879-86.

90. Cummins JM, Rago C, Kohli M, Kinzler KW, Lengauer C, Vogelstein B. Tumour suppression: disruption of HAUSP gene stabilizes p53. Nature. 2004;428(6982):1 p following 486.

91. Ritorto MS, Ewan R, Perez-Oliva AB, Knebel A, Buhrlage SJ, Wightman M, et al. Screening of DUB activity and specificity by MALDI-TOF mass spectrometry. Nat Commun. 2014;5:4763.

92. Wertz IE, Murray JM. Structurally-defined deubiquitinase inhibitors provide opportunities to investigate disease mechanisms. Drug Discovery Today: Technologies. 2019.

93. Rouge L, Bainbridge TW, Kwok M, Tong R, Di Lello P, Wertz IE, et al. Molecular Understanding of USP7 Substrate Recognition and C-Terminal Activation. Structure. 2016;24(8):1335-45.

94. O'Dowd CR, Helm MD, Rountree JSS, Flasz JT, Arkoudis E, Miel H, et al. Identification and Structure-Guided Development of Pyrimidinone Based USP7 Inhibitors. ACS Medicinal Chemistry Letters. 2018;9(3):238-43.

95. Gavory G, O'Dowd CR, Helm MD, Flasz J, Arkoudis E, Dossang A, et al. Discovery and characterization of highly potent and selective allosteric USP7 inhibitors. Nature Chemical Biology. 2017;14:118.

96. Lamberto I, Liu X, Seo H-S, Schauer NJ, Iacob RE, Hu W, et al. Structure-Guided Development of a Potent and Selective Non-covalent Active-Site Inhibitor of USP7. Cell Chemical Biology. 2017;24(12):1490-500.e11.

97. Kategaya L, Di Lello P, Rougé L, Pastor R, Clark KR, Drummond J, et al. USP7 small-molecule inhibitors interfere with ubiquitin binding. Nature. 2017;550:534.

98. Di Lello P, Pastor R, Murray JM, Blake RA, Cohen F, Crawford TD, et al. Discovery of Small-Molecule Inhibitors of Ubiquitin Specific Protease 7 (USP7) Using Integrated NMR and in Silico Techniques. Journal of Medicinal Chemistry. 2017;60(24):10056-70.

99. Turnbull AP, Ioannidis S, Krajewski WW, Pinto-Fernandez A, Heride C, Martin ACL, et al. Molecular basis of USP7 inhibition by selective small-molecule inhibitors. Nature. 2017;550:481.

100. Wang X, Liu Z, Zhang L, Yang Z, Chen X, Luo J, et al. Targeting deubiquitinase USP28 for cancer therapy. Cell Death Dis. 2018;9(2):186.

101. Wrigley JD, Gavory G, Simpson I, Preston M, Plant H, Bradley J, et al. Identification and Characterization of Dual Inhibitors of the USP25/28 Deubiquitinating Enzyme Subfamily. ACS Chem Biol. 2017;12(12):3113-25.

102. Guerin DJ, Bair KW, Caravella JA, Ioannidis S, LANCIA JDR, Li H, et al., inventors; FORMA THERAPEUTICS, INC., assignee. Thienopyrazine carboxamides as ubiquitin-specific protease inhibitors 2017 17.08.2017.

103. Evans PR, Murshudov GN. How good are my data and what is the resolution? Acta Crystallogr D Biol Crystallogr. 2013;69(Pt 7):1204-14.

104. Baker NA, Sept D, Joseph S, Holst MJ, McCammon JA. Electrostatics of nanosystems: application to microtubules and the ribosome. Proc Natl Acad Sci U S A. 2001;98(18):10037-41.

105. Blanc E, Roversi P, Vonrhein C, Flensburg C, Lea SM, Bricogne G. Refinement of severely incomplete structures with maximum likelihood in BUSTER-TNT. Acta Crystallogr D Biol Crystallogr. 2004;60(Pt 12 Pt 1):2210-21.

106. Cowtan K. The Buccaneer software for automated model building. 1. Tracing protein chains. Acta Crystallogr D Biol Crystallogr. 2006;62(Pt 9):1002-11.

107. Winn MD, Ballard CC, Cowtan KD, Dodson EJ, Emsley P, Evans PR, et al. Overview of the CCP4 suite and current developments. Acta Crystallogr D Biol Crystallogr. 2011;67(Pt 4):235-42.

108. Emsley P, Lohkamp B, Scott WG, Cowtan K. Features and development of Coot. Acta Crystallogr D Biol Crystallogr. 2010;66(Pt 4):486-501.

109. Skubak P, Pannu NS. Automatic protein structure solution from weak X-ray data. Nat Commun. 2013;4:2777.

110. Holm L, Laakso LM. Dali server update. Nucleic Acids Res. 2016;44(W1):W351-5.

111. Gasteiger E, Hoogland C, Gattiker A, Duvaud S, Wilkins MR, Appel RD, et al. Protein Identification and Analysis Tools on the ExPASy Server. In: Walker JM, editor. The Proteomics Protocols Handbook: Humana Press; 2005. p. 571-607.

112. Cowtan K. Recent developments in classical density modification. Acta Crystallogr D Biol Crystallogr. 2010;66(Pt 4):470-8.

113. Dolinsky TJ, Nielsen JE, McCammon JA, Baker NA. PDB2PQR: an automated pipeline for the setup of Poisson-Boltzmann electrostatics calculations. Nucleic Acids Res. 2004;32(Web Server issue):W665-7.

114. Krissinel E, Henrick K. Secondary-structure matching (SSM), a new tool for fast protein structure alignment in three dimensions. Acta Crystallogr D Biol Crystallogr. 2004;60(Pt 12 Pt 1):2256-68.

115. Krissinel E, Henrick K. Inference of macromolecular assemblies from crystalline state. J Mol Biol. 2007;372(3):774-97.

116. McCoy AJ, Grosse-Kunstleve RW, Adams PD, Winn MD, Storoni LC, Read RJ. Phaser crystallographic software. J Appl Crystallogr. 2007;40(Pt 4):658-74.

117. Adams PD, Afonine PV, Bunkoczi G, Chen VB, Davis IW, Echols N, et al. PHENIX: a comprehensive Python-based system for macromolecular structure solution. Acta Crystallogr D Biol Crystallogr. 2010;66(Pt 2):213-21.

118. Berman HM, Westbrook J, Feng Z, Gilliland G, Bhat TN, Weissig H, et al. The Protein Data Bank. Nucleic Acids Res. 2000;28(1):235-42.

119. Schrodinger, LLC. The PyMOL Molecular Graphics System, Version 1.8. 2015.

120. Källberg M, Wang H, Wang S, Peng J, Wang Z, Lu H, et al. Template-based protein structure modeling using the RaptorX web server. Nat Protoc. 2012;7(8):1511-22.

121. Murshudov GN, Skubak P, Lebedev AA, Pannu NS, Steiner RA, Nicholls RA, et al. REFMAC5 for the refinement of macromolecular crystal structures. Acta Crystallogr D Biol Crystallogr. 2011;67(Pt 4):355-67.

122. Tickle IJ, Flensburg C, Paciorek W, Sharff A, Vonrhein C, Bricogne G. STARANISO [Server]. 2019 [updated 04-Feb-2019. Available from: http://staraniso.globalphasing.org/cgi-bin/staraniso.cgi.

123. Notredame C, Higgins DG, Heringa J. T-Coffee: A novel method for fast and accurate multiple sequence alignment. J Mol Biol. 2000;302(1):205-17.

124. UniProt Consortium T. UniProt: the universal protein knowledgebase. Nucleic Acids Res. 2018;46(5):2699.

125. Kabsch W. Xds. Acta Crystallogr D Biol Crystallogr. 2010;66(Pt 2):125-32.

126. Sauer F, Klemm T, Kollampally RB, Tessmer I, Nair RK, Popov N, et al. Differential Oligomerization of the Deubiquitinases USP25 and USP28 Regulates Their Activities. Mol Cell. 2019;74(3):421-35 e10.

127. Li MZ, Elledge SJ. Harnessing homologous recombination in vitro to generate recombinant DNA via SLIC. Nat Methods. 2007;4(3):251-6.

128. Lawrence AM, Besir HU. Staining of proteins in gels with Coomassie G-250 without organic solvent and acetic acid. J Vis Exp. 2009(30).

129. Komander D, Lord CJ, Scheel H, Swift S, Hofmann K, Ashworth A, et al. The structure of the CYLD USP domain explains its specificity for Lys63-linked polyubiquitin and reveals a B box module. Mol Cell. 2008;29(4):451-64.

130. Gersch M, Gladkova C, Schubert AF, Michel MA, Maslen S, Komander D. Mechanism and regulation of the Lys6-selective deubiquitinase USP30. Nat Struct Mol Biol. 2017;24(11):920-30.

131. Ekkebus R, van Kasteren SI, Kulathu Y, Scholten A, Berlin I, Geurink PP, et al. On terminal alkynes that can react with active-site cysteine nucleophiles in proteases. J Am Chem Soc. 2013;135(8):2867-70.

132. Renatus M, Parrado SG, D'Arcy A, Eidhoff U, Gerhartz B, Hassiepen U, et al. Structural basis of ubiquitin recognition by the deubiquitinating protease USP2. Structure. 2006;14(8):1293-302.

133. Ernst A, Avvakumov G, Tong J, Fan Y, Zhao Y, Alberts P, et al. A strategy for modulation of enzymes in the ubiquitin system. Science. 2013;339(6119):590-5.

134. Hu M, Li P, Song L, Jeffrey PD, Chenova TA, Wilkinson KD, et al. Structure and mechanisms of the proteasome-associated deubiquitinating enzyme USP14. EMBO J. 2005;24(21):3747-56.

135. Sato Y, Goto E, Shibata Y, Kubota Y, Yamagata A, Goto-Ito S, et al. Structures of CYLD USP with Met1- or Lys63-linked diubiquitin reveal mechanisms for dual specificity. Nat Struct Mol Biol. 2015;22(3):222-9.

136. Bekes M, van der Heden van Noort GJ, Ekkebus R, Ovaa H, Huang TT, Lima CD. Recognition of Lys48-Linked Di-ubiquitin and Deubiquitinating Activities of the SARS Coronavirus Papain-like Protease. Mol Cell. 2016;62(4):572-85.

137. Altschul SF, Gish W, Miller W, Myers EW, Lipman DJ. Basic local alignment search tool. J Mol Biol. 1990;215(3):403-10.

138. Robert X, Gouet P. Deciphering key features in protein structures with the new ENDscript server. Nucleic Acids Res. 2014;42(Web Server issue):W320-4.

139. Tate JG, Bamford S, Jubb HC, Sondka Z, Beare DM, Bindal N, et al. COSMIC: the Catalogue Of Somatic Mutations In Cancer. Nucleic Acids Res. 2019;47(D1):D941-D7.

140. Wu G, Diaz AK, Paugh BS, Rankin SL, Ju B, Li Y, et al. The genomic landscape of diffuse intrinsic pontine glioma and pediatric non-brainstem high-grade glioma. Nat Genet. 2014;46(5):444-50.

141. Pickering CR, Zhou JH, Lee JJ, Drummond JA, Peng SA, Saade RE, et al. Mutational Landscape of Aggressive Cutaneous Squamous Cell Carcinoma. Clin Cancer Res. 2014;20(24):6582-92.

142. Fujimoto A, Totoki Y, Abe T, Boroevich KA, Hosoda F, Nguyen HH, et al. Whole-genome sequencing of liver cancers identifies etiological influences on mutation patterns and recurrent mutations in chromatin regulators. Nat Genet. 2012;44(7):760-4.

143. Totoki Y, Tatsuno K, Yamamoto S, Arai Y, Hosoda F, Ishikawa S, et al. High-resolution characterization of a hepatocellular carcinoma genome. Nat Genet. 2011;43(5):464-9.

144. Schülein-Völk C, Wolf E, Zhu J, Xu W, Taranets L, Hellmann A, et al. Dual Regulation of Fbw7 Function and Oncogenic Transformation by Usp28. Cell Reports. 2014;9(3):1099-109.

145. Hao B, Oehlmann S, Sowa ME, Harper JW, Pavletich NP. Structure of a Fbw7-Skp1-cyclin E complex: multisite-phosphorylated substrate recognition by SCF ubiquitin ligases. Mol Cell. 2007;26(1):131-43.

146. Ng RWM, Arooz T, Yam CH, Chan IWY, Lau AWS, Poon RYC. Characterization of the cullin and F-box protein partner Skp1. 1998;438(3):183-9.

147. Shang S, Hua F, Hu ZW. The regulation of beta-catenin activity and function in cancer: therapeutic opportunities. Oncotarget. 2017;8(20):33972-89.

148. Gersch M, Wagstaff JL, Toms AV, Graves B, Freund SMV, Komander D. Distinct USP25 and USP28 Oligomerization States Regulate Deubiquitinating Activity. Mol Cell. 2019;74(3):436-51 e7.

149. Liu B, Sureda-Gomez M, Zhen Y, Amador V, Reverter D. A quaternary tetramer assembly inhibits the deubiquitinating activity of USP25. Nat Commun. 2018;9(1):4973.

150. Reyes-Turcu FE, Shanks JR, Komander D, Wilkinson KD. Recognition of polyubiquitin isoforms by the multiple ubiquitin binding modules of isopeptidase T. J Biol Chem. 2008;283(28):19581-92.

151. Manczyk N, Veggiani G, Teyra J, Strilchuk AW, Sidhu SS, Sicheri F. The ubiquitin interacting motifs of USP37 act on the proximal Ub of a di-Ub chain to enhance catalytic efficiency. Scientific reports. 2019;9(1):4119.

152. Basters A, Geurink PP, Rocker A, Witting KF, Tadayon R, Hess S, et al. Structural basis of the specificity of USP18 toward ISG15. Nat Struct Mol Biol. 2017;24(3):270-8.

153. Avvakumov GV, Walker JR, Xue S, Finerty PJ, Jr., Mackenzie F, Newman EM, et al. Amino-terminal dimerization, NRDP1-rhodanese interaction, and inhibited catalytic domain conformation of the ubiquitin-specific protease 8 (USP8). J Biol Chem. 2006;281(49):38061-70.

154. Pruneda JN, Komander D. Evaluating enzyme activities and structures of DUBs. Methods Enzymol. 2019;618:321-41.

155. Wrighton KH. p53: Understanding the actions of 53BP1. Nat Rev Mol Cell Biol. 2016;17(10):608.

156. Welcker M, Clurman BE. FBW7 ubiquitin ligase: a tumour suppressor at the crossroads of cell division, growth and differentiation. Nat Rev Cancer. 2008;8(2):83-93.

157. Welcker M, Clurman BE. Fbw7/hCDC4 dimerization regulates its substrate interactions. Cell Division. 2007;2(1):1-13.

158. Welcker M, Larimore EA, Swanger J, Bengoechea-Alonso MT, Grim JE, Ericsson J, et al. Fbw7 dimerization determines the specificity and robustness of substrate degradation. Genes Dev. 2013;27(23):2531-6.

159. Kim RQ, Sixma TK. Regulation of USP7: A High Incidence of E3 Complexes. J Mol Biol. 2017;429(22):3395-408.

160. Kim RQ, Geurink PP, Mulder MPC, Fish A, Ekkebus R, El Oualid F, et al. Kinetic analysis of multistep USP7 mechanism shows critical role for target protein in activity. Nat Commun. 2019;10(1):231.

161. Clerici M, Luna-Vargas MPA, Faesen AC, Sixma TK. The DUSP–Ubl domain of USP4 enhances its catalytic efficiency by promoting ubiquitin exchange. Nature Communications. 2014;5:5399.

VI. Appendix

VI.1 Abbreviations

Table VI-1: List of abbreviations. For amino acids, the one or three letter code was used, according to the International Union of Pure and Applied Chemistry (IUPAC) regulations.

Abbreviation	Name
53BP1	P53 binding protein 1
6-FAM	Fluorescein (FAM)-maleimide, 6-Isomer
A_{280}	Absorbance at 280
aa	Amino acid
AAA ATPase	ATPases associated with various cellular activities
ACTA1	Actin alpha 1
A_{max}	Maximal absorbance
Amp	Ampicillin
AMSH	Associated molecule with the SH3 domain of STAM
APC/C (Cdh1)	Anaphase-promoting complex/ cyclosome (Cadherin-1)
APP	β-Amyloid precursor protein
APS	Ammonium persulfate
ATM	Ataxia-telangiectasia mutated
ATP	Adenosine-5'-triphosphate disodium salt
ATXN3	Ataxin 3
AUC	Analytical ultracentrifuge
BAP1	BRCA1-associated protein 1
BL	Blocking loop
BLAST	Basic local alignment search tool
BRCA1	Breast cancer early-onset 1
BRCC36	BRCA1/BRCA2-containing complex subunit 36
BRCT	Breast cancer susceptibility gene 1 COOH terminus
BSA	Bovine serum albumin
$CaCl_2$	Calcium chloride dihydrate
Cam	Chloramphenicol
Catalytic domain	Cat
CBD	Chitin binding domain
CCT4	Chaperonin containing TCP1 subunit 4
CD	Catalytic dead
CD	Circular dichroism

CD3δ	Cluster of differentiation 3δ
CD44	Cluster of differentiation 44
CDC34	Ubiquitin-conjugating enzyme E2-34 kDa
CF	Correction factor
Chk1, Chk2	Checkpoint kinase 1, 2
COSMIC	Catalogue of somatic mutations in cancer
c_{prot}	Protein concentration
CT	C-terminal domain
Cul1	Cullin 1
CYLD	Cylindromatosis
d	Distance for the path length
dATP	2'-Deoxyadenosine 5'-triphosphate
dCTP	2'-Deoxycytidine 5'-triphosphate
DD	Dimerization domain
DDR	DNA damage response
dGTP	2'-Deoxyguanosine 5'-triphosphate
DMSO	Dimethyl sulfoxide
dRI	Differential refractive index
DTT	Dithiothreitol
dTTP	2'-Deoxythymidine 5'-triphosphate
DUB	Deubiquitinase
DUSP	Domain in USP
E. coli	*Escherichia coli*
EDTA	Ethylenediaminetetraacetic acid
EMBL	European molecular biology laboratory
$\mathcal{E}_{prot}$	Extinction coefficient
ER	Endoplasmatic reticulum
ERAD	ER-associated degradation
ESCRT	Endosomal sorting complex required for transport
ESRF	European synchrotron radiation facility
FAM	Fluorescein
FBW7	F-box/WD repeat-containing protein 7
$Fe(II)SO_4$	Iron(II) sulfate heptahydrate
fl	Full length
FLNC	Filamin C

FOM	Figure of merit
Fw	Forward primer
H-bond	Hydrogen bond
HCl	Hydrochloric acid
HEPES	4-(2-hydroxyethyl)-1-piperazineethanesulfonic acid
HRD1	HMG-CoA reductase degradation protein 1
IFN	Type I interferons
IL-17	Interleukin 17
IPTG	Isopropyl-β-D-thiogalactopyranoside
IR	Ionizing irradiation
IRF7	Interferon regulatory factor 7
ITC	Isothermal titration calorimetry
IUPAC	the International Union of Pure and Applied Chemistry
JAMM/ MPN+	JAB1/ MPN/ MOV34
K_2HPO_4	Dipotassium hydrogen phosphate
Kan	Kanamycin sulfate
KH_2PO_4	Potassium dihydrogen phosphate
LB	Lysogeny broth
LPS	Lipopolysaccharide
LSD1	Lysine-specific demethylase 1
MDM2	Mouse double minute 2 homolog
MESNa	Sodium 2-mercaptoethanesulfonate
$MgCl_2$	Magnesium chloride
$MgSO_4$	Magnesium sulfate
MINDY	MIU containing novel DUB family
MIU	Motif interacting with ubiquitin
MJD	Machado Joseph Disease
MMS2	Ubiquitin-conjugating enzyme variant
MR	Molecular replacement
MyBPC1	Myosin binding protein C1
MYC	Avian myeloblastosis virus oncogene cellular homolog
Na_2HPO_4	Disodium hydrogen phosphate
NaCl	Sodium chloride
NaH_2PO_4	Sodium dihydrogen phosphate
NaOH	Sodium hydroxide

NF-κB	Nuclear factor κB
NH_4Cl	Ammonium chloride
NICD1	Notch intracellular domain 1
NSCLC	Non-small cell lung cancer
OD	Optical density
OTU	Ovarian tumor protease
PA	Propargylamine
PAMPs	Pathogen-associated patterns
PARP	Poly-ADP-ribosyl-polymerase
PARsylated	Poly-ADP-ribosylated
PCR	Polymerase chain reaction
PDB	Protein Data Bank
PEG	Polyethylen glycol
POI	Protein of interest
PUMA	P53 upregulated modulator of apoptosis
qRT-PCR	Quantitative real-time PCR
RMSD	Rout mean square deviation
RNF146	Ring finger protein 146
rv	Reverse primer
RVZ	Rudolf Virchow Zentrum
S1	Subsite 1
SAD	Single wavelength anomalous dispersion
SAM	Sterile alpha motif
SARS PLpro	SARS-coronavirus papain-like protease
SAXS	Small-angle X-ray scattering
SCF	Skp1/Cul1/F-box protein
SD	Superdex
SDS	Sodium dodecyl sulfate
SDS-PAGE	SDS polyacrylamide gel electrophoresis
SEC	Size exclusion chromatography
SEC-MALS	Size exclusion chromatography coupled to multi-angle light scattering
SeMet	Seleno methionine
SIM	SUMO interacting motif
SKP1	S-phase kinase-associated protein 1

SL	Switching loop
SLIC	Sequence and ligation independent cloning
$SrCl_2$	Strontiumchloride hexahydrate
Strep	Streptomycin sulfate
sub	Subdomain
SUMO	Small-ubiquitin-like modifier
SV-AUC	Sedimentation velocity analytical ultracentrifugation
SYK	Spleen Tyrosin Kinase
TB	Terrific Broth
TCEP	Tris-(2-carboxyethyl)-phosphine
TEMED	Tetramethylethylenediamin
TLR4	Toll-like receptor 4
TNKS	Tankyrases
TNKS-ANK	Tankyrase-ankyrin repeats
TRAF3	Tumor necrosis factor receptor-associated factor 3
TRiC	Chaperon TCP-1 ring complex
Tris	Tris-(hydroxymethyl)-aminomethan
trx	Thioredoxin
Ub	Ubiquitin
UBA	Ubiquitin associated domain
UBA1	Ubiquitin-like modifier-activating enzyme 1
Ub-AMC	Ubiquitin with 7-amino-4-methylcoumarin
Ubc13	Ubiquitin-conjugating enzyme E2 13
Ube2K	Ub conjugating enzyme E2 K
UBL	Ubiquitin-like
UbPA	Ubiquitin propargylamide
UBR	Ubiquitin binding region
UbRh110	Ubiquitin-rhodamine110Gly
UCH	Ubiquitin C-terminal hydrolase
UCID	USP25/28 catalytic domain inserted domain
UCID	USP25/28 Catalytic domain inserted domain
UIM	Ubiquitin interacting motif
USP	Ubiquitin specific protease
USP25m	USP25 muscle specific isoform
VCP	Valosin-containing protein

VRK2	Vaccinia-related kinase 2
WEHI	Walter and Eliza Hall Institute of Medical Research
wt	Wild type
ZnF UBPs	Zinc finger ubiquitin specific protease domain
ZUFSP	Zinc finger with UFM1-specific peptidase domain protein

VI.2 Expression constructs

Table VI-2: Expression constructs for recombinant expression in *E.coli*.

Name	Region/ *Mutation	Vector	-tag
USP28 full-length	1-1045	pColA-22	trx-6xHis-3C
USP28 1-665	1-665	pColA-22	trx-6xHis-3C
USP28cat	149-707	pCDF-22	trx-6xHis-3C
USP28 114-730	114-730	pCDF-22	trx-6xHis-3C
USP28 114-1045	114-1045	pColA-22	trx-6xHis-3C
USP28cat ΔDD	149-425-GSSG-560-707	pCDF-22	trx-6xHis-3C
USP28cat Δtip	149-458-SGSG-529-707	pCDF-22	trx-6xHis-3C
USP28cat L545E	149-707/ *L545E	pCDF-22	trx-6xHis-3C
USP28cat E593D	149-707/ *E593D	pCDF-22	trx-6xHis-3C
Ubiquitin (Ub)	1-76	pET30A	6xHis-3C
Ub K48R/S20C	1-76/ *K48R, *S20C	pET30A	6xHis-3C
Ub G76W	1-76/ *G76W	pTXB1	---
USP25cat	157-706	pCDF-14	6xHis-3C
USP25cat Δtip	157-464-GSGS-538-706	pCDF-14	6xHis-3C
USP25cat F458E/L552E	157-706/ *F458E, *L552E	pCDF-14	6xHis-3C
USP25cat Δtip F458E/ L552E	157-464-GSGS-538-706/ *F458E, *L552E	pCDF-14	6xHis-3C
USP28-tip-chimera	(USP28)149-457-(USP25)465-534-(USP28)528-707	pETM-14	6xHis-3C
USP28-roof-chimera	(USP28)149-427-(USP25)433-562-(USP28)555-707	pCDF-22	trx-6xHis-3C

USP25-roof-chimera	(USP25)157-434(USP28)428-555(USP25)563-706	pCDF-14	6xHis-3C
USP25 UCID	415-583	pETM-14	6xHis-3C
USP25cat Δtip R385Q	157-464-GSGS-538-706/ *R385Q	pCDF-14	6xHis-3C
USP28cat Q378R	149-707/ *Q378R	pCDF-22	trx-6xHis-3C
USP25cat P535S	157-706/ *P535S	pCDF-14	6xHis-3C
USP25cat P535L	157-706/ *P535L	pCDF-14	6xHis-3C
USP25cat E600D	157-706/ *E600D	pCDF-14	6xHis-3C
USP25cat Δtip E600D	157-464-GSGS-538-706/ *E600D	pCDF-14	6xHis-3C
USP25cat Δtip E600N	157-464-GSGS-538-706/ *E600N	pCDF-14	6xHis-3C
USP25cat Δtip E600A	157-464-GSGS-538-706/ *E600A	pCDF-14	6xHis-3C
FBW7 262-707	262-707	pCDF-22	trx-6xHis-3C
FBW7 247-707	247-707	pCDF-22	trx-6xHis-3C
SKP1	1-163	pColA-22	trx-6xHis-3C
TNKS-ANK	171-957	pETM-22	trx-6xHis-3C
USP25cat-ct	157-1055	pCDF-22/ pETM-14	trx-6xHis-3C 6xHis-3C
USP25cat-ct P535L	157-1055/ *P535L	pCDF-14	6xHis-3C
USP25cat C178S	157-706/ *C178S	pCDF-14	6xHis-3C
USP25CT	765-1055	pETM-14	6xHis-3C
USP28CT	723-1045	pColA-22	trx-6xHis-3C
USP28CT-2	754-1045	pCDF-22	trx-6xHis-3C

Table VI-3: Expression constructs for eukaryotic expression. All experiments *in vivo*, including cloning of the USP variants, were performed by our collaboration partners Ravi B. Kollampally and Nikita Popov, PhD.

Name	Region/ *Mutation	Vector	-tag
USP28 fl	1-1045	pcDNA3	HA
USP28 L545E	1-1045/ *L545E	pcDNA3	HA
USP28 fl	1-1045	pcDNA3	FLAG
USP25 wt	1-1055	pWZL	HA
USP25 C178A	1-1055/ *C178A	pWZL	HA

USP25 Δtip	1-464-GSGS-538-1055	pWZL	HA
USP25 Δtip C178A	1-464-GSGS-538-1055/ *C178A	pWZL	HA
USP25 P535L	1-1055/ *P535L	pWZL	HA
USP25 P535L/ C178A	1-1055/ *P535L, *C178A	pWZL	HA
USP25 E600D	1-1055/ *E600D	pWZL	HA

VI.3 Extinction coefficients

Table VI-4: Extinction coefficients, molecular weights and the absorption values for each protein at OD280 for all recombinantly expressed proteins.

Protein name	Extinction coefficient (M^{-1} cm^{-1}) assuming all Cys residues reduced	Molecular Weight (Da)	Absorption at A280 (1g/l) assuming all Cys residues reduced
USP28 full-length	136600	119121	1.147
USP28 1-665	87780	75759	1.159
USP28cat	94770	64936	1.46
USP28 114-730	101760	71329	1.427
USP28 114-1045	136600	107182	1.274
USP28cat ΔDD	84800	49916	1.699
USP28cat Δtip	94770	57763	1.641
USP28cat L545E	94770	64952	1.459
USP28cat E593D	94770	64922	1.460
Ubiquitin (Ub)	1490	8565	0.174
Ub K48R/S20C	1490	8609	0.173
Ub G76W	6990	8694	0.804
USP25cat	73800	63961	1.154
USP25cat Δtip	73800	56757	1.300
USP25cat F458E/L552E	73800	63959	1.154
USP25cat Δtip F458E/ L552E	73800	56755	1.300
USP28-tip-chimera	94770	65232	1.453
USP28-roof-chimera	94770	65024	1.457
USP25-roof-chimera	73800	64230	1.149
USP25 UCID	12950	19015	0.681

USP25cat Δtip R385Q	73800	56729	1.301
USP28cat Q378R	94770	64964	1.459
USP25cat P535S	73800	63951	1.154
USP25cat P535L	73800	63977	1.154
USP25cat E600D	73800	63947	1.154
USP25cat Δtip E600D	73800	56743	1.301
USP25cat Δtip E600N	73800	56742	1.301
USP25cat Δtip E600A	73800	56699	1.302
FBW7 262-707	81930	50304	1.629
FBW7 247-707	81930	51876	1.579
SKP1	17990	18658	0.964
TNKS-ANK	47330	85076	0.556
USP25cat-ct	104170	104868	0.993
USP25cat-ct P535L	104170	104884	0.993
USP25cat C178S	73800	63945	1.154
USP25CT	28880	34485	0.837
USP28CT	34840	36594	0.952
USP28CT-2	34840	33420	1.042

VI.4 Supplementary Figures

Purification of USP28 variants

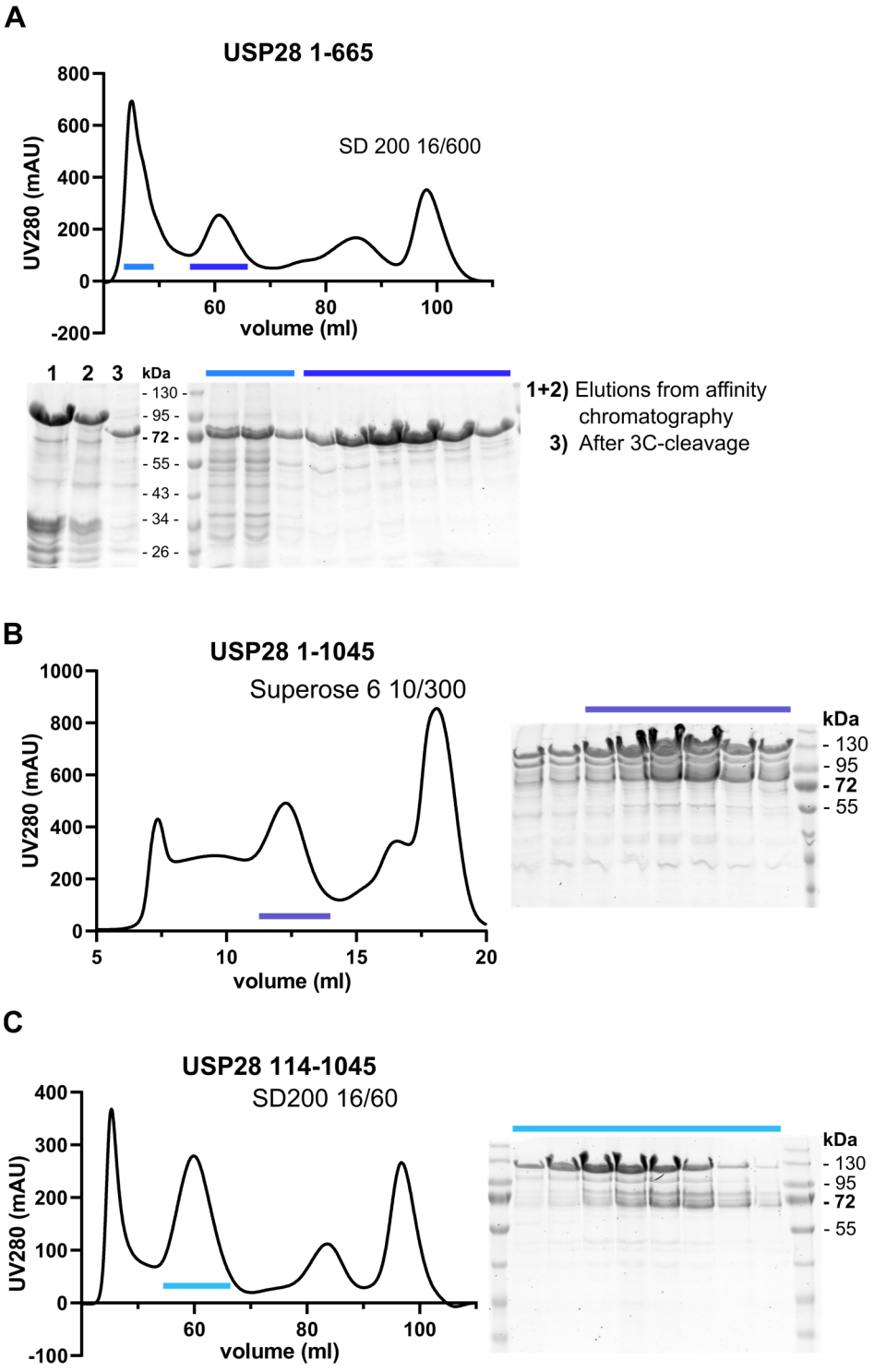

Figure 53: Purifications of USP28 variants. **A)** SEC of USP28 1-665 on a SD200 16/600 column with the appropriate SDS-PAGE. Corresponding fractions on the gels are indicated. Samples on the left side are elution fractions from Ni-IDA affinity chromatography (1+2) and after 3C-cleavage (3). **B)** SEC of USP28 fl 1-1045 on a Superose 6 10/300 column and **C)** SEC of USP28 114-1045 on a SD 200 16/600 column with appropriate SDS-PAGE. Corresponding fractions on the gels are indicated.

Conservation of Ub-binding in USPs

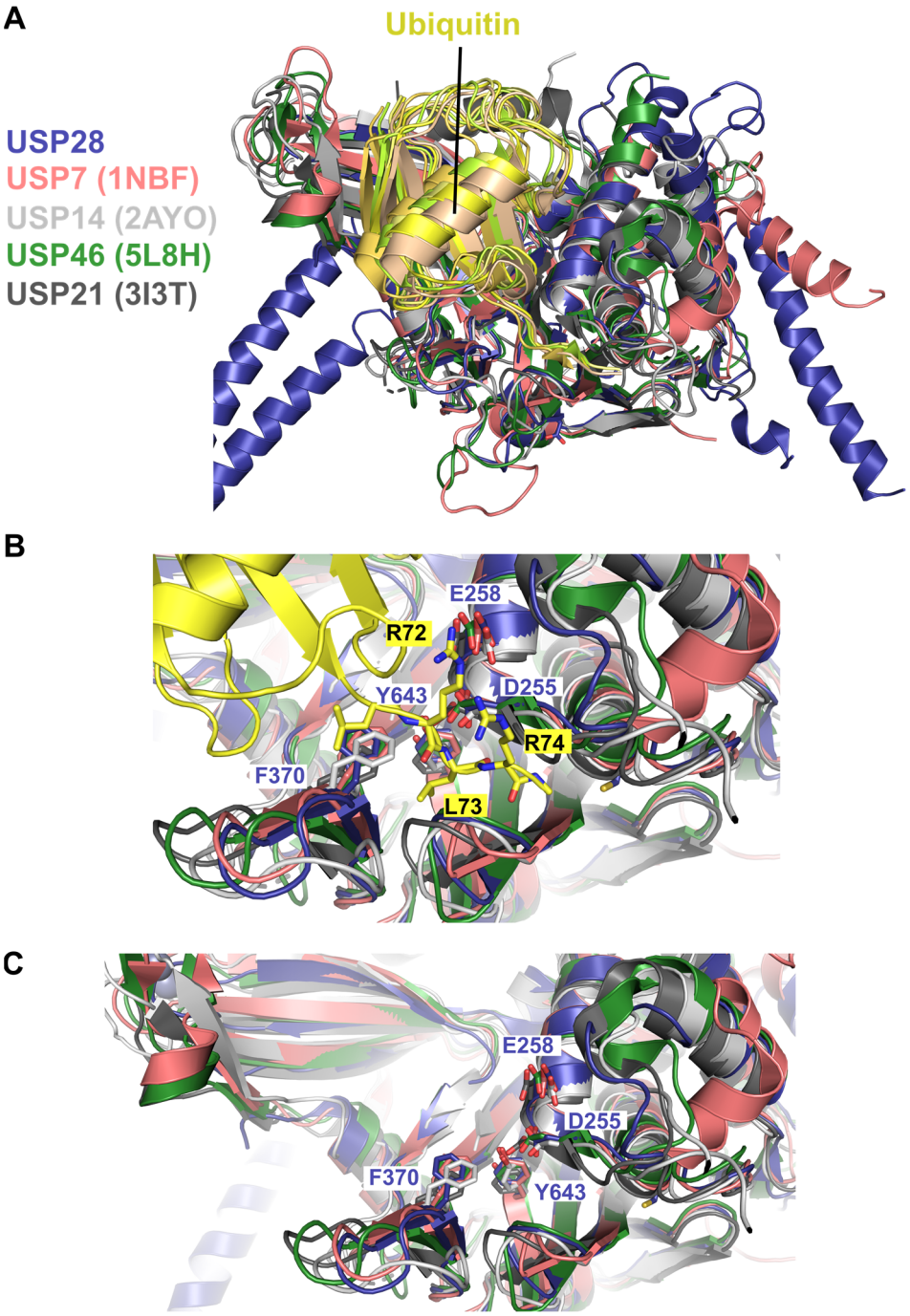

Figure 54: Conserved Ub-binding in USPs. **A)** Superposition of USP28-UbPA (blue and yellow respectively) with the Ub-bound structures of USP7 (PDB: 1NBF, red), USP14 (PDB: 2AYO, light grey), USP46 (PDB: 5L8H, green) and USP21 (PDB: 3I3T, dark grey). The ubiquitins of the different structures are colored in different shades of yellow. Overall Ub binding to the S1-site is similar between the different USPs. **B)** Detailed view of the superimposed USP structures with the tail of only one Ub shown. The Ub-tail and the conserved amino acids of the USPs are shown as sticks, with only the Ub and the USP28 amino acids labeled. **C)** Detailed view of the superimposed USP structures without Ub in the same orientation as above. The conserved amino acids participating in Ub-tail stabilization are shown as sticks. Only USP28 amino acids are labeled. For B) and C) the same color code as in A) was used.

Ubiquitin purification and Ub-chain synthesis

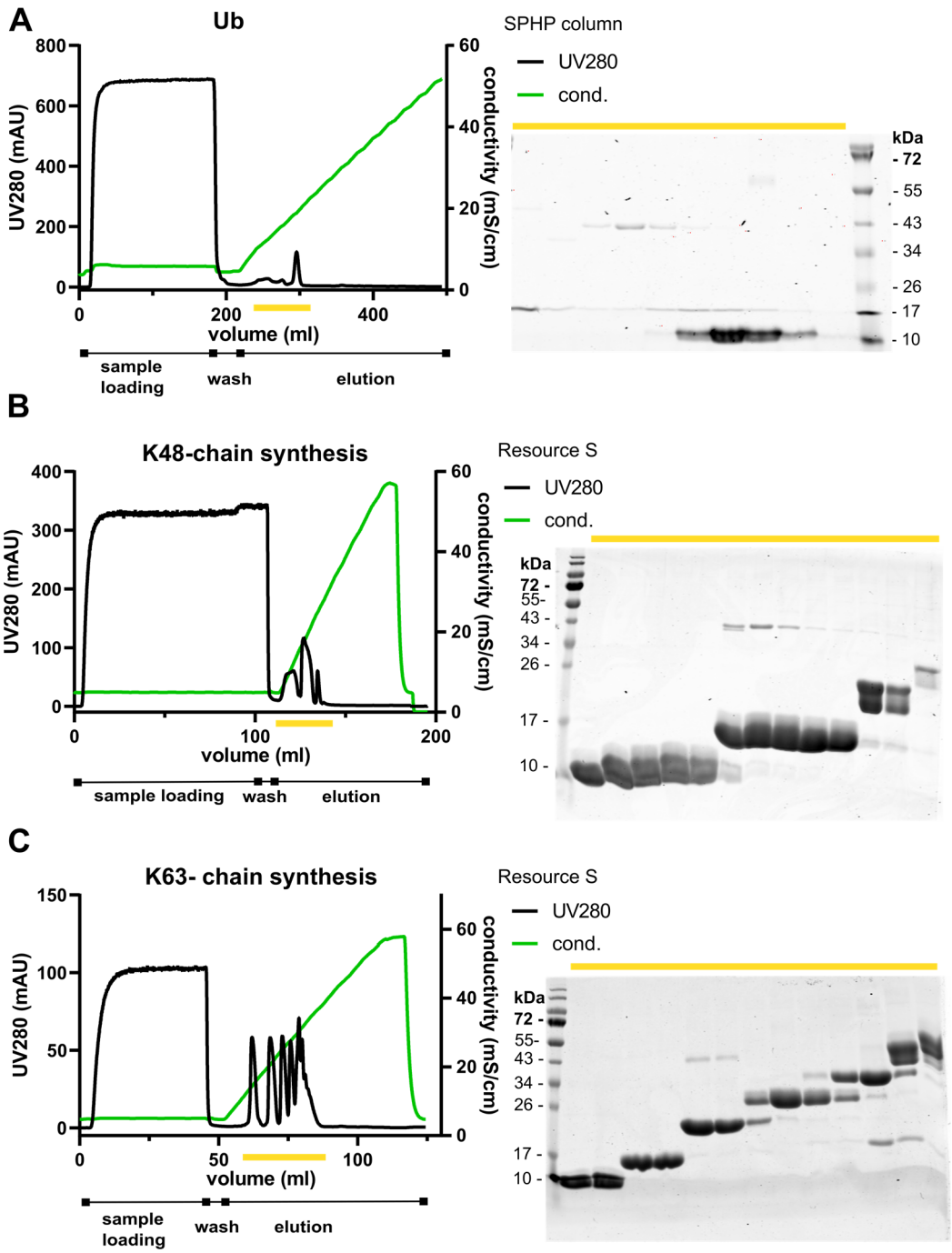

Figure 55: Ubiquitin purification and chain synthesis. **A)** Ub purification on a SPHP column. Ub was loaded after a precipitation step on a SPHP column and eluted with a linear gradient of 0-600 mM NaCl (indicated by the increasing conductivity (cond.), in green). Eluted protein fractions (underlined in yellow) were analyzed by SDS-PAGE. **B)** Ub K48-chain synthesis and **C)** Ub K63-chain synthesis. After incubation with the E1 and E2 enzymes, Ub-chains were loaded on a Resource S column and separated by a linear gradient of 0-600 mM NaCl (indicated by the increasing cond., in green). Eluted chains (yellow) were analyzed by SDS-PAGE.

Purification of FBW7 263-707/ SKP1

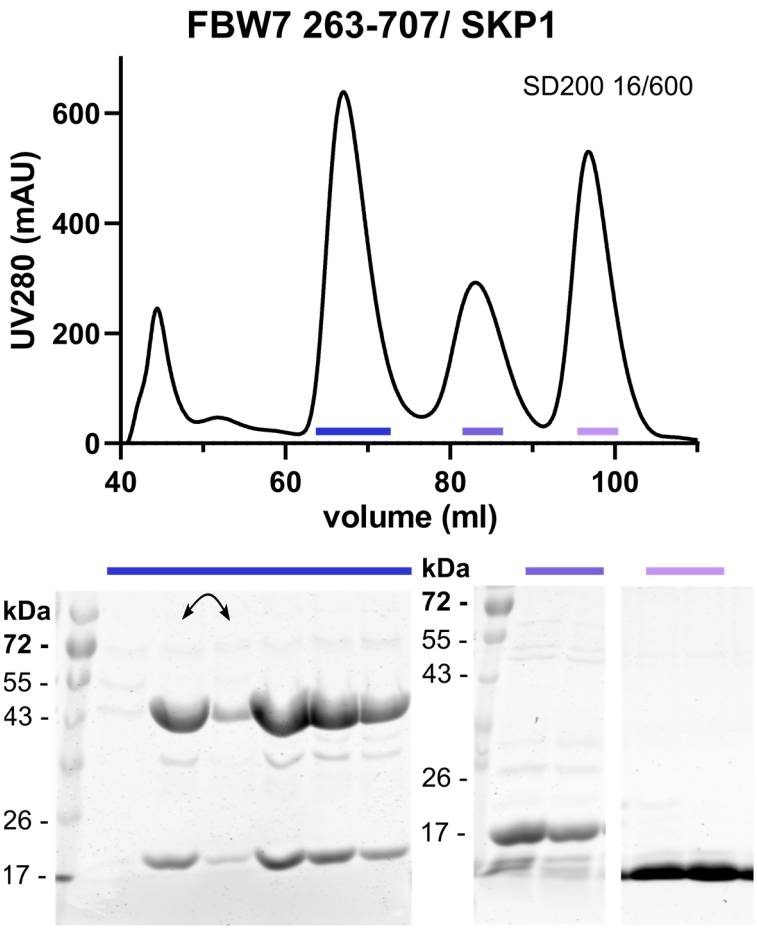

Figure 56: SEC of FBW7 263-707 in complex with SKP1. After affinity chromatography, SEC was performed using a SD200 16/600 column. The elution fractions of the indicated peaks were analyzed by SDS-PAGE.

Purification of USP25 157-1055

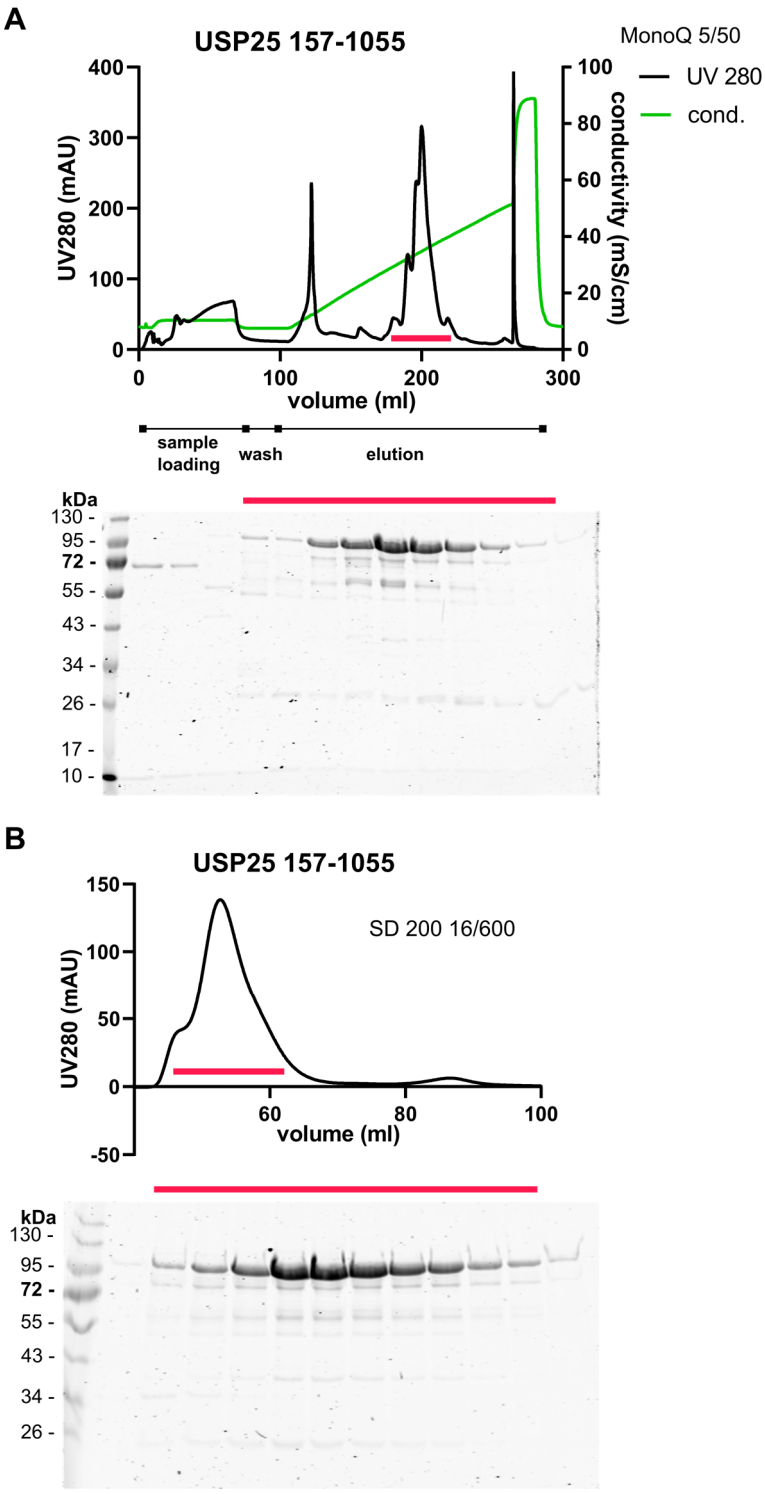

Figure 57: Purification of USP25 157-1055. **A)** Ion exchange chromatography of USP25 157-1055. Following affinity chromatography and dialysis, the protein was loaded on a MonoQ 5/50 column. After a washing-step, the protein was eluted y a linear gradient of 50-500 mM NaCl, indicated in the chromatogram by the increasing conductivity (cond., in green). The peak fractions (indicated by a red line) were analyzed by SDS-PAGE. **B)** SEC of USP25 157-1055. SEC was performed after ion-exchange chromatography on a SD 200 16/600 column. The eluting protein was analyzed by SDS-PAGE as indicated.

Purification of TNKS

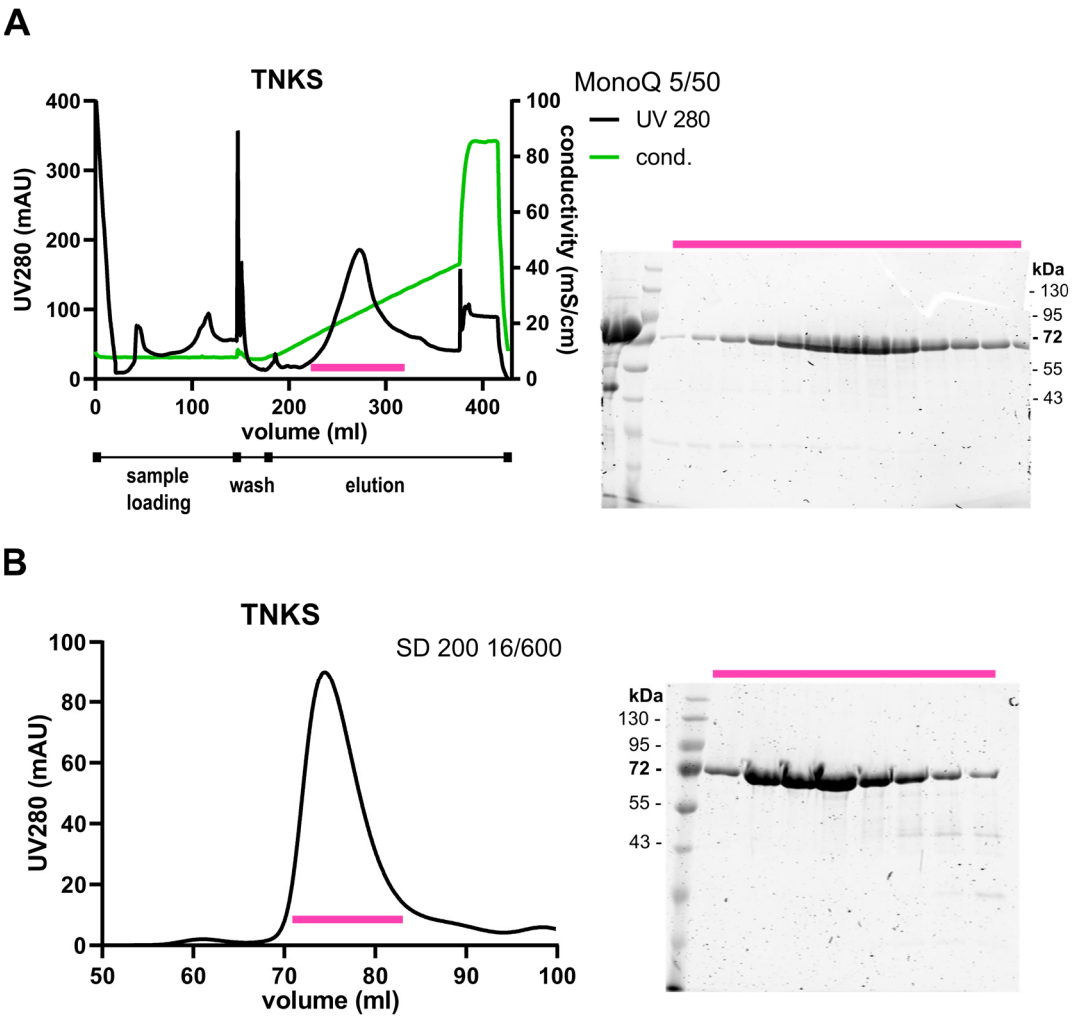

Figure 58: Purification of TNKS. **A)** Ion exchange chromatography of TNKS. The protein was loaded on a MonoQ 5/50 column after affinity chromatography and subsequent dialysis. After a washing step, the protein was eluted by a linear gradient of 0-800 mM NaCl, indicated by the increasing conductivity (cond., in green). The eluted peak fractions (indicated in pink) were analyzed by SDS-PAGE. Left to the marker, a sample of the eluted protein from the affinity chromatography was loaded. **B)** SEC of TNKS. SEC was performed after ion-exchange chromatography, on a SD 200 16/600 column. Elution fractions (indicated in pink) were analyzed by SDS-PAGE.

Purification of USP25 157-1055 P535L

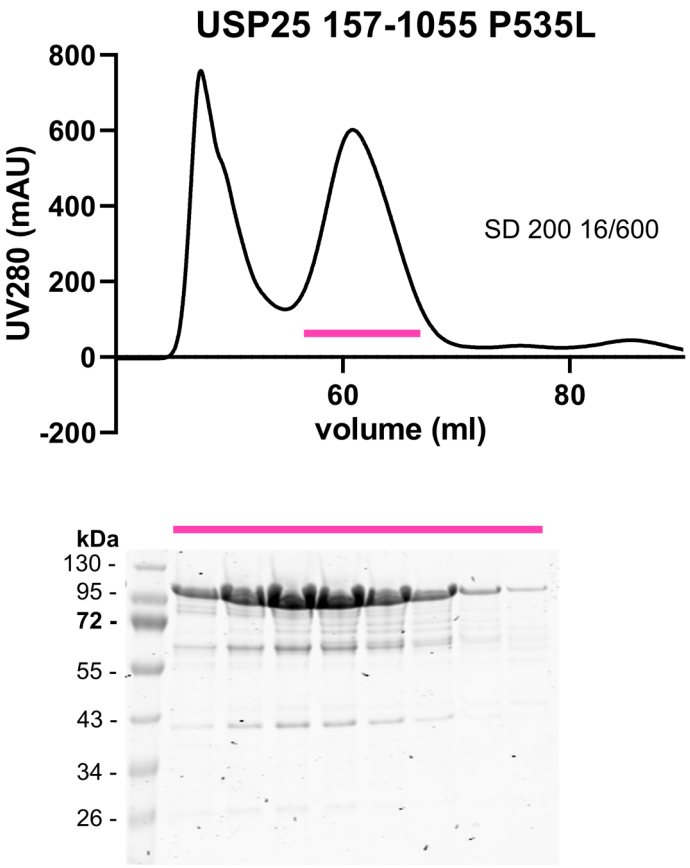

Figure 59: Purification of USP25 157-1055 P535L. After affinity chromatography, a SEC was performed on a SD 200 16/600 column. The elution fractions analyzed by SDS-PAGE are indicated.

Purification of USP25CT

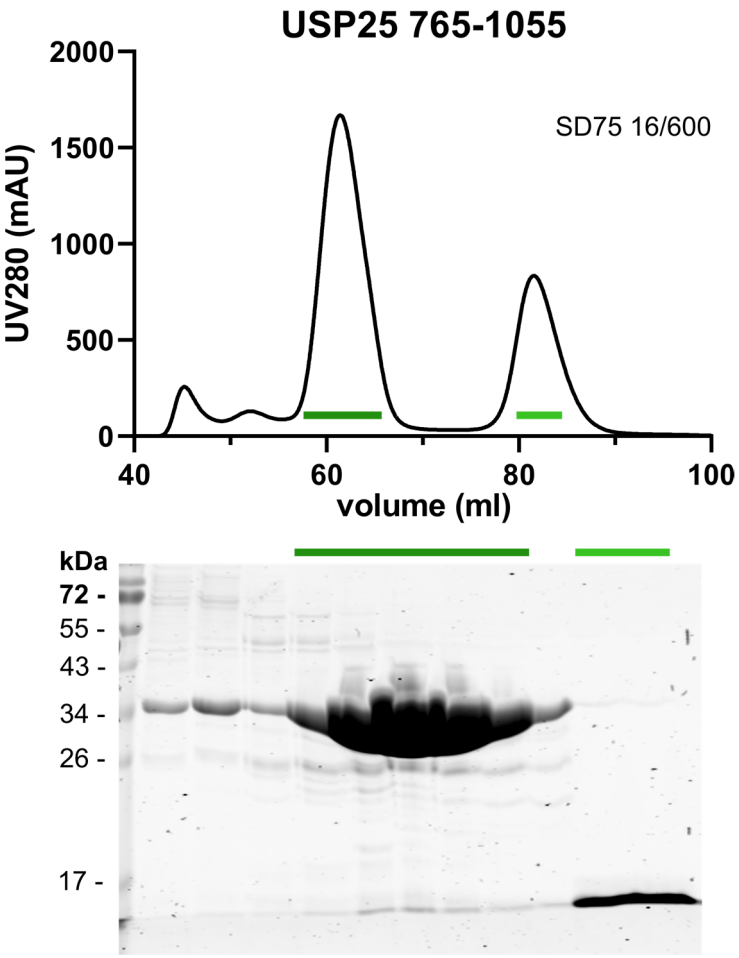

Figure 60: Purification of USP25CT. After affinity chromatography, SEC was performed utilizing the SD75 16/600 column. The eluting peak fractions were analyzed by SDS-PAGE as indicated. USP25Ct domain (fractions indicated in dark green) is separated from its His-tag (indicated in light green), that was cleaved during dialysis by the 3C protease, after affinity chromatography.

Purification of USP28CT-2

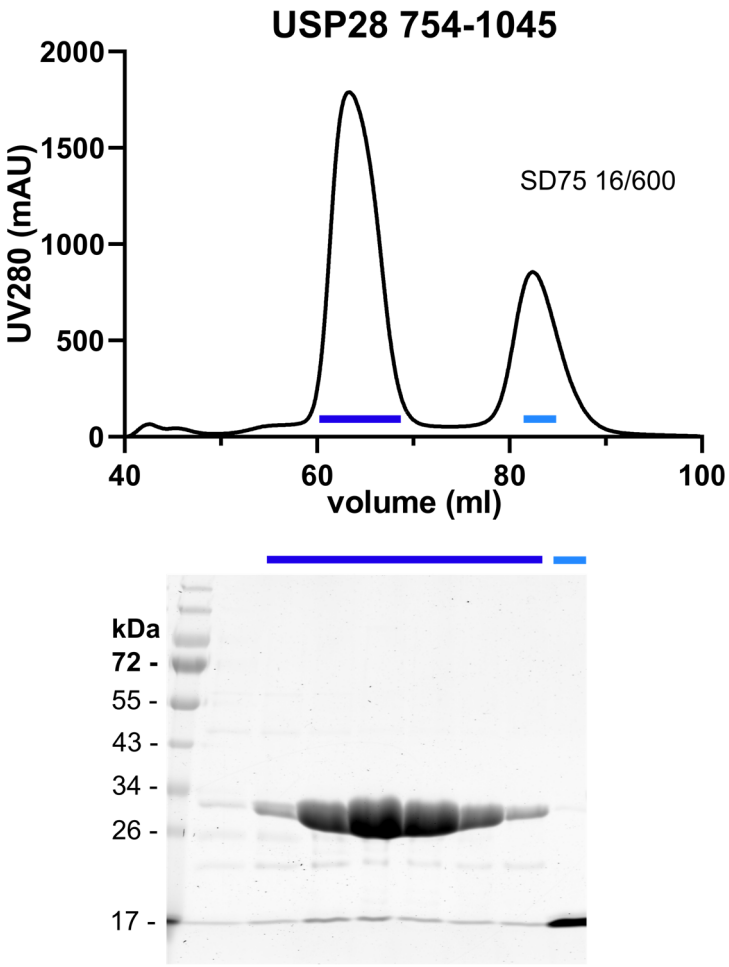

Figure 61: Purification of USP28CT-2. After affinity chromatography, SEC was performed utilizing the SD75 16/600 column. The eluting peak fractions were analyzed by SDS-PAGE as indicated. USP28CT-2 (fractions indicated in dark blue) is separated from its Trx-his-tag (indicated in light blue), that was cleaved by the 3C-protease during dialysis after affinity chromatography.

VII. List of Publications

Publications

Sauer F *, **Klemm T*** , Kollampally RB, Tessmer I, Nair RK, Popov N, Kisker C. Differential Oligomerization of the Deubiquitinases USP25 and USP28 Regulates Their Activities. Mol Cell. 2019;74(3):421-35 e10.

* These authors contributed equally

Ramirez YA, Adler TB, Altmann E, **Klemm T**, Tiesmeyer C, Sauer F, *et al*. Structural Basis of Substrate Recognition and Covalent Inhibition of Cdu1 from Chlamydia trachomatis. ChemMedChem. 2018;13(19):2014-23.

Selle M, Hertlein T, Oesterreich B, **Klemm T**, Kloppot P, Müller E, *et al*. Global antibody response to Staphylococcus aureus live-cell vaccination. Scientific reports. 2016;6:24754.

Congress Contributions

17th - 19th of June 2019: Deubiquitylases: from mechanism to physiology, in Edinburgh, UK. Poster presentation: “Regulation of USP activity by Oligomerization”.

17th – 22nd of June 2018: FASEB Ubiquitin & Cellular Regulation, in Snowmass village CO, USA. Poster presentation: “Characterization of the DUBs USP25 and USP28”.

11th /12th of October 2017: 12th international GSLS Student Symposium “EUREKA! 2017”, in Würzburg, Germany. Poster presentation: “Regulation of DUB Activity by Oligomerization”.

12th /13th of October 2016: 11th international GSLS Student Symposium “EUREKA! 2016”, in Würzburg, Germany. Poster presentation: “Structural insights into the Ubiquitin specific Protease USP28”.

14th /15th of October 2015: 10th international GSLS Student Symposium “EUREKA! 2015”, in Würzburg, Germany. Poster presentation: “Characterization of the catalytic activity of USP28 and its interaction with FBW7”.

VIII. Curriculum vitae

IX. Acknowledgements

At the end of this thesis, I want to take the chance to thank several people, who supported and accompanied me during the last four years of my PhD.

First of all, I want to thank my primary supervisor Caroline Kisker, who admitted me in her research group and trusted me to work on this promising new project in the DUB field. Despite the exciting but stressful time, I really enjoyed writing and editing the manuscript of our paper with her. I wanted to thank her for the constant advice, the ‘‘open door‘‘ and especially for making the right call in difficult situations.

I am deeply grateful to Florian Sauer, who shared the project with me and taught me everything I know about protein purification, characterization and crystallization. His great ideas formed the project and he became my mentor and friend, who went together with me through thick and thin.

Moreover, I would like to thank my second and third supervisors Alexander Buchberger and Nikita Popov, for useful advice, great ideas and their professional support.

Without our collaboration partners, Ingrid Tessmer (who performed and analyzed the AUC data) and Ravi B. Kollampally, Radhika K. Nair and Nikita Popov (who performed all the cell-based work) our paper (and this thesis) would not be as good as it is. Thank you all for your hard work, your ideas and knowledge.

Thanks to Jochen Kuper, who helped me in the analysis of the enzyme assays and always had good suggestions and ideas and to Wolfgang Kölmel, who not only took care of all the crystallization robots but also wrote a program that was facilitating the analysis of my enzymatic assay data.

Teresa Frank and Andrea Schott-Heinzmann are the heart of the Kisker and Schindelin groups, thank you for the caring support and all the administrative work.

I am really grateful to Bernhard Fröhlich and Roland Markert, for their constant IT-support and especially for their help when my laptop broke, several times.

Thanks to Nicole Bader, Monika Kuhn, Michelle Endres, Gudrun Sander and Julia Wörner for their organizing, ordering, sorting and running the lab.

I want to thank all the colleagues from the structural biology department, the research groups Kisker, Schindelin, Lorenz, Tessmer and Böttcher for the nice working atmosphere, especially Radhika K. Nair, Anabel Pacios Michelena, Jeannette Kappenberger, Mohit Misra and Sebastian Kaiser, who became good friends.

Thanks to Hannah Heil and Sara Eisenbart (“Die Genießerbande“). Delicious food is always a good distraction.

I want to thank Anna Maierhofer and Felix Mattern for encouraging breakfasts and dinners in our quadripartite-shared flat.

Thanks to my good friends Franziska Karl and Anna Molitor for the best lunch breaks and party nights and that both of them are always there.

I am grateful to have my best friend Julia Rammler who cheered me up from far far away, with an Adventskalender, motivating postcards and phone calls.

I especially want to thank my parents Kornelia and Fritz Klemm and my siblings Isabel Stritzel and Christopher Klemm, who unconditionally supported me, always had an open ear and encouraged me throughout. I am also grateful for the rest of my joint family, showing their constant interest and support.

Finally, I want to thank my boyfriend Martin Kraus, with whom I could share the best and the worst moments of my PhD and who stayed through it all.

Affidavit

I hereby confirm that my thesis entitled "**Minor differences cause major effects: How differential oligomerization regulates the activities of USP25 and USP28**" is the result of my own work. I did not receive any help or support from commercial consultants. All sources and/or

materials applied are listed and specified in the thesis.

Furthermore, I confirm that this thesis has not yet been submitted as part of another examination process neither in identical nor in similar form.

Würzburg, …… ……

(Date) (Signature)

Eidesstattliche Erklärung

Hiermit erkläre ich an Eides statt, dass die Dissertation „**Kleine Unterschiede mit großer Auswirkung: Wie differenzielle Oligomerisierung die Aktivitäten von USP25 und USP28 reguliert"** eigenständig, d.h. insbesondere selbstständig und ohne Hilfe eines kommerziellen Promotionsberaters, angefertigt und keine anderen als die von mir angegebenen Quellen und Hilfsmittel verwendet zu haben. Ich erkläre außerdem, dass die Dissertation weder in gleicher noch in ähnlicher Form bereits in einem anderen Prüfungsverfahren vorgelegen hat.

Würzburg, …… ……

(Datum) (Unterschrift)